Phenotypic High-Throughput Screening to Identify Small-Molecule Inhibitors of Beta-Cell Glucolipotoxicity

Citation

Permanent link

Terms of Use

Share Your Story

[Accessibility](#)

HARVARD UNIVERSITY
Graduate School of Arts and Sciences

DISSERTATION ACCEPTANCE CERTIFICATE

The undersigned, appointed by the

Department of Chemical Biology

have examined a dissertation entitled

Phenotypic High-Throughput Screening to Identify Small-Molecule Inhibitors of Beta-Cell Glucolipotoxicity

presented by Jonnell Candice Small

candidate for the degree of Doctor of Philosophy and hereby certify that it is worthy of acceptance.

Signature _____

Typed name: Bridget K. Wagner, Ph.D.

Signature _____

Typed name: Prof. Christina M. Woo, Ph.D.

Signature _____

Typed name: Prof. Stuart L. Schreiber, Ph.D.

Signature _____

Typed name: Prof. Rohit N. Kulkarni, M.D., Ph.D,
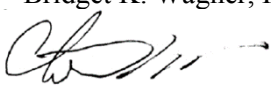
Date: March 31, 2022

Phenotypic High-Throughput Screening to Identify Small-Molecule Inhibitors of Beta-Cell

Glucolipotoxicity

A Dissertation Presented

By

Jonnell Candice Small

To the Committee On Higher Degrees in Chemical Biology

In Partial Fulfillment of the Requirements

For the Degree of

Doctor of Philosophy

In the Subject of

Chemical Biology

Harvard University

Cambridge, Massachusetts

March, 2022

Phenotypic High-Throughput Screening to Identify Small-Molecule Inhibitors of Beta-Cell Glucolipotoxicity

Abstract

The global type 2 diabetes (T2D) epidemic continues to grow and by 2045, it is estimated 780 million adults will live with the disease. T2D is characterized by progressive pancreatic β-cell failure and loss of β-cell mass due to several pathophysiological factors including increased levels of circulating glucose and free fatty acids (FFAs). In fact, the growing prevalence of T2D is correlated with rapidly rising obesity rates, especially in low- and middle-income countries. Poor nutrition in early life, combined with overnutrition in later life appear to accelerate the T2D epidemic in these populations experiencing changing food habits and reduced physical activity. The onset of obesity is associated with elevated FFAs which contribute to T2D development by promoting insulin resistance, pancreatic β-cell dysfunction, and pancreatic β-cell death. Exposure to elevated glucose compounds the toxicity of elevated FFAs, leading to β-cell glucolipotoxicity (GLT). GLT is characterized by impaired glucose-stimulated insulin secretion (GSIS), decreased insulin gene transcription, attenuation of β-cell-specific transcription factors like PDX1, and induction of apoptosis through caspase activation. There are currently no therapeutics which address this facet of T2D.

Phenotypic high-throughput screening (HTS) is a target-agnostic therapeutic discovery strategy that strives to preserve the functional cellular context of disease relevant molecular pathways. Unlike target-based drug discovery, phenotypic screening is less biased, allowing the model system to reveal the target(s) crucial to a disease phenotype. Phenotypic HTS is useful for the discovery of novel biological probes and for the repurposing of previously identified drugs to

new disease contexts. Phenotypic HTS relies on the design of model system that near accurately mimic the clinical manifestation of diseases of interest.

In this dissertation, I explore the application of phenotypic screening to the discovery of β-cell GLT-protective small molecules. After optimizing GLT assays in the INS-1E cell line and dissociated human islets, *in vivo* models of pancreatic β-cells, I screened a total of 20,876 small molecules and validated ten compounds which recovered β-cell viability in both human islets and INS-1E. These compounds were validated in several secondary screening assays highlighting hallmark aspects of GLT including caspase activation, mitochondrial depolarization, calcium influx, and decreased expression of β-cell transcription factor *Pdx1*.

KD025 was identified as GLT-protective from the phenotypic HTS, and I sought to investigate the beta-cell target responsible for its activity. KD025 is a known Rho-associated kinase 2 (ROCK2) inhibitor and I hypothesized ROCK2 inhibition may mediate its GLT-protectivity. Subsequent experiments revealed *Rock2* loss did not affect INS-1E viability in GLT-conditions. Kinase profiling revealed KD025 had potent casein kinase 2 (CK2) α/α' activity and lead to the validation of CK2α as the mediator of GLT-induced β-cell death. CK2α loss improved INS-1E viability in GLT-conditions and CK2α overexpression ablated KD025 GLT-protectivity. RNA-sequencing analysis additionally revealed KD025 partially reversed the GLT-induced gene expression signature, including recovering the expression of several pancreatic β-cell genes and reducing the expression of genes involved in hypoxia and the inflammation response.

Table of Contents

Acknowledgements

I am immensely grateful to my advisors Dr. Bridget K. Wagner and Dr. Stuart L. Schreiber for providing me with the opportunity to train and learn from them as I conducted my dissertation studies. I am especially grateful for the welcoming nature of both, which served as a source of comfort during a trying time in my dissertation studies. Dr. Wagner and Dr. Schreiber welcomed me into their groups and provided me with a sense of belonging. As scientific advisors, they gave me the freedom to drive this project, but were always available for constructive feedback and advice when I needed it. Additionally, Dr. Wagner and Dr. Schreiber were exemplary sources of support as I explored career development opportunities during my studies, giving me the freedom to explore internship opportunities and learn from them. I cannot imagine more supportive advisors for my doctoral studies and I will carry their goodwill with me through future career choices and mentorship of others.

I would also like to thank the members of the Wagner and Schreiber laboratories for facilitating my growth as an experimentalist, a mentor, and a scientist. I may have started as an introvert with rudimentary understanding of beta-cell biology but I have since grown, advancing this project and making new discoveries.

I thank my dissertation advisory committee: Dr. Christina Woo, Dr. Rohit Kulkarni, and Dr. Bridget Wagner for guiding me through my project and providing crucial feedback necessary to advance my studies. My DAC meetings were instrumental in guiding my development as a scientist.

I am also extremely thankful to Dr. Carol Khodier, Dr. Maria Kost-Alimova, and Dr. Paul A. Clemons for their support and guidance as my dissertation project progressed. They were all extremely necessarily to my scientific growth, teaching me new methods and guiding me through steep learning curves.

To my parents Andrea Small and James Small, thank you for everything. Thank you for the sacrifices you had to make for me, especially to support my education. Thank you for your belief in me, even when I sometimes loss track of it myself. Mom you said it best, "Big things start small" and now more than ever I feel the weight of those words. Thank you, thank you, thank you. I have achieved the dream of dreamers who dared me to dream.

And at last I thank the community of friends and colleagues I have gained in my time at Harvard. You have challenged me to lead, you have challenged me to grow, and I say without you all I would have floundered. You saw potential in me where I faintly knew it existed and reminded me life was more than the sum of successes and failures. Thank you.

Dedication

To the girl in the mirror and her lovely dark skin. There was a time the others said her future was dictated by its tint. May those words never again be uttered by friend or foe. Let all children freely bask in the yellow of the sun. I rise so you rise. I grow so you know too, the future is not written. It is waiting for you.

Chapter 1

Introduction

1.1 Glucose Homeostasis: The Who, What, Where, and When

It is almost lunch time and you are famished. You have skipped breakfast and the echo of a wild animal issues from your stomach, compelling a visit to the vending machine for a quick fix. Since dinner last night at 10 PM your plasma blood glucose has slowly decreased as your muscles and liver absorb the energy source. The α-cells located in the islets of Langerhans of your pancreas secrete glucagon in response to the decreasing blood glucose, stimulating a signal cascade to prevent blood glucose levels from bottoming out. Glucagon, like insulin, is an endocrine hormone released from the pancreas to maintain normoglycemia in the blood. Normoglycemia is the basal concentration of glucose available in the blood when in a fasting state between meals. In order to prevent blood glucose from crashing and causing hypoglycemia, the body utilizes glucagon to stimulate hepatic and renal glucose production (gluconeogenesis) and hepatic glucose release (glycogenolysis).[1] While these are great temporary sources of glucose, they will eventually run out, hence the need replace lost stores with glucose from food.
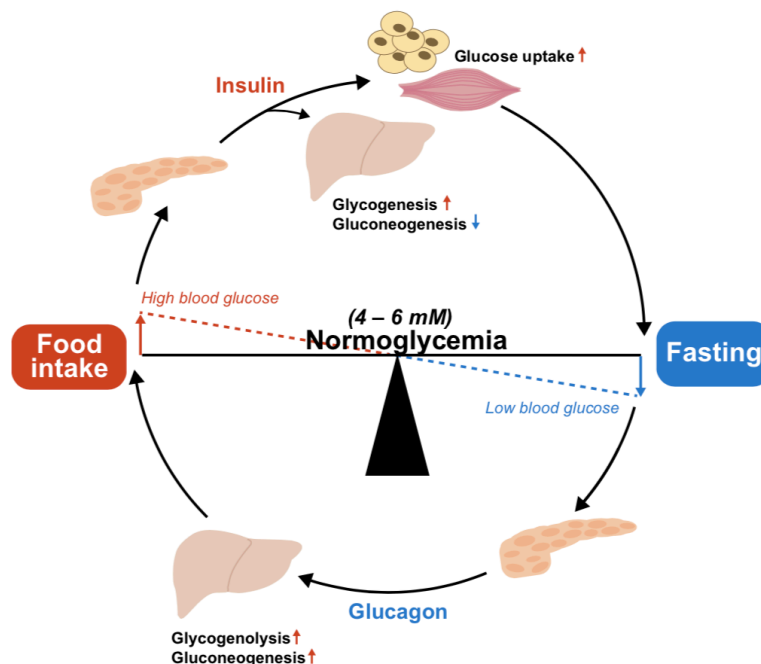
Figure 1.1.1. Glucose homeostasis mediated by insulin and glucagon. When blood glucose is low, glucagon is secreted to increase hepatic glycogenolysis and gluconeogenesis. After eating, blood glucose rises and insulin is secreted to trigger glucose uptake in adipose, muscle, and hepatic tissue.

You have indulged in a chocolate bar and a new signal cascade begins. In your gut, enteroendocrine cells release glucagon-like peptide 1 (GLP1) and glucose-dependent insulinotropic peptide (GIP), which bind to their receptors on β-cells in your islets of Langerhans to stimulate insulin release.[1] Glucose, amino acids, and free fatty acids released from digestion of the chocolate bar stimulate this GLP1 and GIP release.[1] Rapidly rising blood glucose levels due to intestinal glucose absorption stimulate glucose uptake from the glucose transporter 2 (GLUT2) on the β-cell. Once inside, glucose is metabolized to produce ATP, the increased levels of which stimulate closure of ATP-sensitive potassium channels. The depolarized β-cell membrane then triggers the influx of calcium through voltage-gated calcium channels, resulting in the exocytosis of insulin granules and the secretion of insulin into the blood.[1] In circulation, insulin acts on several organs to stimulate the uptake of glucose from the blood, mitigating the onset of hyperglycemia. In the liver, insulin stimulates the uptake of glucose and its conversion into its storage form glycogen. Insulin also turns off hepatic gluconeogenesis. In adipose and muscle tissue insulin stimulates uptake of glucose through GLUT4. The uptake of glucose in adipose tissue leads to the release of leptin, which acts on receptors in the hypothalamus to stop food intake and induce satiety.[1]

Unfortunately, the insulin released by your β-cells now has a limited effect on hepatic, adipose, and muscle glucose absorption. Years of an increasingly sedentary lifestyle has induced weight gain and insulin resistance in critical tissues of your body. You are entering a phase known as prediabetes and, if left unchecked, will progress to full fledge type 2 diabetes.

1.2 Type 2 Diabetes & Obesity

In 2016 the World Health Organization (WHO) released a report on the global burden of diabetes. Most shockingly, it revealed an estimated 422 million adults were living with a form of diabetes in 2014, compared to 108 million in 1980.[2] In 2021 the International Diabetes Federation

(IDF) updated these estimates and concluded 537 million people have diabetes worldwide and this number is expected to exceed 780 million by 2045 (Fig. 1.2.1).[3,4] The global prevalence of diabetes has nearly doubled in the last three decades, from 4.7% of the adult population to 8.5% sounding alarms across the world.[2] What is causing this rapid increase in diabetes and what, if anything, can be done to slow it down?
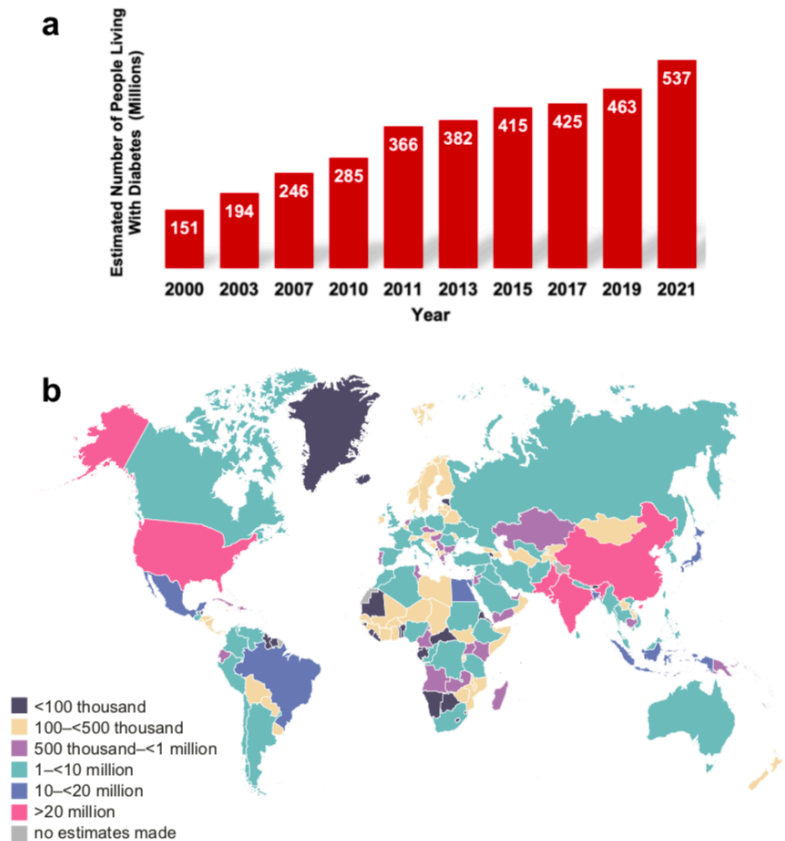
Figure 1.2.1. Estimates of global prevalence of diabetes in the 20-79 age group. a) The estimated number of individuals living with type 2 diabetes has more than tripled since 2000. Data from reference ([4]). b) Estimated total number of adults with diabetes in 2021. Adapted from IDF Diabetes Atlas, 10th Edition (2021).

Diabetes, as it is commonly known, refers to three separate forms of diabetes mellitus: type 1 diabetes (T1D), type 2 diabetes (T2D), and gestational diabetes (GDM). All three forms result in elevated blood glucose levels known as hyperglycemia. There is a fourth category referred to by the WHO and IDF as "other specific types," and it includes monogenic diabetes that results from

a single gene mutation; however, monogenic diabetes is much less common and represents 1.5-2% of diabetes cases.[4]

Type 1 diabetes, previously known as childhood-onset diabetes because it was commonly observed to develop in children, is characterized by insulin deficiency due to β-cell loss.[2,5] T1D is a chronic autoimmune disease, where immune system recognition of insulin producing β-cells leads to their targeted destruction. As such, T1D patients are insulin-dependent and must constantly monitor their blood glucose levels and appropriately dose themselves with insulin.

Type 2 diabetes on the other hand is a chronic metabolic disorder resulting in hyperglycemia due to impaired insulin secretion, insulin resistance or a combination of both.[6,7] T2D is characterized by β-cell dysfunction as well as dysregulated carbohydrate, lipid, and protein metabolism.[7] Therefore, it should be more wholistically considered a metabolic disease, rather than an insufficiency of the pancreas. T2D is the most common form of diabetes (representing >90% of all cases) and has increasingly become a major global health problem closely linked with the growing obesity epidemic.[6,7] Unlike T1D, environmental factors like obesity, unhealthy diet, and lack of exercise largely contribute to the multiple pathophysiological disturbances that impair glucose homeostasis in T2D.[7] In recent decades, genome wide association studies (GWAS) have revealed genetic factors that contribute to the development of T2D; however, environmental factors remain the primary instigator for the development of the disease.[8,9] While insulin resistance and impaired insulin secretion are the primary defects of T2D, several other pathophysiological abnormalities contribute to the dysregulation of glucose metabolism, necessitating the use of multiple antidiabetic agents to maintain normal blood glucose levels (Figure 1.2.2).[7]
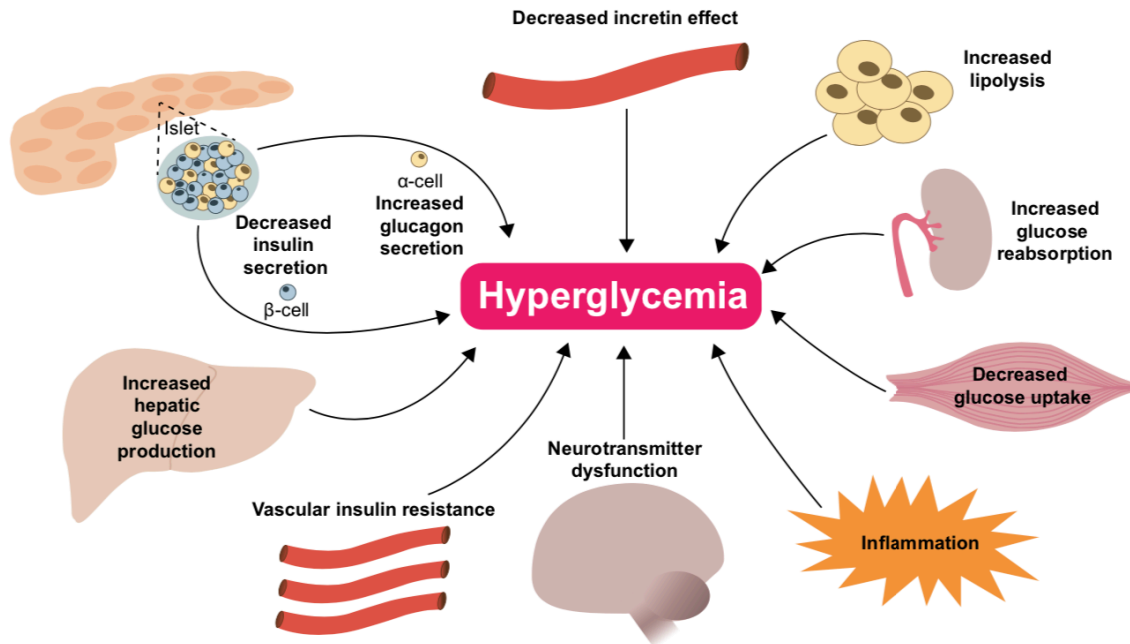
Figure 1.2.2. Multiple pathophysiological disturbances impair glucose homeostasis in type 2 diabetes. Insulin resistance in the muscle and liver combined with impaired insulin secretion by pancreatic β-cells are the main defects contributing to type 2 diabetes. Insulin resistance in fat storing adipocytes accelerate fat breakdown (lipolysis) and increases plasma free fatty acid levels. Increased renal glucose reabsorption maintains hyperglycemia. Resistance to appetite suppressing hormones (ex. Insulin, leptin, GLP1) contribute to weight gain. Inflammation and vascular insulin resistance promote hyperglycemia.

To this end, there is still a need to develop medications addressing these abnormalities of T2D, including those that enhance insulin sensitivity, prevent pancreatic β-cell failure and prevent or reverse microvascular complications.[7]

Gestational diabetes occurs during pregnancy and increases the likelihood of developing T2D. Blood glucose levels are above normal but below the T2D range and increase the risk of pregnancy complications.[2] Unlike T1D and T2D diabetes which are often undiagnosed for years or diagnosed through patient symptoms like frequent urination, fatigue, or weight loss, GDM is identified through prenatal screening only and patients are immediately placed on treatment regimens to normalize blood glucose.

Type 2 diabetes stands apart from type 1 diabetes and gestational diabetes due its shear prevalence. In 2013, over 382 million adults aged 20-70 had T2D and 80% of this group lived in low- and middle-income countries.[7] From an epidemiological standpoint these data seemed

6

counterintuitive because, as is well documented, T2D is largely due to environmental factors like nutritional excess leading to obesity. However, in China and India, prevalence of T2D has dramatically increased despite the low prevalence of obesity, revealing the limitations of using body mass index (BMI) to define obesity.[7,10] Asians have a higher percentage of body fat mass, abdominal obesity and less lean muscle, potentially explaining their increased disposition to T2D.[11] Additionally, poor nutrition in early life, combined with overnutrition in later life appears to accelerate the T2D epidemic in populations experiencing changing food habits and reduced physical activity.[7] In summary, increasing adiposity is the single most important risk factor for T2D and research continues to support the conclusion that the rising obesity epidemic, and not genetic mutations, explain the increasing prevalence of T2D (Figure 1.2.3).[7,12]
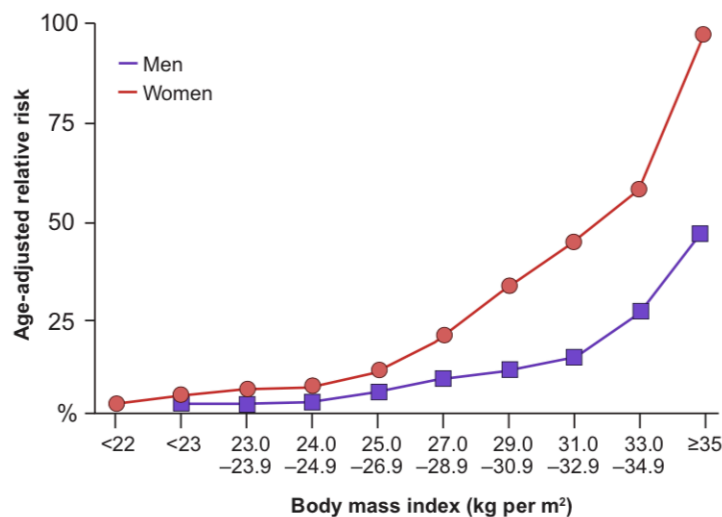
Figure 1.2.3. Association between body mass index (BMI) and type 2 diabetes. For both men and women, risk for T2D increases with increasing BMI. Data obtained from references ([7,13,14]).

T2D is frequently diagnosed based on three parameters: glycated hemoglobin A1c (HbA1c), fasting plasma glucose, and two-hour plasma oral glucose tolerance test (OGTT). As shown in Table 1.2.4, T2D is characterized by HbA1c $\geq 6.5\%$, fasting plasma glucose ≥ 126 mg per dl, and two-hour plasma OGTT ≥ 200 mg per dl. Also shown in Table 1.2.4 is the condition known as prediabetes, wherein a patient shows elevated blood glucose parameters. The overt

hyperglycemia observed in T2D is preceded by prediabetes, a high-risk condition which, if left untreated, progresses to T2D. Prediabetes is characterized by impaired fasting glucose levels, impaired glucose tolerance, and increased HbA1c.[7] The annual conversion rate of prediabetics to T2D ranges from 3-11%, as such, screening these at risk individuals is crucial because 30-45% of T2D patients remain undiagnosed.[3,7]

Table 1.2.4. Type 2 diabetes diagnostic reference values.

Parameters	Normal*	Prediabetes	T2D
Hemoglobin A1c	<5.7%‡ <6.0%§	5.7–6.4%‡ 6.0–6.4%§	≥6.5%
Fasting plasma glucose	<100 mg per dl‡ (<5.55 mM) <110 mg per dl§ (<6.11 mM)	100–125 mg per dl‡ (5.55–6.94 mM) 110–125 mg per dl§ (6.22–6.94 mM)	≥126 mg per dl (≥7.0 mM)
Two-hour plasma OGTT	<140 mg per dl (<7.77 mM)	140–199 mg per dl (7.77–11.0 mM)	≥200 mg per dl (≥11.1 mM)

OGTT, oral glucose tolerance test; T2D, type 2 diabetes. *Normal glucose metabolism. ‡American Diabetes Association. §World Health Organization.

When type 2 diabetes is left unmanaged or undiagnosed complications develop which can affect overall health and quality of life. Over time, hyperglycemia can damage the heart, nerves, and blood vessels in the eyes and kidneys, leading to increased incidence of heart disease, stroke, kidney failure, nerve damage in the feet (neuropathy), and blindness (diabetic retinopathy).[2] Finally, type 2 diabetes impacts not only patient lives, but the economic output of countries.[2,15] Current estimates calculate $1.7 trillion USD of global GDP from 2011–2030 will be lost due to direct and indirect costs associated with diabetes.[2,15]

1.3 Type 2 Diabetes Drugs: Diverse Mechanisms of Action

Therapeutic interventions have been approved for eight of the ten pathophysiological disturbance described in Figure 1.2.2 that contribute to impaired glucose homeostasis in T2D; the

exceptions are therapeutics targeting inflammation and vascular insulin resistance.[7] FDA-approved antidiabetic therapeutic strategies fall into eight categories: metformin, thiazolidinediones (TZDs), sodium/glucose co-transporter 2 (SGLT2) inhibitors, glucagon-like peptide 1 receptor agonists (GLP1 RA), dipeptidyl peptidase 4 (DPP4) inhibitors, α-glucosidase inhibitors (AGIs), sulfonylureas, and insulin (Table. 1.3.1).[7,16]

Table 1.3.1. Glycemic efficacy and mechanism of action for current FDA-approved antidiabetic agents.

Drugs	Glycemic efficacy (HbA1c levels)	Mechanism of action	Administration
Metformin	↓↓	↓↓ Hepatic glucose production (HGP)	Oral
TZDs	↓↓	↑↑ Insulin sensitivity ↑↑ β-cell function	Oral
SGLT2 inhibitors	↓↓	↑↑ Glucosuria ↓↓ Glucotoxicity	Oral
GLP1 receptor agonists	↓↓	↑↑ Insulin secretion ↓↓ Glucagon secretion	Injection
DPP4 inhibitors	↓	↓ Glucagon secretion ↑ Insulin secretion	Oral
AGIs	↓	↓ Carbohydrate absorption	Oral
Sulfonylureas	↓↓	↑↑ Insulin secretion	Oral
Insulin	↓↓	↓ HGP ↑ Glucose uptake in muscle	Injection

Number of arrows indicate intensity of response.

The small molecule metformin is not itself a drug category. Rather, metformin functions so uniquely from all seven other categories and has such an excellent safety profile, it is placed in a category of its own. Re-discovered in 1957 by the French physician Jean Sterne, metformin was the first small molecule used to treat diabetic hyperglycemia and has become the preferred first-line oral blood glucose lowering antidiabetic.[17] Metformin partially functions by lowering hepatic glucose production and in recent years has been shown to decrease cardiovascular risk factors

in patients who take it long-term.[7,16,17] However, though widely prescribed and heralded as a safe drug, molecular validation of metformin cellular targets remains largely unknown and lowering hepatic glucose production does not fully explain all its effects.[18,19] The primary site of metformin action is thought to be in the mitochondria where it inactivates mitochondrial complex I, however, metformin is also known to inhibit enzymes responsible for the breakdown and synthesis of glucose, and for the activation of AMP-activated protein kinase (AMPK), whereby it affects lipid metabolism.[18,19]

Table 1.3.1 reveals the general mechanisms of action for FDA-approved antidiabetic agents. These include reducing hepatic glucose production, increasing insulin secretion, decreasing glucagon secretion, increasing insulin sensitivity, and increasing muscle glucose absorption. It is worth noting that several FDA-approved antidiabetic agents have multiorgan effects and work systemwide to regulate plasma glucose concentration. Decreasing glucagon secretion functions as a successful plasma glucose lowering strategy because the glucagon hormone increases blood glucose concentration as described in section 1.1. The opposing functions of insulin and glucagon in modulating plasma blood glucose therefore necessitates controlling both to effectively treat T2D.

In T2D patients with significant insulin resistance, insulin sensitizing agents like TZDs are priority. In fact, insulin resistance often precedes the development of T2D by many years, impacting the processing of glucose in several tissues.[7] TZDs are the only counter to insulin resistance in the current antidiabetic toolbox and their efficacy is offset only by the weight-gain associated with their use, which tends to decrease patient adherence.[7,16] TZDs increase insulin action in the liver, adipocytes, and skeletal and cardiac muscles, in addition to improving and preserving insulin secretion in β-cells.[20–22] The molecular mechanisms of TZDs include stimulation of the transcription factor peroxisome proliferator-activator receptor-γ (PPARγ); coactivation of PPARγ coactivator 1 (PGC1), which leads to fat oxidation; activation of genes involved in

lipogenesis (fat synthesis) and adipocyte proliferation; reduction of plasma levels of free fatty acids; reduction of circulating inflammatory cytokines; and stimulation of several enzymes involved in glucose metabolism.[7,20]

SGLT2 inhibitors by contrast increase weight loss due to the caloric loss of glucose through the urine.[7] SGLT2 inhibitors work by blocking glucose absorption in the proximal renal tubule, via SGLT2, decreasing maximum renal glucose reabsorption capacity and decreasing the threshold at which glucose transfers to the urine.[7,23–26]

GLP1 RA and DPP4 inhibitors both work to overcome β-cell glucagon-like peptide 1 (GLP1) resistance in T2D patients.[7,27–29] DPP4 inhibitors extend the half-life of endogenously secreted GLP1 by blocking its enzymatic destruction by DPP4.[7] However, to significantly reduce HbA1c in the background of severe GLP1 resistance, DPP4 inhibitors must be supplemented with GLP1 RA because they stimulate insulin secretion.[7,27] GLP1 RA also have the effect of decreasing glucagon secretion, thereby functioning like metformin to decrease hepatic glucose production.[7] Unlike metformin however, GLP1 RA are administered via injections and are the first prescribed injectable before insulin in T2D management.[16] Due to their HbA1c lowering efficacy SGLT2 inhibitors and GLP1 RA are often second-line treatments for the management of T2D.[29]

AGIs decrease carbohydrate absorption from the intestine by inhibiting α-glucosidase, an enzyme that breaks down starch to more easily absorbed carbohydrates.[30] AGIs also increase GLP1 secreted during meals. The HbA1c lowering capacity of AGIs is similar to DPP4 inhibitors but they remain in common use because they have been shown to decrease the conversion from prediabetes to T2D and their adverse effects are minimal.[7,31]

Sulfonylureas improve insulin secretion and decrease HbA1c, however the HbA1c lowering effect is temporary because sulfonylureas have no β-cell protective effect.[7] Literature evidence even suggests sulfonylureas facilitate β-cell failure in T2D.[32] Sulfonylureas act on the regulator subunits of ATP-sensitive potassium ion channels present in β-cells causing them to close and induce insulin secretion.[33]

Insulin supplementation is the last resort for plasma glucose management in T2D patients and is only prescribed once all other antidiabetic agents have failed to normalize HbA1c.[7] Insulin resistance is often present in these poorly responding patients, requiring large doses of insulin daily. However, even in these cases, insulin supplementation is still combined with other antidiabetic agents like TZDs, metformin, GLP1 RA, and SGLT2 inhibitors to improve glycemic control.[7,34–36]

While the current antidiabetic toolkit makes T2D treatment manageable, none of these therapeutics target the maintenance of β-cell mass, and in the case of sulfonylureas, some accelerate β-cell loss. Therefore, there is a current need to develop therapeutic strategies which counter β-cell dysfunction and loss in T2D.

1.4 Mechanisms of β-cell Death: Glucotoxicity, Lipotoxicity, and Glucolipotoxicity

The earliest detectable abnormality in individuals at risk for developing T2D is insulin resistance, however, true T2D does not occur unless β-cells are unable to secrete enough insulin to overcome insulin resistance.[37–41] Several factors contribute to this β-cell dysfunction and failure including insulin resistance itself[37,42], aging[43–45], genetic abnormalities[8,9,46], incretin hormone (GLP1, and gastric inhibitory polypeptide (GIP)) resistance and/or deficiency[47,48], hypersecretion of islet amyloid polypeptide (IAPP)[49–52], reactive oxygen stress[53–55], inflammation[56–59], and lipid or glucose dependent lipotoxicity[60–63], glucotoxicity[32,64], and glucolipotoxicity[65–68]. In experimental models, exposure to elevated levels of lipids (hyperlipidemia), glucose (hyperglycemia), or both leads to decreased β-cell mass through activation of β-cell apoptosis. More relevantly, in humans, poor diet and obesity are associated with decreased β-cell mass and onset of T2D.

β-cells metabolize free fatty acids (FFAs) and glucose to generate ATP, however, unlike adipose or muscle cells, excess of both or either can be detrimental, leading to dysfunction and

ultimately apoptotic death. In low glucose conditions, β-cells oxidize FFAs, generating ATP and acetyl-CoA.[69] In high glucose conditions, they metabolize glucose and generate enough ATP to depolarize their membranes and induce insulin secretion.[1,69] Chronic high glucose conditions overwork the insulin production and secretion machinery, stressing β-cells and leading to dysfunction. Chronic FFA exposure leads to lipid accumulation, as the growing level of stored lipids cannot be quickly detoxified. Chronic high glucose and FFAs leads to diminished lipid detoxification as β-cells switch to a glycolytic state to metabolize glucose and secrete insulin.[69] Recent research has focused on the role FFAs play in β-cell dysfunction and the detrimental effect of saturated FFAs over unsaturated FFAs.

It turns out not all FFAs are created equal. Saturated FFAs, found more in animal fats and highly processed foods, are difficult to detoxify because they aggregate and form lipid droplets within β-cells. Unsaturated FFAs however, are bent due to one or more double bonds in their carbon-carbon chain and it is more difficult for these fatty acids to aggregate and form cytoplasmic lipid droplets. In β-cells, lipotoxicity and glucolipotoxicity inhibit insulin secretion, decrease insulin expression, and decrease expression of β-cell specific transcription factors pancreatic duodenal homeobox-1 (PDX1) and MAFA.[70,71] Elevated levels of FFA are often observed in obesity because of reduced FFA clearance and expanded adipose tissue mass, providing a mechanistic link between obesity and the onset of T2D.[72]

The induction of apoptosis in β-cells experiencing glucotoxicity, lipotoxicity, or glucolipotoxicity occurs via multiple mechanisms, the vast majority of which affect the expression of apoptotic genes. Mammalian sterile 20-like kinase 1 (MST1, also known as STK4) for example, is a known regulator of β-cell death and dysfunction.[73,74] In diabetogenic conditions MST1 activity leads to mitochondrial proapoptotic pathway activation and caspase-3 activation. The full activation of MST1 is itself dependent on caspase cleavage, allowing MST1 to amplify the apoptotic signaling pathway.[73] MST1 also phosphorylates PDX1, resulting in its ubiquitination and degradation.[73]

When MST1 is inactivated, β-cell function is restored *in vitro* and *in vivo*, validating it as a therapeutic target for future drug development.[73]

Exposure to elevated glucose or FFA also stimulates the secretion of interleukin-1β (IL-1β) from β-cells and intraislet macrophages, activating β-cell apoptosis via inflammation.[75] Treating patients with a IL-1β deactivating antibody reduces expression of inflammatory markers, improves β-cell function, and improves glycemic control.[76–78] Toxic oligomers of islet amyloid polypeptide (IAPP) in the β-cells of T2D patients activate endoplasmic reticulum (ER) stress and reveals the role of impaired clearance of misfolded proteins in β-cell dysfunction.[79] This impaired clearance leads to a deficiency in ubiquitin carboxyl-terminal hydrolase L1 (UCH-L1), which prevents the ubiquitination and degradation of proteins, ultimately compromising β-cell viability.[79] Exposure to elevated FFA and glucose also generates reactive oxygen species (ROS) in β-cells due to their limited anti-oxidative defense mechanisms.[80] While short-term ROS increases glucose stimulated insulin secretion (GSIS), excessive ROS impairs GSIS.[81,82]

In summary β-cell death brought on by glucotoxicity, lipotoxicity, and glucolipotoxicity is mediated through several molecular mechanisms, some dependent on internal β-cell triggers and some depending on factors produced by other organs and cells. Considering the diverse causes of β-cell death in type 2 diabetes, future drug discovery campaigns may benefit from taking a phenotypic approach to screening rather than focusing on one specific mechanism of β-cell death like ER stress or ROS. Several β-cell models exists which are applicable to the phenotypic screening process and include the INS-1 and INS-1E rat insulinoma cell lines, the MIN6 mouse insulinoma cell line, the recently developed EndoC-βH1 human β cell line, rat islets, and human islets.[60,61,63,83]

1.5 Pancreatic β-Cell Models

Phenotypic drug discovery requires model systems that accurately, nor near accurately mimic the clinical manifestations of their disease of interest. In comparison to target-based drug discovery

methods, phenotypic screening is less biased, allowing the cell system to reveal the target(s) crucial to the disease phenotype. To properly utilize this advantage of phenotypic screening, the model system used must be biologically relevant, or the resulting hit compounds may not address the actual disease. While there are several rodent models of T2D (Table 1.5.1) available for investigating the organism wide efficacy of potential antidiabetics, these are not amenable to phenotypic screening which requires a more focused look on a phenotype of interest; for example, insulin resistance, insulin or hepatic glucose production, β-cell replication, transdifferentiation, or death, and more.

Table 1.5.1. Frequently used rodent models of type 2 diabetes.

Strain or Method	Species	Obesity	Hyper-glycaemia	Insulin Resistance	Hyper-insulinaemia	T2D
Monogenic						
Lep$^{ob/ob}$	Mouse	++	+	++	++	-
Lepr$^{db/db}$	Mouse	++	+	++	++	+
ZDF	Rat	-	+	++	+	+
Polygenic						
C57BL/6J	Mouse	+	-	+	-	-
C57BL/6N	Mouse	-	+	++	-	-
KK	Mouse	-	+	++	+	+
KK-A^y	Mouse	+	+	++	+	+
NZO	Mouse	++	+	++	+	+
TALLYO/Jng	Mouse	+	+	++	+	+
Chemical-induced						
HFD/STZ	Mouse, Rat	+	+	+	+	+

-, absent; +, mild; ++, severe. Lep$^{ob/ob}$: mouse model with mutation in leptin. Lepr$^{db/db}$: mouse model deficient in the leptin receptor. ZDF: a strain of Zucker Fatty rats with severe insulin resistance. C57BL/6J: diet-induced obesity (DIO) model. C57BL/6N: diet-induced obesity (DIO) model. KK: model spontaneously develops diabetic characteristics. KK-A^y: KK mice crossed with yellow obese gene (A^y). NZO: New Zealand obese mouse. TALLYO/Jng: spontaneously develop T2D. HFD/STZ: high-fat diet/streptozotocin-treated. Adapted from source: Fang J-Y et al. ([84]).

Several *in vitro* models have also been developed which enable focus on the pancreatic β-cell and while these cell lines do not perfectly mimic primary β-cell physiology, they still serve as value

tools to study the molecular biology governing β-cell function, dysfunction, and death (Table 1.5.2). Insulinoma-derived cell lines have the advantage of unlimited growth in tissue culture, however, for many there is a vast difference in their glucose stimulated insulin secretion (GSIS) compared to primary β-cells.[85] Beta-hyperplastic islet-derived cells (βHC) and EndoC-βH1 were derived from SV40 transformed preneoplastic islets and fetal pancreas respectively.[86,87] Rat insulinoma (RINm, RINm5F, RINr), insulinoma cell line (INS-1), and Cambridge rat insulinoma-G1 (CRI-G1) cell lines were generated from irradiated cells.[86,88–90] The βTC1 cell line does not secret insulin in response to glucose, though it does produce insulin.[91] βHC-9, BRIN-BD11, MIN6, INS-1, and EndoC-βH1 on the other hand all have normal GSIS and insulin content.[83,85,87,89,92–94] The INS-1E cell line is a clonal derivative of the nonclonal INS-1 cell line and can be stably cultured over extended periods (40-100 passages) while maintaining GSIS similar to rat islets.[95] RINm5F and RINr cells were both reported to have abnormal glucose transport and phosphorylation and both exhibit abnormal sensitivity to glucose.[96] The INS-1 and INS-1E cell lines exhibit several important characteristics of the β-cell including high insulin content (20% of normal rat β-cells) and responsiveness to glucose in the physiological range.[89,95] The MIN6 cell line originates from a transgenic C57Bl/6 mouse insulinoma expressing an insulin-promoter/t-antigen construct.[93] It has been observed that MIN6 cells can randomly lose GSIS.

Table 1.5.2. *In vitro* models of pancreatic β-cells.

Cell line	Cell origin	Species	Methods	Advantages	Disadvantages	References
βHC	Hyperplastic islets	Mouse	SV40 T-antigen	Normal GSIS	Only clone 9 (βHC9) responds to glucose stimulation.	[86,92]
βTC1	Insulinoma	Mouse	SV40 T-antigen	-	No GSIS	[91]
MIN6	Insulinoma	Mouse	SV40 T-antigen	Normal GSIS	Needs nicotinamide to be responsive to glucose.	[88,93]
BRIN-BD11	Insulinoma and normal β-cells	Rat	Electrofusion derived	Near normal GSIS	-	[94]
CRI-G1	Insulinoma	Rat	Radiation induced	-	No GSIS	[90]
INS-1 INS-1E	Insulinoma	Rat	Radiation induced	Normal GSIS. Relatively high insulin content.	Require βME in culture medium.	[89,95]
RINm	Insulinoma	Rat	Radiation induced	-	No GSIS	[97]
RINm5F	Insulinoma	Rat	Radiation induced	-	Inadequate sensitivity to glucose.	[96–98]
RINr	Insulinoma	Rat	Radiation induced	-	Inadequate sensitivity to glucose.	[97,98]
EndoC-βH1	Fetal pancreas	Human	SV40LT, hTERT	Normal GSIS. High insulin content.	Difficult to culture and slow growth	[83,87]

Glucose-stimulated insulin secretion (GSIS). β-mercaptoethanol (βME). EndoC-βH1 is the only extensively validated immortal human β-cell line. Adopted from Skelin M. *et al.* ([85]).

In addition to immortalized cell lines, primary β-cells can be obtained from rats, mice and human donors. Mouse, rat, and human donor islets are untransformed, glucose responsive, insulin secreting cells. They can be used to study β-cells in the most near-native environment outside of a living organism and experience limited gene-expression changes when cultured *ex-vivo* for a short period time (<7 days).[99–101] There are however limitations to using isolated islets, including

limited availability, especially for human islets, inability to be expanded to generate more cells, variability, especially between human donors, limited experimental handling before onset of dysfunction, limited transfection efficiency, and limited gene-editing efficiency. Due to the fragile nature of these cells, long-term experiments requiring more than a week, for example stable transfections or gene editing, are difficult to execute without risking dedifferentiation of islet cell populations. Additionally, due to the diverse cell types contained in an islet, specific focus on β-cell function requires multiplexed approaches to identify and isolate β-cells. My own work has shown that the high zinc content of β-cells enables the use of zinc-activated fluorophores like DA-ZP1 to identify, sort, and enrich β-cells from islet samples and differentiated β-like cells. (Appendix 1 & 2).

1.6 Phenotypic Screening & Lead Discovery

Equipped with an adequate model system or cell line, phenotypic high-throughput screening (HTS) can be a valuable strategy to probe the molecular mechanisms of complex phenotypes. This approach has been utilized in the pharmaceutical industry for years to generate candidate entities for therapeutic discovery and can be applied to the screening of small molecules, peptides, and even genes through overexpression, knockdown, and CRISPR-Cas9 mediated knockout.[102–105] For years, the connection between mechanistic knowledge and physiological effects was absent for prescribed therapeutics. Many novel drugs like insulin, penicillin, and aspirin were given to patients without knowledge of how they worked. What was known about these drugs was what physicians observed: phenotypic changes in treated patients like decreased glucose content in urine, reduced fever in septicemic shock patients, or reduced pain.[106] Case in point, metformin, the first-line therapeutic for T2D treatment is not much removed from a medieval herbal remedy. Even today, the complete elucidation of the specific molecular mechanisms which govern metformin action in the body has yet to be achieved.

In addition to an appropriate model system, the success of HTS phenotypic screening also depends on the availability of large libraries, be these small molecules or pooled CRISPR-Cas9 lentiviruses. In this case more is actually more, and considerable effort has been spent by pharmaceutical companies to generate small molecule libraries containing compounds in the millions and tens of millions. Screening such large libraries of small molecules has required developments in robotics and liquid handling to automize the entire process and computational capacity, to analyze the results. When selecting a small molecule library for phenotypic screening, consideration should be given to the quality metrics used to generate the library. That is, have small molecules with problematic functionalities been removed (i.e. Pan Assay Interference Compounds (PAINS) or nuisance compounds)?[107,108] Have compounds with low aqueous solubility been removed (i.e. molecules breaking Lipinski's rule of five: molecule with a molecular mass ≤ 500 Da, ≤ 5 hydrogen bond donors, ≤ 10 hydrogen bond acceptors, and an octanol–water partition coefficient log P ≤ 5)?[106,109,110] Is the library enriched in biologically active small molecules (i.e. Has an analysis like Cell Painting been performed to enrich for compounds with biological activity?)?)[111,112] Is the library chemically diverse as classified by the four components of structural diversity (i.e. appendage diversity, functional group diversity, stereochemical diversity, scaffold diversity)?[113] If these quality metrics have been verified, the library is of higher quality and is more likely to generate relevant hit compounds.

The Broad Institute of Harvard and MIT has expended considerable effort to generate libraries meeting such quality benchmarks, and in fact was among the first to pioneer multiplexed assays like Cell Painting to quickly screen small molecule libraries for morphological activity in cells.[112] The Diversity-oriented synthesis (DOS) library at the Broad Institute contains ≥10,000 compounds varying in stereochemistry, scaffolds, and functional groups. It was generated using DOS, which increases the diversity of compounds generated from a common set of chemical reactions by

utilizing a combination of reagent-based and substrate-based strategies (Figure 1.6.1).[113] The

Broad Institute also has developed a next-generation drug library and information resource known

as the Drug Repurposing Hub which consists of 4,707 hand-curated compounds annotated with

their literature-reported targets.[114] The collection includes 3,422 drugs tested in human trials or

marketed around the world and makes biologically active, annotated small molecules available

for screening. Drug repurposing, that is, taking a therapeutic for a specific disease and applying

to another is much cheaper than *de novo* drug development because much of the work profiling

the small molecules of interest have already been done.[114] The Broad Institute libraries are

therefore perfect for phenotypic high-throughput screening to identify small-molecule inhibitors of

β-cell glucolipotoxicity.
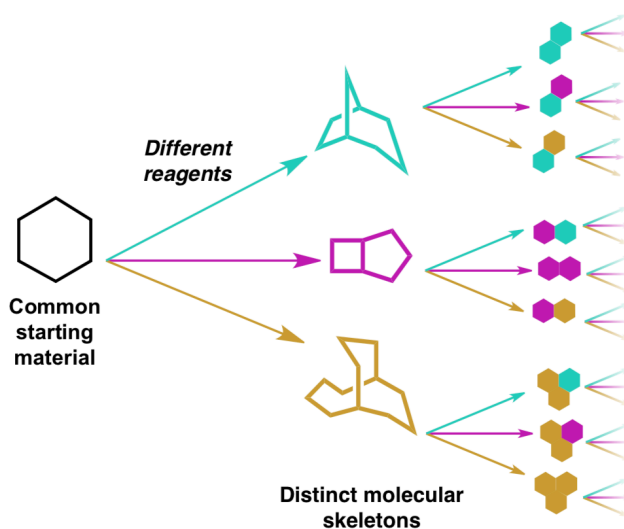
Figure 1.6.1: Schematic of Diversity-oriented synthesis (DOS) strategy. To maximize the four components of structural diversity DOS utilizes reagent-based and substrate-based strategies. The reagent-based strategy uses a common starting material and different chemical reagents to generate diversity. The substrate-based strategy uses different starting materials and common reaction conditions.

1.7 Dissertation Outline

The following chapters detail my efforts to identify small molecules that confer protection against the glucolipotoxic response in β-cells.

- **Chapter 2** describes the optimization of the glucolipotoxicity assay in INS-1E cells and the development of secondary assays to validate and interrogate the efficacy of hit compounds.

- **Chapter 3** summarizes the results of the primary screen in INS-1E and subsequent validation in human islets.

- **Chapter 4** details efforts to identify the target of the primary screen hit KD025.

- **Chapter 5** summarizes the findings of my dissertation and discusses future experimental directions.

1.8 References

1.   Röder, P. V, Wu, B., Liu, Y. & Han, W. Pancreatic regulation of glucose homeostasis. *Exp. Mol. Med.* **48**, e219–e219 (2016).

2.   World Health Organization. *Global Report on Diabetes*. *WHO Press* (WHO Press, 2016).

3.   International Diabetes Federation. *IDF Atlas 10th Edition 2021*. (2021).

4.   Sun, H. *et al.* IDF Diabetes Atlas: Global, regional and country-level diabetes prevalence estimates for 2021 and projections for 2045. *Diabetes Res. Clin. Pract.* **183**, 109119 (2022).

5.   Katsarou, A. *et al.* Type 1 diabetes mellitus. *Nat. Rev. Dis. Prim.* **3**, 17016 (2017).

6.   Type 2 diabetes mellitus. *Nat. Rev. Dis. Prim.* **1**, 15039 (2015).

7.   DeFronzo, R. A. *et al.* Type 2 diabetes mellitus. *Nat. Rev. Dis. Prim.* **1**, 15019 (2015).

8.   Xue, A. *et al.* Genome-wide association analyses identify 143 risk variants and putative regulatory mechanisms for type 2 diabetes. *Nat. Commun.* **9**, 2941 (2018).

9.   Cai, L. *et al.* Genome-wide association analysis of type 2 diabetes in the EPIC-InterAct study. *Sci. Data* **7**, 393 (2020).

10.   Hu, F. B. Globalization of diabetes: the role of diet, lifestyle, and genes. *Diabetes Care* **34**, 1249–1257 (2011).

11.   Chan, J. C. N. *et al.* Diabetes in asia: epidemiology, risk factors, and pathophysiology. *JAMA* **301**, 2129 (2009).

12.   Wang, Y. C., McPherson, K., Marsh, T., Gortmaker, S. L. & Brown, M. Health and economic burden of the projected obesity trends in the USA and the UK. *Lancet* **378**, 815–825 (2011).

13.   Colditz, G. A. Weight gain as a risk factor for clinical diabetes mellitus in women. *Ann. Intern. Med.* **122**, 481 (1995).

14.   Chan, J. M., Rimm, E. B., Colditz, G. A., Stampfer, M. J. & Willett, W. C. Obesity, fat distribution, and weight gain as risk factors for clinical diabetes in men. *Diabetes Care* **17**, 961–969 (1994).

15.   Smith-Spangler, C. M., Bhattacharya, J. & Goldhaber-Fiebert, J. D. Diabetes, its treatment,

and catastrophic medical spending in 35 developing countries. *Diabetes Care* **35**, 319–326 (2012).

16. Lee, D. S. U. & Lee, H. Adherence and persistence rates of major antidiabetic medications: a review. *Diabetol. Metab. Syndr.* **14**, 12 (2022).

17. Bailey, C. J. Metformin: historical overview. *Diabetologia* **60**, 1566–1576 (2017).

18. Rena, G., Hardie, D. G. & Pearson, E. R. The mechanisms of action of metformin. *Diabetologia* **60**, 1577–1585 (2017).

19. Pernicova, I. & Korbonits, M. Metformin—mode of action and clinical implications for diabetes and cancer. *Nat. Rev. Endocrinol.* **10**, 143–156 (2014).

20. Nanjan, M. J., Mohammed, M., Prashantha Kumar, B. R. & Chandrasekar, M. J. N. Thiazolidinediones as antidiabetic agents: a critical review. *Bioorg. Chem.* **77**, 548–567 (2018).

21. Eldor, R., DeFronzo, R. A. & Abdul-Ghani, M. In vivo actions of peroxisome proliferator–activated receptors. *Diabetes Care* **36**, S162–S174 (2013).

22. Gastaldelli, A. *et al.* Thiazolidinediones improve β-cell function in type 2 diabetic patients. *Am. J. Physiol. Metab.* **292**, E871–E883 (2007).

23. DeFronzo, R. A. *et al.* Characterization of renal glucose reabsorption in response to dapagliflozin in healthy subjects and subjects with type 2 diabetes. *Diabetes Care* **36**, 3169–3176 (2013).

24. Kramer, C. K. & Zinman, B. Sodium–glucose cotransporter–2 (SGLT-2) inhibitors and the treatment of type 2 diabetes. *Annu. Rev. Med.* **70**, 323–334 (2019).

25. Scheen, A. J. Sodium–glucose cotransporter type 2 inhibitors for the treatment of type 2 diabetes mellitus. *Nat. Rev. Endocrinol.* **16**, 556–577 (2020).

26. Sano, R., Shinozaki, Y. & Ohta, T. Sodium–glucose cotransporters: functional properties and pharmaceutical potential. *J. Diabetes Investig.* **11**, 770–782 (2020).

27. Aroda, V. R. *et al.* Efficacy of GLP-1 receptor agonists and DPP-4 Inhibitors: meta-analysis

and systematic review. *Clin. Ther.* **34**, 1247-1258.e22 (2012).

28. Trujillo, J. M., Nuffer, W. & Smith, B. A. GLP-1 receptor agonists: an updated review of head-to-head clinical studies. *Ther. Adv. Endocrinol. Metab.* **12**, 204201882199732 (2021).

29. Brown, E., Heerspink, H. J. L., Cuthbertson, D. J. & Wilding, J. P. H. SGLT2 inhibitors and GLP-1 receptor agonists: established and emerging indications. *Lancet* **398**, 262–276 (2021).

30. Dirir, A. M., Daou, M., Yousef, A. F. & Yousef, L. F. A review of alpha-glucosidase inhibitors from plants as potential candidates for the treatment of type-2 diabetes. *Phytochem. Rev.* (2021). doi:10.1007/s11101-021-09773-1

31. Chiasson, J.-L. *et al.* Acarbose for prevention of type 2 diabetes mellitus: the STOP-NIDDM randomised trial. *Lancet* **359**, 2072–2077 (2002).

32. Shyr, Z. A., Wang, Z., York, N. W., Nichols, C. G. & Remedi, M. S. The role of membrane excitability in pancreatic β-cell glucotoxicity. *Sci. Rep.* **9**, 6952 (2019).

33. Hinke, S. A. Epac2: a molecular target for sulfonylurea-induced insulin release. *Sci. Signal.* **2**, (2009).

34. Gough, S. C. L. *et al.* Efficacy and safety of a fixed-ratio combination of insulin degludec and liraglutide (IDegLira) compared with its components given alone: results of a phase 3, open-label, randomised, 26-week, treat-to-target trial in insulin-naive patients with type 2 di. *Lancet Diabetes Endocrinol.* **2**, 885–893 (2014).

35. Wilding, J. P. H. Long-term efficacy of dapagliflozin in patients with type 2 diabetes mellitus receiving high doses of insulin. *Ann. Intern. Med.* **156**, 405 (2012).

36. Holman, R. R. *et al.* Three-year efficacy of complex insulin regimens in type 2 diabetes. *N. Engl. J. Med.* **361**, 1736–1747 (2009).

37. DeFronzo, R. A. From the triumvirate to the ominous octet: a new paradigm for the treatment of type 2 diabetes mellitus. *Diabetes* **58**, 773–795 (2009).

38. Martin, B. C. *et al.* Role of glucose and insulin resistance in development of type 2 diabetes

mellitus: results of a 25-year follow-up study. *Lancet* **340**, 925–929 (1992).

39. De Jesus, D. F. & Kulkarni, R. N. Epigenetic modifiers of islet function and mass. *Trends Endocrinol. Metab.* **25**, 628–636 (2014).

40. Ferrannini, E. & Mari, A. β-Cell function in type 2 diabetes. *Metabolism* **63**, 1217–1227 (2014).

41. Kahn, S. E., Cooper, M. E. & Del Prato, S. Pathophysiology and treatment of type 2 diabetes: perspectives on the past, present, and future. *Lancet* **383**, 1068–1083 (2014).

42. DeFronzo, R. A. Insulin resistance, lipotoxicity, type 2 diabetes and atherosclerosis: the missing links. The Claude Bernard Lecture 2009. *Diabetologia* **53**, 1270–1287 (2010).

43. He, W. *et al.* Ageing potentiates diet-induced glucose intolerance, β-cell failure and tissue inflammation through TLR4. *Sci. Rep.* **8**, 2767 (2018).

44. De Tata, V. Age-related impairment of pancreatic beta-cell function: pathophysiological and cellular mechanisms. *Front. Endocrinol. (Lausanne).* **5**, (2014).

45. Muller, D. C., Elahi, D., Tobin, J. D. & Andres, R. Insulin response during the oral glucose tolerance test: The role of age, sex, body fat and the pattern of fat distribution. *Aging Clin. Exp. Res.* **8**, 13–21 (1996).

46. the DIAbetes Genetics Replication And Meta-analysis (DIAGRAM) Consortium. Large-scale association analysis provides insights into the genetic architecture and pathophysiology of type 2 diabetes. *Nat. Genet.* **44**, 981–990 (2012).

47. Nauck, M. A., Vardarli, I., Deacon, C. F., Holst, J. J. & Meier, J. J. Secretion of glucagon-like peptide-1 (GLP-1) in type 2 diabetes: what is up, what is down? *Diabetologia* **54**, 10–18 (2011).

48. Madsbad, S. The role of glucagon-like peptide-1 impairment in obesity and potential therapeutic implications. *Diabetes, Obes. Metab.* **16**, 9–21 (2014).

49. Kanatsuka, A., Kou, S. & Makino, H. IAPP/amylin and β-cell failure: implication of the risk factors of type 2 diabetes. *Diabetol. Int.* **9**, 143–157 (2018).

50. Westermark, P., Andersson, A. & Westermark, G. T. Islet amyloid polypeptide, islet amyloid, and diabetes mellitus. *Physiol. Rev.* **91**, 795–826 (2011).

51. Pilkington, E. H. *et al.* Pancreatic β-cell membrane fluidity and toxicity induced by human islet amyloid polypeptide species. *Sci. Rep.* **6**, 21274 (2016).

52. Montemurro, C. *et al.* IAPP toxicity activates HIF1α/PFKFB3 signaling delaying β-cell loss at the expense of β-cell function. *Nat. Commun.* **10**, 2679 (2019).

53. Collins, S., Pi, J. & Yehuda-Shnaidman, E. Uncoupling and reactive oxygen species (ROS) – A double-edged sword for β-cell function? "Moderation in all things". *Best Pract. Res. Clin. Endocrinol. Metab.* **26**, 753–758 (2012).

54. Gerber, P. A. & Rutter, G. A. The role of oxidative stress and hypoxia in pancreatic beta-cell dysfunction in diabetes mellitus. *Antioxid. Redox Signal.* **26**, 501–518 (2017).

55. Newsholme, P., Keane, K. N., Carlessi, R. & Cruzat, V. Oxidative stress pathways in pancreatic β-cells and insulin-sensitive cells and tissues: importance to cell metabolism, function, and dysfunction. *Am. J. Physiol. Physiol.* **317**, C420–C433 (2019).

56. Nordmann, T. M. *et al.* The role of inflammation in β-cell dedifferentiation. *Sci. Rep.* **7**, 6285 (2017).

57. Khodabandehloo, H., Gorgani-Firuzjaee, S., Panahi, G. & Meshkani, R. Molecular and cellular mechanisms linking inflammation to insulin resistance and β-cell dysfunction. *Transl. Res.* **167**, 228–256 (2016).

58. Eguchi, K. & Nagai, R. Islet inflammation in type 2 diabetes and physiology. *J. Clin. Invest.* **127**, 14–23 (2017).

59. Donath, M. Y., Böni-Schnetzler, M., Ellingsgaard, H. & Ehses, J. A. Islet inflammation impairs the pancreatic β-cell in type 2 diabetes. *Physiology* **24**, 325–331 (2009).

60. Lee, S. H. *et al.* High-throughput screening and bioinformatic analysis to ascertain compounds that prevent saturated fatty acid-induced β-cell apoptosis. *Biochem. Pharmacol.* **138**, 140–149 (2017).

61. Ciregia, F. *et al.* Palmitate-induced lipotoxicity alters acetylation of multiple proteins in clonal β cells and human pancreatic islets. *Sci. Rep.* **7**, 13445 (2017).

62. Stone, V. M. *et al.* The cytoprotective effects of oleoylethanolamide in insulin-secreting cells do not require activation of GPR119. *Br. J. Pharmacol.* **165**, 2758–2770 (2012).

63. Xiong, X. *et al.* SIRT6 protects against palmitate-induced pancreatic β-cell dysfunction and apoptosis. *J. Endocrinol.* **231**, 159–165 (2016).

64. Bensellam, M., Laybutt, D. R. & Jonas, J.-C. The molecular mechanisms of pancreatic β-cell glucotoxicity: recent findings and future research directions. *Mol. Cell. Endocrinol.* **364**, 1–27 (2012).

65. Prentki, M. & Corkey, B. E. Are the β-cell signaling molecules malonyl-CoA and cystolic long-chain acyl-CoA implicated in multiple tissue defects of obesity and NIDDM? *Diabetes* **45**, 273–283 (1996).

66. Poitout, V. *et al.* Glucolipotoxicity of the pancreatic beta cell. *Biochim. Biophys. Acta - Mol. Cell Biol. Lipids* **1801**, 289–298 (2010).

67. Kim, J.-W. & Yoon, K.-H. Glucolipotoxicity in pancreatic β-cells. *Diabetes Metab. J.* **35**, 444 (2011).

68. Rojas, J. *et al.* Pancreatic beta cell death: novel potential mechanisms in diabetes therapy. *J. Diabetes Res.* **2018**, 1–19 (2018).

69. Poitout, V. & Robertson, R. P. Glucolipotoxicity: fuel excess and β-Cell dysfunction. *Endocr. Rev.* **29**, 351–366 (2008).

70. Leung, M. B. W., Choy, K. W., Copp, A. J., Pang, C. P. & Shum, A. S. W. Hyperglycaemia potentiates the teratogenicity of retinoic acid in diabetic pregnancy in mice. *Diabetologia* **47**, 515–522 (2004).

71. Hagman, D. K., Hays, L. B., Parazzoli, S. D. & Poitout, V. Palmitate inhibits insulin gene expression by altering Pdx-1 nuclear localization and reducing MafA expression in isolated rat islets of langerhans. *J. Biol. Chem.* **280**, 32413–32418 (2005).

72. Boden, G. Obesity and free fatty acids. *Endocrinol. Metab. Clin. North Am.* **37**, 635–646 (2008).

73. Ardestani, A. *et al.* MST1 is a key regulator of beta cell apoptosis and dysfunction in diabetes. *Nat. Med.* **20**, 385–397 (2014).

74. Ardestani, A. *et al.* Neratinib protects pancreatic beta cells in diabetes. *Nat. Commun.* **10**, 1–17 (2019).

75. Ardestani, A. *et al.* Neutralizing interleukin-1β (IL-1β) induces β-cell survival by maintaining PDX1 protein nuclear localization. *J. Biol. Chem.* **286**, 17144–17155 (2011).

76. Larsen, C. M. *et al.* Interleukin-1–receptor antagonist in type 2 diabetes mellitus. *N. Engl. J. Med.* **356**, 1517–1526 (2007).

77. Donath, M. Y., Böni-Schnetzler, M., Ellingsgaard, H., Halban, P. A. & Ehses, J. A. Cytokine production by islets in health and diabetes: cellular origin, regulation and function. *Trends Endocrinol. Metab.* **21**, 261–267 (2010).

78. Maedler, K., Dharmadhikari, G., Schumann, D. M. & Størling, J. Interleukin-1 beta targeted therapy for type 2 diabetes. *Expert Opin. Biol. Ther.* **9**, 1177–1188 (2009).

79. Costes, S. *et al.* β-Cell dysfunctional ERAD/ubiquitin/proteasome system in type 2 diabetes mediated by islet amyloid polypeptide–induced UCH-L1 deficiency. *Diabetes* **60**, 227–238 (2011).

80. Sharma, R. B. & Alonso, L. C. Lipotoxicity in the pancreatic beta cell: not just survival and function, but proliferation as well? *Curr. Diab. Rep.* **14**, 492 (2014).

81. Mohammed, A. M., Syeda, K., Hadden, T. & Kowluru, A. Upregulation of phagocyte-like NADPH oxidase by cytokines in pancreatic beta-cells: Attenuation of oxidative and nitrosative stress by 2-bromopalmitate. *Biochem. Pharmacol.* **85**, 109–114 (2013).

82. Graciano, M. F., Valle, M., Kowluru, A., Curi, R. & Carpinelli, A. Regulation of insulin secretion and reactive oxygen species production by free fatty acids in pancreatic islets. *Islets* **3**, 213–223 (2011).

83. Tsonkova, V. G. *et al.* The EndoC-βH1 cell line is a valid model of human beta cells and applicable for screenings to identify novel drug target candidates. *Mol. Metab.* **8**, 144–157 (2018).

84. Fang, J.-Y., Lin, C.-H., Huang, T.-H. & Chuang, S.-Y. In vivo rodent models of Type 2 diabetes and their usefulness for evaluating flavonoid bioactivity. *Nutrients* **11**, 530 (2019).

85. Skelin, M., Rupnik, M. & Cenič, A. Pancreatic beta cell lines and their applications in diabetes mellitus research. *ALTEX* 105–113 (2010). doi:10.14573/altex.2010.2.105

86. Radvanyi, F., Christgau, S., Baekkeskov, S., Jolicoeur, C. & Hanahan, D. Pancreatic beta cells cultured from individual preneoplastic foci in a multistage tumorigenesis pathway: a potentially general technique for isolating physiologically representative cell lines. *Mol. Cell. Biol.* **13**, 4223–4232 (1993).

87. Ravassard, P. *et al.* A genetically engineered human pancreatic β cell line exhibiting glucose-inducible insulin secretion. *J. Clin. Invest.* **121**, 3589–3597 (2011).

88. Ishihara, H. *et al.* Pancreatic beta cell line MIN6 exhibits characteristics of glucose metabolism and glucose-stimulated insulin secretion similar to those of normal islets. *Diabetologia* **36**, 1139–1145 (1993).

89. Asfari, M. *et al.* Establishment of 2-mercaptoethanol-dependent differentiated insulin-secreting cell lines. *Endocrinology* **130**, 167–178 (1992).

90. Carrington, C. A., Rubery, E. D., Pearson, E. C. & Hales, C. N. Five new insulin-producing cell lines with differing secretory properties. *J. Endocrinol.* **109**, 193-NP (1986).

91. Efrat, S. *et al.* Beta-cell lines derived from transgenic mice expressing a hybrid insulin gene-oncogene. *Proc. Natl. Acad. Sci.* **85**, 9037–9041 (1988).

92. Liang, Y. *et al.* Glucose metabolism and insulin release in mouse beta HC9 cells, as model for wild-type pancreatic beta-cells. *Am. J. Physiol. Metab.* **270**, E846–E857 (1996).

93. Miyazaki, J.-I. *et al.* Establishment of a pancreatic beta cell line that retains glucose-inducible insulin secretion: special reference to expression of glucose transporter isoforms.

Endocrinology **127**, 126–132 (1990).

94.   McClenaghan, N. H. *et al.* Characterization of a novel glucose-responsive insulin-secreting cell line, BRIN-BD11, produced by electrofusion. *Diabetes* **45**, 1132–1140 (1996).

95.   Merglen, A. *et al.* Glucose sensitivity and metabolism-secretion coupling studied during two-year continuous culture in INS-1E insulinoma cells. *Endocrinology* **145**, 667–678 (2004).

96.   Halban, P. A., Praz, G. A. & Wollheim, C. B. Abnormal glucose metabolism accompanies failure of glucose to stimulate insulin release from a rat pancreatic cell line (RINm5F). *Biochem. J.* **212**, 439–443 (1983).

97.   Gazdar, A. F. *et al.* Continuous, clonal, insulin- and somatostatin-secreting cell lines established from a transplantable rat islet cell tumor. *Proc. Natl. Acad. Sci.* **77**, 3519–3523 (1980).

98.   Praz, G. A. *et al.* Regulation of immunoreactive-insulin release from a rat cell line (RINm5F). *Biochem. J.* **210**, 345–352 (1983).

99.   Carter, J. D., Dula, S. B., Corbin, K. L., Wu, R. & Nunemaker, C. S. A practical guide to rodent islet isolation and assessment. *Biol. Proced. Online* **11**, 3 (2009).

100. Corbin, K. L. *et al.* A practical guide to rodent islet isolation and sssessment revisited. *Biol. Proced. Online* **23**, 7 (2021).

101. Kayton, N. S. *et al.* Human islet preparations distributed for research exhibit a variety of insulin-secretory profiles. *Am. J. Physiol. Metab.* **308**, E592–E602 (2015).

102. Wagner, B. K. & Schreiber, S. L. The power of sophisticated phenotypic screening and modern mechanism-of-action methods. *Cell Chem. Biol.* **23**, 3–9 (2016).

103. Watt, P. M. *et al.* Chapter 17. Phylomer libraries: a rich source of peptide hits in phenotypic and target-directed screens. in *Drug Discovery* 497–517 (Royal Society of Chemistry, 2017). doi:10.1039/9781788011532-00497

104. Mohr, S., Bakal, C. & Perrimon, N. Genomic screening with RNAi: results and challenges.

Annu. Rev. Biochem. **79**, 37–64 (2010).

105. Bock, C. *et al.* High-content CRISPR screening. *Nat. Rev. Methods Prim.* **2**, 8 (2022).

106. Swinney, D. C. Chapter 1. Phenotypic Drug Discovery: History, Evolution, Future. in *Drug Discovery* 1–19 (Royal Society of Chemistry, 2020). doi:10.1039/9781839160721-00001

107. Baell, J. B. & Holloway, G. A. New substructure filters for removal of pan assay interference compounds (PAINS) from screening libraries and for their exclusion in bioassays. *J. Med. Chem.* **53**, 2719–2740 (2010).

108. Dahlin, J. L. *et al.* Nuisance compounds in cellular assays. *Cell Chem. Biol.* **28**, 356–370 (2021).

109. Goodwin, R. J. A., Bunch, J. & McGinnity, D. F. Mass spectrometry imaging in oncology drug discovery. *Adv* 133–171 (2017). doi:10.1016/bs.acr.2016.11.005

110. Lipinski, C. A., Lombardo, F., Dominy, B. W. & Feeney, P. J. Experimental and computational approaches to estimate solubility and permeability in drug discovery and development settings. *Adv. Drug Deliv. Rev.* **46**, 3–26 (2001).

111. Gerry, C. J. *et al.* Real-time biological annotation of synthetic compounds. *J. Am. Chem. Soc.* **138**, 8920–8927 (2016).

112. Bray, M.-A. *et al.* Cell Painting, a high-content image-based assay for morphological profiling using multiplexed fluorescent dyes. *Nat. Protoc.* **11**, 1757–1774 (2016).

113. Galloway, W. R. J. D., Isidro-Llobet, A. & Spring, D. R. Diversity-oriented synthesis as a tool for the discovery of novel biologically active small molecules. *Nat. Commun.* **1**, 80 (2010).

114. Corsello, S. M. *et al.* The Drug Repurposing Hub: a next-generation drug library and information resource. *Nat. Med.* **23**, 405–408 (2017).

Chapter 2

Generating a Cell-Based Toolkit to Study Glucolipotoxicity in β-Cells

2.1 Abstract

This chapter details the optimization of a high-throughput glucolipotoxicity (GLT) assay in INS-1E cells and human islets, with the aim of generating optimal Z'-scores for high-throughput phenotypic screening. Also described are secondary assays used to validate GLT primary screen hits. These include detection of INS-1E viability using CellTiter-Glo and detection of apoptosis using Caspase Glo; development of a high-content fluorescent microscopy (HCFM) method to quantify INS-1E cell number and percent viability; and quantification of percent C-peptide positive cells in dissociated human islets treated with GLT media. Three assays are also described that were developed to further probe the effects of validated screen hits on GLT-treated INS-1E heath. The first is a flow cytometry method for detecting mitochondrial depolarization in GLT-treated INS-1E, the second is a fluorescent method for detecting calcium influx in GLT-treated INS-1E, and the third is quantification of *Pdx1* expression in INS-1E cells using qPCR.

2.2 Optimizing Glucolipotoxicity-Assay for High-Throughput Screening

To model the gradual loss of β-cell mass in obese type 2 diabetic patients exposed to chronic hyperglycemia and hyperlipidemia, I sought to design a high glucose, high palmitate media formulation for the INS-1E rat insulinoma cell line. This media formulation when chronically applied to INS-1E cells should result in significant amounts of cell death which could be detected using a viability measuring reagent. INS-1E was selected as the cell line of choice due to its easy culturing method, moderately fast growth rate (~36 hour doubling time), and literature evidence that it was susceptible to high glucose, high palmitate-induced cell death, unlike MIN6 cells.[1] Preliminary experiments I carried out using MIN6 showed there was no glucose-dependent decrease in viability in the presence of excess FFA (Figure 2.2.1).
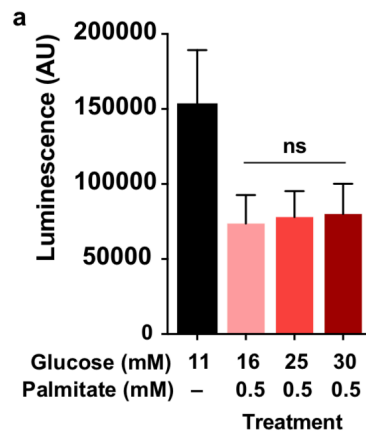
Figure 2.2.1. MIN6 cells do not exhibit glucolipotoxicity. a) MIN6 treated with increasing concentrations of glucose in a constant background of 0.5mM palmitate. Increasing glucose concentration does not decrease MIN6 viability, indicating the absence of the glucolipotoxic response. Cell viability determined using CellTiter-Glo. Statistical significance was evaluated using an unpaired, one-tailed t-test. Ns: not significant. (*, P < 0.0001).

For high-throughput screening, I chose a 384-well plate format and CellTiter-Glo as the viability detection reagent. CellTiter-Glo (Promega) is a cell lysing reagent which becomes luminescent upon ATP-dependent cleavage of luciferin and is widely used in the literature to assess cell viability.[2–4] Consistent with common practice in the field, I aimed to design an assay which

generated a Z'-factor greater than 0.5 for individual 384-well plates. The Z'-factor equation is illustrated below:

$$Z'\text{-factor} = 1 - \frac{3\sigma_{c+} + 3\sigma_{c-}}{\mu_{c+} - \mu_{c-}}$$

Sigma (σ) signifies standard deviation and Mu (μ) signifies average. Subscripts c+ and c- refer to the positive and negative control conditions respectively. As such, the Z'-factor is a ratio of the sum of three standard deviations of the positive and negative controls and the difference of the averages of the positive and negative controls subtracted from one. In more relevant terms, this equation indicates how well separated the positive and negative control populations are from each other. Z'-factors less than 0.5 indicate there is significant overlap of the positive and negative control populations. Z'-factors greater than 0.5 indicate there is limited to no overlap of the positive and negative control populations. For high-throughput screening purposes, limited to no overlap of the positive and negative control populations decreases the prevalence of false positives and negatives, and increases the ability to differentiate hit compounds from the negative control (Fig. 2.2.2).
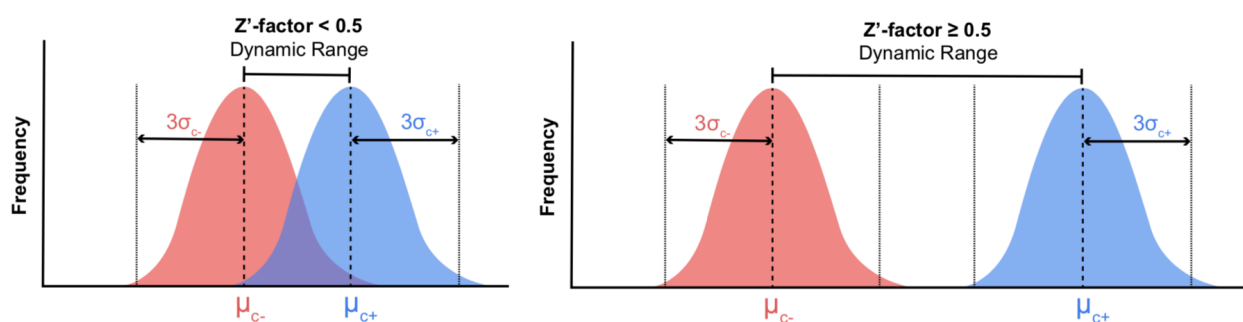
Figure 2.2.2. Visual representation of Z'-factor. Z'-factors greater than 0.5 indicate increased assay dynamic range. σ_{c-}: standard deviation of negative control. σ_{c+}: standard deviation of positive control. μ_{c-}: average of negative control. μ_{c+}: average of positive control.

To select the appropriate glucolipotoxicity (GLT) media formulation, I referred to the literature, where several formulations for INS-1E and other β-cell lines were described.[5–7] Chronic GLT

exposure was frequently modeled by treatments periods greater than or equal to 24 hours and palmitate was consistently used as the lipid source. Additionally, basal INS-1E media contains RPM1 1640 with 11mM glucose. Therefore, GLT media with elevated glucose would require concentrations in excess of 11mM. With these criteria in mind, I developed an INS-1E GLT media formulation beginning with 48-hour incubation. INS-1E cells were plated 5,000 cells/well in 384-well plate format to achieve ~60% confluency at 24 hour and ~90% confluency at 48hrs. Optimization revealed that while elevated glucose alone (16-30mM) did not significantly contribute to INS-1E cell death, elevated palmitate (0.25-0.5mM) significantly decreased viability (Fig. 2.2.3a-b). Glucose dependent decrease in viability was observed only in the presence of 0.5mM palmitate, whereby a glucose concentration of 30mM induced the greatest decrease in INS-1E viability (Fig. 2.2.3c).
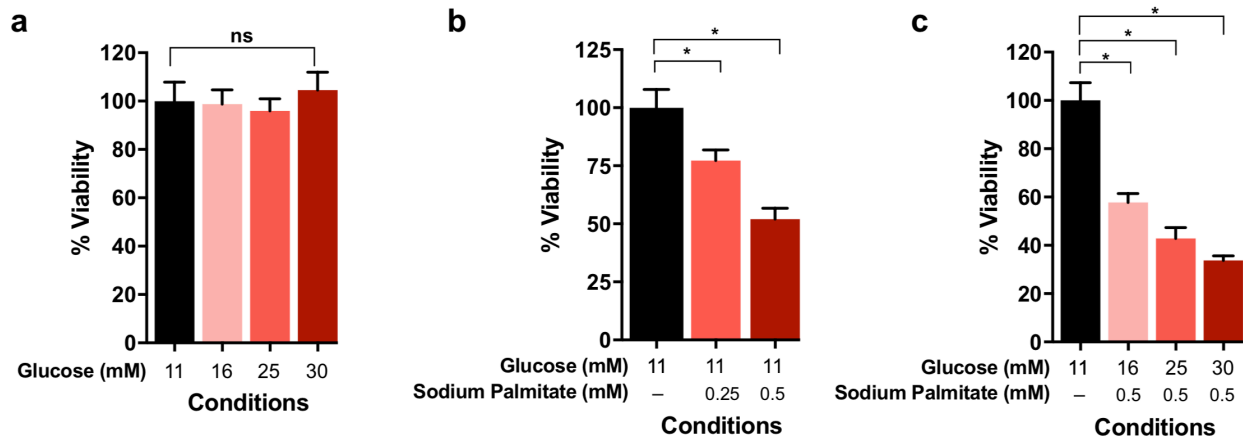
Figure 2.2.3. Optimization of INS-1E GLT media conditions. INS-1E cells were plated in 384-well plate format (5,000 cells/well) and treated with varying GLT media formulations for 48 hours. Percent viability detected using CellTiter-Glo. a) INS-1E viability is unaffected by increasing levels of glucose alone. b) INS-1E viability is decreased with elevated levels of palmitate at basal glucose concentration. c) INS-1E viability decreased with elevated levels of glucose in the presence of 0.5mM palmitate. Statistical significance was evaluated using an unpaired, one-tailed t-test (*, $P < 0.0001$).

The final optimization step was to determine whether incubation time affected the performance of the GLT media formulation. I chose GLT media comprised of 25mM glucose and 0.5mM palmitate as this decreased viability ~50%. I reasoned, decreases in viability greater than 50% would

present a potentially insurmountable challenge to compounds facing an overwhelming cascade of cell death. The results indicated that 48-hour GLT incubation produced the highest Z'-factor in 384-well plate format (Fig. 2.2.4a). Thus, the final high-throughput screening conditions were identified: 48 hour incubation of INS-1E cells with 0.5mM sodium palmitate and 25mM glucose. INS-1E cells were plated 5,000 cells/well, left to rest for 24 hours in basal media before basal media was removed and GLT media added (Fig. 2.2.4b).
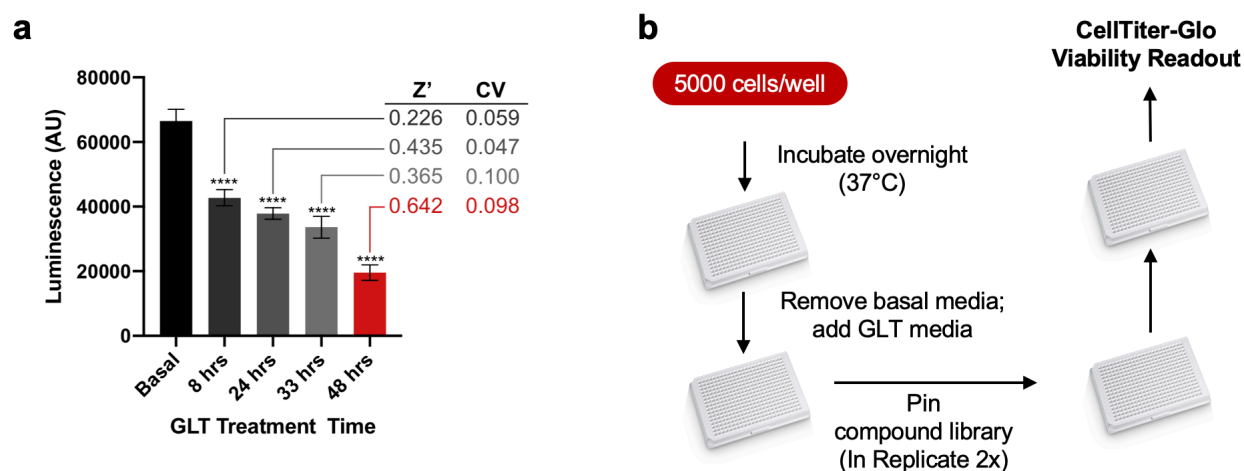
Figure 2.2.4. Effect of GLT incubation time on Z'-factor. a) INS-1E incubated with 0.5mM sodium palmitate and 25mM glucose in 384-well plate format for 48-hours produced the greatest Z'-factor value. Z': Z'-factor. CV: Co-efficient-of-variance. b) Schematic outline of GLT screen in INS-1E. Statistical significance was evaluated using an unpaired, one-tailed t-test (****, $P < 0.0001$).

2.3 Methods for Assaying Cell Viability in Glucolipotoxic Conditions

CellTiter-Glo

CellTiter-Glo (CTG) was used to assess cell viability in the primary and secondary screens. The CTG reagent (Promega) comprises of cell lysing detergent, a proprietary luciferase enzyme, and luciferin, the enzyme substrate. The luciferase enzyme consumes ATP to decarboxylate luciferin and generate the reaction product, oxyluciferin, a luminescent compound. The luminescence of oxyluciferin can be quantified using a plate reader. Because CTG lyses cells, it cannot be used as a beginning or intermediate step in multiplexed assays. One limitation of the CTG reagent is

the direct correlation of cellular ATP levels and luminescent signal. If cellular ATP levels change without an actual increase in cell number, CTG will detect the increase in ATP concentration and produce increased luminescence not corresponding to increase in cell viability. It is for this reason the high-content fluorescent microscopy assay (HCFM) was developed and is further described in section 2.3c.

Caspase Glo

Caspase Glo (Promega) was used to assess caspase-3/7 activation in the secondary screen. Caspase-3 and caspase-7 are members of the caspase family of cysteine proteases. The caspase family is activated in response to various cell death stimuli and help execute a programmed cell death known as apoptosis.[8] Caspase-3 and caspase-7 are the effector caspases responsible for the apoptotic cleavage of cellular proteins. Though not functionally redundant, caspase-3 and caspase-7 both cleave the synthetic DEVD-aminoluciferin substrate of the Caspase Glo reagent. Therefore, when GLT-induced apoptosis is activated in INS-1E cells, activated caspase-3/7 cleave the DEVD-aminoluciferin substrate to generate a luciferin derivate that can be cleaved by a proprietary luciferase to generate a luminescent signal. This luminescent signal can be detected using a plate reader. Once hit compounds were identified from the primary screen, we retested these compounds in 4-point dose, quantifying both viability and caspase activation with CTG and Caspase Glo respectively. Caspase Glo provided complementary data on the performance of hit compounds by indicating whether observed increases in CTG luminescence corresponded to decreases in caspase-3/7 activity, and therefore decrease in apoptosis induction. Figure 2.3.1 shows that all previously tested GLT media formulations increased caspase activation in INS-1E.
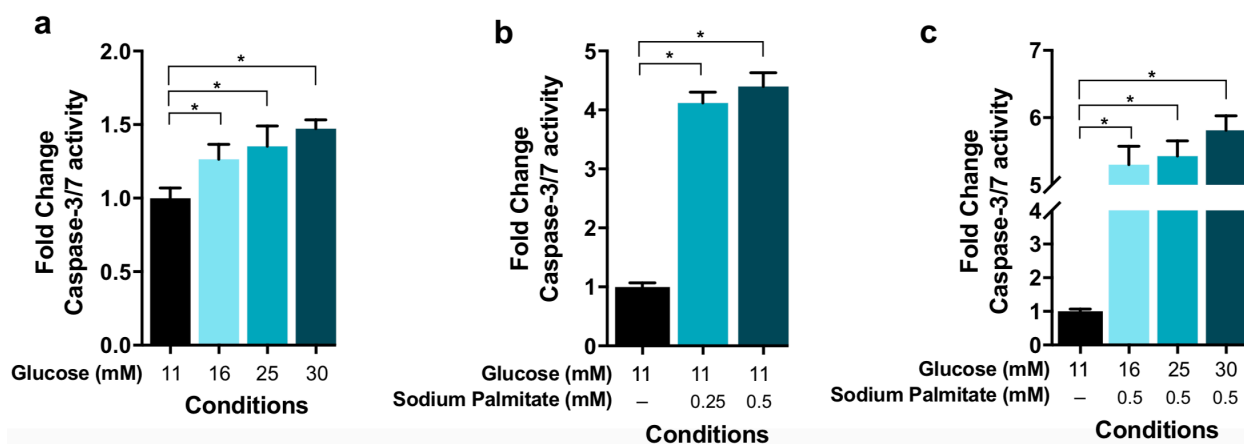
Figure 2.3.1: Optimizing Caspase Glo Assay. INS-1E cells were plated in 384-well plate format (5,000 cells/well) and treated with varying GLT media formulations for 48 hours. Percent viability detected using Caspase Glo. a) Increasing glucose concentration increases caspase activation. b) Caspase activation increased with elevated levels of palmitate at basal glucose concentration. c) Caspase activation increased in the presence of 0.5mM palmitate and elevated glucose levels. Statistical significance was evaluated using an unpaired, one-tailed t-test (*, $P < 0.0001$).

High-Content Fluorescence Microscopy

The high-content fluorescent microscopy (HCFM) assay was developed to quantify cell viability and caspase activation more accurately in INS-1E. When secondary screen hit compound apitolisib showed potent anti-GLT activity using CellTiter-Glo and Caspase Glo, I further attempted to quantify how much viability was improved by the compound using nuclear staining. Using nuclear stain Hoechst 33342, I discovered, that although apitolisib appeared to increase INS-1E viability in GLT conditions using CellTiter-Glo, the increase in luminescence did not correspond to an increase in cell number (Fig. 2.3.2). In fact, apitolisib did not increase cell numbers to levels suggested by the CellTiter-Glo reagent. I therefore concluded that apitolisib was altering ATP concentration in INS-1E cells instead of protecting against GLT. It is interesting to note, that the decrease in caspase activation detected using Caspase Glo was also detected using the HCFM assay, suggesting that apitolisib may be able to mitigate some aspects of caspase-3/7 activation (Fig. 2.3.2b & c).
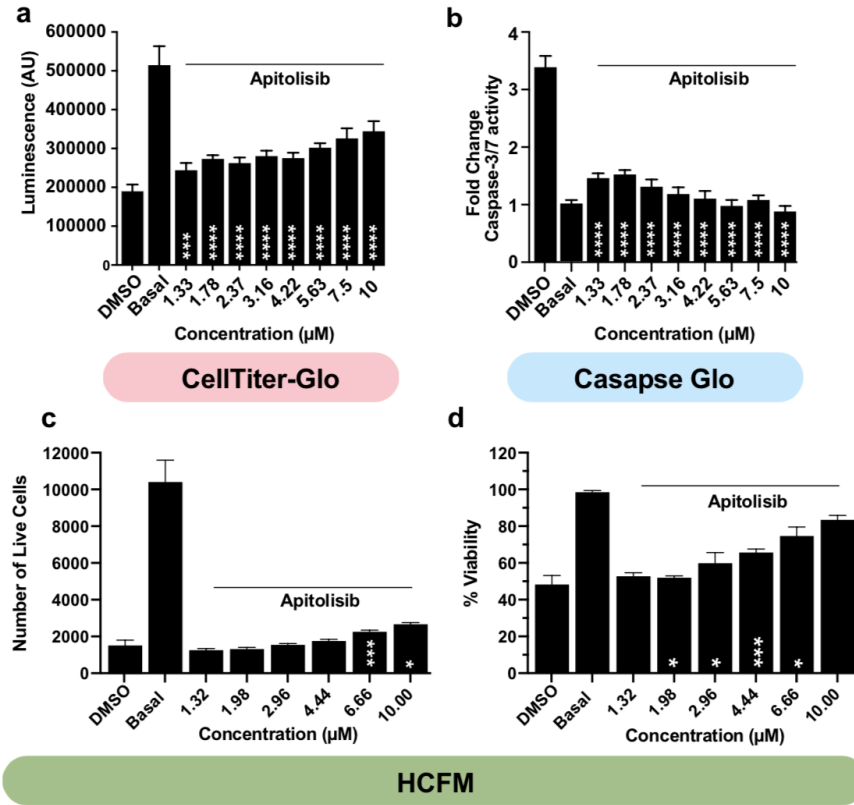
Figure 2.3.2: Comparing the HCFM and CellTiter-Glo/Caspase Glo Viability Assays. a) INS-1E viability detected CellTiter-Glo. b) Caspase-3/7 activation in INS-1E detected using Caspase Glo. c) Quantification of live cell number in INS-1E treated with apitolsib in GLT conditions using HCFM assay nuclear staining. d) Quantification of percent viability using HCFM assay. Statistical significance was evaluated using an unpaired, one-tailed t-test for each compound compared to DMSO. (*, $P < 0.05$; ***, $P < 0.001$; ****, $P < 0.0001$).

The HCFM assay comprises of three fluorescent dyes: 1) nuclear stain Hoechst 33342, 2) live cell impermeable DRAQ7, and 3) caspase-3/7 activated CellEvent™ Caspase-3/7 (Fig. 2.3.3). In conjunction, these three dyes can be used to quantify cell number and cell viability. Hoechst 33342 is a well-known nuclear stain used to identify cells in fluorescent microscopy.[9,10] DRAQ7 is a recently developed live cell impermeable nuclear stain used to quantify dead cells.[11–13] The compromised cell membranes of dead cells allows DRAQ7 to bind to nuclear DNA. CellEvent™ Caspase-3/7, like Caspase Glo is cleaved by caspase-3/7 to produce a fluorescent compound which can be used to quantify caspase activation in cells.[14,15] Analysis of the images collected using the HCFM assay is simplified by the absence of emission spectra overlap between the three

fluorescent dyes. Hoechst 33342 has a maximum emission at 461nm. DRAQ7 has a maximum emission at 678-697nm. CellEvent™ Caspase-3/7 has a maximum emission at 530nm. Total cell number was quantified using Hoechst to count cell nuclei. Live cell number was quantified by selecting the population of cell nuclei negative for the DRAQ7 and Caspase-3/7 dyes. Percent viability was therefore calculated by dividing the total number of cells by the number of cells without DRAQ7 and Caspase-3/7 staining.
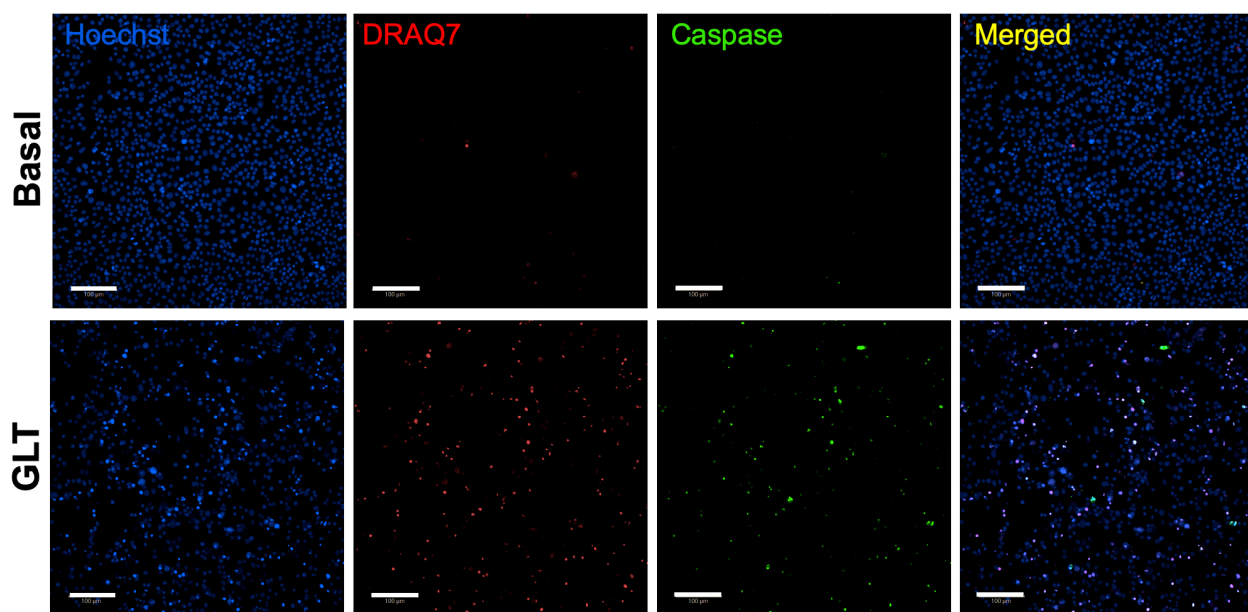
Figure 2.3.3. HCFM Assay Example Images. Images taken in 10x on Operetta Phenix. White bar indicates 100μm. Top row: INS-1E treated with basal media. Bottom row: INS-1E treated with GLT media for 48 hours. Harmony software is used to analyze images. Scale bar: 100μM.

Dissociated Human Islets

Screen hits validated using secondary assays were then tested in dissociated human islets to ascertain whether they retained their anti-GLT activity. This required the optimization of the GLT assay in dissociated human islets and a method for quantifying β-cell viability in the mixed endocrine and exocrine population of dissociated islets. Unfortunately, the HCFM assay using DRAQ7 and CellEvent™ Caspase-3/7 failed to work in dissociated human islets. These dyes did not remain in dissociated human islet samples after fixation, permeabilization, and C-peptide

staining. However, using C-peptide staining and Hoechst 33342, I was able to quantify β-cell

number in islet samples. I reasoned islet β-cell number should decrease with GLT treatment and

used C-peptide positive cells to quantify β-cell abundance in sample wells. C-peptide can be used

as an alternative insulin detection/quantification method. When preproinsulin, translated from

insulin mRNA, is cleaved into mature insulin it losses a signal peptide and its C-peptide domain.[16]

Therefore, there is a stoichiometric equivalence of C-peptide and mature insulin within β-cells and

C-peptide can be used as an alternate insulin detection marker.[17] Using C-peptide quantification,

I tested 25mM glucose and 0.5mM sodium palmitate in human islets for both 48-hour incubation

and 120-hour (5-day) incubation. 5-day incubation was tested to mimic a more chronic GLT

exposure as that experienced by obese type 2 diabetic patients. Prior experiments in our lab had

indicated a weeklong culture of dissociated islets would not affect sample viability. With 25mM

glucose and 0.5mM palmitate, I detected no significant decrease in C-peptide positive cells (Fig.

2.3.4a).
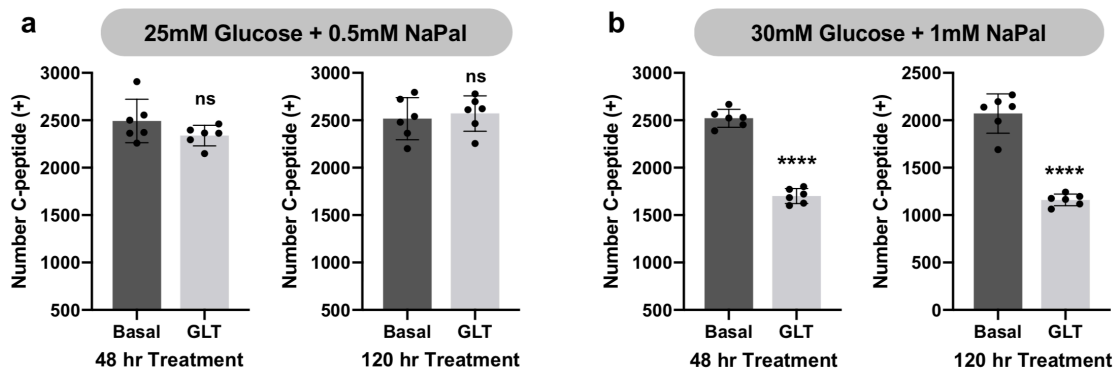
Figure 2.3.4. GLT Assay optimization in human islets. Dissociated human islets plated 5,000 cells/well. a) Human islets treated with 25mM glucose and 0.5mM sodium palmitate (NaPal) for 48 and 120 hours. b) Human islets treated with 30mM glucose and 1mM sodium palmitate for 48 and 120 hours. Statistical significance was evaluated using an unpaired, one-tailed t-test for each compound compared to DMSO. (****, $P < 0.0001$).

Therefore, I increased the concentration of glucose and sodium palmitate to 30mM and 1mM

respectively. I found that 30mM glucose and 1mM sodium palmitate significantly decreased C-

peptide number in dissociated human islets treated for 48 and 120 hours (Fig. 2.3.4b). Since 48-hour incubation performed as well as 120-hour incubation, this timepoint was used for future human islet GLT studies. Subsequent analysis of human islets treated with GLT utilized a normalized percent C-peptide quantification, where percent C-peptide positive cells was calculated for each sample and then normalized to basal control. Normalized percent C-peptide also decreased with 48-hour incubation (Fig. 2.3.5).
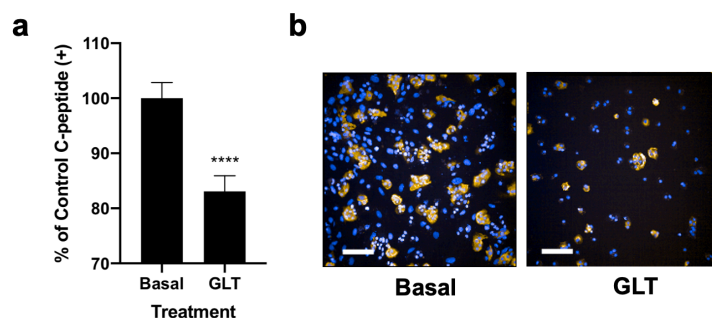
Figure 2.3.5. Normalized percent C-peptide in human islets. a) Human islets treated with 30mM glucose and 1mM sodium palmitate for 48 hours. b) Representative images of dissociated human islets stained for C-peptide. Scale bar: 100μM. Statistical significance was evaluated using an unpaired, one-tailed t-test for each compound compared to basal treatment. (****, $P < 0.0001$).

2.4 Methods for Assaying β-Cell Functionality in Glucolipotoxic Conditions

Detecting Mitochondrial Depolarization

Though viability was a sufficient means of identifying GLT-protective compounds, investigating how these compounds affected other markers of GLT was an attractive avenue for probing compound mechanism of action. Mitochondrial depolarization is a known marker of β-cell GLT and the JC-1 dye has frequently been used to detect and quantify this depolarization.[18,19] JC-1 accumulates in functional, polarized mitochondria and emits a 1:1 ratio of Red:Green fluorescence. When mitochondrial depolarization occurs, JC-1 leaks from mitochondrial and a decrease in red fluorescence occurs. Thus in depolarized mitochondria the Red:Green fluorescence will decrease. I first attempted to detect mitochondrial depolarization in INS-1E cells

using 15.3µM JC-1 and high-content confocal microscopy, however, I could observe no induction

of mitochondrial depolarization with two-hour valinomycin treatment. Valinomycin is a known

mitochondrial depolarizing agent.[20]   I therefore tried using flow cytometry to quantify the

Red:Green fluorescence of JC-1 in valinomycin treated INS-1E cells and observed a decreased

Red:Green ratio (Fig. 2.4.1). This Red:Green ratio decrease was not observed in basal treated

INS-1E (Fig. 2.4.1). Applying this flow cytometry to INS-1E treated with GLT for 48 hours, I

detected decreased Red:Green ratio. Therefore, this flow cytometry method was used to

interrogate HCFM-validated GLT-protective compounds.
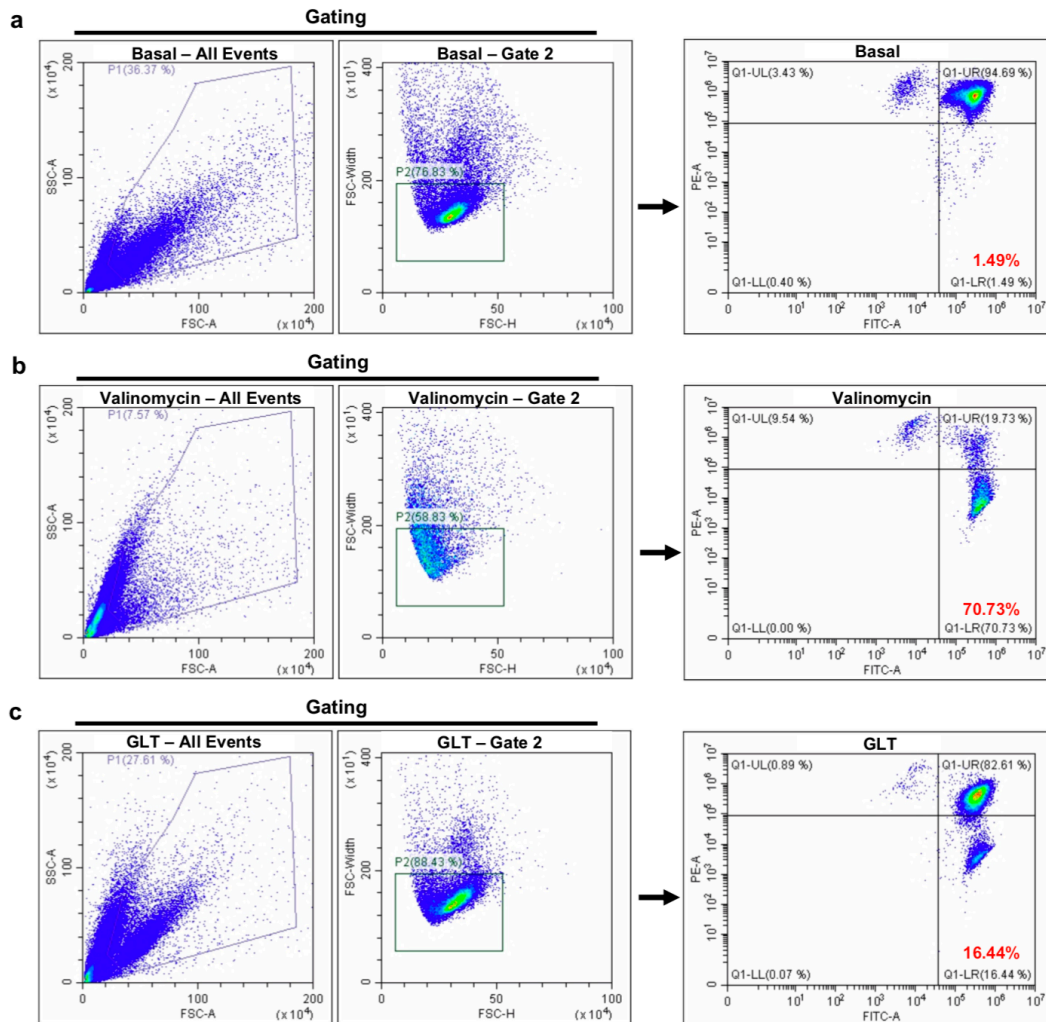
Figure 2.4.1

Figure 2.4.1 (Continued). Detecting mitochondrial depolarization detection via flowcytometry. a) – c) Gating used for basal, valinomycin, and GLT treated INS-1E cells. b) Valinomycin is used as a positive control to induce mitochondrial depolarization (decrease in JC-1 Red:Green ratio). c) GLT treatment induces mitochondrial depolarization in INS-1E (i.e. decrease in JC-1 Red:Green ratio). PE-A: red fluorescence. FITC-A: green fluorescence.

Detecting Calcium Flux

Increased calcium influx is a well-known marker of β-cell dysfunction, and more recently GLT-induced β-cell dysfunction.[7,21,22] I therefore sought to develop an assay to detect calcium influx in INS-1E cells treated with GLT. The calcium 6 dye is a proprietary compound developed by Molecular Devices which binds to intracellular calcium to generate a fluorescent signal.[23] The dye is most frequently used in the Fluorescent Imaging Plate Reader (FLIPR) to quantify calcium content in cells. The FLIPR instrument provides continual calcium flux data for samples over variable periods of time, however required multiple wash steps to image cells. Previous optimization efforts of the HCFM assay had shown that wash steps greatly reduced cell number remaining in GLT-treated samples. Therefore, I opted not to use the FLIPR instrument to image calcium 6, but the Operetta Phenix high-content microscope. Using the Phenix, I imaged INS-1E cells treated with GLT media for 48 hours incubated with calcium 6 for 1 hour. PerkinElmer Harmony software was then used to analyze green fluorescence of activated calcium 6 dye. Completed analysis revealed that 48-hour GLT exposure increased green fluorescence and therefore calcium content of INS-1E cells (Fig. 2.4.2).
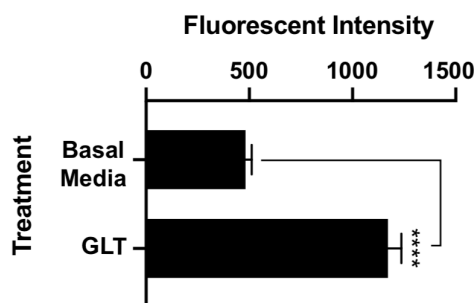
Figure 2.4.2. Detecting calcium flux in INS-1E. GLT treatment increases fluorescent intensity of GLT-treated INS-1E incubated with calcium 6 dye. Statistical significance was evaluated using an unpaired, one-tailed t-test for each compound compared to basal treatment. (****, $P < 0.0001$)

Glucose Stimulated Insulin Secretion

Detecting glucose stimulated insulin secretion (GSIS) remains the gold standard for assessing β-cell functionality in response to stress or drug treatment. While insulin secretion is usually detected by ELISA, the Wagner laboratory previously developed an INS-1E cell line co-secreting *Gaussia* luciferase with insulin.[24] Insulin is secreted at a 1:1 ratio with *Gaussia* luciferase in this cell line, allowing insulin secretion to be detected by quantifying luciferase activity using the coelenterazine substrate (NanoLight).[24] While efforts were made utilize this cell line to investigate the effect of GLT on insulin secretion, validated GLT-protective compounds like anandamide or neratinib did not perform as positive controls to restore diminished insulin secretion.[6,25] Believing this was an issue with lack of normalization across conditions, attempts were made to normalize luminescence to cell number. However, I found that GLT-treated INS-1E easily washed away from plate surfaces, preventing the quantification of cell number by microscopy and resulting in inconsistent glucose-stimulated luciferase secretion (GSLS) results. Thus, viability was the primary metric utilized to validate primary screen hits. To supplement the lack of a GSIS assay, I also investigated whether compounds recovered the expression of *Pdx1* in GLT-treated INS-1E cells. *Pdx1* is a β-cell specific transcription factor and its expression is known to decrease with GLT treatment.[26] I was able to confirm this decrease in GLT-treated INS-1E and utilized this to validate screen hits (Figure 2.4.3).
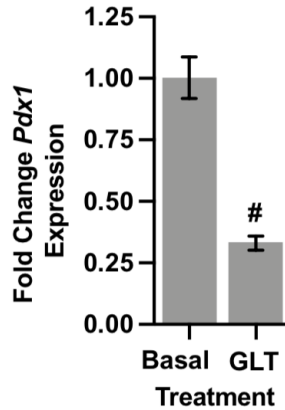
Figure 2.4.3. GLT decreases *Pdx1* expression in INS-1E. 32-hours GLT treatment. and AT-9283. Statistical significance was evaluated using an unpaired, one-tailed t-test for each compound compared to GLT alone. (#, P < 0.0001)

2.5 Methods

Cell culture. INS-1E cells (generously provided by Claes Wollheim and Pierre Maechler, University of Geneva, Switzerland) cultured in RPMI 1640 supplemented with 10% FBS, 1% Pen/Strep, 1% sodium pyruvate, and 50 µM β-mercaptoethanol. Cells were maintained in flasks precoated with diluted supernatant (1:10) from the rat 804G cell line (804G matrix). 804G cells are a rat cancer cell line known to secrete a laminin-5 rich extracellular matrix. 804G cells were a generous gift of Susan Bonner-Weir Lab, Joslin Diabetes Center. GLT media for INS-1E consisted of RPMI 1640 supplemented with 1% FBS, 1% Pen/Strep, 1% fatty acid free BSA, 50 µM β-mercaptoethanol, 25 mM glucose, and 0.5 mM sodium palmitate. Sodium palmitate was dissolved in warmed 4% BSA in PBS before being added to RPMI 1650.

High-throughput screening. INS-1E cells were plated at 5,000 cells/well in 384-well plates pretreated with supernatant from 804G cells. After 24 hours in regular media conditions, media was removed from and GLT media was added at 35 µL/well. Following 48-hour incubation in GLT media CellTiter-Glo (Promega) diluted 1:3 in PBS was added. Viability (luminescence) was quantified using an Envision plate reader (PerkinElmer). A 3-σ (z-score $\geq$ 3) cut off was used to

identify hit compounds from the primary screen. Caspase-3/7 activity was quantified using Caspase Glo (Promega). Briefly, Caspase Glo was added at 1:1 ratio to wells, plates incubated for one hour at room temperature, then luminescence quantified using an Envision plate reader (PerkinElmer).

Human islets. Islets obtained from the Integrated Islet Distribution Program (IIDP) and Prodo Laboratories, and cultured in CMRL 1066 supplemented with 10% FBS, 1% Pen/Strep, and 2 mM GlutaMAX. Islets were washed with PBS, incubated with acutase for 20 minutes at 37°C, and cell culture media added to terminate enzymatic dissociation. Cells were then strained, counted and plated on flasks pre-treated with conditioned media from the human bladder carcinoma cell line HTB-9[27]. GLT media for human islets consisted of CMRL 1066 supplemented with 1% fatty acid free BSA, 1% FBS, 30 mM glucose and 1 mM sodium palmitate.

Z' and z-score calculations. Z' factor was calculated as previously described using Genedata Screening software (Genedata)[28]. z-score was calculated using Genedata Screener software (Genedata).

Microscopy.

High-Content Fluorescent Microscopy (HCFM) Assay: Live INS-1E cells were stained with Hoechst 33342, CellEvent™ Caspase-3/7, and DRAQ7 all at 1:5000 dilution for 1.5 hours. Cells imaged at the magnification 5X and 10X using an Opera Phenix High-Content Imaging Instrument (PerkinElmer). Caspase-negative/positive and DRAQ7-negative/positive cells were quantified using Harmony software (PerkinElmer).

Human Islet Staining: Human islets were fixed with 3% PFA for 20 minutes, permeabilized with 0.2% Triton X-100 in PBS for 20 minutes, blocked with 2% BSA in PBS for 2-3 hours at room

temperature with gentle shaking, and then incubated with C-peptide antibody (Developmental Studies Hybridoma Bank, GN-ID4) in 2% BSA in PBS overnight at 4°C. After thorough washing with PBS and 1% BSA in PBS, cells were incubated with secondary antibody conjugated to AlexaFluor 568 (Invitrogen) and Hoechst 33342, all in 2% BSA dissolved in PBS for 1 hour at room temperature. Cells are washed five times with PBS and then stored at 4°C. Cells were imaged at the magnification 10X and 20X using an Opera Phenix High-Content Imaging Instrument (PerkinElmer), and percent C-peptide positive cells quantified using Harmony software (PerkinElmer).

Calcium content. INS-1E cells plated in 384-well plates were incubated with GLT media and compound treatment for 48 hours. Lyophilized Calcium 6 dye (VWR Scientific) was resuspended in GLT media and added at 1:1 volume to each well. Plates were incubated for 2 hours at 37°C where Hoechst 33342 was added at a 1:1000 ratio at 1.5 hours, and imaged with 10X and 20X air objectives using an Operetta automated microscope (PerkinElmer). Increased calcium flux was estimated by quantifying FITC emission. Increased fluorescence in the FITC channel correlated with increased calcium content. Per cell FITC fluorescence was quantified using Hoechst to identify cell nucleus and nearby cytoplasm.

Flow cytometry. Mitochondrial depolarization in INS-1E detected using JC-1 dye and flow cytometry. Four million treated INS-1E cells were incubated with 15.3 mM JC-1 for 10 minutes, washed with dye-free RPMI 1640 medium, then trypsinized and resuspended in dye-free RPMI 1640. Cells were sorted on a flow cytometer (Cytoflex, Beckman Coulter) and resulting data analyzed using FlowJo flow cytometry analysis software (BD Biosciences).

Gene Expression. Cellular RNA was isolated from INS-1E cells 32-hours after GLT treatment using an RNeasy Plus Mini Kit (Qiagen). qPCR was performed using purified RNA, TaqMan RNA-to-Ct 1-Step Kit (ThermoFisher), and the following TaqMan probes (ThermoFisher): Hprt1 (Rn01527840_m1), Mrpl19 (Rn01425270_m1), and Pdx1 (Rn00755591_m1). qPCR samples were normalized to Hprt1 and Mrpl19 expression levels. Pdx1 expression levels were normalized relative to basal treated INS-1E.

Statistical Analysis. *In vitro* experiments were performed at least three times and quantitative data are presented as mean ± SD. Group means were compared using ANOVA assuming Gaussian distribution followed by a one-way *t*-test. Statistical analyses were performed using GraphPad Prism software version 8 (GraphPad Software).

2.6 Discussion

The methods described is this chapter are robust and low variability means to identify and interrogate primary screen hits with GLT-protectivity. While mitochondrial depolarization and calcium influx are easily detected effects of GLT in β-cells, there are other effects including endoplasmic reticulum stress (ER), activation of the unfolded protein response, and oxidative stress via the generation of reactive oxygen species (ROS). Though it would have been beneficial to interrogate the effects of primary screens hits on ROS production or oxidative stress in GLT-treated INS-1E, attempts to develop such an assay failed to show strong and repeatable activation of oxidative stress or ROS generation using fluorophores like H2DCFDA and CellROX and flow cytometry or confocal microscopy readouts.[29,30] Additionally, there are few high-throughput methods for detecting ER stress. The method most utilized in the literature is Western blot detection of proteins cleaved and phosphorylated under ER stress. These proteins include: phosphorylated IRE1α, spliced XBP-1, phosphorylated PERK, phosphorylated eIFα, cleaved

ATFα, and CHOP, and ATF4.[31] Development of an ER stress detection assay was impeded by poor antibody detection of protein targets and the large quantity of cells needed to extract enough protein for Western blotting multiple protein targets. ER stress detection via Western blotting was attempted using GLT-treated INS-1E cells and GLT-treated human islets however neither sample could be used to detect markers of ER stress. Overall, secondary effects of GLT were investigated in this chapter and robust assays to detect a few were developed. Future mechanism of action studies for validated primary screen hits will benefit from more assays to detect the components of GLT in β-cells.

2.7 References

1. Sol, E. M., Sargsyan, E., Akusjärvi, G. & Bergsten, P. Glucolipotoxicity in INS-1E cells is counteracted by carnitine palmitoyltransferase 1 over-expression. *Biochem. Biophys. Res. Commun.* **375**, 517–521 (2008).

2. Gebert, B., Fischer, W., Weiss, E., Hoffmann, R. & Haas, R. Helicobacter pylori vacuolating cytotoxin inhibits T lymphocyte activation. *Science (80-.).* **301**, 1099–1102 (2003).

3. Mathews Griner, L. A. *et al.* High-throughput combinatorial screening identifies drugs that cooperate with ibrutinib to kill activated B-cell–like diffuse large B-cell lymphoma cells. *Proc. Natl. Acad. Sci.* **111**, 2349–2354 (2014).

4. Hata, A. N. *et al.* Tumor cells can follow distinct evolutionary paths to become resistant to epidermal growth factor receptor inhibition. *Nat. Med.* **22**, 262–269 (2016).

5. Lee, S. H. *et al.* High-throughput screening and bioinformatic analysis to ascertain compounds that prevent saturated fatty acid-induced β-cell apoptosis. *Biochem. Pharmacol.* **138**, 140–149 (2017).

6. Ardestani, A. *et al.* Neratinib protects pancreatic beta cells in diabetes. *Nat. Commun.* **10**, 1–17 (2019).

7. Vogel, J. *et al.* A phenotypic screen identifies calcium overload as a key mechanism of β-cell glucolipotoxicity. *Diabetes* **69**, 1032–1041 (2020).

8. Walsh, J. G. *et al.* Executioner caspase-3 and caspase-7 are functionally distinct proteases. *Proc. Natl. Acad. Sci.* **105**, 12815–12819 (2008).

9. Lin, K. K. & Goodell, M. A. Detection of hematopoietic stem cells by flow cytometry. in 21–30 (2011). doi:10.1016/B978-0-12-385493-3.00002-4

10. Mazzini, G. & Danova, M. Fluorochromes for DNA staining and quantitation. in 239–259 (2017). doi:10.1007/978-1-4939-6788-9_18

11. Wlodkowic, D. *et al.* Kinetic viability assays using DRAQ7 probe. *Curr. Protoc. Cytom.* **65**, 1–10 (2013).

12. Kudryavtsev, I., Serebryakova, M., Solovjeva, L., Svetlova, M. & Firsanov, D. Rapid detection of apoptosis in cultured mammalian cells. in 105–111 (2017). doi:10.1007/978-1-4939-7187-9_8

13. Akagi, J. *et al.* Real-time cell viability assays using a new anthracycline derivative DRAQ7®. *Cytom. Part A* **83A**, 227–234 (2013).

14. Wong, D. W., Gan, W. L., Teo, Y. K. & Lew, W. S. Interplay of cell death signaling pathways mediated by alternating magnetic field gradient. *Cell Death Discov.* **4**, 49 (2018).

15. Hasegawa, T., Shimada, S., Ishida, H. & Nakashima, M. Chafuroside B, an oolong tea polyphenol, ameliorates UVB-induced DNA damage and generation of photo-immunosuppression related mediators in human keratinocytes. *PLoS One* **8**, e77308 (2013).

16. Liu, M., Wright, J., Guo, H., Xiong, Y. & Arvan, P. Proinsulin entry and transit through the endoplasmic reticulum in pancreatic beta cells. in 35–62 (2014). doi:10.1016/B978-0-12-800174-5.00002-8

17. Leighton, E., Sainsbury, C. A. & Jones, G. C. A ractical review of C-peptide testing in diabetes. *Diabetes Ther.* **8**, 475–487 (2017).

18. Lytrivi, M., Castell, A. L., Poitout, V. & Cnop, M. Recent insights into mechanisms of β-cell lipo- and glucolipotoxicity in type 2 diabetes. *J. Mol. Biol.* **432**, 1514–1534 (2020).

19. Perelman, A. *et al.* JC-1: alternative excitation wavelengths facilitate mitochondrial membrane potential cytometry. *Cell Death Dis.* **3**, e430–e430 (2012).

20. Furlong, I. J., Mediavilla, C. L., Ascaso, R., Rivas, A. L. & Collins, M. K. Induction of apoptosis by valinomycin: mitochondrial permeability transition causes intracellular acidification. *Cell Death Differ.* **5**, 214–221 (1998).

21. Zhou, Y. *et al.* Inhibition of calcium influx reduces dysfunction and apoptosis in lipotoxic pancreatic β-cells via regulation of endoplasmic reticulum stress. *PLoS One* **10**, e0132411 (2015).

22. Klec, C., Ziomek, G., Pichler, M., Malli, R. & Graier, W. F. Calcium signaling in ß-cell physiology and pathology: a revisit. *Int. J. Mol. Sci.* **20**, 6110 (2019).

23. Law, B. Y. K. *et al.* N-desmethyldauricine induces autophagic cell death in apoptosis-defective cells via Ca2+ mobilization. *Front. Pharmacol.* **8**, (2017).

24. Burns, S. M. *et al.* High-throughput luminescent reporter of insulin secretion for discovering regulators of pancreatic Beta-cell function. *Cell Metab.* **21**, 126–137 (2015).

25. Stone, V. M. *et al.* The cytoprotective effects of oleoylethanolamide in insulin-secreting cells do not require activation of GPR119. *Br. J. Pharmacol.* **165**, 2758–2770 (2012).

26. Hagman, D. K., Hays, L. B., Parazzoli, S. D. & Poitout, V. Palmitate inhibits insulin gene expression by altering Pdx-1 nuclear localization and reducing MafA expression in isolated rat islets of langerhans. *J. Biol. Chem.* **280**, 32413–32418 (2005).

27. Walpita, D. & Wagner, B. K. Evaluation of compounds in primary human islet cell culture. *Curr. Protoc. Chem. Biol.* **6**, 157–168 (2014).

28. Zhang, J. H., Chung, T. D. Y. & Oldenburg, K. R. A simple statistical parameter for use in evaluation and validation of high throughput screening assays. *Journal of Biomolecular Screening* **4**, 67–73 (1999).

29. Mehmeti, I., Lortz, S., Avezov, E., Jörns, A. & Lenzen, S. ER-resident antioxidative GPx7 and GPx8 enzyme isoforms protect insulin-secreting INS-1E β-cells against lipotoxicity by improving the ER antioxidative capacity. *Free Radic. Biol. Med.* **112**, 121–130 (2017).

30. Pyle, J. R., Sy Piecco, K. W. E., Vicente, J. R. & Chen, J. In situ sensing of reactive oxygen species on dye-stained single DNA molecules under illumination. *Langmuir* **35**, 11308–11314 (2019).

31. Oslowski, C. M. & Urano, F. Measuring ER stress and the unfolded protein response using mammalian tissue culture system. *Methods Enzym.* 71–92 (2011). doi:10.1016/B978-0-12-385114-7.00004-0

Chapter 3

Phenotypic Screening For Small Molecules That Protect β-Cells From Glucolipotoxicity

3.1 Attribution

Jonnell C. Small, Aidan Joblin-Mills, Kaycee Carbone, Maria Kost-Alimova, Kumiko Ayukawa, Carol Khodier, Vlado Dancik, Paul A. Clemons, Andrew B. Munkacsi, and Bridget K. Wagner*

Author Contributions

JCS and AJM executed primary screen. JCS conducted validation screen, developed secondary assays for viability detection and functionalization, and wrote the manuscript. KC conducted cytokine treatment experiments and assisted with flow cytometry. MKA assisted with high-content imaging and analysis. JCS and KA dissociated and plated human islets. CK assisted with primary screen data collection. VD and PAC assisted with primary screen data analysis. ABM and BKW conceived of study, participated in its design, and wrote the manuscript. Final manuscript was read and approved by all authors.

This chapter was adapted from

Small, J et al. Phenotypic Screening For Small Molecules That Protect β-Cells From Glucolipotoxicity. (2022) *ACS Chem Bio.* 10.1021/acschembio.2c00052

3.2 Abstract

Type 2 diabetes is marked by progressive β-cell failure, leading to loss of β-cell mass. Increased levels of circulating glucose and free fatty acids associated with obesity lead to β-cell glucolipotoxicity. There are currently no therapeutic options to address this facet of β-cell loss in obese type 2 diabetes patients. To identify small molecules capable of protecting β-cells, we performed a high-throughput screen of 20,876 compounds in the rat insulinoma cell line INS-1E in the presence of elevated glucose and palmitate. We found 312 glucolipotoxicity-protective small molecules (1.49% hit rate) capable of restoring INS-1E viability and we focused on seventeen with known biological targets. Sixteen of the seventeen compounds were kinase inhibitors with activity against specific families including but not limited to cyclin-dependent kinases (CDK), PI-3 kinase (PI3K), janus kinase (JAK), and Rho-associated kinase 2 (ROCK2). Seven of the sixteen kinase inhibitors were PI3K inhibitors. Validation studies in dissociated human islets identified ten of the seventeen compounds, namely KD025, ETP-45658, BMS-536924, AT-9283, PF-03814735, torin-2, AZD5438, CP-640186, ETP-46464, and GSK2126458 that reduced glucolipotoxicity-induced β-cell death. These ten compounds decreased markers of glucolipotoxicity including caspase activation, mitochondrial depolarization, and increased calcium flux. Together, these results provide a path forward toward identifying novel treatments to preserve β-cell viability in the face of glucolipotoxicity.

3.3 Introduction

Obesity is a critical risk factor for the development of type 2 diabetes (T2D). Elevated levels of free fatty acids (FFA) are observed in obesity because of expanded adipose tissue mass and reduced FFA clearance[1]. Increasing evidence suggests that elevated FFAs may contribute to T2D pathogenesis and represent a mechanistic link between obesity and diabetes. FFAs induce insulin resistance and pancreatic β-cell dysfunction, two major defects underlying T2D pathophysiology[2]. Prolonged FFA exposure has inhibitory effects on insulin secretion[3]. When co-infused with glucose, FFA elevation inhibits the stimulatory effect of hyperglycemia on β-cell function[3], and individuals genetically predisposed to T2D show increased susceptibility to FFA-dependent β-cell dysfunction[4,5]. Exposure to elevated glucose exerts synergistic effects with FFAs, leading to glucolipotoxicity (GLT)[6–9]. GLT is characterized by impaired glucose-stimulated insulin secretion (GSIS), decreased insulin gene transcription, attenuation of β-cell-specific transcription factors PDX1 and MAFA, and induction of apoptosis through activated caspase, mitochondrial depolarization, increased calcium flux, oxidative stress, and the unfolded protein response[10,11].

The absence of strategies to suppress GLT-induced loss of β-cell function and mass in T2D has inspired the search for β-cell-protective small molecules. Recent high-throughput screening (HTS) campaigns have identified anti-apoptotic small molecules in β-cell models of lipotoxicity and glucolipotoxicity. These include the polyunsaturated fatty acid amide and endogenous endocannabinoid anandamide[12], the FDA-approved HER2/EGFR dual kinase inhibitor neratinib[13], and L-type calcium channel blockers nifedipine and verapamil[14]. Polyunsaturated fatty acids, especially anandamide, protect against saturated fatty acid-induced lipotoxicity by binding to β-cell fatty acid receptors and decreasing uptake of toxic saturated fatty acids. Neratinib is β-cell protective by inhibiting the serine-threonine kinase STK4/MST1, a key regulator of β-cell apoptosis and dysfunction in diabetes. L-type calcium channel blockers like nifedipine and

verapamil protect against GLT by decreasing calcium influx, which induces apoptosis. The discovery of these small molecules and their diverse mechanisms of action suggest there are multiple avenues through which β-cell function and survival can be promoted and maintained.

HTS has long been utilized in the pharmaceutical industry for therapeutic discovery, and its application in the academic setting has spurred the discovery of novel biological probes for perturbing and investigating cellular mechanisms[15]. Phenotypic HTS has become especially attractive because such screens preserve the functional cellular context of targets of compounds. Additionally, it is possible to conduct compound discovery that is target agnostic (i.e., identify compounds that induce similar phenotypic changes through different cellular targets). Phenotypic HTS has therefore been very useful in identifying compounds important for β-cell survival, insulin degradation, and β-cell replication[16–18].

Identifying novel β-cell protective small molecules using phenotypic HTS is advantageous on two fronts. First, it enables the potential discovery of novel mechanisms regulating β-cell survival and function, which can be further investigated to generate a more holistic understanding of β-cell biology. Second, it provides novel chemical matter that can be further optimized to generate lead candidates for the treatment of T2D. Motivated by both questions, we performed a screen of 20,876 compounds in INS-1E cells, with the goal of identifying novel compounds with β-cell protective activity. We identified two diversity-oriented synthesis (DOS)-derived scaffolds with GLT-suppressive activity. We also found 17 small molecules with known biological targets capable of suppressing GLT in both INS-1E cells and human islets. Several of these compounds reveal a critical role for kinase inhibition in promoting β-cell survival and function. These results suggest new mechanisms for promoting β-cell survival and provide further evidence that multiple cellular processes govern β-cell function in obese and T2D patients.

3.4 Methods

Cell culture. INS-1E cells (generously provided by Claes Wollheim and Pierre Maechler, University of Geneva, Switzerland) were cultured in RPMI 1640 supplemented with 10% FBS, 1% Pen/Strep, 1% sodium pyruvate, and 50 µM β-mercaptoethanol. Cells were maintained in flasks precoated with diluted supernatant (1:10) from the rat 804G cell line (804G matrix). 804G cells are a rat cancer cell line known to secrete a laminin-5 rich extracellular matrix. 804G cells were a generous gift of Susan Bonner-Weir Lab, Joslin Diabetes Center. The 804G matrix induces spreading, improves glucose-stimulated insulin secretion, and increases survival and proliferation of rat pancreatic β-cells.[19] GLT media for INS-1E consisted of RPMI 1640 supplemented with 1% FBS, 1% Pen/Strep, 1% fatty acid free BSA, 50 µM β-mercaptoethanol, 25 mM glucose, and 0.5 mM sodium palmitate. Sodium palmitate was dissolved in warmed 4% BSA in PBS before being added to RPMI1650.

Human islets. Islets were obtained from the Integrated Islet Distribution Program (IIDP) and Prodo Laboratories, and cultured in CMRL 1066 supplemented with 10% FBS, 1% Pen/Strep, and 2 mM GlutaMAX. Islets were washed with PBS, incubated with acutase for 20 minutes at 37°C, and cell culture media added to terminate enzymatic dissociation. Cells were then strained, counted and plated on flasks pre-treated with conditioned media from the human bladder carcinoma cell line HTB-9[20]. GLT media for human islets consisted of CMRL 1066 supplemented with 1% fatty acid free BSA, 1% FBS, 30 mM glucose and 1 mM sodium palmitate.

High-throughput screening. INS-1E cells were plated at 5,000 cells/well in 384-well plates pretreated with supernatant from 804G cells. After 24 hours in regular media conditions, media was removed from plates using a Multidrop Combi plate dispenser (ThermoFisher), and GLT media was added at 35 µL/well. Following 48-hour incubation in GLT media, plates were left to

equilibrate to room temperature before CellTiter-Glo (Promega) was added. Luminescence (viability) was quantified using an Envision plate reader (PerkinElmer). A 3-σ (z-score ≥ 3) cut off was used to identify hit compounds from the primary screen, which were then retested at four concentrations. CaspaseGlo (Promega) was also used to quantify caspase-3/7 activity.

Z' and z-score calculations. Z' factor was calculated as previously described using Genedata Screening software (Genedata)[21]. z-score was calculated using Genedata Screener software (Genedata).

Compounds. Compounds in the DOS Informer, DOS-A, Repurposing and Bioactive libraries were maintained in the Broad Institute and printed into 96- and 384-well plates using a Tecan D300e drug printer. A subset of the repurposed compounds were purchased commercially for validation studies: PIK-93, GSK2126458 (Omipalisib), Duvelisib (IPI-145, INK1197), KD025 (SLx-2119), LY2784544, Palbociclib, Torin-2, AZD8186, AT-9283, and AZD5438 (Selleckchem); ETP-45658 (R&D Systems); ETP-46464, CP-640186, and BMS-536924 (Sigma-Aldrich); PF-03814735, TGX-221, and Taselisib (GDC-0032) (Cayman Chemical); Anandamide (VWR Scientific); AM404 (Santa Cruz Biotech) and Oleylethanolamide (Combi Blocks). Stock solutions were prepared in DMSO and stored as per manufacturer instructions.

Target enrichment. To evaluate the screening results from the Repurposing collection, we imported target annotation from the Broad Repurposing Hub (clue.io/repurposing-app), and filtered for compounds with annotating targets (4,829 of the 5,440 screened). We then imported a list of gene symbols for 401 human kinases from Discoverx KinomeScan (https://www.discoverx.com/services/drug-discovery-development-services/kinase-profiling/kinomescan/gene-symbol), and found that 623 of the 4,829 compounds had at least one kinase inhibitory activity. Of the 623 compounds, 58 were determined to be screening hits (as

opposed to 59 of the other 4,147). We calculated a nominal p-value for these results using Fisher's exact text, implemented in MATLAB release R2018b.

Microscopy. *High-Content Fluorescent Microscopy (HCFM) Assay*: Live INS-1E cells were stained with DNA dye Hoechst 33342 (all cells), Caspase 3/7 activation dye CellEvent™ Caspase-3/7 (apoptotic cells), and live cell impermeable DNA dye DRAQ7 (dead cells) all at 1:5000 dilution for 1.5 hours. Cells were imaged at the magnification 5X and 10X using an Opera Phenix High-Content Imaging Instrument (PerkinElmer). Caspase-negative/positive and DRAQ7-negative/positive cells were quantified using Harmony software (PerkinElmer).

Human Islet Staining: Human islets were fixed with 3% PFA for 20 minutes, permeabilized with 0.2% Triton X-100 in PBS for 20 minutes, blocked with 2% BSA in PBS for 2-3 hours at room temperature with gentle shaking, and then incubated with C-peptide antibody (Developmental Studies Hybridoma Bank, GN-ID4) in 2% BSA in PBS overnight at 4°C. After thorough washing with PBS and 1% BSA in PBS, cells were incubated with secondary antibody conjugated to AlexaFluor 568 (Invitrogen) and Hoechst 33342, all in 2% BSA dissolved in PBS for 1 hour at room temperature. Cells are washed five times with PBS and then stored at 4°C. Cells were imaged at the magnification 10X and 20X using an Opera Phenix High-Content Imaging Instrument (PerkinElmer), and percent C-peptide positive cells quantified using Harmony software (PerkinElmer).

Calcium content. Intracellular calcium content was quantified as previously described.[14] INS-1E cells plated in 384-well plates were incubated with GLT media and compound treatment for 48 hours. Lyophilized Calcium 6 dye (VWR Scientific) was resuspended in GLT media and added at 1:1 volume to each well. Plates were incubated for 2 hours at 37°C where Hoechst 33342 was

added at a 1:1000 ratio at 1.5 hours, and imaged with 10X and 20X air objectives using an Operetta automated microscope (PerkinElmer). Increased calcium flux was estimated by quantifying FITC emission. Increased fluorescence in the FITC channel correlated with increased calcium content. Per cell FITC fluorescence was quantified using Hoechst to identify cell nucleus and nearby cytoplasm.

Proinflammatory cytokine treatment. Immune stress was induced as previously described.[22] INS-1E cells were plated at 8,000 cells per well in a 384-well plate coated with 804G matrix and incubated at 37°C overnight. Basal media was then removed and replaced with media containing cytokines (R&D Systems) specifically RPMI media, 1% FBS, 10 ng/mL IL-1β , 100 ng/mL IFN-γ , and 25 ng/mL TNF-α. Working concentrations of compounds were printed into the 384-well plates using a Tecan D300e drug printer. Plates were incubated at 37°C for 48 hours and cell viability was detected using HCFM assay.

Flow cytometry. Mitochondrial depolarization in INS-1E was detected using flow cytometry via the JC-1 dye. Four million treated INS-1E cells were incubated with 15.3 ⌈M JC-1 for 10 minutes, washed with dye-free RPMI 1640 medium, then trypsinized and resuspended in dye-free RPMI 1640. Cells were sorted on a flow cytometer (Cytoflex, Beckman Coulter) and resulting data analyzed using FlowJo flow cytometry analysis software (BD Biosciences).

Statistical Analysis. *In vitro* experiments were performed at least three times and quantitative data are presented as mean ± SD. Group means were compared using ANOVA assuming Gaussian distribution followed by a one-way *t*-test. Statistical analyses were performed using GraphPad Prism software version 8 (GraphPad Software).

Gene Expression. Cellular RNA was isolated from INS-1E cells 24-48hrs after GLT treatment using an RNeasy Plus Mini Kit (Qiagen). qPCR was performed using purified RNA, TaqMan RNA-to-Ct 1-Step Kit (ThermoFisher), and the following TaqMan probes (ThermoFisher): Hprt1 (Rn01527840_m1), Mrpl19 (Rn01425270_m1), and Pdx1 (Rn00755591_m1). qPCR samples were normalized to Hprt1 and Mrpl19 expression levels. Pdx1 expression levels were normalized relative to basal treated INS-1E.

3.5 Results and Discussion

Primary Screen Identifies β-Cell-Protective Compounds.

We performed a primary screen (Figure 3.5.1a) in INS-1E cells to identify compounds that protected β-cells from GLT as measured by cell viability detected using CellTiter-Glo. Optimized GLT media contained 25 mM glucose and 0.5 mM sodium palmitate, which induced ~70% INS-1E cell death after 48-hour treatment (Figure 3.5.2a). Sodium palmitate was the major contributor to INS-1E cell death in GLT conditions via reduced INS-1E viability by 25% and 50% at 0.25 mM and 0.5 mM, respectively, compared to control (Figure 3.5.1c–f). Sodium palmitate is well documented to induce lipotoxicity and glucolipotoxicity in β-cell models including INS-1E, INS-1, BRIN-BD11, and MIN6.[12,23–25]
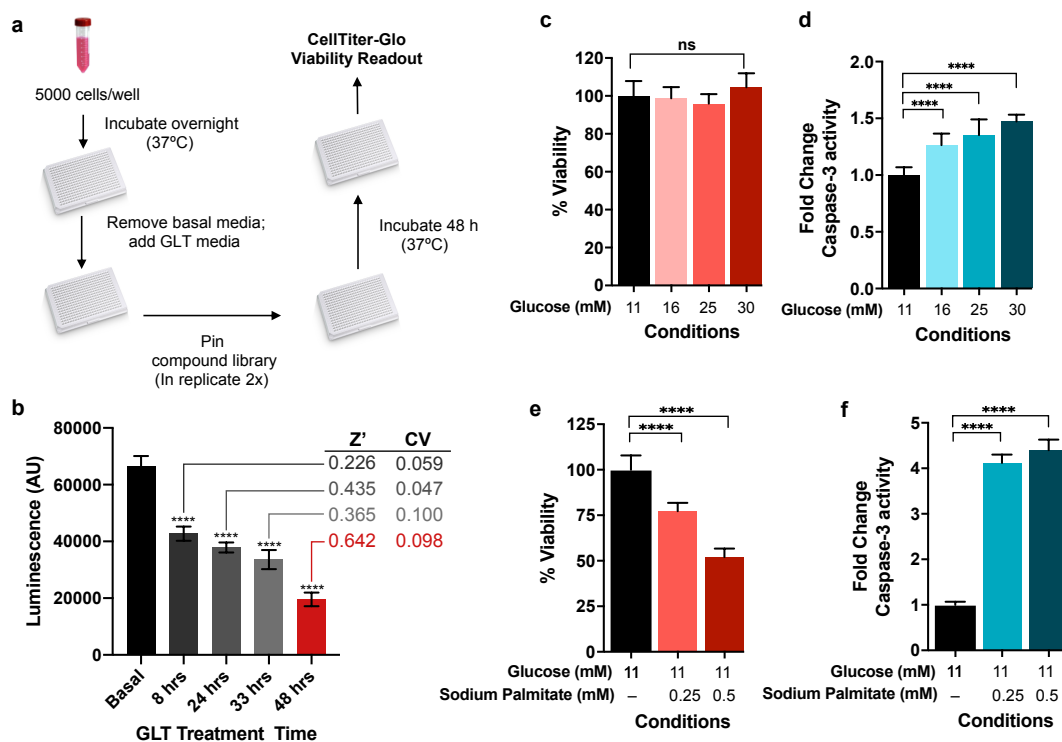
Figure 3.5.1. Glucolipotoxicity induction in INS-1E cells. a) Schematic outline of GLT phenotypic screen in INS-1E cells. b) Z' factor and CV were calculated for 8, 24, 33, and 48hr GLT treatment in 384-well plate format using Cell-Titer Glo viability readout. c) INS-1E viability is unaffected by increasing levels of glucose alone however is coincident with a d) dose-dependent increase in caspase-3 activation. e) Increased cell death and f) caspase activation is observed with increasing levels of palmitate. Statistical significance was evaluated using an unpaired, one-tailed t-test (****, $P < 0.0001$).
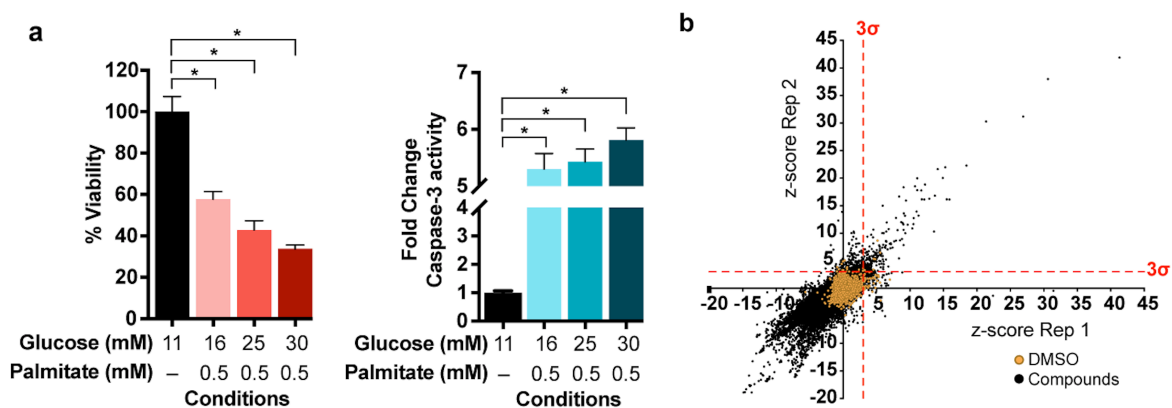
Figure 3.5.2. Optimization of glucolipotoxicity media for INS-1E cells and phenotypic screening of glucolipotoxicity-suppressing compounds. a) Cell death and caspase-3 activation are significantly enhanced in GLT media conditions with increasing levels of glucose and 0.5 mM sodium palmitate. *, $P < 0.0001$, as determined by unpaired t test. b) Scatter plot showing HTS results from 20,876 compounds (black dots) where compounds were screened at concentrations between 5–10 µM in duplicate and z-scores were calculated from CellTiter-Glo readouts for compounds relative to DMSO control using Genedata Screener. A z-score of ≥ 3 (3σ) was used as a threshold for hit calling (red-dotted line).

Compounds Known To Protect β-Cells Validate Primary Screen Performance.

We selected four chemical libraries (20,876 total compounds) for screening. First, the DOS Informer Set is a subset of the Broad Institute DOS library[26,27], containing 9,510 compounds (192 hits – 2.02% hit rate) representing ~30 diverse structural families. Second, the DOS-A library (3,840 compounds, 29 hits – 0.76% hit rate) is a collection of DOS compounds selected for performance diversity based on a combination of gene expression analysis and Cell Painting[28]. Finally, the Broad Repurposing Collection (5,440 compounds, 81 hits – 1.49% hit rate)[29] and Bioactive Libraries (2,086 compounds, 10 hits – 0.48% hit rate) contain FDA-approved drugs, candidates in development, and known tool compounds. We screened compounds at a typical screening concentration of 10 μM in 384-well plate format for 48 hours to identify those that improved INS-1E viability, as determined by calculated z-scores (Figure 3.5.2b). Using a hit-calling threshold of z-score $\geq$ 3 (3σ, relative to DMSO) in two replicates, we identified 312 total hits (1.49% overall hit rate). This hit rate of 1.49% was more than 100 times the average hit rate of 0.01–0.14% for most high-throughput screens[30]. Due to availability, 160 hits were selected for retesting at four concentration points (1.25, 2.5, 5, and 10 μM) to determine their effects on INS-1E cell viability and caspase activation in GLT conditions.

Anandamide (AEA), a polyunsaturated fatty acid amide with z-scores >40 in both replicates of the primary screen, was validated as a potent hit with a dose-dependent increase in INS-1E viability and dose-dependent decrease in caspase activity in GLT conditions. AEA recovered INS-1E viability and decreased caspase activity by ~90% and ~70% compared to basal media control, respectively (Figure 3.5.3a). The AEA derivative AM404 (z-scores >18 in both replicates) also showed similar activity at 10 μM, recovering INS-1E viability to ~90% of the control and decreasing caspase activity to 86% of the control (Figure 3.5.3b). Our results are consistent with previous studies that confirmed AEA and AM404 as GLT- and lipotoxicity-protective small molecules in

INS-1, INS-1E, and BRIN-BD11 cells[12,24]. The monounsaturated fatty acid amide oleoylethanolamide (OEA) exhibited z-scores of > 6 in both replicates of the primary screen, and showed maximum activity at 10µM where it recovered INS-1E viability to ~60% of control and decreased caspase activity to 33% of control (Figure 3.5.3c). Consistently, OEA had also been previously identified as lipotoxicity-protective in BRIN-BD11 cells[24]. SU9516 (z-scores > 9 in both replicates) recovered only 65% of INS-1E viability compared to control and this was associated with an increase in caspase activity using the Caspase-Glo 3/7 assay (Figure 3.5.3d). Similar to the aforementioned compounds, SU9516 has been shown to be GLT-protective in INS-1 cells[12]. Literature confirmation of primary screen hits AEA, AM404, OEA, and SU9516 thus provided evidence that the primary screen successfully identified GLT-protective small molecules from the four libraries.
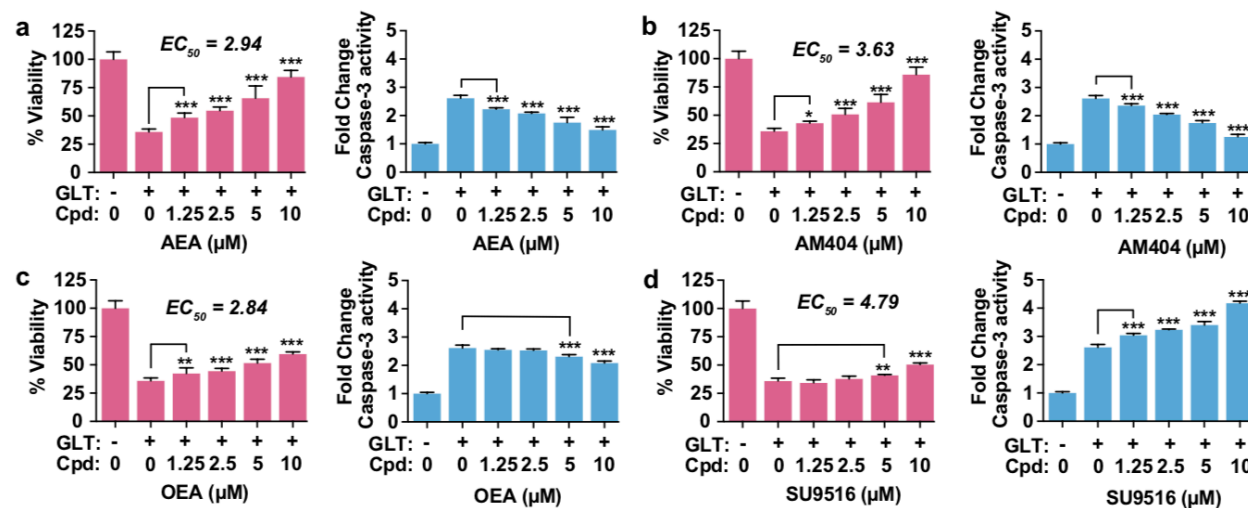
Figure 3.5.3. Confirmation of GLT-protective activity. Four compounds previously reported to protect against GLT provide proof-of-principle results for the detection of novel bioactivity in the HTS. a & b) Anandamide (AEA) and the AEA derivative (AM404) increased INS-1E viability and decreased caspase-3 activity in a dose-dependent manner. c) Oleylethanolamide (OEA) increased INS-1E viability and moderately decreased caspase-3 activity. d) SU9156 moderately protected at 5µM and 10µM, with more dramatically increased caspase-3 activation. Data represents mean ± SD of 5 replicates. Statistical significance was evaluated using an unpaired, one-tailed t-test for each compound compared to GLT alone (*, $P < 0.05$; **, $P < 0.001$; ***, $P < 0.0001$).

Though initial validation studies confirming primary screen hits AEA, AM404, OEA, and SU9516 utilized the CellTiter-Glo reagent, we learned this reagent can yield false positive results. Apitolisib showed dose-dependent increase in luminescence with the CellTiter-Glo readout, suggesting it was a GLT-protective compound; however, this activity was not validated with cell number quantification using nuclear staining (Figure 3.5.4a,b). High-content microscopy revealed that apitolisib did not proportionally increase INS-1E cell number above control cells treated with GLT and DMSO. We speculated that apitolisib induced changes in cellular ATP levels in INS-1E that resulted in increased CellTiter-Glo luminescence. We therefore developed a high-content fluorescent microscopy (HCFM) assay utilizing the live-cell-impermeable dye DRAQ7[31–33] and the CellEvent™ Caspase-3/7 dye[34,35] to quantify total number of live (DRAQ7 negative, caspase negative) cells and percent viability (% DRAQ negative, caspase negative cells) (Figure 3.5.4b,c). This assay revealed that while some compounds were able to increase percent viability, they had little or no effect on the total number of live cells (as was the case for apitolisib). The decrease in caspase-3 activation by apitolisib detected via Caspase Glo and the HCFM assay was not associated with an increase in cell number, and we speculate that apitolisib may be arresting INS-1E cell growth while protecting the viability of the non-mitotic cells. The HCFM assay is therefore appropriate for high-throughput investigations of cell viability, especially in GLT where it generated Z'-factor values > 0.4 (Figure 3.5.4d,e). The HCFM assay was subsequently used in validation studies of primary screen hits.
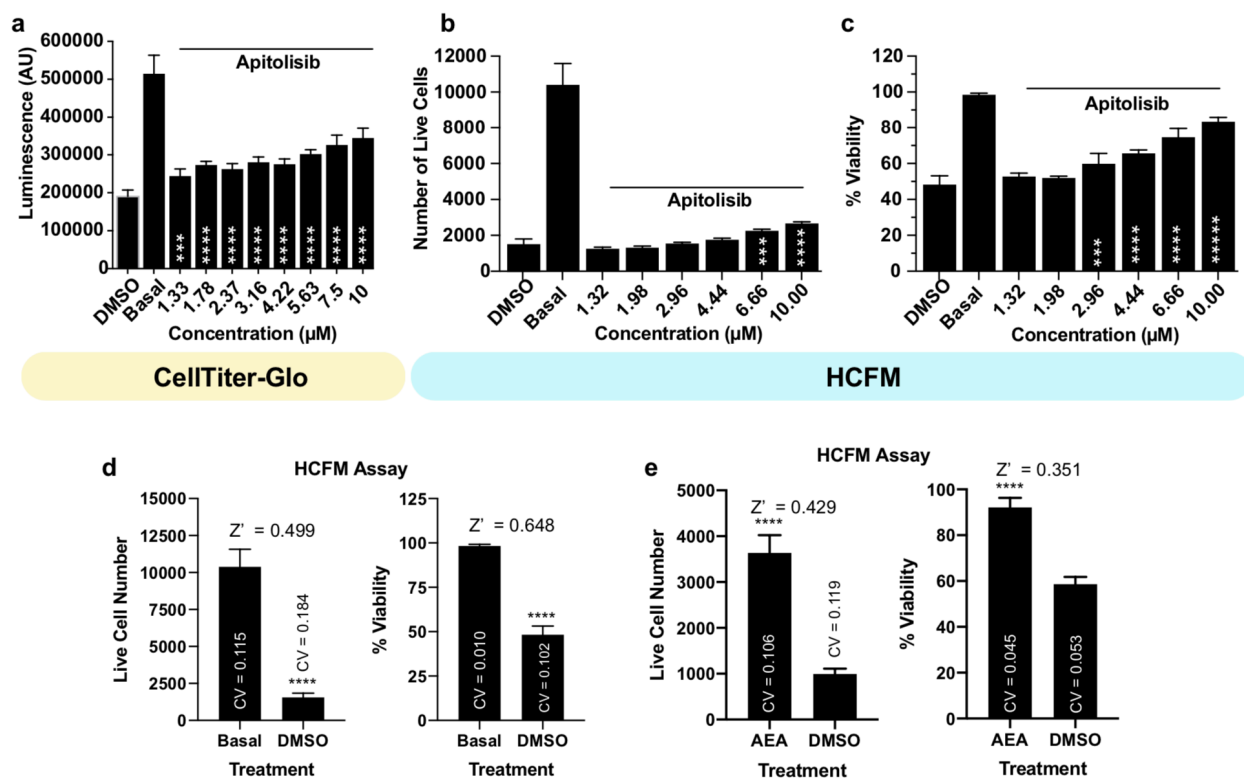
Figure 3.5.4. High-content fluorescent microscopy (HCFM) assay reveals limitations of CellTiter-Glo. (a) Apitolisib treatment results in concentration-dependent increase in INS-1E viability in GLT conditions with CellTiter-Glo (luminescence dependent on ATP concentration (n=7). (b) HCFM analysis of nuclei as a marker of cell number reveals apitolisib did not recover cell number in GLT conditions (n=3). (c) The HCFM assay developed herein captures viability using DRAQ7 (a nuclear marker for dead cells) and a caspase-activated fluorescent probe. Live cells were classified as DRAQ7 (-), Caspase (-). (d, e) Z'-factor analysis of the HCFM assay using both basal and anandamide (AEA) positive controls). Statistical significance was evaluated using an unpaired, one-tailed t-test for each compound compared to DMSO (***, *P* < 0.001; ****, P < 0.0001).

Azetidine Monoketopiperazine and Pictet-Spengler Scaffolds Protect INS-1E Cells from GLT.

Many of the DOS primary hits came from the azetidine monoketopiperazine[36] (AMK, 1.25% hit-rate) and Pictet-Spengler[37] (0.63% hit-rate) libraries (Figure 3.5.5a–c). We observed structure-activity relationships that defined active and inactive compounds (Figure 3.5.5d–e, Tables 3.5.6 & 3.5.7). For AMK compounds, stereochemistry around the monoketopiperazine core was a key determinant of activity (Figure 3.5.5c). BRD4935 (*R,S,S* stereochemistry in the monoketopiperazine core) was the most potent AMK compound, recovering INS-1E viability to 100% of AEA control (Figure 3.5.5d). Stereochemistry around the monoketopiperazine core

became less of a predictor of activity among AMK compounds containing different R_1 and R_2 groups. BRD3476 (*S,R,S*) was the second-most active AMK compound and at 2.96 µM increased the number of live INS-1E cells nearly 3-fold over the GLT control, while recovering INS-1E viability to 70% (Figure 3.5.5d).
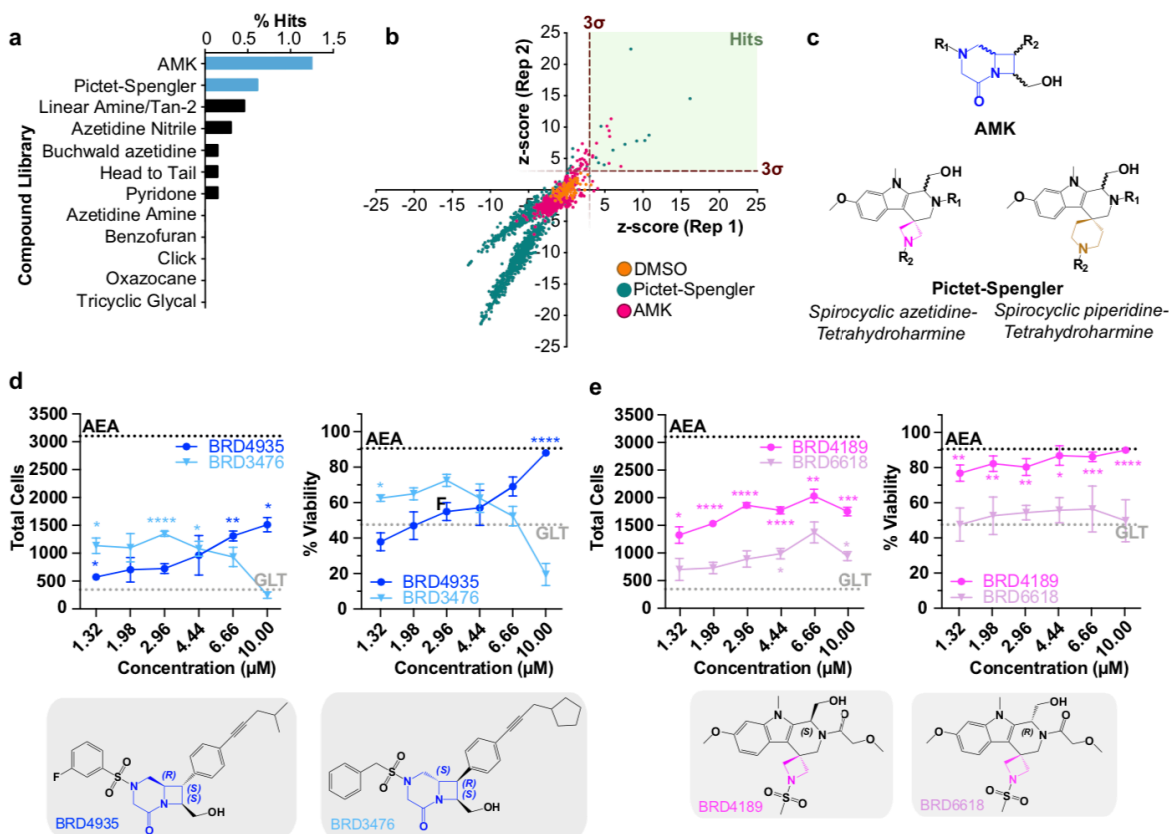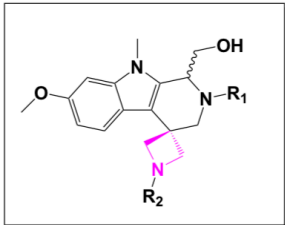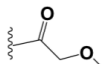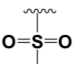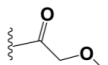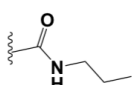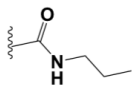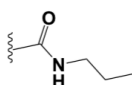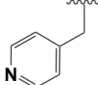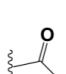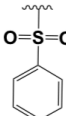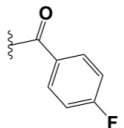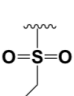
Figure 3.5.5. Validation of GLT-protective compounds in the Pictet-Spengler and Azetidine monoketopiperazine (AMK) libraries. a) Hit-rate distribution across compound libraries within the DOS Informer Set. Light blue bars indicate the AMK and Pictet-Spengler libraries from which hit compounds BRD4935 and BRD4189 were found. b) Scatter plot showing results of the Pictet-Spengler and AMK libraries (1920 compounds); compounds were screened at 10 µM. A z-score of 3 (3σ) was used as a threshold for hit calling (red-dotted line). Data points in yellow, teal, and pink represent the DMSO control, the Pictet-Spengler library, and the AMK library, respectively. c) Compounds in the AMK library contain a monoketopiperazine core (blue) with three chiral carbons (wavy bonds) and two R groups (R_1 and R_2). Compounds in the Pictet-Spengler library contains two spirocyclic β-carboline cores with either an azetidine (magenta) or piperidine (gold) ring, in addition to two R groups (R_1 and R_2) and one chiral carbon (wavy bond). d–e) Dose-dependent increases in GLT protection were validated in INS-1E cells for d) BRD4935 (n=3, from the AMK library), BRD3476 (n=3, from the AMK library), and BRD4189 (n=3, from the Pictet-Spengler library) using the HCFM assay where INS-1E cells were treated with GLT media and compounds for 48 hours. The decreased potency BRD6618 highlights the crucial role of stereochemistry in the activity of BRD4189. Statistical significance was evaluated using an unpaired, one-tailed t-test for each compound compared to GLT alone (*, $P < 0.05$; **, $P < 0.01$; ***, $P < 0.001$; ****, $P < 0.0001$).

Table 3.5.6. Maximum recovered viability and EC$_{50}$ (µM) values of structurally related spirocyclic azetidine-β-carbolines in the DOS library.

	R$_1$	R$_2$	Stereochemistry	z-score$_1$	z-score$_2$	Max Recovered Viability (%)	EC$_{50}$ (µM)
1		O=S=O	S	4.52	7.28	51.3	1.79
2		"	R	1.10	1.33	12.6	3.38
3		"	S	3.56	2.98	39.2	4.18
4		"	R	-1.43	-1.77	9.0	4.82
5			S	3.73	4.61	29.5	4.35
6		O=S=O	S	3.07	4.07	48.2	2.19
7		O=S=O	S	3.71	2.89	26.1	3.24

Pictet-Spengler (PS) library members were more active than AMK members. BRD4189 (**1**), the most potent PS hit, recovered INS-1E viability a maximum of 51% of basal media control using the CellTiter-Glo reagent and about 100% of the AEA control using the HCFM assay (Table 3.5.6, Figure 3.5.5e). The identity of the R$_1$ and R$_2$ side chains of the azetidine (magenta) and piperidine (gold) spirocyclic Tetrahydroharmine (THH) cores drastically affected PS compound activity. For example, with the same *S* stereochemistry, **1** was 20% more active than **5** but only 3% more active than **6** (BRD2892) (Table 3.5.6). However, stereochemistry of the methylhydroxyl group on

71

the spirocyclic azetidine-THH cores had a significant effect on activity. While **1** (*S* stereochemistry) recovered INS-1E viability 51.3% of basal media control and 100% of the AEA control, BRD6618 (**2**) (*R* stereochemistry) recovered INS-1E viability 12.6% of basal media control and 50% of the AEA control (Table 3.5.6, Fig 3.5.5E). For spirocyclic piperidine-THH compounds, changing the stereochemistry of the methylhydroxyl group moderately affected activity. **8** (*S* stereochemistry) recovered INS-1E viability by 48%, while **9** (*R* stereochemistry) recovered INS-1E viability by 42.9% (Table 3.5.7). One exception is made for compound **20**, which when inverted to *S* stereochemistry (**21**) lost more than 25% activity (Table 3.5.7). The azetidine-THH scaffold BRD4189 (**1**) was the most GLT-protective small molecule of the DOS compounds tested and provides a promising novel compound class for future structure-activity relationship (SAR) and mechanism-of-action investigations. To rule out promiscuity, we also performed cross-reactivity analysis[38] on BRD4189 and several other spirocyclic azetidine-THH compounds. We found these compounds were not frequent hits in other screening assays (Table 3.5.8).

Table 3.5.7. Maximum recovered viability and EC_{50} (µM) values of structurally related spirocyclic piperidine-β-carbolines in the DOS library.

	R₁	R₂	Stereochemistry	z-score₁	z-score₂	Max Recovered Viability (%)	EC₅₀ (µM)
8	(acetyl)	(2-fluorophenyl amide)	S	6.50	5.87	48.0	1.55
9	(acetyl)	"	R	2.89	3.18	42.9	1.80
10	—H	"	R	3.04	3.99	50.4	1.69
11	(4-pyridylmethyl)	(4-pyridyl ketone)	R	2.83	6.00	30.4	2.99
12	(4-pyridylmethyl)	"	S	1.68	3.69	48.3	4.05
13	—Me	"	R	3.39	2.48	45.5	1.80
14	—Me	"	S	2.36	2.92	35.3	3.87
15	(ethylsulfonyl)	"	R	2.84	1.34	N/A	N/A
16	(ethylsulfonyl)	(3-pyridyl ketone)	R	1.17	3.03	29.1	5.27
20	—Me	"	R	1.90	4.43	30.6	4.96
21	—Me	"	S	3.42	1.57	9.7	3.67
22	—H	(ethylsulfonyl)	R	2.57	3.20	18.2	5.20
23	(acetyl)	(butanoyl)	S	1.49	2.79	38.0	4.99

Table 3.5.8. Summary of Cross-Reactivity Analysis.

Compound	N_Tested	N_Hit	Promiscuity Probability
BRD4189 (**1**)	12	1	0.031
BRD6618 (**2**)	23	0	0
3	21	3	0.054
6	23	0	0

DOS compounds BRD4189 and BRD6618 scored low promiscuity probabilities of 0.031 and 0.054 respectively indicating they were not frequently identified as hits in other Broad Institute screens.

Acetyl-CoA Carboxylase Inhibition Protects β-Cells From GLT. CP-640186 is here identified as a novel β-cell GLT-protective small molecule with nanomolar potency. We validated CP-640186 as a potent GLT-protective small molecule that recovered INS-1E viability 97% of the control with an EC_{50} of 410 nM (Figure 3.5.9, Table 3.5.10).
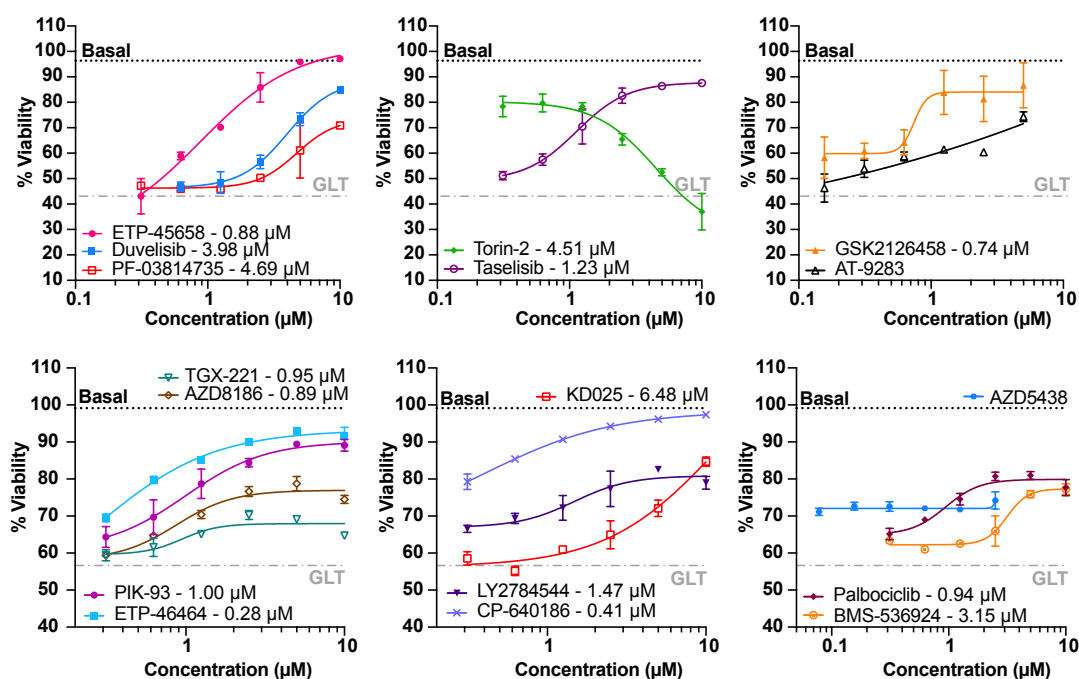
Figure 3.5.9. Validation of GLT-protective compounds in the Repurposing Library using the HCFM assay. INS-1E cells were treated with GLT media and compounds (n = 3). Numbers adjacent compound labels indicate EC_{50}. Black dotted line (n = 24) represents percent viability of INS-1E cells incubated in basal culture media. Grey dotted line (n = 18) represents percent viability of INS-1E cells treated with GLT media and DMSO. See Table S2 for annotation of all compounds in this figure.

Table 3.5.10. EC$_{50}$ values and maximum recovered viability for GLT-protective compounds in the Repurposing Library.

Category	Compound	EC$_{50}$ (µM)	Max Viability (%)	Targets and IC$_{50}$
Kinase Inhibitor	ETP-45658	0.88	97.1	PI3Kα (22 nM), PI3Kδ (30 nM), DNA-PK (70.6 nM), PI3Kβ (129 nM), mTOR (152 nM), and PI3Kγ (710 nM)
Kinase Inhibitor	ETP-46464	0.28	91.6	mTOR (0.6 nM) and ATR (14 nM)
Kinase Inhibitor	PIK-93	1.00	89.1	PI3Kγ (16 nM), PI4KIIβ (19 nM), PI4Kα (39 nM), DNA-PK (64 nM), PI3Kδ (120 nM), PI3Kβ (590 nM)
Kinase Inhibitor	Taselisib (GDC-0032)	1.23	87.6	PI3Kδ (0.12 nM), PI3Kα (0.29 nM), and PI3Kγ (0.97 nM)
Kinase Inhibitor	GSK2126458 (Omipalisib)	0.74	86.7	PI3Kα (0.019 nM), PI3Kδ (0.024 nM), PI3Kγ (0.06 nM), PI3Kβ (0.13 nM), and mTORC1/2 (0.18/0.3 nM)
Kinase Inhibitor	Duvelisib (IPI-145, INK1197)	3.98	84.9	PI3Kδ (1 nM) and PI3Kγ (50 nM)
Kinase Inhibitor	KD025 (SLx-2119)	6.48	84.7	ROCK2 (60 nM)
Kinase Inhibitor	LY2784544	1.47	82.6	JAK2 (3 nM), FLT3 (4 nM), and JAK1 (19.3 nM)
Kinase Inhibitor	Palbociclib (PD-0332991)	0.94	81.0	CDK4 (11 nM) and CDK6 (16 nM)
Kinase Inhibitor	Torin-2	4.51	79.8	mTOR (0.25 nM)
Kinase Inhibitor	AZD8186	0.89	78.8	PI3Kβ (4 nM) and PI3Kδ (12 nM)
Kinase Inhibitor	BMS-536924	3.15	77.3	Inuslin receptor (73 nM), IGF-1R (100 nM), FAK (150 nM), MEK (182 nM), LCK (341 nM)
Kinase Inhibitor	AT-9283	-	74.4	JAK3 (1.1 nM), JAK2 (1.2 nM), Aurora B (3 nM), and Abl1 (4 nM)
Kinase Inhibitor	AZD5438	-	74.2	CDK2 (6 nM), CDK1 (16 nM), and CDK9 (20 nM)
Kinase Inhibitor	PF-03814735	4.69	70.9	Aurora A (0.8 nM), Aurora B (5 nM), FLT1 (10 nM), FAK 22 nM), TrkA (30 nM), Met (100 nM), and FGFR1 (100 nM)
Kinase Inhibitor	TGX-221	0.95	70.3	PI3Kβ (5 nM)
Misc.	CP-640186	0.41	97.4	Acetyl-CoA carboxylase 1/2 (50 nM)

The HCFM assay was used to generate these data. Annotation of the category, target and IC$_{50}$ value for each compound were determined using www.selleckchem.com and the Broad Institute Repurposing Hub[29].

CP-640186 is an isozyme-nonselective acetyl-CoA carboxylase (ACC) inhibitor that inhibits fatty acid synthesis, fatty acid oxidation and triglyceride synthesis[39]. The identification of CP-640186 as GLT protective was an intriguing result in our study. This result was further validated in INS-1E cells via reductions in GLT-induced mitochondrial depolarization and calcium influx (Figures 3.5.12a, 3.5.13g). While we are not sure these are specific mechanisms of CP-640186 GLT-protectivity, ample literature evidence indicates that decreasing calcium influx improves β-cell function and viability.[14] CP-640186 was first identified for its ability to reduce fatty acid synthesis and increase fatty acid oxidation[39]. In the context of β-cell GLT, these activities likely decrease

fatty load in β-cells and allow them to circumvent the deleterious effects associated with fatty acid accumulation. There are currently no FDA approved ACC inhibitors, however given the crucial role fatty acid metabolism plays in cell viability, ACC inhibition is being explored as a potential therapeutic strategy in several diseases including nonalcoholic fatty liver disease (NAFLD) and non-alcoholic steatohepatitis (NASH). ACC inhibition is therefore a potentially beneficial therapeutic strategy for the treatment of T2D.

Numerous Kinase Inhibitors Protect β-Cells From GLT.

Several lead compounds from the Broad Repurposing Collection were annotated kinase inhibitors (Table 3.5.10). We found that 623 of the 4,829 compounds with annotated targets had at least one kinase as a target, and that of these, 58 were screening hits (nominal p-value $1.8 * 10^{-22}$). These included inhibitors of cyclin-dependent kinases (CDK) (AZD5438 and palbociclib), PI-3 kinase (PI3K) (AZD8186, TGX-221, PIK-93, ETP-45658, taselisib (GDC-0032), GSK2126458 (omipalisib), and duvelisib), mTOR (ETP-46464 and torin-2), Rho-associated kinase 2 (ROCK2) (KD025 (SLx-2119)), JAK2 (LY2784544 and AT-9283), and Aurora A/B kinase (PF-03814735). Using the HCFM assay, we calculated EC_{50} values for these kinase inhibitors and identified ETP-45658, ETP-46464, PIK-93, taselisib, and GSK2126458 as potent compounds that recovered INS-1E viability >85% compared to control (Figure 3.5.9, Table 3.5.10). The kinase inhibitor neratinib was previously identified as GLT-protective in INS-1E and rodent models.[13] The mechanism by which it was shown to be GLT-protective was via STK4/MST1 inhibition, a novel activity for the FDA-approved dual HER2/EGFR inhibitor. Our study reveals that a wide selection of inhibitors against several kinase families are β-cell protective, suggesting a variety of kinases regulate β-cell viability and function. However, further studies will be needed to investigate whether these kinases are their β-cell relevant targets, or if like neratinib other novel targets are responsible. We also found that several of these kinases were able to partially restore Pdx1

expression in INS-1E cells treated with GLT media (Figure 3.5.11). Pdx1 is a β-cell specific

transcription factor and its expression is known to decrease in β-cells experiencing GLT.[13,40]

Encouragingly, top hits ETP-45658, ETP-46464, PIK-93, and taselisib significantly restored Pdx1

expression.
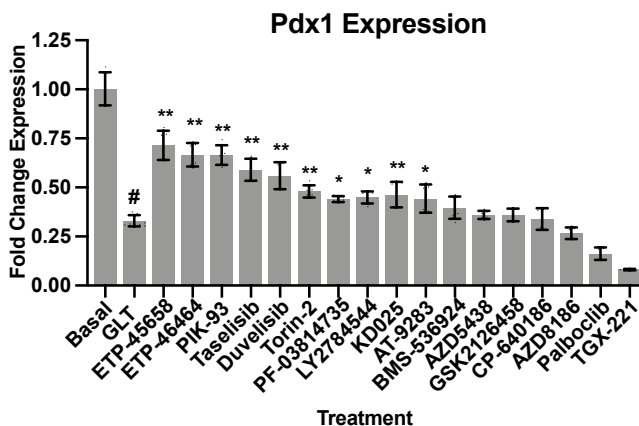
Figure 3.5.11. Pdx1 expression in GLT treated INS-1E cells. 32 hours of GLT treatment decreases Pdx1 expression. Several compounds significantly increase Pdx1 expression, namely: ETP-45658, ETP-46464, PIK-93, taselisib, duvelisib, torin, PF-03814735, LY2784544, KD025, and AT-9283. Statistical significance was evaluated using an unpaired, one-tailed t-test for each compound compared to GLT alone. (#, P < 0.0001; *, P < 0.001; **, P < 0.0001).

Decreased Calcium Flux and Mitochondrial Re-polarization Coincide with GLT-Protectivity.

The significance of calcium flux and calcium signaling in β-cell survival and health has recently

been implicated via the identification of compounds that protected INS-1E cells from GLT by

decreasing cellular calcium content.[14] GLT treatment impairs β-cell calcium flux, and specifically

increases β-cell calcium content. Using the Calcium 6 dye that generates a fluorescent signal

upon binding to intracellular calcium, we tested whether the kinase inhibitors decreased cellular

calcium influx in INS-1E cells treated with GLT media.[41] KD025 significantly decreased calcium

influx to levels below the GLT control at all concentrations tested (2.5-10 µM) (Figure 3.5.12a).

ETP-45658, ETP-46464, PIK-93, taselisib, duvelisib, palbociclib, TGX-221, and AZD8186

moderately decreased calcium flux to levels below GLT control (2.5-10 µM) (Figure 3.5.12a).

Additionally, we found that the ACC1 inhibitor CP-640186, a non-kinase inhibitor, significantly

decreased GLT-induced calcium influx (Figure 3.5.12a). All other six compounds (torin-2, GSK2126458, LY2784544, AT-9283, BMS-536924, PF-03814735) either had no effect on calcium influx or increased calcium influx (Figure 3.5.12b). Since not all Repurposing Library hits decreased cellular calcium flux, we conclude β-cell protection from GLT can be achieved without lowering cellular calcium content. GLT is also known to affect mitochondrial function, therefore we investigated mitochondrial polarity using flow cytometry and the JC-1 dye.[2,42] Mitochondria were depolarized in INS-1E cells treated with GLT media for 48 hours (Figure 3.5.13a–g). Several of our lead compounds (ETP-45658, ETP-46464, PIK-93, KD025, and CP-640186) reduced GLT-induced mitochondrial depolarization (Figure 3.5.13c–g). The most potent reduction of mitochondrial depolarization was observed with ETP-45658 and CP-640186 (Figure 3.5.13c,g).
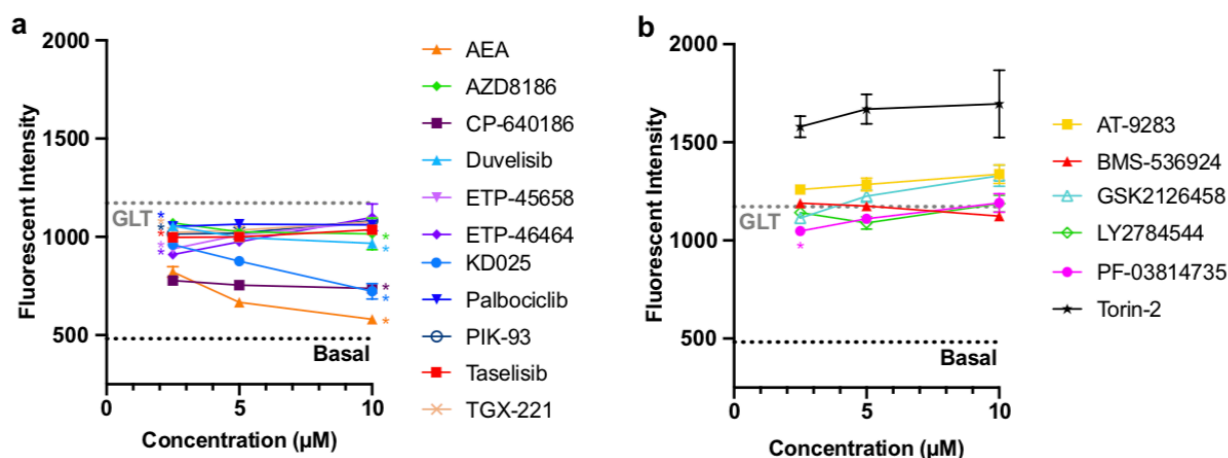
Figure 3.5.12. Lead compounds protect against GLT via decreased calcium flux. a–b) INS-1E cells incubated with Calcium 6 dye to detect cellular calcium content (n=3). Relative to GLT treatment that increased fluorescent intensity in INS-1E cells (i.e., compare fluorescent intensity for basal media control and GLT control), there were a) compounds that significantly decreased GLT-induced calcium flux in a dose dependent manner as well as b) compounds that had little effect on decreasing GLT induced calcium flux. All compounds were treated at n=3. Black dotted line (n=72) represents fluorescent intensity of INS-1E cells incubated in basal culture media. Grey dotted line (n=32) represents fluorescent intensity of INS-1E cells treated with GLT media and DMSO. Statistical significance was evaluated using an unpaired, one-tailed t-test for each compound compared to GLT alone (*, $P < 0.0001$).
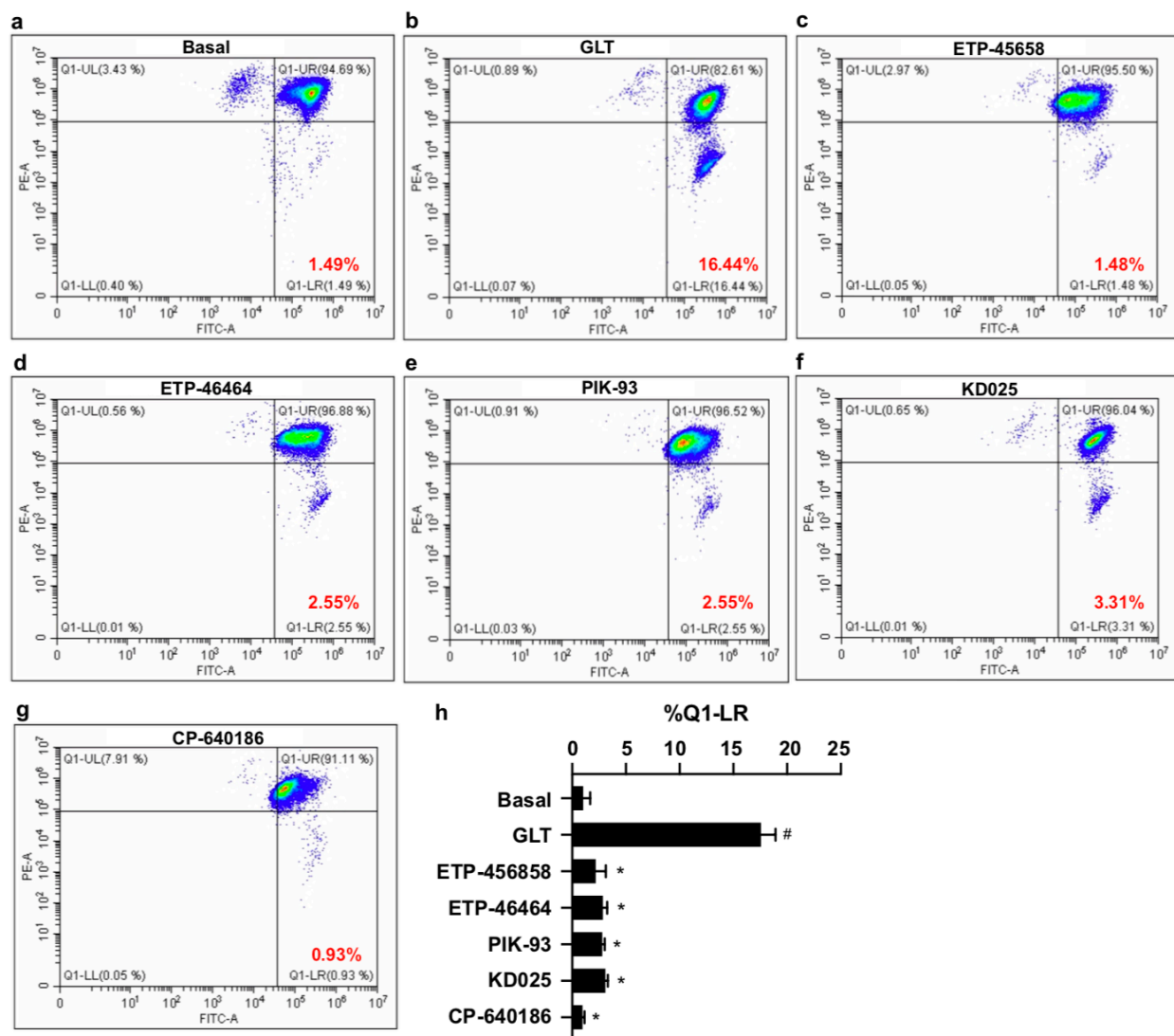
Figure 3.5.13. Lead compounds protect against GLT via decreased mitochondrial depolarization. a–g) INS-1E cells incubated with JC-1 dye to detect mitochondrial depolarization (n=3). For more gating details see Figure 3.4.14. a) JC-1 accumulates in polarized mitochondria and emits Red:Green fluorescence at a 1:1 ratio. b) Moderate mitochondrial depolarization in INS-1E cells as indicated by the decrease in Red:Green ratio. c–d) ETP-45658, ETP-46464, PIK-93, KD025, and CP-640186 improve GLT-induced mitochondrial depolarization. Representative flow graphs from three experiments. h) Quantification of flow cytometry detection of mitochondrial depolarization (n=3). Statistical significance was evaluated using an unpaired, one-tailed t-test (#, P< 0.001 – Basal vs GLT; *, $P < 0.0001$ GLT vs Compound).
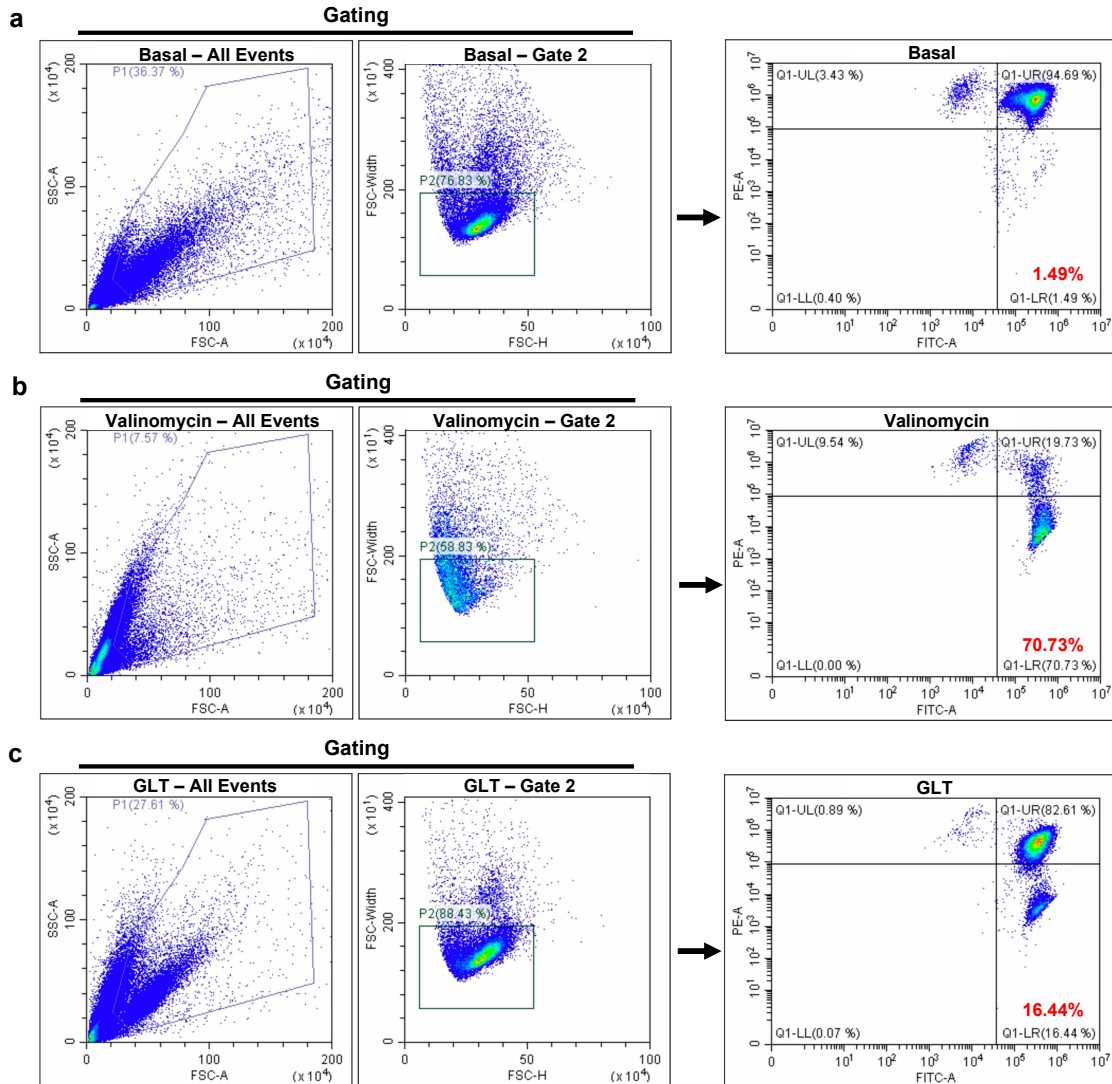
Figure 3.5.14. Gating details for mitochondrial depolarization detection via flowcytometry. a) – c) Gating used for basal, valinomycin, and GLT treatment conditions in INS-1E. b) Valinomycin is used as a positive control to induce mitochondrial depolarization (i.e. decrease in JC-1 Red:Green ratio). c) GLT treatment induces mitochondrial depolarization in INS-1E (i.e. decrease in JC-1 Red:Green ratio).

GLT-Protective Compounds Can Decrease Cytokine Mediated β-Cell Death. We next sought

to determine the specificity of GLT-protective compounds by measuring their effects on

proinflammatory cytokine-induced stress. We treated INS-1E cells with a cocktail of IL-1β, IFN-γ,

and TNF-α without GLT for 48 hours and quantified viability using the HCFM assay. Several

compounds (AT-9283, LY2784544, AZD5438, PF-03814735, and BMS-536924) significantly

recovered INS-1E viability in the presence of cytokines (Figure 3.5.15). AT-9283 and LY2784544 are both JAK inhibitors and JAK inhibition is known to protect diabetic mice and β-cells from cytokine mediated stress.[43,44] AZD5438 is a CDK 1,2, and 9 inhibitor. PF-03814735 and BMS-536924 are multitarget kinase inhibitors with nanomolar potency against several kinase families. The compounds AZD8186, duvelisib, ETP-45658, ETP-46464, KD025, palbocilib, and PIK-93 were toxic at concentrations above 1 μM. GSK2126458, taselib, and torin-2 were toxic at all concentrations tested with cytokine treatment. CP-640186 and TGX-221 though non-toxic, did not recover INS-1E viability. These results indicate that less than half of the seventeen GLT-protective hits were generally β-cell protective.
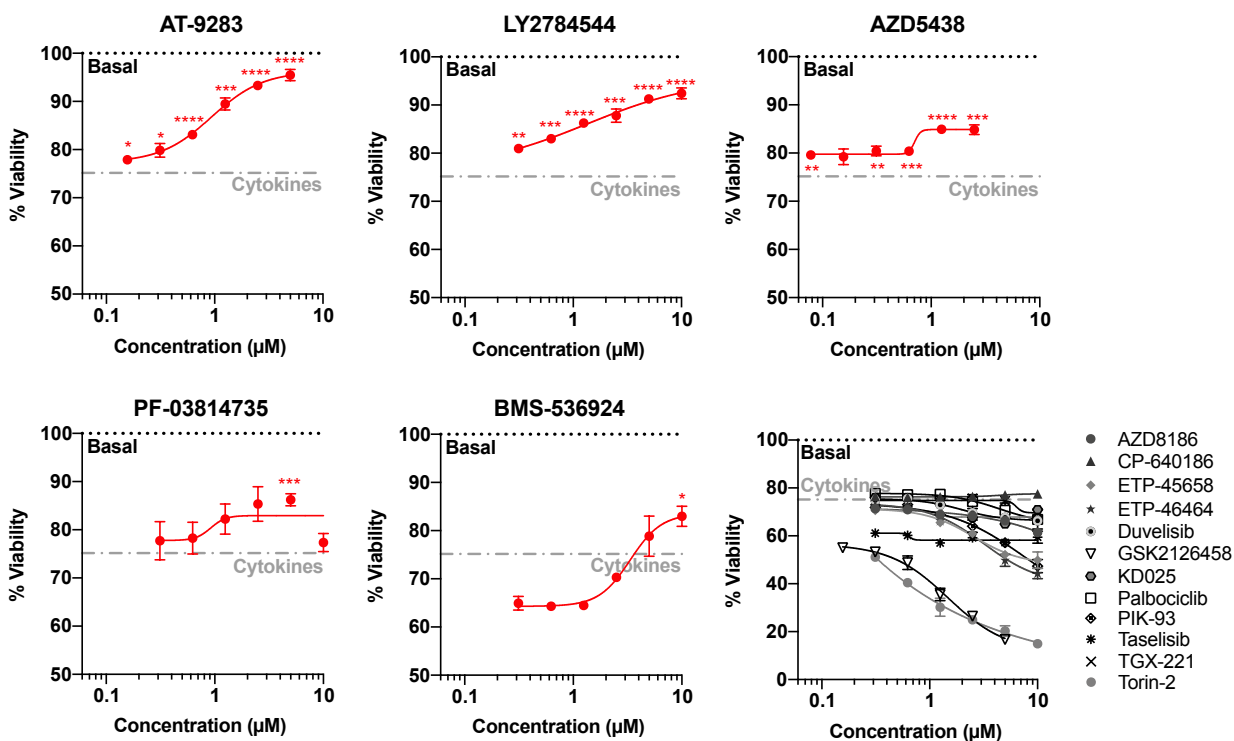
Figure 3.5.15. Compounds variably protect against immune stress. INS-1E cells were treated with compounds and a cytokine cocktail (IL-1β, IFN-γ, and TNF-α). Percent viability classified as DRAQ (-) cells (n=3). Black dotted line (n=24) represents percent viability of cells incubated in basal culture media. Grey dotted line (n=6) represents percent viability of cells treated with cytokine cocktail and DMSO. Statistical significance was evaluated using an unpaired, one-tailed t-test for each compound compared to cytokine treatment alone (*, $P < 0.05$; **, $P < 0.01$; ***, $P < 0.001$; ****, $P < 0.0001$).

Validation in Human Islets.

To further validate the Repurposing Library hits, we tested these compounds in human islets, pancreatic cells that include β-cells and exhibit reduced function in obesity and T2D. Induction of GLT decreased the percent of C-peptide-positive cells by 25% in dissociated islet cells acquired from three donors (Figure 3.5.16). C-peptide is produced in the maturation of insulin. Preproinsulin, translated from insulin mRNA, is cleaved into mature insulin in the ER via the excision of a signal peptide and its C-peptide domains.[45] Therefore, there is a stoichiometric equivalence of C-peptide and mature insulin within β-cells and C-peptide can be used as an alternative insulin detection/quantification method. C-peptide staining is often used to quantify β-cell abundance in patient islets or to quantify blood insulin levels.[46] T2D islets are known to show decreased staining for C-peptide, indicating decreased β-cell mass in these patients. In a potentially therapeutic manner, several compounds (KD025, AZD5438, PF-03814735, ETP-45658, CP-640186, torin-2, BMS-536924, ETP-46464, GSK2126458AT-9283, and AT-9283) significantly increased percent C-peptide-positive cells (Figure 3.5.16). KD025 increased percent C-peptide-positive cells to 110% of basal media (i.e., no evidence of GLT) in several donor samples. Likewise, the other lead compounds (AZD5438, PF-0314735, ETP-45658, CP-640186, torin-2, BMS-536924, ETP-46464) increased percent C-peptide-positive cells albeit these improvements varied between 85-90% compared to the control. CP-640186 was mildly beneficial in human islets increasing percent C-peptide positive cells to approximately 85% of control. The remaining compounds were found to be either inactive or toxic (Figure 3.5.16). Overall, these results in islets validate our results in β-cells and demonstrate these compounds are consistent with the therapeutic strategy of treating diabetes by decreasing β-cell loss in patients.
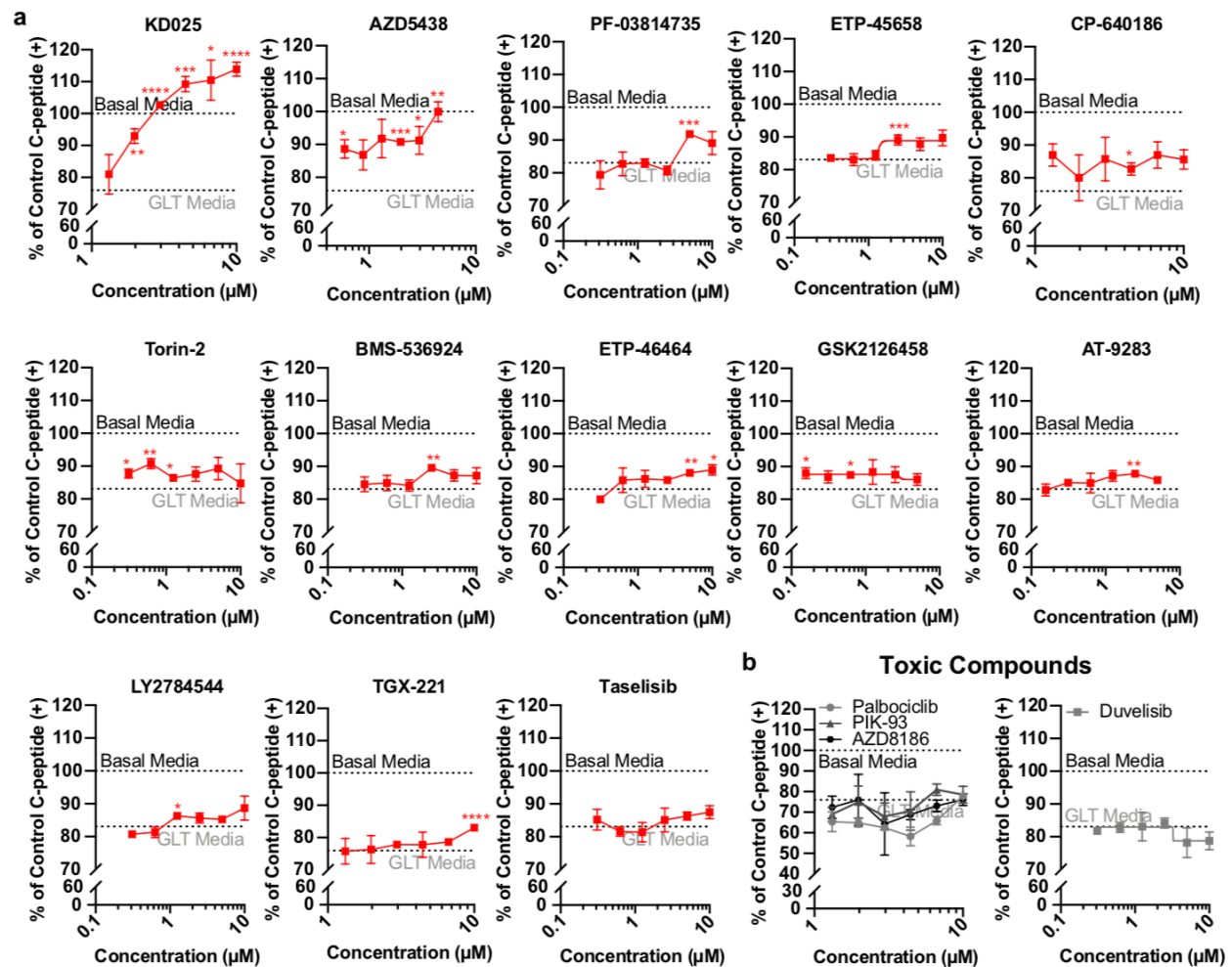
Figure 3.5.16. Compounds protective against GLT in INS-1E cells are also protective in human islets. Quantification of percent C-peptide positive cells relative to basal control revealed a) compounds active in INS-1E cells and human islets and b) compounds active in INS-1E cells but inactive or toxic in human islets (n=3 for all compounds). Black dotted line (n=10 or 18) represents normalized percent of C-peptide positive cells in dissociated human islets incubated in basal culture media for 48 hours. Grey dotted line (n=10 or 18) represents normalized percent of C-peptide positive cells in dissociated human islets incubated in GLT media for 48 hours. These results are representative data from 1-3 donors (Table 3.5.17). Statistical significance was evaluated using an unpaired, one-tailed t-test for each compound compared to GLT alone (*, $P < 0.05$; **, $P < 0.005$; ***, $P < 0.0005$; ****, $P < 0.00005$).

Islet Preparation	1	2	3
Unique identifier	HP-20228-01	SAMN15851500	HP-20252-01
Donor age (years)	36	33	59
Donor sex (M/F)	F	F	F
Donor BMI (kg/m2)	25.8	44.2	28.3
Donor HbA1c or other measure of blood glucose control	5.50%	–	5.50%
Donor Ethnicity	White	White	Hispanic
Origin/source of islets	Prodo Labs	IIDP	Prodo Labs
Islet isolation center	Prodo Labs	University of Wisconsin	Scharp-Lacy Research Institute
Donor history of diabetes? Yes/No	No	No	No
Donor cause of death	Anoxic event	Anoxia	Stroke
Estimated purity (%)	85-90%	85%	90%
Estimated viability (%)	95%	98%	95%

Table 3.5.17. Human Islet Donors. Background information on the three donors of islets used to validate lead compounds in this study.

3.6 Conclusion

In summary, the results of our HTS screen in INS-1E cells and subsequent validation in islets provide new tool compounds for the investigation of β-cell biology in the context of T2D and GLT. Several secondary screening approaches enabled us to eliminate toxic compounds and false positives, which ultimately led to the identification of the herein described β-cell-protective small molecules. Previously validated compounds AEA, AM404, OEA, and SU9516 were identified as GLT protective in our primary screen, in addition to two DOS-derived chemical scaffolds, an ACC inhibitor, and sixteen kinase inhibitors. It was notable that we identified seven phosphoinositide 3-kinase (PI3K) inhibitors as protective against GLT (Table 3.5.10). The PI3K/Akt/FoxO1 signaling pathway has long been implicated in the protection of β-cells from lipotoxic and glucolipoxic stress[47,48]. Our findings contrast with this view and suggest that PI3K signaling may be dispensable for β-cell survival. There are four isoforms of PI3K (α, β, δ, and γ) and partial inhibition of one over the other can have different cellular effects. PI3Kβ inhibition, for example, is known to induce the differentiation and maturation of human embryonic stem cells to β-cells and increase insulin expression[49]. ETP-45658, PIK-93, taselisib, GSK2126458, duvelisib, and AZD8186 all share potent activity towards PI3Kδ. It is thus possible that these annotated PI3K inhibitors are protective against GLT via specific PI3K isoforms and their cellular targets. Future studies examining kinase profiling and gene expression will help shed light on this uncertainty as well as reveal new mechanisms integral to the complex biology underlying the health and survival of β-cells in obesity and T2D.

3.7 References

1.   Boden, G. Obesity and free fatty acids. *Endocrinol. Metab. Clin. North Am.* **37**, 635–646 (2008).

2.   Lytrivi, M., Castell, A. L., Poitout, V. & Cnop, M. Recent insights into mechanisms of β-cell lipo- and glucolipotoxicity in type 2 diabetes. *J. Mol. Biol.* **432**, 1514–1534 (2020).

3.   Leung, M. B. W., Choy, K. W., Copp, A. J., Pang, C. P. & Shum, A. S. W. Hyperglycaemia potentiates the teratogenicity of retinoic acid in diabetic pregnancy in mice. *Diabetologia* **47**, 515–522 (2004).

4.   Kashyap, S. *et al.* A sustained increase in plasma free fatty acids impairs insulin secretion in nondiabetic subjects genetically predisposed to develop type 2 diabetes. *Diabetes* **52**, 2461–2474 (2003).

5.   Storgaard, H., Jensen, C. B., Vaag, A. A., Vølund, A. & Madsbad, S. Insulin secretion after short- and long-term low-grade free fatty acid infusion in men with increased risk of developing type 2 diabetes. *Metabolism* **52**, 885–894 (2003).

6.   Prentki, M. & Corkey, B. E. Are the β-cell signaling molecules malonyl-CoA and cystolic long-chain acyl-CoA implicated in multiple tissue defects of obesity and NIDDM? *Diabetes* **45**, 273–283 (1996).

7.   Poitout, V. *et al.* Glucolipotoxicity of the pancreatic beta cell. *Biochim. Biophys. Acta - Mol. Cell Biol. Lipids* **1801**, 289–298 (2010).

8.   Kim, J.-W. & Yoon, K.-H. Glucolipotoxicity in pancreatic β-cells. *Diabetes Metab. J.* **35**, 444 (2011).

9.   Rojas, J. *et al.* Pancreatic beta cell death: novel potential mechanisms in diabetes therapy. *J. Diabetes Res.* **2018**, 1–19 (2018).

10.   Hagman, D. K., Hays, L. B., Parazzoli, S. D. & Poitout, V. Palmitate inhibits insulin gene expression by altering Pdx-1 nuclear localization and reducing MafA expression in isolated rat islets of langerhans. *J. Biol. Chem.* **280**, 32413–32418 (2005).

11. Kim, J. H., Kim, D. J., Jang, H. C. & Choi, S. H. Epidemiology of micro- and macrovascular complications of type 2 diabetes in Korea. *Diabetes Metab. J.* **35**, 571 (2011).

12. Lee, S. H. *et al.* High-throughput screening and bioinformatic analysis to ascertain compounds that prevent saturated fatty acid-induced β-cell apoptosis. *Biochem. Pharmacol.* **138**, 140–149 (2017).

13. Ardestani, A. *et al.* Neratinib protects pancreatic beta cells in diabetes. *Nat. Commun.* **10**, 1–17 (2019).

14. Vogel, J. *et al.* A phenotypic screen identifies calcium overload as a key mechanism of β-cell glucolipotoxicity. *Diabetes* **69**, 1032–1041 (2020).

15. Wagner, B. K. & Schreiber, S. L. The power of sophisticated phenotypic screening and modern mechanism-of-action methods. *Cell Chem. Biol.* **23**, 3–9 (2016).

16. Chou, D. H. C. *et al.* Synthesis of a novel suppressor of β-cell apoptosis via diversity-oriented synthesis. *ACS Med. Chem. Lett.* **2**, 698–702 (2011).

17. Maianti, J. P. *et al.* Substrate-selective inhibitors that reprogram the activity of insulin-degrading enzyme. *Nat. Chem. Biol.* **15**, 565–574 (2019).

18. Wang, P. *et al.* A high-throughput chemical screen reveals that harmine-mediated inhibition of DYRK1A increases human pancreatic beta cell replication. *Nat. Med.* **21**, 383–388 (2015).

19. Parnaud, G. *et al.* Signaling pathways implicated in the stimulation of β-Cell proliferation by extracellular matrix. *Mol. Endocrinol.* **23**, 1264–1271 (2009).

20. Walpita, D. & Wagner, B. K. Evaluation of compounds in primary human islet cell culture. *Curr. Protoc. Chem. Biol.* **6**, 157–168 (2014).

21. Zhang, J. H., Chung, T. D. Y. & Oldenburg, K. R. A simple statistical parameter for use in evaluation and validation of high throughput screening assays. *Journal of Biomolecular Screening* **4**, 67–73 (1999).

22. Chou, D. H. C. *et al.* Inhibition of histone deacetylase 3 protects beta cells from cytokine-

induced apoptosis. *Chem. Biol.* **19**, 669–673 (2012).

23. Ciregia, F. *et al.* Palmitate-induced lipotoxicity alters acetylation of multiple proteins in clonal β cells and human pancreatic islets. *Sci. Rep.* **7**, 13445 (2017).

24. Stone, V. M. *et al.* The cytoprotective effects of oleoylethanolamide in insulin-secreting cells do not require activation of GPR119. *Br. J. Pharmacol.* **165**, 2758–2770 (2012).

25. Xiong, X. *et al.* SIRT6 protects against palmitate-induced pancreatic β-cell dysfunction and apoptosis. *J. Endocrinol.* **231**, 159–165 (2016).

26. Clemons, P. A. *et al.* The use of informer sets in screening: perspectives on an efficient strategy to identify new probes. *SLAS Discov.* **26**, 855–861 (2021).

27. Gerry, C. J. & Schreiber, S. L. Chemical probes and drug leads from advances in synthetic planning and methodology. *Nat. Rev. Drug Discov.* **17**, 333–352 (2018).

28. Wawer, M. J. *et al.* Toward performance-diverse small-molecule libraries for cell-based phenotypic screening using multiplexed high-dimensional profiling. *Proc. Natl. Acad. Sci. U. S. A.* **111**, 10911–10916 (2014).

29. Corsello, S. M. *et al.* The drug repurposing hub: a next-generation drug library and information resource. *Nat. Med.* **23**, 405–408 (2017).

30. Zhu, T. *et al.* Hit identification and optimization in virtual screening: practical recommendations based on a critical literature analysis. *J. Med. Chem.* **56**, 6560–6572 (2013).

31. Wlodkowic, D. *et al.* Kinetic viability assays using DRAQ7 probe. *Curr. Protoc. Cytom.* **65**, 1–10 (2013).

32. Kudryavtsev, I., Serebryakova, M., Solovjeva, L., Svetlova, M. & Firsanov, D. Rapid detection of apoptosis in cultured mammalian cells. in 105–111 (2017). doi:10.1007/978-1-4939-7187-9_8

33. Akagi, J. *et al.* Real-time cell viability assays using a new anthracycline derivative DRAQ7®. *Cytom. Part A* **83A**, 227–234 (2013).

34. Wong, D. W., Gan, W. L., Teo, Y. K. & Lew, W. S. Interplay of cell death signaling pathways mediated by alternating magnetic field gradient. *Cell Death Discov.* **4**, 49 (2018).

35. Hasegawa, T., Shimada, S., Ishida, H. & Nakashima, M. Chafuroside B, an oolong tea polyphenol, ameliorates UVB-induced DNA damage and generation of photo-immunosuppression related mediators in human keratinocytes. *PLoS One* **8**, e77308 (2013).

36. Lowe, J. T. *et al.* Synthesis and profiling of a diverse collection of azetidine-based scaffolds for the development of CNS-focused lead-like libraries. *J. Org. Chem.* **77**, 7187–7211 (2012).

37. Maji, B. *et al.* A high-throughput platform to identify small-molecule inhibitors of CRISPR-Cas9. *Cell* **177**, 1067-1079.e19 (2019).

38. Dančík, V. *et al.* Connecting small molecules with similar assay performance profiles leads to new biological hypotheses. *J. Biomol. Screen.* **19**, 771–781 (2014).

39. Harwood, H. J. *et al.* Isozyme-nonselective N-substituted bipiperidylcarboxamide acetyl-CoA carboxylase inhibitors reduce tissue malonyl-CoA concentrations, inhibit fatty acid synthesis, and increase fatty acid oxidation in cultured cells and in experimental animals. *J. Biol. Chem.* **278**, 37099–37111 (2003).

40. Kornelius, E. *et al.* Liraglutide protects against glucolipotoxicity-induced RIN-m5F β-cell apoptosis through restoration of PDX1 expression. *J. Cell. Mol. Med.* **23**, 619–629 (2019).

41. Law, B. Y. K. *et al.* N-desmethyldauricine induces autophagic cell death in apoptosis-defective cells via Ca2+ mobilization. *Front. Pharmacol.* **8**, (2017).

42. Perelman, A. *et al.* JC-1: alternative excitation wavelengths facilitate mitochondrial membrane potential cytometry. *Cell Death Dis.* **3**, e430–e430 (2012).

43. Chou, D. H.-C. *et al.* Kinase-independent small-molecule inhibition of JAK-STAT signaling. *J. Am. Chem. Soc.* **137**, 7929–7934 (2015).

44. Trivedi, P. M. *et al.* Repurposed JAK1/JAK2 inhibitor reverses established autoimmune

insulitis in NOD mice. *Diabetes* **66**, 1650–1660 (2017).

45. Liu, M., Wright, J., Guo, H., Xiong, Y. & Arvan, P. Proinsulin entry and transit through the endoplasmic reticulum in pancreatic beta cells. in 35–62 (2014). doi:10.1016/B978-0-12-800174-5.00002-8

46. Leighton, E., Sainsbury, C. A. & Jones, G. C. A ractical review of C-peptide testing in diabetes. *Diabetes Ther.* **8**, 475–487 (2017).

47. Joly, E. *et al.* Glucagon-like peptide-1 prevents beta cell glucolipotoxicity. *Diabetologia* **47**, 806–815 (2004).

48. Shao, S. *et al.* Protective action of liraglutide in beta cells under lipotoxic stress via PI3K/Akt/FoxO1 pathway. *J. Cell. Biochem.* **115**, 1166–1175 (2014).

49. Mao, G. hong *et al.* Role of PI3K p110β in the differentiation of human embryonic stem cells into islet-like cells. *Biochem. Biophys. Res. Commun.* **488**, 109–115 (2017).

Chapter 4

KD025 Suppresses Glucolipotoxicity by Inhibiting Casein Kinase 2

4.1 Attribution

Jonnell C. Small, Kaycee Carbon, Ayushi Agrawal, Amedeo Vetere, and Bridget K. Wagner*

Author Contributions

JCS screened ROCK inhibitors in INS-1E, performed knockdown and overexpression experiments, completed the RNA-Sequencing analysis and visualization, and wrote the manuscript. AV assisted with overexpression experiments. KC conducted cytokine treatment experiments. AA assisted with RNA-Sequencing analysis. BKW participated in design of study.

Acknowledgements

This chapter is a draft of a manuscript in preparation.

4.2 Abstract

We previously identified KD025 as a glucolipotoxicity (GLT)-protective compound in INS-1E and dissociated human islets. KD025 is annotated as a ROCK2 inhibitor and we screened other pan-ROCK inhibitors like SR3677 and H-1152 to determine whether ROCK2 inhibition was responsible for KD025 GLT-protectivity. We found that KD025 was the only ROCK inhibitor to be GLT-protective in INS-1E and *Rock2* knockdown in GLT-treated INS-1E had no effect on viability. We then profiled the kinase targets for KD025, SR3677, and H-1152 to identify KD025 specific targets. We found that KD025 potently inhibited casein kinase 2 (CK2) subunits α (CK2α) and α' (CK2α'). CX4945, a potent CK2 inhibitor, was equally as GLT-protective as KD025 in INS-1E. Knockdown experiments validated that CK2α but not CK2α' loss improved INS-1E viability in GLT. Overexpression of CK2α in INS-1E ablated KD025 GLT-protectivity. We therefore concluded KD025 was GLT-protective due to CK2 inhibition. RNA-sequencing analysis of GLT-treated INS-1E cells co-incubated with 10 µM KD025 for 6, 12, and 24hr hours revealed KD025 partially reverses the GLT-induced gene signature in INS-1E. KD025 treatment reverses genes found in the Hallmark Hypoxia, Hallmark Inflammatory Response, and Hallmark TNFα Signaling via NFκB gene sets. KD025 treatment also recovered the expression of Hallmark Pancreas Beta Cells genes decreased by GLT treatment.

4.3 Introduction

The global obesity and type 2 diabetes (T2D) epidemics continue to grow.[1] In 2045, it is estimated 780 million adults will live with T2D.[2] While there are several approved therapeutic strategies to treat T2D, none address the underlying issue of β-cell dysfunction, failure, and ultimate death in patients.[3] The onset of obesity is associated with elevated free fatty acids (FFAs) due to reduced FFA clearance and expansion of adipose tissue, and these elevated FFAs are thought to contribute to T2D development by promoting insulin resistance and pancreatic β-cell dysfunction.[4,5] Elevated plasma glucose in conjunction with elevated FFAs exert a synergistic effect on β-cell dysfunction known as glucolipotoxicity (GLT).[6–9] GLT decreases insulin gene expression, impairs glucose-stimulated insulin secretion (GSIS), and activates β-cell apoptotic machinery.[10] Motivated by the absence of strategies to suppress GLT-induced β-cell loss in T2D, we previously performed a phenotypic screen in INS-1E and identified KD025, also known as SLx-2119 and Belumosudi, as GLT-protective (Chapter 3).[11,12] We showed that KD025 reversed several hallmarks of the GLT-response in β-cells, including decreasing mitochondrial depolarization, decreasing calcium influx, and increasing *Pdx1* expression (Chapter 3).

KD025 is a ROCK2 inhibitor with specificity that is rare among the Rho-associated kinase (ROCK) inhibitor class.[13] When bound to GTP, RhoA activates ROCK1/2 which go on to phosphorylate several substrates.[14] The isoforms ROCK1 and ROCK2 share ~90% sequence homology in their kinase domain, making it extremely challenging to develop isoform specific inhibitors.[15] ROCK inhibition as a therapeutic strategy gained popularity with the discovery of Rho/ROCK pathway involvement in several diseases, including vascular disease, cancer, asthma, glaucoma, kidney failure, osteoporosis, and neuronal degenerative disease.[14,16] The pan-ROCK inhibitor fasudil was the first to be clinically approved in Japan in 1995 for the treatment of cerebral vasospasm, but more recently, KD025 has been FDA-approved for the treatment of chronic graft-versus-host disease (GVHD).[12] The ROCK2 specificity of this small molecule sets it apart from several family

members and therefore presented a fascinating hypothesis: was the ROCK2 inhibition of KD025 responsible for its GLT-protective activity?

ROCK inhibition with H-1152 was recently shown to promote maturation of human pluripotent stem cells (hPSCs) to β-like cells by increasing the expression of β-cell markers *NKX6.1, INS, UCN3, G6PC2,* and *MAFA*.[17] RNA-sequencing analysis revealed H-1152 increased the expression of genes associated with improved glucose-sensitivity and β-cell maturation.[17] Knockdown experiments then showed *ROCK2* but not *ROCK1* loss phenocopied H-1152 treatment, increasing insulin positive cells produced from differentiated hPSCs, increasing expression of β-cell maturity markers, and improving glucose stimulation.[17]

Motivated to determine the mechanism of KD025 GLT-protectivity, we screened seven pan-ROCK inhibitors in GLT-treated INS-1E to identify any that were GLT-protective. We found that KD025 alone recovered both INS-1E viability and percent C-peptide in dissociated human islets treated with GLT media. Additionally, *Rock2* knockdown in GLT-treated INS-1E had no effect on viability. Hypothesizing that some other kinase target was responsible for KD025 GLT-protectivity, we kinase profiled KD025, SR3677, and H-1152 and found KD025 alone had potent inhibitory activity towards *Csnk2a1*, *Csnk2a2, and Mrckb*. Co-treatment of potent casein kinase 2 (CK2) inhibitor CX4945 improved GLT-treated INS-1E viability similarly as KD025 and knockdown studies revealed *Csnk2a1*, but not *Csnk2a2* loss improved GLT-treated INS-1E viability. Overexpression of *Csnk2a1* completely ablated INS-1E KD025 GLT-protectivity. We therefore concluded casein kinase 2α (CK2α) inhibition was the means through which KD025 was GLT-protective. RNA-sequencing analysis of GLT-treated INS-1E showed that KD025 partially reversed the GLT-gene signature, recovering expression of Hallmark Pancreas Beta Cell genes and downregulating genes involved in hypoxia, inflammatory response, and TNFα signaling through NFκB. These results further clarify the role of casein kinase 2 in mediating β-cell

apoptosis in GLT and suggest casein kinase inhibition is a feasible therapeutic strategy for mitigating β-cell death in T2D.

4.4 Methods

Cell culture. INS-1E cells (generously provided by Claes Wollheim and Pierre Maechler, University of Geneva, Switzerland) were cultured in RPMI 1640 supplemented with 10% FBS, 1% Pen/Strep, 1% sodium pyruvate, and 50 µM β-mercaptoethanol. Cells were maintained in flasks precoated with diluted supernatant (1:10) from the rat 804G cell line (804G matrix). 804G cells are a rat cancer cell line known to secrete a laminin-5 rich extracellular matrix. 804G cells were a generous gift of Susan Bonner-Weir Lab, Joslin Diabetes Center. The 804G matrix induces spreading, improves glucose-stimulated insulin secretion, and increases survival and proliferation of rat pancreatic β-cells.[18] GLT media for INS-1E consisted of RPMI 1640 supplemented with 1% FBS, 1% Pen/Strep, 1% fatty acid free BSA, 50 µM β-mercaptoethanol, 25 mM glucose, and 0.5 mM sodium palmitate. Sodium palmitate was dissolved in warmed 4% BSA in PBS before being added to RPMI1650.

Human islets. Islets were obtained from the Integrated Islet Distribution Program (IIDP) and Prodo Laboratories, and cultured in CMRL 1066 supplemented with 10% FBS, 1% Pen/Strep, and 2 mM GlutaMAX. Islets were washed with PBS, incubated with acutase for 20 minutes at 37°C, and cell culture media added to terminate enzymatic dissociation. Cells were then strained, counted and plated on flasks pre-treated with conditioned media from the human bladder carcinoma cell line HTB-9[19]. GLT media for human islets consisted of CMRL 1066 supplemented with 1% fatty acid free BSA, 1% FBS, 30 mM glucose and 1 mM sodium palmitate.

Compounds. Compounds were purchased commercially for ROCK1/2 and CK2 inhibition studies: CX4945 (Silimitasertib), KD025 (SLx-2119), Y-27632, Fasudil, (Selleckchem); Rho Kinase Inhibitor V, SR3677 (Sigma-Aldrich); and AS-1892802, GSK429286A, (S)-H-1152, RKI-1447 (Cayman Chemical). Stock solutions were prepared in DMSO and stored as per manufacturer instructions. Compounds were added to 96- and 384-well plates using Tecan D300e drug printer.

Microscopy.

High-Content Fluorescent Microscopy (HCFM) Assay: Live INS-1E cells were stained with DNA dye Hoechst 33342 (all cells), Caspase 3/7 activation dye CellEvent™ Caspase-3/7 (apoptotic cells), and live cell impermeable DNA dye DRAQ7 (dead cells) all at 1:5000 dilution for 1.5 hours. Cells were imaged at the magnification 5X and 10X using an Opera Phenix High-Content Imaging Instrument (PerkinElmer). Caspase-negative/positive and DRAQ7-negative/positive cells were quantified using Harmony software (PerkinElmer).

Immunofluorochemistry. INS-1E cells were fixed with 3% PFA for 20 minutes, permeabilized with 0.2% Triton X-100 in PBS for 20 minutes and blocked with 2% BSA in PBS for 2-3 hours at room temperature with gentle shaking. Cells were incubated with Flag antibody (Sigma-Aldrich, Cat. no: F1804) overnight at 4°C. After thorough washing with PBS and 1% BSA in PBS, cells were incubated with secondary antibody conjugated to Alex Fluor 594 (Invitrogen, #A11037) and Hoechst 33342, all in 2% BSA in PBS for 1 hour at room temperature. Cells are washed five times with PBS and then stored at 4°C. Cells were imaged at the magnification 20X using an Opera Phenix High-Content Imaging Instrument (PerkinElmer).

Human Islet Staining: Human islets were fixed with 3% PFA for 20 minutes, permeabilized with 0.2% Triton X-100 in PBS for 20 minutes, blocked with 2% BSA in PBS for 2-3 hours at room temperature with gentle shaking, and then incubated with C-peptide antibody (Developmental Studies Hybridoma Bank, GN-ID4) in 2% BSA in PBS overnight at 4°C. After thorough washing with PBS and 1% BSA in PBS, cells were incubated with secondary antibody conjugated to AlexaFluor 568 (Invitrogen) and Hoechst 33342, all in 2% BSA dissolved in PBS for 1 hour at room temperature. Cells are washed five times with PBS and then stored at 4°C. Cells were imaged at the magnification 10X and 20X using an Opera Phenix High-Content Imaging Instrument (PerkinElmer), and percent C-peptide positive cells quantified using Harmony software (PerkinElmer).

Induction of ER Stress with Thapsigargin. INS-1E cells were plated at 5,000 cells/well in 384-well plates pretreated with supernatant from 804G cells. After 24 hours in regular media conditions, media was removed from plates using a Multidrop Combi plate dispenser (ThermoFisher), and basal INS-1E media supplemented with 6.67 µM thapsigargin added at 35 µL/well.

Proinflammatory cytokine treatment. Immune stress was induced as previously described.[20] INS-1E cells were plated at 8,000 cells/well in a 384-well plate coated with 804G matrix and incubated at 37°C overnight. Basal media was then removed and replaced with media containing cytokines (R&D Systems) specifically RPMI media, 1% FBS, 10 ng/mL IL-1β, 100 ng/mL IFN-γ , and 25 ng/mL TNFα. Working concentrations of compounds were printed into the 384-well plates using a Tecan D300e drug printer. Plates were incubated at 37°C for 48 hours and cell viability was detected using CellTiter-Glo (Promega).

Kinase Profiling. Kinase profiling of KD025, SR3677, and H-1152 was performed by Eurofins DiscoverX KINOMEscan™ scanMAX agains 468 targets.[21] KD025, SR3677, and H-1152 were both screened at 1000 nM. Briefly, streptavidin-coated magnetic beads were treated with biotinylated small molecule ligands for 30 minutes at room temperature to generate affinity resins for kinase assays. Liganded beads were blocked with excess biotin and washed with blocking buffer to remove unbound ligand and reduce non-specific binding. Binding reactions were assembled by combining kinases, ligand affinity beads, and test compounds in binding buffer. Test compounds were prepared as 40x stocks in DMSO and directly diluted into assay. Assay reactions were performed in 384-well plate and incubated at room temperature. Beads were re-suspended in elution buffer and incubated at room temperature with shaking for 30 minutes. The kinase concentration in the eluates was measured by qPCR and used to calculate percent kinase activity compared to control.

siRNA Knockdown. Lipofectamine RNAiMAX was used for siRNA transfection in INS-1E. INS-1E cells were plated 5,000 cells per well in 96-well plate format and transfected with 10 pmol of siRNA. Transfected cells were left to incubate for 72-96 hours at 37°C. For GLT treatment, basal media was removed, GLT media added and cells incubated for another 48 hours at 37°C. siRNA knockdown was validated via Western blotting and qPCR. siRNA was purchased from Sigma-Aldrich: *Rock2* (SASI_Rn01_00030374), *Csnk2a1* (SASI_Rn01_00051446), and *Csnk2a2* (SASI_Rn02_00228536).

Overexpression. Lipofectamine RNAiMAX was used for transfection of INS-1E cells with *Csnk2a1-Flag* expression clone EX-Rn14990-M14 (Genecopoeia). INS-1E cells were plated 5,000 cells per well in 96-well plate format and transfected with 300ng of EX-Rn14990-M14 vector. Transfected cells were left to incubate for 72 hours at 37°C. For GLT treatment, basal

media was removed, GLT media added and cells incubated for another 48 hours at 37°C. CK2α overexpression was validated via Western blotting using anti-Flag.

Gene Expression. Cellular RNA was isolated from INS-1E cells 72 hours after transfection using RNeasy Plus Mini Kit (Qiagen). qPCR was performed using purified RNA, TaqMan RNA-to-Ct 1-Step Kit (ThermoFisher), and the following TaqMan probes (ThermoFisher): Hprt1 (Rn01527840_m1), Mrpl19 (Rn01425270_m1), Pdx1 (Rn00755591_m1), Csnk2a1 (Rn01535979_m1), and Csnk2a2 (Rn01574256_m1). qPCR samples were normalized to Hprt1 and Mrpl19 expression levels. Pdx1 expression levels were normalized relative to basal treated INS-1E.

Western Blotting. INS-1E cells transfected with siRNA or *Csnk2a1-Flag* vector were trypsinized, washed twice with cold PBS and pelleted for storage at -80°C. Thawed cell pellets were lysed in RIPA lysis buffer (Thermo Fisher) containing 25 mM Tris-HCl pH 7.6, 150 mM NaCl, 1%NP-40, 1% sodium deoxycholate, and 0.1% SDS. Protein concentration was quantified using BCA protein assay (Thermo Fisher). Approximately 20-35 µg of protein lysate was run on a Bolt 4-12% Bis-Tris SDS-Page gel (Thermo Fisher) and electrically transferred to PVDF membranes either by wet transfer (ROCK2) using XCell II Blot Module (Thermo Fisher) or semi-dry transfer using iBlot 2 system (Csnk2a1/2) (Thermo Fisher). PVDF membranes were washed with TBST and incubated with SuperBlock Blocking Buffer in TBS (ROCK2) (Thermo Fisher) or Intercept (TBS) Blocking Buffer (Csnk2a1/2) (Li-Cor) for 1 hour at room temperature. Primary antibody incubation was 1:1000 overnight at 4°C: mouse anti-ROCK2 (BD Biosciences, Cat no: 610623), rabbit anti-actin-β (Cell Signaling, #4967), rabbit anti-Csnk2a1 (Thermo Fisher, Cat no: PA5-28686), rabbit anti-Csnk2a2 (Thermo Fisher, Cat no: PA5-109601), rabbit anti-Hprt1 (Thermo Fisher, Cat no: PA5-22281). Secondary antibody incubation was for 1 hour at room temperature: anti-Rabbit

HRP-linked (#7074), anti-Mouse HRP-linked (#7076) (Cell Signaling), anti-Rabbit IRDye 680 RD (Li-Cor), anti-Rabbit IRDye 800 CW (Li-Cor). Membranes incubated with HRP-linked antibodies were developed using Azure c600 imager (Azure Biosystems). Membranes incubated with Li-Cor antibodies developed using Odyssey DLx imager (Li-Cor). Uncropped scans of all Western blots available.

RNA-sequencing analysis.

Differential Expression. INS-1E cells were incubated with basal media, GLT media, or GLT media supplemented with 1 or 10 µM KD025 for 6, 12, or 24 hours. Cells were trypsinized, pelleted, and RNA extracted using RNeasy Mini Kit (Qiagen). RNA sequencing was performed by Genewiz using Illumina HiSeq paired-end sequencing. FastQC (v.0.11.9) was used to quality check RNA-sequencing results, which performed with an average of 35-42 million reads per sample. Paired-end sequences where then trimmed with Trimmomatic (v.0.39) and RNA-sequencing reads aligned to the *R. norvegicus* genome (mRatBN7.2) using STAR (v.2.7.5c). An average of ~87% reads were uniquely mapped and quantified. Differential expression analysis was performed using DESeq2. DESeq2 analysis accounted for the experimental design of basal media and GLT treated INS-1E. Log transformed gene counts were converted to z-scores and visualized using R pheatmap function.

Gene Set Enrichment Analysis. Normalized gene counts were loaded into GSEA (v.4.1.0) and analyzed using the h.all.v7.5.symbols.gmt gene set database, using 1000 permutations, and the Rat_ENSEMBL_Gene_ID_Human_Orthologs_MSigDB.v7.5.chip Chip platform.[22] All other settings were left at default.

Statistical Analysis. *In vitro* experiments were performed at least three times and quantitative data are presented as mean ± SD. Group means were compared using ANOVA assuming

Gaussian distribution followed by a one-way *t*-test. Statistical analyses were performed using GraphPad Prism software version 8 (GraphPad Software).

4.5 Results

KD025 GLT-protectivity is not Dependent on ROCK2 Inhibition

KD025 is a GLT-protective small molecule in both INS-1E and human islets (Figure 4.5.1a-c). To investigate whether KD025 GLT-protectivity was a result of its ROCK2 activity, we tested several pan-ROCK inhibitors including SR3677, H-1152, Y-27632, fasudil, Rho Kinase Inhibitor V, AS-1892802, GSK429286A, and RKI-1447 in INS-1E and human islets treated with GLT media (Table 4.5.2). We found that KD025 alone preserved β-cell viability in GLT (Figure 4.5.1b-c). Additionally, we found that specific knockdown of *Rock2* in INS-1E did not confer protection against glucolipotoxicity (Figure 4.5.1e-f). KD025 β-cell protectivity extended to thapsigargin treated INS-1E cells but not cytokine treated INS-1E, indicating it is not generally β-cell protective (Figure 4.5.3).
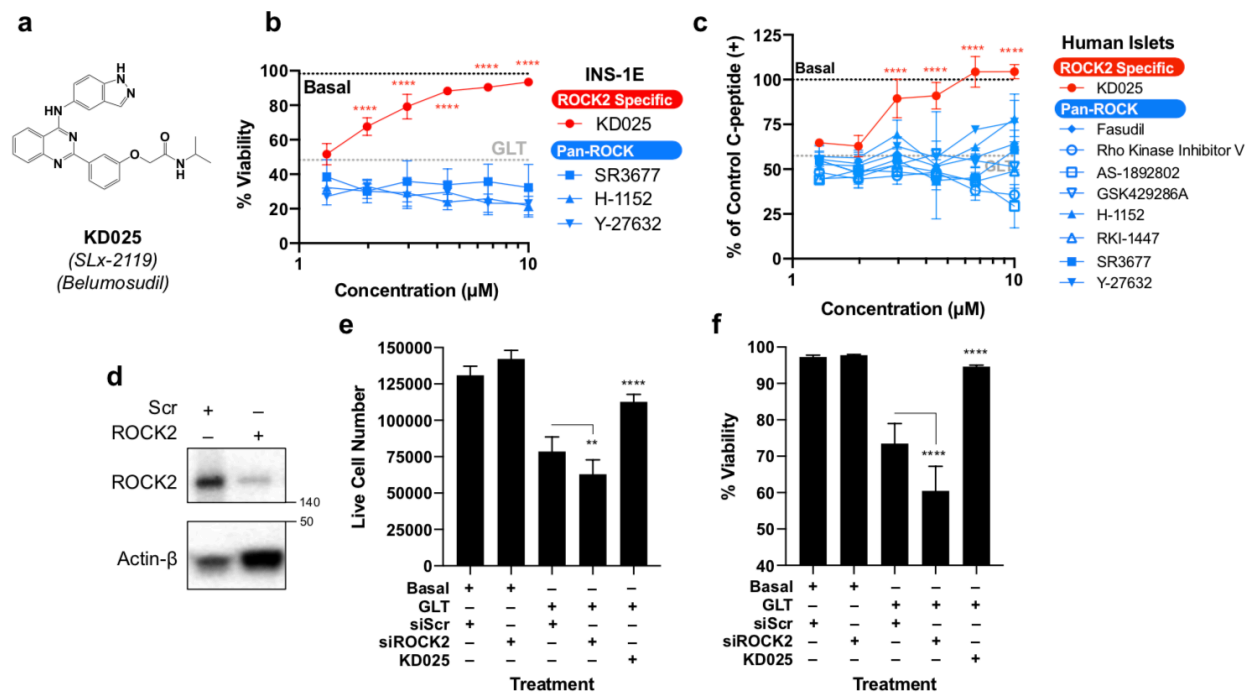
Figure 4.5.1

Figure 4.5.1 (Continued). KD025 is GLT protective in INS-1E and human islets. a) Chemical structure of KD025. b) & c) KD025 recovers the viability of INS-1E cells and human islets treated with GLT media for 48 hours (n=3). Black dotted line (n = 24) represents percent viability of INS-1E cells or human islets incubated in basal culture media. Grey dotted line (n = 24) represents percent viability of INS-1E cells or human islets treated with GLT media and DMSO. d) Validation of 72-hour *Rock2* siRNA knockdown in INS-1E. e) & f) *Rock2* siRNA knockdown does not recover GLT-treated INS-1E viability (n=8), while 10 µM KD025 does. Statistical significance was evaluated using an unpaired, one-tailed t-test for each compound compared to GLT alone. (**, P < 0.01, ****, P < 0.0001).

Table 4.5.2. Comparison of known ROCK1 and ROCK2 IC_{50} values.

ROCK Inhibitor	IC_{50} ROCK1 (nM)	IC_{50} ROCK2 (nM)
KD025	24000	105
Fasudil	267	153
Rho Kinase Inhibitor V	*NA*	1.5
AS-1892802	122	52
GSK429286A	14	63
H-1152	30	12
RKI-1447	14.5	6.2
SR3677	56	32
Y-27632	$K_i = 140$	$K_i = 300$

KD025 is the only ROCK2 specific inhibitor. NA: Rho Kinase Inhibitor V ROCK1 inhibition has not been tested. IC_{50} values were sourced from www.selleckchem.com.
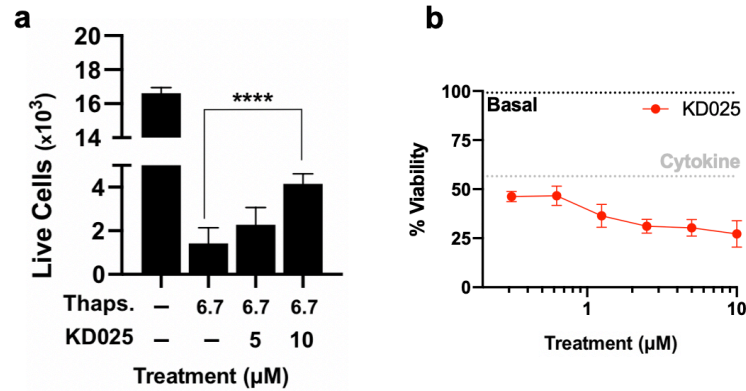
Figure 4.5.3. KD025 is not generally β-cell protective. a) KD025 improves the viability of INS-1E cells treated with 6.7 µM of thapsigargin (ER-stress inducer) for 48 hours (n=4). b) KD025 does not improve the viability of INS-1E cells treated with cytokines for 48 hours (n=3). Statistical significance was evaluated using an unpaired, one-tailed t-test for each compound compared to GLT alone. (****, $P < 0.0001$).

KD025 is a Casein Kinase Inhibitor

We speculated some other target was responsible for KD025 activity and used kinase profiling to screen KD025, SR3677, and H-1152 against 468 kinase targets (Appendix 3.1). The results, summarized in Figure 4.5.4a, show KD025 has potent activity towards casein kinase 2 (CK2) subunits *CSNK2A1* (CK2α) and *CSNK2A2* (CK2α') while pan-ROCK inhibitors SR3677 and H-1152 do not. KD025 also had mild activity towards myotonic dystrophy protein kinase-like β (MRCKB). Kinase profiling revealed H-1152 is a non-selective kinase inhibitor with activity towards several kinase families (Figure 4.5.4b). SR3677 on the other hand had a cleaner inhibition profile than H-1152. To test whether other CK2 inhibitors could also be GLT protective, we tested CX4945 in INS-1E cells treated with 48-hour GLT. We found that potent CK2 inhibitor CX4945 (IC_{50} = 1 nM) was as effective as KD025 at restoring INS-1E viability (Figure 4.5.5).[23]
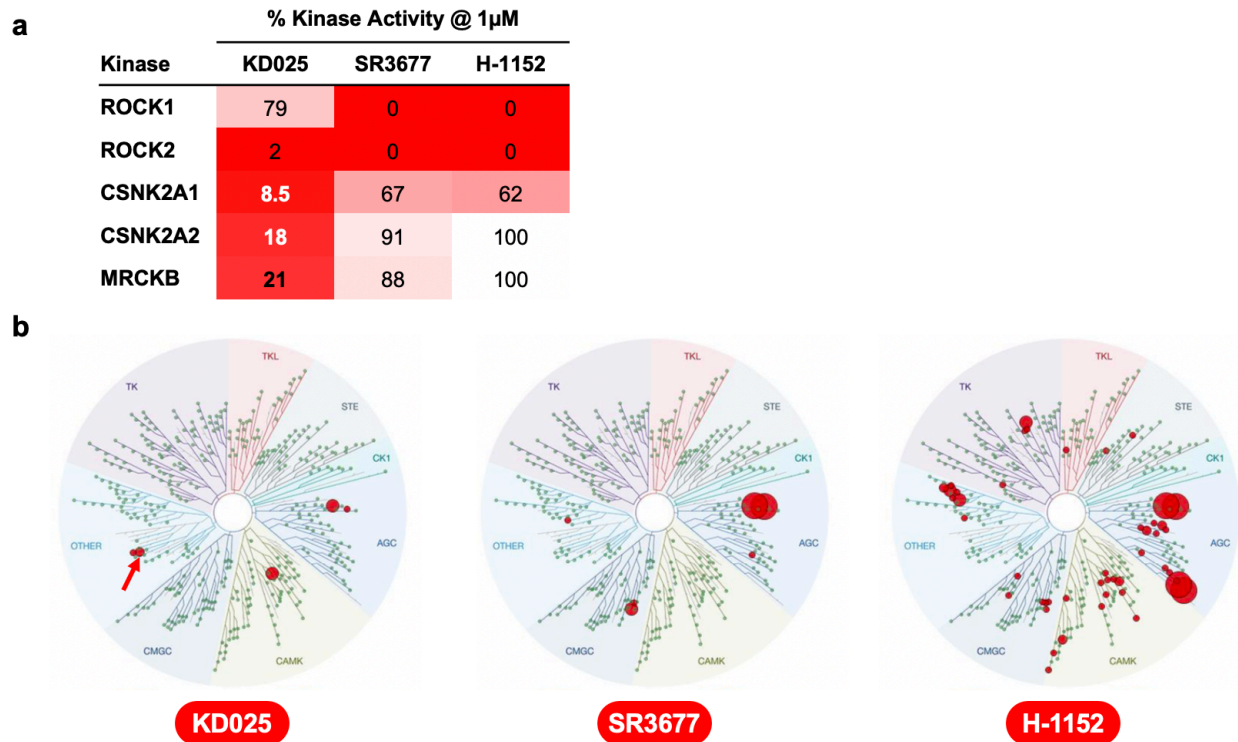
Figure 4.5.4. KD025 is a casein kinase 2 inhibitor. a) Summary of KD025 specific kinase targets from kinase profiling. KD025, SR3677, and H-1152 profiled at 1 µM. b) TREE*spot* visualization of kinase targets for KD025, SR3677, and H-1152. While KD025 and SR3677 are more specific compounds, H-1152 has activity towards several targets. Image generated using TREE*spot*™ Software Tool and reprinted with permission from KINOME*scan®*, a division of DiscoveRx Corporation, © DISCOVERX CORPORATION 2010.
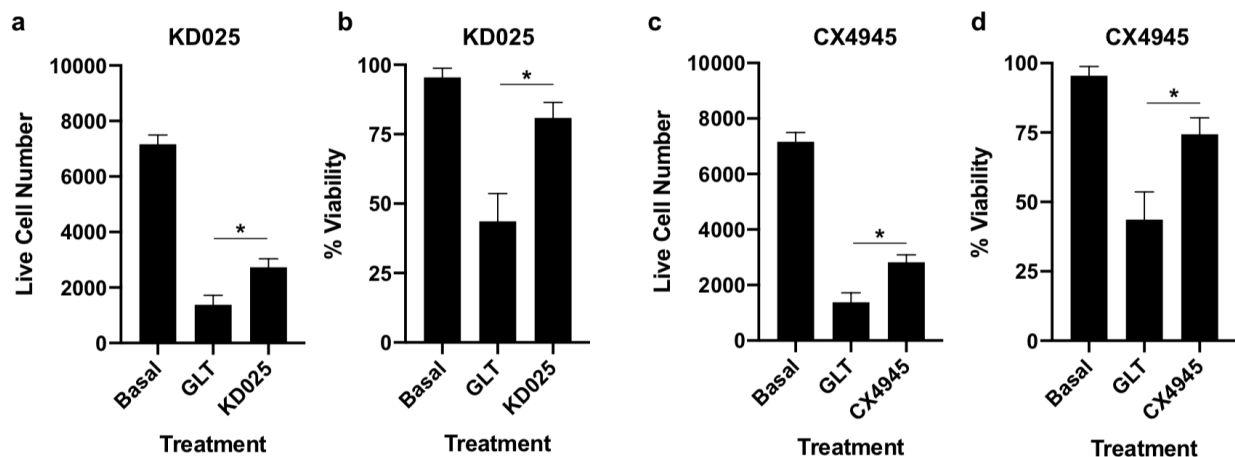
Figure 4.5.5. CK2 inhibition is GLT protective in INS-1E. a) & b) KD025 (10 µM) is GLT-protective in INS-1E treated with GLT media for 48-hours (n=6). c) & d) CX4945 (10 µM) is GLT protective in INS-1E treated with GLT media for 48-hours (n=6). Basal and GLT treatment alone (n=18). Percent viability was determined using the HCFM assay method described in Chapter 2. Statistical significance was evaluated using an unpaired, one-tailed t-test for each compound compared to GLT alone. (*, P < 0.0001).

Casein Kinase 2 inhibition Improves INS-1E Viability in GLT

To validate whether casein kinase 2 (CK2) inhibition was responsible for KD025 GLT-protectivity, we knocked down both isoforms of the catalytically active kinase subunits of CK2 (*Csnk2a1* and *Csnk2a2*) and found that *Csnk2a1* but not *Csnk2a2* knockdown improved INS-1E viability in the presence of GLT media for 48 hours (Figure 4.5.6). We validated *Csnk2a1/2* knockdown down in INS-1E in via qPCR and Western blotting (Figure 4.5.6a,d). While *Csnk2a1* knockdown was not able to increase GLT-treated INS-1E cell number to similar levels as KD025, *Csnk2a1* knockdown improved INS-1E viability to ~65% compared to GLT control (~55%) (Figure 4.5.6b,c). KD025 increased GLT-treated INS-1E viability to ~85% (Figure 4.5.6b,c). Interestingly, *Csnk2a1* knockdown plus 10 μM KD025 treatment improved the viability of GLT-treated INS-1E more than KD025 treatment alone, however, this was accompanied with a decrease in the total number of live cells (Figure 4.5.6c). The knockdown of *Csnk2a2* had no effect on GLT-treated INS-1E viability (Figure 4.5.6e,f). Though *Csnk2a2* knockdown slightly increased INS-1E cell number compared to GLT control, percent viability of these cells was similar to GLT control (Figure 4.5.6e,f). These data suggest there may be differential functions for the two catalytic subunits of CK2 in β-cells.
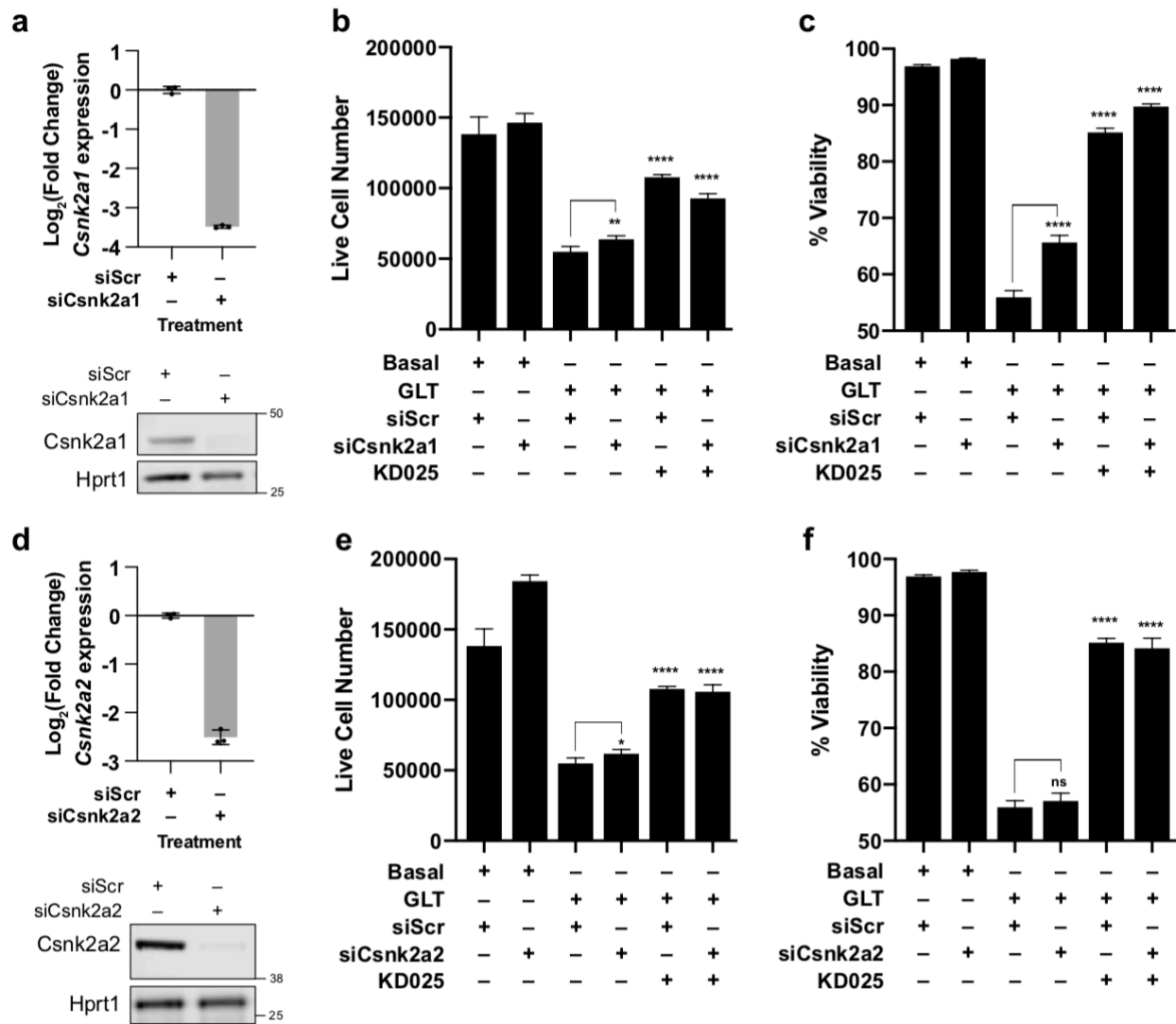
Figure 4.5.6. *Csnk2a1* **knockdown improved GLT-treated INS-1E viability.** a) qPCR validation of 72-hour *Csnk2a1* knockdown in INS-1E. b) Live cell number for INS-1E cells treated with basal or GLT media, with or without *Csnk2a1* knockdown, and with or without 10 µM KD025 treatment (n=6). c) Percent viability for INS-1E cells treated with basal or GLT media, with or without *Csnk2a1* knockdown, and with or without 10 µM KD025 treatment (n=6). d) qPCR validation of 72-hour *Csnk2a2* knockdown in INS-1E. e) Live cell number for INS-1E cells treated with basal or GLT media, with or without *Csnk2a2* knockdown, and with or without 10 µM KD025 treatment (n=6). f) Percent viability for INS-1E cells treated with basal or GLT media, with or without *Csnk2a2* knockdown, and with or without 10 µM KD025 treatment. Statistical significance was evaluated using an unpaired, one-tailed t-test for each compound compared to GLT alone. (*, $P < 0.05$; **, $P < 0.01$; ****, $P < 0.0001$).

Casein Kinase 2 Overexpression Decreases KD025 activity in GLT

We further investigated the role of CK2 inhibition in mediating KD025 GLT-protectivity activity by

overexpressing *Csnk2a1* in INS-1E. We transfected INS-1E with a C-terminal Flag *Csnk2a1*

vector and validated *Csnk2a1*-Flag overexpression via Western blotting and immunofluorescence (Figure 4.5.7a,d). Overexpression of *Csnk2a1*-Flag significantly decreased the viability of INS-1E treated with GLT media for 48 hours (Figure 4.5.7b,c). *Csnk2a1*-Flag expression also seemed to decrease the viability of basal media treated INS-1E, suggesting that overexpression of the kinase activates apoptotic signaling (Figure 4.5.7b,c). When INS-1E overexpressing *Csnk2a1*-Flag were treated with KD025 and GLT media, the GLT-protectivity of KD025 was totally eliminated confirming that *Csnk2a1* inhibition is key to KD025 β-cell activity (Figure 4.5.7b,c).

KD025 Partially Reverses GLT Gene Signature in INS-1E

To investigate KD025 effect on GLT-induced gene expression we performed RNA-sequencing analysis on INS-1E treated with 10 µM KD025 and GLT media for 6, 12, and 24 hours (Figure 4.5.8). We found that the ability of KD025 to reverse the INS-1E GLT-gene signature was dependent on time, with the most GLT-induced gene expression reversal occurring at 24 hours (Figure 4.5.8). GLT-treatment increased the expression of 443, 726, and 1110 genes at 6, 12, and 24 hours in INS-1E and decreased the expression of 157, 331, and 566 genes at 6, 12, and 24 hours in INS-1E (Appendix 3.2.xlsx). GSEA analysis of the 1110 upregulated and 566 downregulated genes at 24 hours revealed enrichment of several Hallmark gene sets involved in stress including: HALLMARK_PEROXISOME, HALLMARK_P53_PATHWAY, HALLMARK_ HYPOXIA, HALLMARK_TNFA_SIGNALING_ VIA_NFKB, HALLMARK_INTERFERON_ ALPHA_RESPONSE, HALLMARK_APOPTOSIS, HALLMARK_INFLAMMATORY_RESPONSE, and HALLMARK_REACTIVE_OXYGEN_ SPECIES_PATHWAY (Figure 4.5.9).
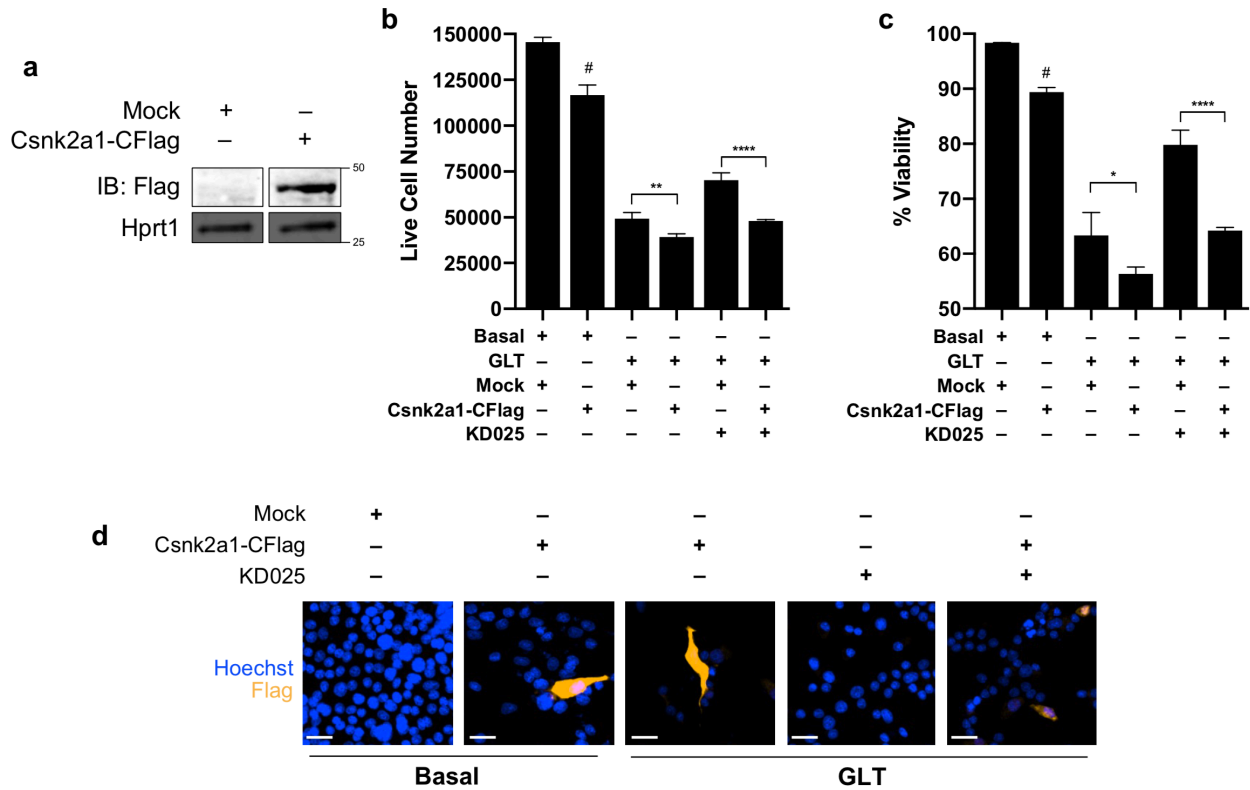
Figure 4.5.7. *Csnk2a1* **overexpression eliminates KD025 GLT-protectivity in INS-1E.** a) Western blot confirmation of C-terminal *Csnk2a1*-Flag fusion overexpression in INS-1E. B) *Csnk2a1* overexpression decreases the live cell number of basally- and GLT-treated INS-1E. INS-1E treated with GLT media for 48 hours. *Csnk2a1* overexpression eliminated KD025 GLT-protectivity in INS-1E (n=4). c) *Csnk2a1* overexpression decreases the percent viability of basally- and GLT-treated INS-1E. INS-1E treated with GLT media for 48 hours. *Csnk2a1* overexpression eliminates KD025 activity in INS-1E (n=4). d) Representative images of immunofluorescence confirmation of *Csnk2a1*-CFlag overexpression in INS-1E treated with and without GLT media and 10 µM KD025. Scale bar: 20nm. Statistical significance was evaluated using an unpaired, one-tailed t-test for each compound compared to GLT alone. (#, P < 0.0001) (*, P < 0.05; **, P < 0.01; ****, P < 0.0001)
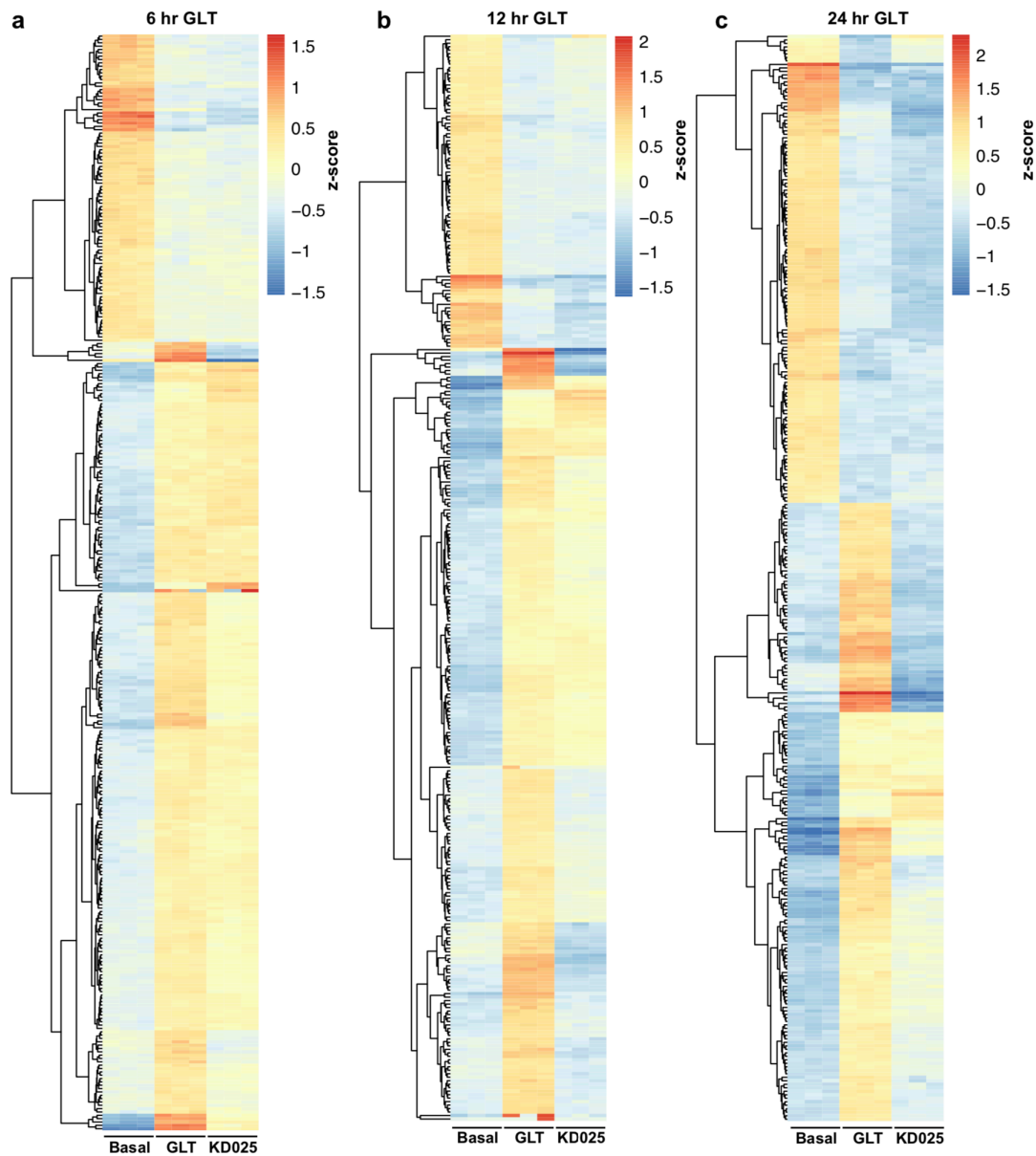
Figure 4.5.8. KD025 partially reverses GLT-induced gene expression signature in INS-1E. a-c) Visualization of RNA-sequencing data for top 300 genes with large variance between z-scores (relative expression) in the basal control and 6, 12, or 24-hour GLT control. N=3 for each treatment condition: basal, 48-hour GLT, and 10 μM KD025. Gene z-score (relative expression) calculated by determining log transformed gene expression variance across each treatment condition. Gene hierarchical clustering represented on left of each figure.
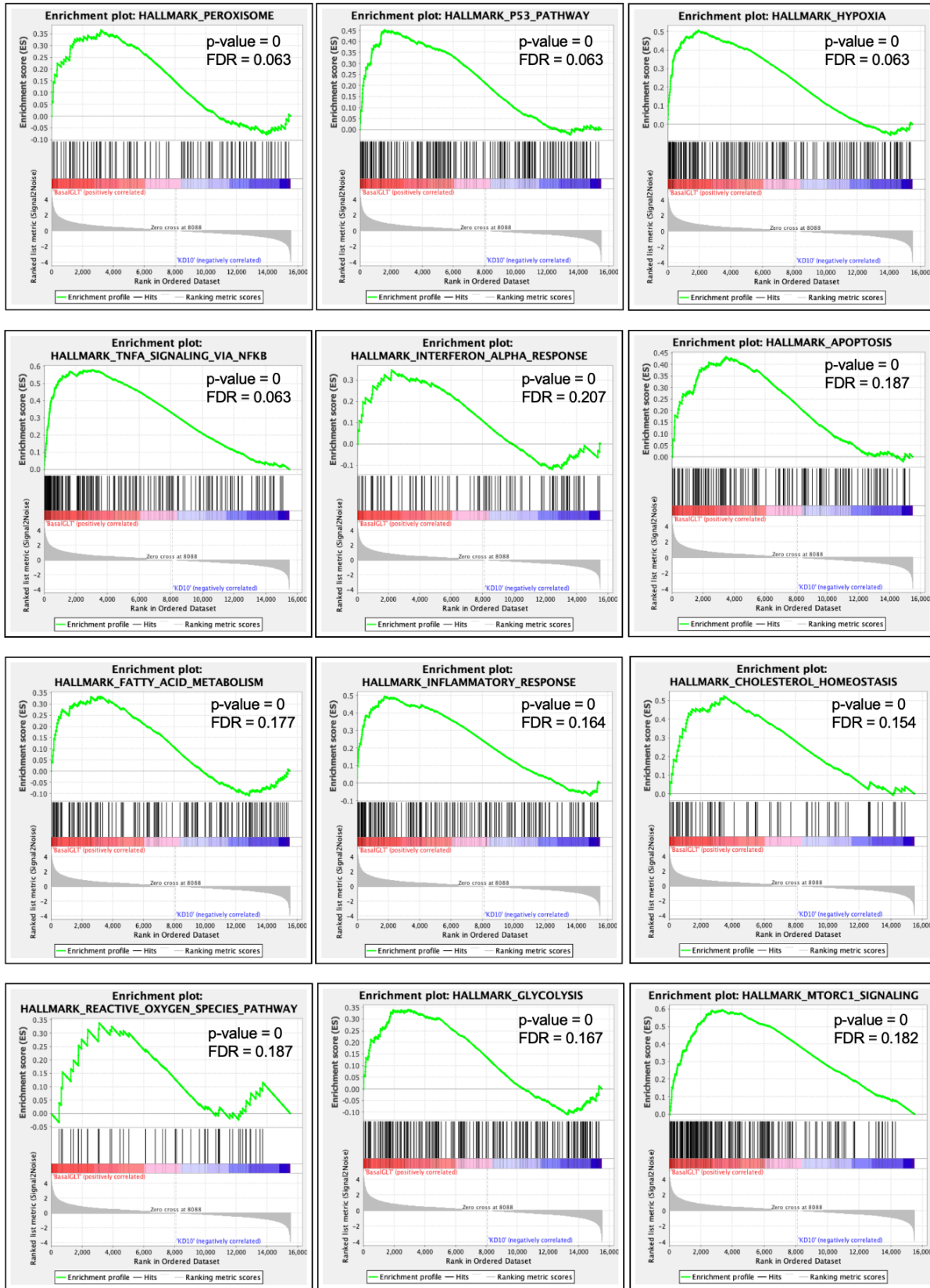
Figure 4.5.9

Figure 4.5.9 (Continued). GSEA analysis of Hallmark gene sets enriched in 24-hour GLT-treated INS-1E. GSEA Analysis performed by comparing GLT-treated INS-1E co-incubated with DMSO or 10 µM KD025. Gene counts normalized to INS-1E treated with basal media.

We further investigated GLT-induce gene expression changes reversed by KD025 by computing overlaps between these genes and the Hallmark gene sets in the Molecular Signatures Database (MSigDB).[22,24,25]

We found that GLT-induced gene expression changes reversed by KD025 included genes in the HALLMARK_HYPOXIA, HALLMARK_INFLAMMATORY_RESPONSE, and HALLMARK_TNFA_ SIGNALING_VIA_NFKB gene sets (Figure 4.5.10a). In the HALLMARK_HYPOXIA gene set KD025 decreased GLT-induced upregulation of *Pfkfb3, Ppp1r3c, Efna3, Bhlhne40, and S100a4* (Figure 4.5.10c). In the HALLMARK_INFLAMMATORY_RESPONSE gene set KD025 decreased GLT-induced upregulation of *Prok2, Hbegf, Il2rb, Slc4a4, and Cd40* (Figure 4.5.10d). In the HALLMARK_TNFA_SIGNALING_VIA_NFKB gene set KD025 decreased GLT-induced upregulation of *Klf10, Pfkfb3, G0s2, Bhlhe40, and Hbegf* (Figure 4.5.10e). KD025 also decreased the expression of GLT-induced upregulated genes in the HALLMARK_P53_PATHWAY, HALLMARK_INTERFERON_GAMMA_RESPONSE, HALLMARK_ MTORC1_SIGNALING, AND HALLMARK_IL6_JAK_STAT3_ SIGNALING gene sets (Figure 4.5.10a). Of note is KD025-dependent decrease in *Slc7a11* and *Txnip* expression in GLT-treated INS-1E. Slc7a11 is a cysteine/glutamine antitransporter implicated in ferroptosis suppression and *Txnip* is upregulated in diabetes, where it promotes oxidative stress, inhibits insulin production, and facilitates β-cell apoptosis.[26–29] KD025 also had an effect on a selection of genes that do not fall into any Hallmark data set and are here classified as the unique KD025 signature (Figure 4.5.10b). Encouragingly, we also found that KD025 recovered expression of several downregulated HALLMARK_PANCREAS_BETA_CELLS genes, including *Pdx1, Nkx6.1, Isl1, Nkx2.2, Dpp4, Pax6, Dcx, Pax4, Neurod1, and Syt13* (Figure 4.5.11).
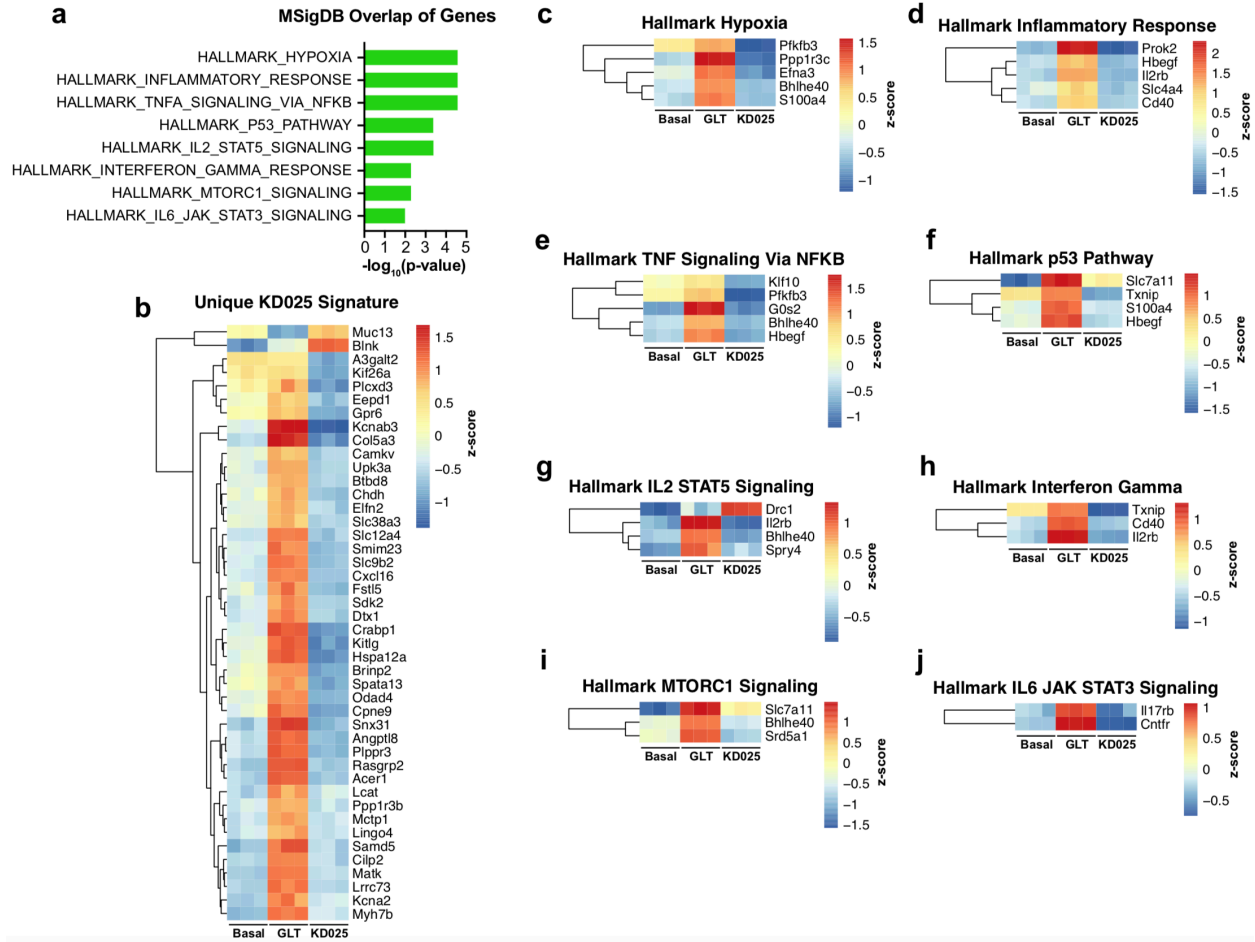
Figure 4.5.10. Hallmark gene set overlap of genes affected by KD025 treatment. a) Molecular Signatures Database (MSigDB) hallmark gene set overlap of GLT-upregulated genes reverted by KD025 treatment in INS-1E after 24 hours. b) Genes which comprise the unique signature for KD025 treatment in GLT-treated INS-1E at 24 hours. c-d) Hallmark gene set overlaps of genes specifically downregulated by KD025 in 24-hour GLT-treated INS-1E.
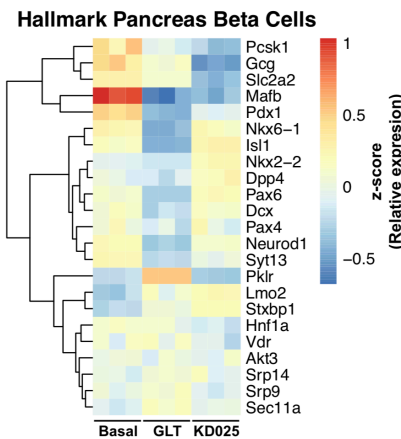
Figure 4.5.11. KD025 recovers downregulated Hallmark Pancreas Beta Cells genes. INS-1E cells treated with 24-hour basal media, GLT media, or GLT media supplemented with 10 µM KD025.

113

Of particular interest were those genes not affected by INS-1E KD025 treatment, including genes upregulated by GLT-treatment or downregulated by GLT treatment. We found that the largest Hallmark gene set overlap of genes unaffected by KD025 treatment was the HALLMARK_E2F_TARGETS gene set (4.5.12a,b). These genes, which encode cell cycle related targets of E2F transcription factors are upregulated in mitotic cells.[25] We believe this gene signature is unique to the INS-1E insulinoma cell line which, when unstressed continues to grow. INS-1E cells treated with GLT media halt their growth phenotype and this was represented by the decrease in HALLMARK_E2F_TARGETS, HALLMARK_G2M_CHECKPOINT, and HALLMARK_MITOTIC_SPINDLE gene set expression in GLT treated INS-1E (Figure 4.5.12b-d). It was interesting to see 24-hour KD025 treatment did not return several HALLMARK_HYPOXIA genes back to basal levels (Figure 4.5.12e). Instead, some like *Atf3, Stbd1,* and *Ddit3* were slightly decreased, while others like *Fos, Pparg1a, Ppfia4, and Aldoc* were increased. Similarly, 24-hour KD025 treatment did not return select HALLMARK_MTORC1_SIGNALING genes back to basal levels (Figure 4.5.12g). Other Hallmark gene sets largely unchanged include HALLMARK_GLYCOLYSIS and HALLMARK_KRAS _SIGNALING_UP (Figure 4.5.12f,g). There were also some hallmark gene set members decreased by 24-hour KD025 treatment that are upregulated in basal INS-1E, including HALLMARK_PI3K_AKT_MTOR_SIGNALING and HALLMARK_TNFA_SIGNALING_VIA_NFKB (Figure 4.5.12i,j). Finally, there remained a group of GLT-upregulated genes that were not affected by 24-hour KD025 treatment and did not overlap with any Hallmark gene sets (Figure 4.5.13).
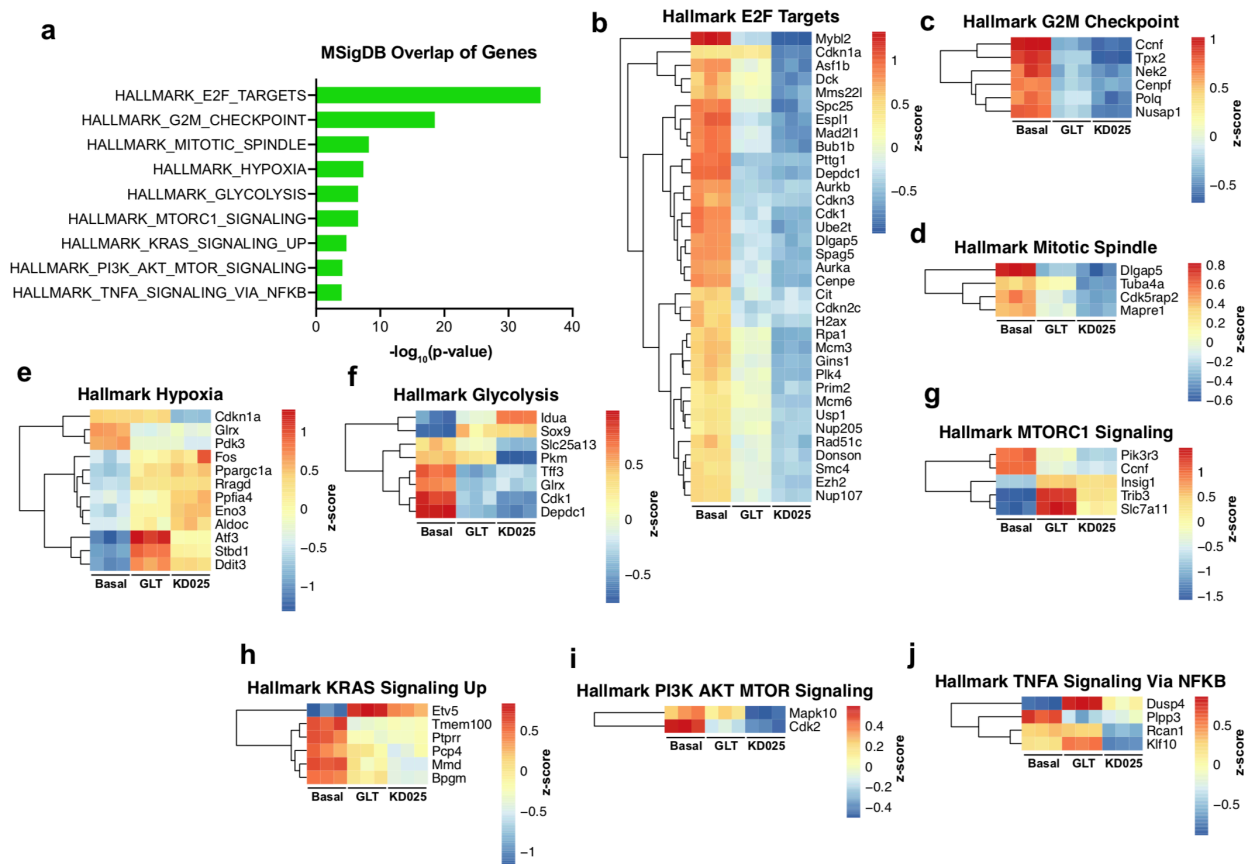
Figure 4.5.12. Hallmark gene set overlap of INS-1E genes not returned to basal levels by KD025 treatment. a) Molecular Signatures Database (MSigDB) hallmark gene set overlap of GLT-upregulated genes that did not return to basal INS-1E levels by 24-hour KD025 treatment. b-j) Visualization of Hallmark gene set overlaps of genes not returned to basal INS-1E levels after 24-hour KD025 treatment in GLT-treated INS-1E.
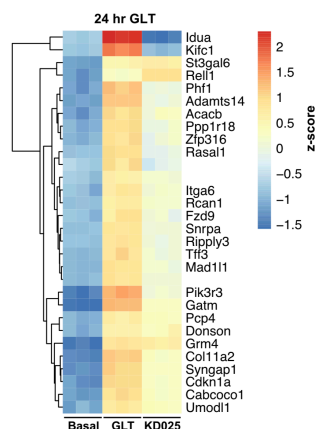
Figure 4.5.13. Genes not returned to basal levels by KD025, absent Hallmark gene set overlap. 10 µM KD025 24-hour co-treatment in GLT-treated INS-1E does not return the expression of these genes to back to basal levels.

4.6 Discussion

The discovery of KD025 as GLT-protective suggested a role for ROCK2 inhibition in GLT-mediated death in β-cells. However, by screening several pan-ROCK inhibitors and knocking down *Rock2* in INS-1E, we showed that ROCK2 inhibition was not the GLT-relevant target for KD025 (Figure 4.5.1). We also showed that KD025 was not generally β-cell protective. KD025 does not protect against cytokine-mediated death and moderately protects against thapsigargin-induced ER stress (Figure. 4.5.3). This suggested to us KD025 activity was specific to the GLT-response, possibly through decreasing GLT-induced ER stress in combination with reducing previously described mitochondrial depolarization and calcium influx (Chapter 3). By kinase profiling KD025, SR3677, and H-1152 we were able to directly compare the kinase targets for these three ROCK inhibitors and discover that KD025 had unique targets (Table 4.5.2). These were *Csnk2a1, Csnk2a2, and Mrckb*. *Csnk2a1 and Csnk2a2* encode the α and α' catalytic subunits for casein kinase 2 (CK2), a previously suggested target for diabetes treatment.[30] CK2 expression is increased in β-cells isolated from human T2D donors compared to nondiabetic donors and treatment of rat and human islets exposed to elevated glucose and fatty acids with potent CK2 inhibitor, CX4945, improved insulin secretion.[31,32] We therefore tested if CX4945 could recover GLT-treated INS-1E viability and found that at 10 μM the compound was just as effective as KD025 (Figure 4.5.5). To further probe the role of CK2α and CK2α' inhibition in β-cell viability, we knocked down *Csnk2a1 and Csnk2a2* and showed that *Csnk2a1,* but not *Csnk2a2,* knockdown improved GLT-treated INS-1E viability (Figure 4.5.6). CK2α and CK2α' share high sequence homology but do differ in their C-termini, suggesting there may be differential targets or functions for the two subunit isoforms in the cell.[33] Overexpression of a C-terminally flagged *Csnk2a1* in GLT-treated INS-1E completely ablated KD025 GLT-protectivity, confirming CK2α as the GLT-relevant target for KD025 in β-cells (Figure 4.5.7).

We RNA-sequenced INS-1E cells treated with KD025 in the presence of GLT media to further probe KD025 mechanism of action and how CK2α inhibition affected GLT-treated INS-1E cells. We found that 10 μM KD025 was able to time-dependently reverse several aspects of the GLT-gene signature, with maximum reversal being observed at 24-hours (Figure 4.5.8). Querying the list of genes KD025 returned to basal INS-1E levels of expression, we found the highest enrichment in Hallmark Hypoxia, Hallmark Inflammatory Response, and Hallmark TNFα Signaling via NFκB gene sets (Figure 4.5.10a). Within the Hallmark Hypoxia gene set, KD025 reversed the upregulation of *Pfkfb3, Ppp1r3c, Efna3, Bhlhe40,* and *S100a4* (Figure 4.5.10c). Upregulation of *Pfkfb3* is observed in the β-cells of type 1 diabetes (T1D) patients and in response to cytokine treatment.[34] The upregulation of *Pfkfb3* by GLT-treatment suggests shared processes with cytokine-induced β-cell death. *Ppp1r3c* is an activator of glycogen synthase and is strongly upregulated in βV59M mice 24-hours after induction of diabetes.[35] The upregulation of this gene by GLT-treatment and subsequent downregulation by KD025, suggest it is a contributor to GLT-mediated β-cell death. *Efna3* is upregulated in T2D patients and is required for insulin secretion, suggesting this gene encoding the Ephrin A3 protein kinase could be upregulated to offset insulin resistance or diminished insulin response.[31] *S100a4* encodes a calcium binding protein regulated by β-cell membrane depolarization agents and is a marker for β-cell excitotoxicity.[36] The upregulation of *S100a4* by GLT-treatment suggests β-cell excitotoxicity may play a role in GLT. Enrichment of the Hallmark Inflammatory Response gene set in GLT harkens to the observation that obesity-induced chronic inflammation is a risk factor for T2D.[37] For example, *Hbegf* expression is upregulated in β-cells in response to glucose and infusing rats with lipids increase *Hbegf* mRNA expression.[38,39] *Slc4a4* is overexpressed in the β-cells of T2D patients and is associated with loss of β-cell transcriptional identity and β-cell dysfunction.[40,41] *Slc4a4* knockout mice were protected from high-fat-diet-induced glucose intolerance and β-cell dysfunction, and showed improved mitochondrial function and β-cell gene expression.[40,41] *Cd40* is known to be upregulated by proinflammatory cytokines and is a means by which GLT initiates β-cell death

117

through TNFR5/CD40-mediated STAT1 and NF-κB activation.[42] KD025 treatment downregulates the expression of *Hbegf, Slc4a4,* and *Cd40* (Figure 4.5.10d). In the enriched Hallmark p53 pathway, it was interesting to find *Slc7a11* and *Txnip* upregulated in GLT-treatment (Figure. 4.5.10f). *Slc7a11* is a cystine/glutamate transporter known to suppress the activation of ferroptosis.[26] The involvement of ferroptosis in β-cell mediated death in T2D remains to be investigated, however, overexpression of *Slc7a11* could be in response to lipid peroxidation in INS-1E cells. *Txnip* is also upregulated by GLT-treatment and is known to be upregulated in T2D, where it inhibits insulin production and β-cell function and promotes oxidative stress and induction of apotosis.[29] *Txnip* deficiency is known to protect against T2D by promoting β-cell survival and a recently developed small molecule which decreases *Txnip* expression lowers blood glucose in obesity-induced diabetes in mice.[43,44] RNA-sequencing also revealed a selection of genes not enriched in any Hallmark gene set which are downregulated by 24-hour KD025 treatment (Figure 4.5.10b). Interestingly, KD025-treatment lowers the expression of some of these genes even lower than basal media treated INS-1E. Future investigations will determine whether this is to the benefit or detriment of overall β-cell function. We also observed that KD025 treatment increased the expression of Hallmark Pancreas Beta Cell genes downregulated by GLT-treatment including *Pdx1, Nkx6.1, Isl1, Nkx2.2, Dpp4, Pax6, Dcx, Pax4, Neurod1,* and *Syt13* (Figure 4.5.11). These results suggest that KD025 is able to improve β-cell identity lost by GLT-treatment and conform with previous results that KD025 increases GLT-reduced *Pdx1* expression (Chapter 3).

KD025 was not able to revert to basal the expression of several genes involved in the Hallmark E2F Targets gene set; however this was less concerning as these genes are associated with a mitotic phenotype and are less relevant in post-mitotic human islets (Figure 4.5.12, 4.5.13). When grown in basal media, INS-1E cells maintain a growth state, doubling approximately every 36 hours. This mitotic phenotype is lost with GLT-treatment and the onset of apoptosis reduces cell number. KD025 does not appear to increase these genes associated with proliferation,

suggesting it does not reactivate the INS-1E mitotic phenotype. As human islets rarely divide, this may suggest KD025 treatment is pushing INS-1E towards a more β-cell, non-mitotic phenotype.

Together, these data show KD025 is GLT-protective because of its CK2α inhibition and that CK2α inhibition protects against GLT-mediated death by upregulating markers of β-cell function, and decreasing markers of hypoxia, inflammation response, and TNFα/NFκB signaling. Future research will benefit from investigating which CK2 phosphorylation substrates are most essential for mediating β-cell dysfunction and death and how CK2 inactivation alters these signaling pathways.

4.7 References

1. DeFronzo, R. A. *et al.* Type 2 diabetes mellitus. *Nat. Rev. Dis. Prim.* **1**, 15019 (2015).

2. International Diabetes Federation. *IDF Atlas 10th Edition 2021*. (2021).

3. Type 2 diabetes mellitus. *Nat. Rev. Dis. Prim.* **1**, 15039 (2015).

4. Boden, G. Obesity and free fatty acids. *Endocrinol. Metab. Clin. North Am.* **37**, 635–646 (2008).

5. Lytrivi, M., Castell, A. L., Poitout, V. & Cnop, M. Recent insights into mechanisms of β-cell lipo- and glucolipotoxicity in type 2 diabetes. *J. Mol. Biol.* **432**, 1514–1534 (2020).

6. Prentki, M. & Corkey, B. E. Are the β-cell signaling molecules malonyl-CoA and cystolic long-chain acyl-CoA implicated in multiple tissue defects of obesity and NIDDM? *Diabetes* **45**, 273–283 (1996).

7. Poitout, V. *et al.* Glucolipotoxicity of the pancreatic beta cell. *Biochim. Biophys. Acta - Mol. Cell Biol. Lipids* **1801**, 289–298 (2010).

8. Kim, J.-W. & Yoon, K.-H. Glucolipotoxicity in pancreatic β-cells. *Diabetes Metab. J.* **35**, 444 (2011).

9. Rojas, J. *et al.* Pancreatic beta cell death: novel potential mechanisms in diabetes therapy. *J. Diabetes Res.* **2018**, 1–19 (2018).

10. Lytrivi, M., Castell, A.-L., Poitout, V. & Cnop, M. Recent insights into mechanisms of β-cell lipo- and glucolipotoxicity in type 2 diabetes. *J. Mol. Biol.* **432**, 1514–1534 (2020).

11. Watanabe, M., Ida, Y., Ohguro, H., Ota, C. & Hikage, F. Diverse effects of pan-ROCK and ROCK2 inhibitors on 2 D and 3D cultured human trabecular meshwork (HTM) cells treated with TGFβ2. *Sci. Rep.* **11**, 15286 (2021).

12. Przepiorka, D. *et al.* FDA approval summary: belumosudil for adult and pediatric patients 12 years and older with chronic gvhd after two or more prior lines of systemic therapy. *Clin. Cancer Res.* clincanres.4176.2021 (2022). doi:10.1158/1078-0432.CCR-21-4176

13. Pan, P. *et al.* Advances in the development of Rho-associated protein kinase (ROCK)

inhibitors. *Drug Discov. Today* **18**, 1323–1333 (2013).

14. Feng, Y., LoGrasso, P. V., Defert, O. & Li, R. Rho kinase (ROCK) inhibitors and their therapeutic potential. *J. Med. Chem.* **59**, 2269–2300 (2016).

15. Nakagawa, O. *et al.* ROCK-I and ROCK-II, two isoforms of Rho-associated coiled-coil forming protein serine/threonine kinase in mice. *FEBS Lett.* **392**, 189–193 (1996).

16. Okumura, N. *et al.* Effect of the rho kinase Inhibitor Y-27632 on corneal endothelial wound healing. *Investig. Opthalmology Vis. Sci.* **56**, 6067 (2015).

17. Ghazizadeh, Z. *et al.* ROCKII inhibition promotes the maturation of human pancreatic beta-like cells. *Nat. Commun.* **8**, 298 (2017).

18. Parnaud, G. *et al.* Signaling pathways implicated in the stimulation of β-Cell proliferation by extracellular matrix. *Mol. Endocrinol.* **23**, 1264–1271 (2009).

19. Walpita, D. & Wagner, B. K. Evaluation of compounds in primary human islet cell culture. *Curr. Protoc. Chem. Biol.* **6**, 157–168 (2014).

20. Chou, D. H. C. *et al.* Inhibition of histone deacetylase 3 protects beta cells from cytokine-induced apoptosis. *Chem. Biol.* **19**, 669–673 (2012).

21. Fabian, M. A. *et al.* A small molecule–kinase interaction map for clinical kinase inhibitors. *Nat. Biotechnol.* **23**, 329–336 (2005).

22. Subramanian, A. *et al.* Gene set enrichment analysis: A knowledge-based approach for interpreting genome-wide expression profiles. *Proc. Natl. Acad. Sci.* **102**, 15545–15550 (2005).

23. Siddiqui-Jain, A. *et al.* CX-4945, an orally bioavailable selective inhibitor of protein kinase CK2, inhibits prosurvival and angiogenic signaling and exhibits antitumor efficacy. *Cancer Res.* **70**, 10288–10298 (2010).

24. Liberzon, A. *et al.* Molecular signatures database (MSigDB) 3.0. *Bioinformatics* **27**, 1739–1740 (2011).

25. Liberzon, A. *et al.* The molecular signatures database hallmark Gene set collection. *Cell*

Syst. **1**, 417–425 (2015).

26. Koppula, P., Zhuang, L. & Gan, B. Cystine transporter SLC7A11/xCT in cancer: ferroptosis, nutrient dependency, and cancer therapy. *Protein Cell* **12**, 599–620 (2021).

27. Chen, J., Saxena, G., Mungrue, I. N., Lusis, A. J. & Shalev, A. Thioredoxin-interacting protein: a critical link between glucose toxicity and beta-cell apoptosis. *Diabetes* **57**, 938–944 (2008).

28. Xu, G., Chen, J., Jing, G. & Shalev, A. Thioredoxin-interacting protein regulates insulin transcription through microRNA-204. *Nat. Med.* **19**, 1141–1146 (2013).

29. Hong, K., Xu, G., Grayson, T. B. & Shalev, A. Cytokines regulate β-cell thioredoxin-interacting protein (TXNIP) via distinct mechanisms and pathways. *J. Biol. Chem.* **291**, 8428–8439 (2016).

30. Ampofo, E., Nalbach, L., Menger, M. D., Montenarh, M. & Götz, C. Protein kinase ck2—a putative target for the therapy of diabetes mellitus? *Int. J. Mol. Sci.* **20**, 4398 (2019).

31. Marselli, L. *et al.* Gene expression profiles of beta-cell enriched tissue obtained by laser capture microdissection from subjects with type 2 diabetes. *PLoS One* **5**, e11499 (2010).

32. Doliba, N. M. *et al.* Inhibition of cholinergic potentiation of insulin secretion from pancreatic islets by chronic elevation of glucose and fatty acids: Protection by casein kinase 2 inhibitor. *Mol. Metab.* **6**, 1240–1253 (2017).

33. St-Denis, N. A. & Litchfield, D. W. From birth to death: The role of protein kinase CK2 in the regulation of cell proliferation and survival. *Cell. Mol. Life Sci.* **66**, 1817–1829 (2009).

34. Nomoto, H. *et al.* Activation of the HIF1α/PFKFB3 stress response pathway in beta cells in type 1 diabetes. *Diabetologia* **63**, 149–161 (2020).

35. Brereton, M. F. *et al.* Hyperglycaemia induces metabolic dysfunction and glycogen accumulation in pancreatic β-cells. *Nat. Commun.* **7**, 13496 (2016).

36. Stancill, J. S. *et al.* Chronic β-Cell depolarization impairs β-cell identity by disrupting a network of Ca2+-regulated genes. *Diabetes* **66**, 2175–2187 (2017).

37. Donath, M. Y., Dinarello, C. A. & Mandrup-Poulsen, T. Targeting innate immune mediators in type 1 and type 2 diabetes. *Nat. Rev. Immunol.* **19**, 734–746 (2019).

38. Maachi, H. *et al.* Hb-egf signaling is required for glucose-induced pancreatic β-cell proliferation in rats. *Diabetes* **69**, 369–380 (2020).

39. Zarrouki, B. *et al.* Epidermal growth factor receptor signaling promotes pancreatic β-cell proliferation in response to nutrient excess in rats through mTOR and FOXM1. *Diabetes* **63**, 982–993 (2014).

40. Brown, M. R. *et al.* Electrogenic sodium bicarbonate cotransporter NBCe1 regulates pancreatic β cell function in type 2 diabetes. *J. Clin. Invest.* **131**, (2021).

41. BROWN, M., HOLMES, H. L., RAKSHIT, K., ROMERO, M. F. & MATVEYENKO, A. Deletion of slc4a4 in pancreatic ß cells protects from high-fat diet–induced glucose intolerance and ß-cell dysfunction. *Diabetes* **67**, (2018).

42. Bagnati, M. *et al.* Glucolipotoxicity initiates pancreatic β-cell death through TNFR5/CD40-mediated STAT1 and NF-κB activation. *Cell Death Dis.* **7**, e2329–e2329 (2016).

43. Shalev, A. Minireview: thioredoxin-interacting protein: regulation and function in the pancreatic β-cell. *Mol. Endocrinol.* **28**, 1211–1220 (2014).

44. Thielen, L. A. *et al.* Identification of an anti-diabetic, orally available small molecule that regulates TXNIP expression and glucagon action. *Cell Metab.* **32**, 353-365.e8 (2020).

Chapter 5

Conclusions and Future Directions

The global obesity and diabetes epidemics show no end in sight. While current type 2 diabetes treatments enable management of the disease, there are no therapeutics that address β-cell loss. Current treatments are therefore palliative not curative. We lack complete understanding of the mechanistic underpinnings of β-cell dysfunction and death in obesity and type 2 diabetes, and this is limiting the development of therapies. Phenotypic screening in β-cell models of death like glucolipotoxicity (GLT) offer new small molecules to probe the molecular biology of β-cell dysfunction and death, possibly identifying disease relevant targets for further therapeutics development.

Chapter 2 describes the development of a high-throughput fluorescent microscopy (HCFM) method to quantify cell number and percent viability. This method is highly reproduceable and can be applied to numerous assay systems to detect cell viability. This method was employed to validate hit compounds from the primary GLT screen. Also described in this chapter are methods to assay β-cell functionality in GLT conditions. These include a flow cytometry method to detect mitochondrial depolarization and a confocal microscopy method to detect calcium influx in INS-1E cells. Future assay development should aim at developing a method for quantifying glucose stimulated insulin secretion (GSIS) from GLT-treated cells in a reproduceable manner. Attempts were made to generate such an assay but faced challenges due to the low attachment properties of GLT-treated cells. This future assay should utilize limited to no wash steps to enable quantification and normalization of insulin secretion by cell number. In the absence of a robust GSIS assay, Chapter 2 details the quantification of *Pdx1* expression in INS-1E cells treated with GLT to further assay β-cell function. Further GLT screening efforts would also benefit from the development of a high-throughput means of assess endoplasmic reticulum (ER) stress in cells. Western blotting for markers of ER stress and the unfolded protein response is the current standard in the field and this limits the throughput for testing whether compound reduce ER stress.

Chapter 3 summarizes the result of the primary GLT screen in INS-1E and the identification of 17 Repurposing library hit compounds and 2 Diversity-Oriented Synthesis (DOS) scaffolds with potent GLT-protective activity. We found an enrichment of kinase inhibitors in our Repurposing library hits, suggesting several pathways of the β-cell GLT response are governed by overactive kinases which activate cell stress and apoptotic pathways. The 17 Repurposing library hits were tested in several assays to investigate their effect on *Pdx1* expression, mitochondrial depolarization, and calcium flux in GLT-treated INS-1E cells. The general β-cell protectivity of these compounds was also tested by applying them to cytokine treated INS-1E cells. We found 5 out of the 17 hits were cytokine protective as well. These 17 small molecules, all but one annotated as a kinase inhibitor, will serve as excellent probes for future studies interrogating the mechanisms of β-cell GLT. Mechanism of action studies to identify the β-cell relevant targets of these compounds may well likely identify new molecular pathways for the treatment of β-cell death and dysfunction in T2D. These studies may include pull-down experiments, *in vivo* validation of antidiabetic effects, and RNA-sequencing to investigate how gene expression changes with and without treatment.

Chapter 4 describes efforts to identify the KD025 target responsible for β-cell GLT-protectivity. KD025 was identified in chapter 3 as a GLT-protective compound that decreased mitochondrial depolarization and calcium influx, increased *Pdx1* expression, and recovered GLT-treated INS-1E viability. KD025 is annotated as a ROCK2 inhibitor and screening of other pan-ROCK inhibitors revealed only KD025 alone was GLT-protective. Additionally, knockdown of *Rock2* in INS-1E had no effect on GLT-treated INS-1E viability. Kinase profiling of KD025 and non-GLT-protective pan-ROCK inhibitors SR3677 and H-1152 revealed KD025 inhibits the α and α' subunits of casein kinase 2 (CK2). These subunits are the catalytic domains of CK2 and mediate its kinase activity. Knockdown of CK2α and CK2α' revealed *siCsnk2a1* (CK2α) improved GLT-treated INS-1E viability, while *siCsnk2a2* (CK2α') loss had no effect. Overexpression of a C-terminal flagged

CK2α fusion in INS-1E completely ablated KD025 GLT-protectivity. I therefore concluded KD025 GLT-protectivity is mediated by CK2 inhibition. RNA-Sequencing analysis of GLT-treated INS-1E revealed that KD025 also partially reverses the GLT-gene signature. Several Hallmark gene sets involved in stress were upregulated in GLT-treated INS-1E and were downregulated by KD025 treatment. This implicates CK2 inhibition in the regulation of several stress pathways in β-cells. Future experiments should aim to dissect which casein kinase 2 substrates are relevant to β-cell function and viability and how CK2 activity in β-cells changes in response to different stressors. KD025 experiments indicate CK2 activity is crucial only to GLT-treated β-cells. Future experiments should aim to understand what differentiates GLT from other β-cell stressors like cytokine stress, oxidative stress, and ER stress.

Appendix 1: Native Zinc Catalyzes Selective and Traceless Release of Small Molecules in β-Cells

Attribution:

Miseon Lee[7], Basudeb Maji[7], Debasish Manna[7], Sevim Kahraman, Ruth M. Elgamal, **Jonnell Small,** Praveen Kokkonda, Amedeo Vetere, Jacob M. Goldberg, Stephen J. Lippard, Rohit N. Kulkarni, Bridget K. Wagner, and Amit Choudhary*

[7]These authors contributed equally to this work

Author Contributions:

JS optimized cell culture methods for INS-1E, alphaTC.6, and PANC-1. JS performed the experiment to characterize the dose and time dependent beta-cell specific hydrolysis of DA-ZP1 in INS-1E (Figure S1).

J|A|C|S

JOURNAL OF THE AMERICAN CHEMICAL SOCIETY

Communication

Native Zinc Catalyzes Selective and Traceless Release of Small Molecules in β-Cells

Miseon Lee,▲ Basudeb Maji,▲ Debasish Manna,▲ Sevim Kahraman, Ruth M. Elgamal, Jonnell Small, Praveen Kokkonda, Amedeo Vetere, Jacob M. Goldberg, Stephen J. Lippard, Rohit N. Kulkarni, Bridget K. Wagner, and Amit Choudhary*

Cite This: *J. Am. Chem. Soc.* 2020, 142, 6477–6482

Read Online

ACCESS | Metrics & More | Article Recommendations | Supporting Information

ABSTRACT: The loss of insulin-producing β-cells is the central pathological event in type 1 and 2 diabetes, which has led to efforts to identify molecules to promote β-cell proliferation, protection, and imaging. However, the lack of β-cell specificity of these molecules jeopardizes their therapeutic potential. A general platform for selective release of small-molecule cargoes in β-cells over other islet cells *ex vivo* or in an organismal context will be immensely valuable in advancing diabetes research and therapeutic development. Here, we leverage the unusually high Zn(II) concentration in β-cells to develop a Zn(II)-based prodrug system to selectively and tracelessly deliver bioactive small molecules and fluorophores to β-cells. The Zn(II)-targeting mechanism enriches the inactive cargo in β-cells as compared to other pancreatic cells; importantly, Zn(II)-mediated hydrolysis triggers cargo activation. This prodrug system, with modular components that allow for fine-tuning selectivity, should enable the safer and more effective targeting of β-cells.

Death and/or dysfunction of β-cells in type 1 and 2 diabetes critically reduces insulin levels, ultimately necessitating insulin injection.[1,2] β-Cells reside in pancreatic islets, together with α-, δ-, ε-, and pancreatic polypeptide (PP)-cells. Multiple avenues in diabetes research and therapeutic development will benefit immensely from methods that selectively release small molecules into β-cells over other islet cells *ex vivo* or other cell-types *in vivo*. First, targeted release of small molecules that induce β-cell proliferation,[3−9] even semispecifically, will be useful in several contexts. For example, the transplantation of β-cells derived from induced pluripotent stem cells is an emerging therapeutic avenue,[10−12] but the yields of mature β-cells are low,[12] requiring selective expansion of β-cells *ex vivo* that can be accomplished by the targeted release of β-cell mitogens.[13] Targeted delivery of β-cell mitogens *in vivo* can also alleviate concerns about nontarget cell proliferation. Second, β-cell-specific release of imaging agents will also be useful in several contexts, including diagnostics. Islets are often transplanted in type 1 diabetes patients,[14] and given the heterogeneous nature of the islets, a nondestructive imaging method for the precise and rapid quantification of β-cell mass in the islets before transplantation would be valuable. Furthermore, the availability of facile β-cell imaging methods would miniaturize small-molecule screening assays employing human islets, which are in scarce supply,[13,15] and improve current *in vivo* β-cell imaging modalities that are only semispecific.[16,17]

Antibody−drug conjugates provide an attractive approach for cell-specific targeting, but the identification of specific β-cell surface markers is challenging. Cell-specific release of small molecules can be accomplished through a prodrug strategy, where an inactive analog of the parent compound is converted to the active agent only in the target cell by an enzyme. Here, we take advantage of an unusually high concentration of zinc ion (Zn(II)) in β-cells to report a β-cell-specific zinc-based prodrug system (ZnPD) that consists of an inactivated small-molecule cargo linked via a scaffold to a Zn(II)-binding ligand. Zn(II) catalyzes the hydrolysis of the bond between the inactive cargo and the scaffold, thereby releasing the active agent. By using this system, we demonstrate the selective release of multiple fluorophores and a β-cell mitogen in human β-cells across several cell types.

The development of ZnPD was motivated by several observations and design principles. First, β-cells have an unusually high Zn(II) concentration in insulin vesicles (up to ∼30 mM, ∼100 μM of which is "loosely bound"),[18] which contrasts with the cytosolic Zn(II) concentration in most cells of ∼400 pM,[19] the concentration in plasma and interstitial fluid of ∼1 nM, and the fact that free Zn(II) concentrations above 100 nM are toxic in cell culture.[20] Indeed, fluorophores bearing Zn(II)-chelating groups have been used extensively over the years to selectively image β-cells.[21−25] Second, Zn(II) can catalyze hydrolytic reactions,[26,27] providing an opportunity to switch the inactive cargo to an active compound, akin to other prodrugs. Furthermore, when the cargo is released from the ZnPD, it can diffuse from the insulin granules to other parts within the β-cell where the cargo targets are likely to
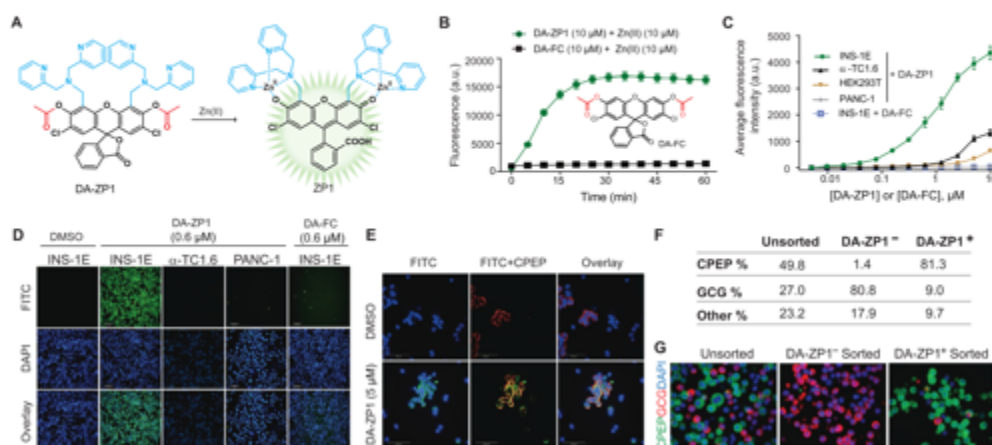
Figure 1. (A) Zn(II)-mediated unmasking of DA-ZP1 releases active fluorophore ZP1. (B) Structure of DA-FC and graph of Zn(II)-mediated fluorescence release of DA-ZP1 and DA-FC. (C) Selective unmasking of DA-ZP1 fluorescence in INS-1E cells compared to other cell types. (D) Representative images of DA-ZP1- or DA-FC-treated cells under the FITC channel (top) measuring ZP1 release, DAPI staining (middle), and the overlay (bottom). (E) Representative confocal images of dissociated human islets treated with DA-ZP1 followed by immunostaining for C-peptide. (F) Quantification of dispersed human islets treated with DA-ZP1 ($n = 4$). See also Figure S3. Human pancreatic donor information is available in Table S1. (G) Dispersed human islets were stained, and DA-ZP1⁺ and DA-ZP1⁻ cells were collected after FACS ($n = 4$). Representative images show C-peptide (green) and glucagon (red) staining in unsorted, DA-ZP1⁺, DA-ZP1⁻ cell populations. Nuclei stained with DAPI (blue).

reside. For most cargoes (e.g., small-molecule inducers of β-cell proliferation), both the activation mechanism and the escape from insulin granules are critical—selective activation prevents proliferation in off-target tissues, whereas the exit from the granules ensures that the small molecule reaches its protein targets. Third, the hydrolytic mechanism allows traceless release of the cargo in its native form, without any modifications, allowing ZnPDs to be developed for small molecules that cannot tolerate modifications without a loss of activity. Fourth, several Zn(II) ligands exist with affinities ranging from pM to mM, allowing the precise fine-tuning of β-cell specificity.[28] Finally, although the aqueous Zn(II) ion is not a potent Lewis acid, multiple tridentate coordinating ligands exist that can be placed proximally to the scissile bond of a ZnPD, thereby facilitating a high effective molarity of Zn(II) with an available coordination site and potent Lewis acidity.

Before constructing ZnPDs, we first determined the rate of Zn(II)-mediated hydrolysis in β-cells compared to other islet cells. We employed a previously reported reaction-based probe, DA-ZP1, a PET-based zinc sensor that requires Zn(II)-triggered hydrolysis of a tethered acetate ester to turn-on fluorescence (Figure 1A) in a way that is selective for Zn(II) over other biologically relevant metal ions.[27] DA-ZP1's activity in β-cells has not been demonstrated. To confirm that the unmasking of DA-ZP1 fluorescence in cells was not catalyzed by an esterase and that proximally located dipicolyl ligands are necessary for hydrolytic cleavage, we tested the compound DA-FC, which lacks the Zn(II)-binding dipicolyl moieties. As expected, DA-FC did not fluoresce in the presence of Zn(II) (Figure 1B).[27] To demonstrate that the high intracellular Zn(II) concentrations could release fluorescent cargo selectively in β-cells, we incubated DA-ZP1 in a β-cell line (INS-1E), an α-cell line (αTC1.6), a ductal cell line (PANC-1), and cells of other lineages (Figures 1C, D and S1A). After a

1 h incubation, the β-cells were highly fluorescent compared to the other cell types, with minimal background fluorescence at concentrations much greater than the K_d of DA-ZP1 (0.6 nM).[26] β-Cells treated with the control compound DA-FC were not fluorescent. Finally, we monitored the kinetics of fluorophore release in β-cells at various concentrations of DA-ZP1 and observed that this release occurred within minutes, confirming the feasibility of our proposed ZnPD approach (Figure S1B and S1C). We further evaluated the intracellular localization of the released ZP1 (Zinpyr1) with nuclear and mitochondrial counterstaining and observed broad cellular distribution (Figure S2A). Finally, we confirmed the direct role of cellular Zn(II) by using a known chelator, N,N,N',N'-tetrakis(2-pyridinylmethyl)-1,2-ethanediamine (TPEN),[27] that depletes Zn(II), preventing DA-ZP1 hydrolysis (Figure S2B). To better mimic human β-cells,[29,30] we also tested DA-ZP1 for β-cell selectivity in human pancreatic islets. Here, we incubated DA-ZP1 in dissociated human islets, costaining for C-peptide (to identify β-cells). We observed a high level of C-peptide staining in DA-ZP1-positive cells (Figure 1E). Subsequent fluorescence-activated cell sorting (FACS) of the treated islets and immunohistochemical quantification of the number of cells positive for C-peptide demonstrated that ~81% of the DA-ZP1-targeted cells were also positive for C-peptide (Figures 1F, G and S3).

These findings prompted us to design our first ZnPD with a rhodamine urea (ZnPD1, Figure 2A) that has a reported pro-fluorophore system.[31] We tested various linkers for connecting the cargo to the scaffold and found that a carbamate linkage (ZnPD1) was stable in buffers and serum-containing cell-culture media (Figure S4A). This stability could be fine-tuned by substituting electron-withdrawing groups at the ortho-/para-position of the scaffold, although ZnPD2 (chloro-substituted) and ZnPD3 (fluoro-substituted) were too labile, prematurely releasing their cargo in INS-1E media (Figure S4B

130
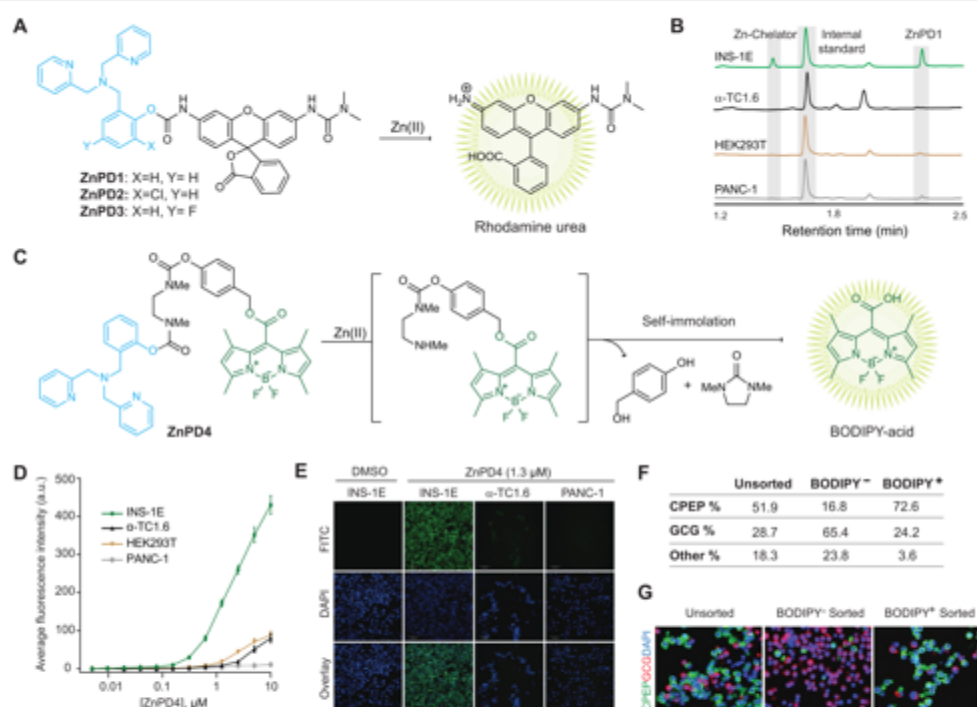
Figure 2. (A) Structures of ZnPD1−3 and their Zn(II)-mediated unmasking of rhodamine urea fluorophore. (B) LC-MS chromatogram of ZnPD1-treated cell extracts. (C) Structures of ZnPD4 and Zn(II)-catalyzed release of BODIPY fluorophore via cascading self-immolation. (D) Selective unmasking of the ZnPD4 fluorophore in INS-1E cells compared to other cells. (E) Representative images of ZnPD4-treated cells under FITC channel (top), DAPI staining (middle), and the overlay (bottom). (F) Quantification of dispersed human islets treated with ZnPD4 (*n* = 3). See also Figure S7. Human pancreatic donor information is available in Table S1. (G) Dispersed human islets were stained, and BODIPY+ and BODIPY− cells were collected after FACS (*n* = 3). Representative images show C-peptide (green) and glucagon (red) staining in unsorted, BODIPY+, BODIPY− cell populations. Nuclei stained with DAPI (blue).

and S4C). ZnPD1, lacking electron-withdrawing groups, released rhodamine urea in a Zn(II)-dependent fashion in PBS (Figure S4A), which was also confirmed by liquid chromatography—mass spectrometry (LC-MS) (Figure S4D). Removing the Zn(II)-binding ligand from ZnPD1 (ZnPD1ctrl, Figure S4E) prevented the release of rhodamine urea (Figure S4F), again confirming the proximity effect. We then demonstrated dose-dependent release of rhodamine urea in INS-1E cells at low micromolar concentrations (Figure S5). Unfortunately, the low fluorescence intensity of rhodamine urea prevented us from performing cell-selectivity studies through fluorescence, although we did confirm selective enrichment by extracting the compound from the cells followed by LC-MS analysis (Figure 2B).

To demonstrate that this prodrug system is generalizable to other cargo types and hydrolyzable bonds, we used a boron dipyrromethene (BODIPY)-based caged probe,[32] where the *meso*-carboxyl moiety of BODIPY was caged with a self-immolative linker (ZnPD4, Figure 2C).[33−35] Upon Zn(II) binding, the carbamate linkage undergoes hydrolysis and triggers self-immolation, yielding the native fluorophore (Figure S6A). With ZnPD4, we observed selective fluorescence emission in only INS-1E cells but no other cell lines (Figure

2D and E), with dose and kinetic studies showing the fast turn-on of BODIPY fluorescence in INS-1E cells (Figure S6B and S6C). After the successful, selective release of BODIPY in INS-1E cells, we used ZnPD4 to capture β-cells from dissociated human islets (Figures 2F, G and S7) and observed an enrichment of 73% in β-cell population.

We next designed ZnPD5 (Figure 3A) based on DA-ZP1 for simultaneous release of fluorescence and a small molecule (GNF-4877) that promotes pancreatic β-cell proliferation.[36,37] We could follow the Zn(II)-triggered hydrolysis of ZnPD5 through a steep rise in fluorescence intensity (Figures 3A, 3B and S8A) followed by saturation, indicating reaction completion that was also confirmed using LC-MS (Figure S8B). Additionally, ZnPD5 was stable in cell culture media and hydrolyzed only in the presence of added Zn(II) (Figure S8C). More importantly, we observed selective fluorescence emission from INS-1E cells when incubated with ZnPD5 (Figures 3C, D and S8D). The direct role of Zn(II) for ZnPD5 was confirmed by using the metal chelator TPEN, whereby INS1E cells preincubated with TPEN failed to hydrolyze ZnPD5 (Figure S8E). Next, we tested ZnPD5 in human islets and observed fluorescence release in β-cells (Figures 3E and S9A, B) as well as dose-dependent induction of proliferation (Figures 3F, S9C

131

Journal of the American Chemical Society
pubs.acs.org/JACS
Communication
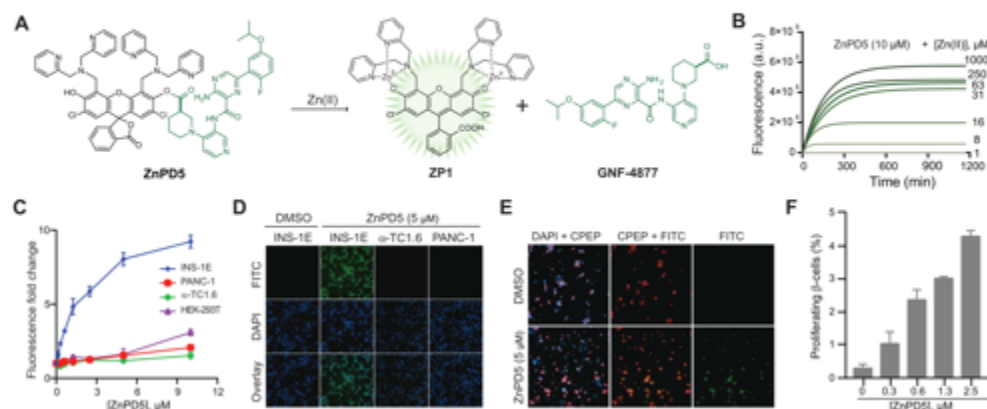
Figure 3. (A) Structures of ZnPD5 and its Zn(II)-catalyzed release of GNF-4877. (B) Reaction kinetics of ZnPD5 with different concentrations of Zn(II) as monitored by fluorescence spectroscopy. (C) Fold change in fluorescence in INS1E cells versus other cells. (D) Representative images of ZnPD5-treated cells under the FITC channel (top), DAPI staining (middle), and the overlay (bottom). (E) Representative fluorescence images of intact human islets showing β-cell selective hydrolysis of ZnPD5 under the FITC channel (green) and C-peptide (red). Intact islet cells were treated with either DMSO (top) or 150 nM of ZnPD5 (bottom). (F) Dose-dependent induction of β-cell proliferation by ZnPD5 in human islets.

and D). The degree of proliferation induced by ZnPD5 is similar to that of GNF-4877 suggesting efficacious release of the cargo (i.e., GNF-4877).

We report the first examples of a rationally designed zinc-based prodrug system for selective and traceless cargo release in β-cells. These ZnPDs are nonenzymatic, cell-permeable, and modular in nature, with a specificity that can be fine-tuned. Furthermore, this approach can deliver various small molecules, including β-cell mitogens. Using controls lacking zinc-binding moieties (e.g., ZnPD1ctrl and DA-FC), we show that cargo release is not due to cellular esterases and confirm the potency of Zn(II) for cleaving various stable bonds (e.g., carbamates) in β-cells. Importantly, this prodrug system uses an inactive analog of the cargo; zinc hydrolysis is required to release the active cargo. Thus, this system should reach a level of selectivity that cannot be achieved by uncleavable systems, which rely on a relative enrichment in the β-cell population.[24] We envision that these studies will propel the development of β-cell targeting approaches for imaging and therapeutic development.

ASSOCIATED CONTENT

Supporting Information
The Supporting Information is available free of charge at https://pubs.acs.org/doi/10.1021/jacs.0c00099.

Experimental details and synthesis methods, and human islet donor information (PDF)

AUTHOR INFORMATION

Corresponding Author
Amit Choudhary − Chemical Biology and Therapeutics Science, Broad Institute of MIT and Harvard, Cambridge, Massachusetts 02142, United States; Department of Medicine, Harvard Medical School, Boston, Massachusetts 02115, United States; Divisions of Renal Medicine and Engineering, Brigham and Women's Hospital, Boston, Massachusetts 02115, United States; Chemical Biology Program, Harvard University, Cambridge, Massachusetts 02138, United States; orcid.org/0000-0002-8437-0150; Email: achoudhary@bwh.harvard.edu

Authors
Miseon Lee − Chemical Biology and Therapeutics Science, Broad Institute of MIT and Harvard, Cambridge, Massachusetts 02142, United States; Department of Medicine, Harvard Medical School, Boston, Massachusetts 02115, United States
Basudeb Maji − Chemical Biology and Therapeutics Science, Broad Institute of MIT and Harvard, Cambridge, Massachusetts 02142, United States; Department of Medicine, Harvard Medical School, Boston, Massachusetts 02115, United States; Divisions of Renal Medicine and Engineering, Brigham and Women's Hospital, Boston, Massachusetts 02115, United States
Debasish Manna − Chemical Biology and Therapeutics Science, Broad Institute of MIT and Harvard, Cambridge, Massachusetts 02142, United States; Department of Medicine, Harvard Medical School, Boston, Massachusetts 02115, United States; Divisions of Renal Medicine and Engineering, Brigham and Women's Hospital, Boston, Massachusetts 02115, United States; orcid.org/0000-0003-4446-7318
Sevim Kahraman − Islet Cell and Regenerative Biology, Joslin Diabetes Center, Boston, Massachusetts 02215, United States; Department of Medicine, Brigham and Women's Hospital, and Harvard Stem Cell Institute, Harvard Medical School, Boston, Massachusetts 02115, United States; orcid.org/0000-0002-2880-6589
Ruth M. Elgamal − Chemical Biology and Therapeutics Science, Broad Institute of MIT and Harvard, Cambridge, Massachusetts 02142, United States; Department of Medicine, Harvard Medical School, Boston, Massachusetts 02115, United States; Divisions of Renal Medicine and Engineering, Brigham and Women's Hospital, Boston, Massachusetts 02115, United States
Jonnell Small − Chemical Biology and Therapeutics Science, Broad Institute of MIT and Harvard, Cambridge,

132

Massachusetts 02142, United States; Chemical Biology Program, Harvard University, Cambridge, Massachusetts 02138, United States

Praveen Kokkonda − Chemical Biology and Therapeutics Science, Broad Institute of MIT and Harvard, Cambridge, Massachusetts 02142, United States; Department of Medicine, Harvard Medical School, Boston, Massachusetts 02115, United States

Amedeo Vetere − Chemical Biology and Therapeutics Science, Broad Institute of MIT and Harvard, Cambridge, Massachusetts 02142, United States

Jacob M. Goldberg − Department of Chemistry, Massachusetts Institute of Technology, Cambridge, Massachusetts 02139, United States; ● orcid.org/0000-0002-8004-3769

Stephen J. Lippard − Department of Chemistry, Massachusetts Institute of Technology, Cambridge, Massachusetts 02139, United States; ● orcid.org/0000-0002-2693-4982

Rohit N. Kulkarni − Islet Cell and Regenerative Biology, Joslin Diabetes Center, Boston, Massachusetts 02215, United States; Department of Medicine, Brigham and Women's Hospital, and Harvard Stem Cell Institute, Harvard Medical School, Boston, Massachusetts 02115, United States

Bridget K. Wagner − Chemical Biology and Therapeutics Science, Broad Institute of MIT and Harvard, Cambridge, Massachusetts 02142, United States; ● orcid.org/0000-0002-2629-361X

Complete contact information is available at:
https://pubs.acs.org/10.1021/jacs.0c00099

Author Contributions

▲M.L., B.M., and D.M. contributed equally to this work

Notes

The authors declare the following competing financial interest(s): Broad Institute has filed PCT/US2018/028660 that claims inventions related to targeted delivery to beta cells.

■ **ACKNOWLEDGMENTS**

■ **REFERENCES**

(1) Butler, A. E.; Janson, J.; Bonner-Weir, S.; Ritzel, R.; Rizza, R. A.; Butler, P. C. beta-cell deficit and increased beta-cell apoptosis in humans with type 2 diabetes. Diabetes 2003, 52, 102−110.

(2) Ferrannini, E. The Stunned beta Cell: A Brief History. Cell Metab. 2010, 11, 349−352.

(3) Tuttle, R. L.; Gill, N. S.; Pugh, W.; Lee, J. P.; Koeberlein, B.; Furth, E. E.; Polonsky, K. S.; Naji, A.; Birnbaum, M. J. Regulation of pancreatic beta-cell growth and survival by the serine/threonine protein kinase Akt1/PKB alpha. Nat. Med. 2001, 7, 1133−1137.

(4) Shen, W.; Tremblay, M. S.; Deshmukh, V. A.; Wang, W.; Filippi, C. M.; Harb, G.; Zhang, Y. Q.; Kamireddy, A.; Baaten, J. E.; Jin, Q.; Wu, T.; Swoboda, J. G.; Cho, C. Y.; Li, J.; Laffitte, B. A.; McNamara, P.; Glynne, R.; Wu, X.; Herman, A. E.; Schultz, P. G. Small-Molecule Inducer of beta Cell Proliferation Identified by High-Throughput Screening. J. Am. Chem. Soc. 2013, 135, 1669−1672.

(5) Vetere, A.; Wagner, B. K. Chemical methods to induce Beta-cell proliferation. Int. J. Endocrinol. 2012, 2012, 925143.

(6) Annes, J. P.; Ryu, J. H.; Lam, K.; Carolan, P. J.; Utz, K.; Hollister-Lock, J.; Arvanites, A. C.; Rubin, L. L.; Weir, G.; Melton, D. A. Adenosine kinase inhibition selectively promotes rodent and porcine islet beta-cell replication. Proc. Natl. Acad. Sci. U. S. A. 2012, 109, 3915−3920.

(7) Andersson, O.; Adams, B. A.; Yoo, D.; Ellis, G. C.; Gut, P.; Anderson, R. M.; German, M. S.; Stainier, D. Y. Adenosine signaling promotes regeneration of pancreatic beta cells in vivo. Cell Metab. 2012, 15, 885−894.

(8) El Ouaamari, A.; Dirice, E.; Gedeon, N.; Hu, J.; Zhou, J. Y.; Shirakawa, J.; Hou, L.; Goodman, J.; Karampelias, C.; Qiang, G.; Boucher, J.; Martinez, R.; Gritsenko, M. A.; De Jesus, D. F.; Kahraman, S.; Bhatt, S.; Smith, R. D.; Beer, H. D.; Jungtrakoon, P.; Gong, Y.; Goldfine, A. B.; Liew, C. W.; Doria, A.; Andersson, O.; Qian, W. J.; Remold-O'Donnell, E.; Kulkarni, R. N. SerpinB1 Promotes Pancreatic beta Cell Proliferation. Cell Metab. 2016, 23, 194−205.

(9) Vetere, A.; Choudhary, A.; Burns, S. M.; Wagner, B. K. Targeting the pancreatic beta-cell to treat diabetes. Nat. Rev. Drug Discovery 2014, 13, 278−289.

(10) Millman, J. R.; Xie, C.; Van Dervort, A.; Gurtler, M.; Pagliuca, F. W.; Melton, D. A. Generation of stem cell-derived beta-cells from patients with type 1 diabetes. Nat. Commun. 2016, 7, 11463.

(11) Pagliuca, F. W.; Melton, D. A. How to make a functional beta-cell. Development 2013, 140, 2472−2483.

(12) Pagliuca, F. W.; Millman, J. R.; Gurtler, M.; Segel, M.; Van Dervort, A.; Ryu, J. H.; Peterson, Q. P.; Greiner, D.; Melton, D. A. Generation of functional human pancreatic beta cells in vitro. Cell 2014, 159, 428−439.

(13) Wang, P.; Alvarez-Perez, J. C.; Felsenfeld, D. P.; Liu, H. T.; Sivendran, S.; Bender, A.; Kumar, A.; Sanchez, R.; Scott, D. K.; Garcia-Ocana, A.; Stewart, A. F. A high-throughput chemical screen reveals that harmine-mediated inhibition of DYRK1A increases human pancreatic beta cell replication. Nat. Med. 2015, 21, 383−388.

(14) Naftanel, M. A.; Harlan, D. M. Pancreatic islet transplantation. PLoS Med. 2004, 1, No. e58.

(15) Mosser, R. E.; Gannon, M. An assay for small scale screening of candidate beta cell proliferative factors using intact islets. BioTechniques 2013, 55, 310−312.

(16) Reiner, T.; Thurber, G.; Gaglia, J.; Vinegoni, C.; Liew, C. W.; Upadhyay, R.; Kohler, R. H.; Li, L.; Kulkarni, R. N.; Benoist, C.; Mathis, D.; Weissleder, R. Accurate measurement of pancreatic islet beta-cell mass using a second-generation fluorescent exendin-4 analog. Proc. Natl. Acad. Sci. U. S. A. 2011, 108, 12815−12820.

(17) Moore, A.; Bonner-Weir, S.; Weissleder, R. Noninvasive in vivo measurement of beta-cell mass in mouse model of diabetes. Diabetes 2001, 50, 2231−2236.

(18) Li, Y. V. Zinc and insulin in pancreatic beta-cells. Endocrine 2014, 45, 178−89.

(19) Carpenter, M. C.; Lo, M. N.; Palmer, A. E. Techniques for measuring cellular zinc. Arch. Biochem. Biophys. 2016, 611, 20−29.

(20) Bozym, R. A.; Chimienti, F.; Giblin, L. J.; Gross, G. W.; Korichneva, I.; Li, Y. A.; Libert, S.; Maret, W.; Parviz, M.; Frederickson, C. J.; Thompson, R. B. Free zinc ions outside a narrow concentration range are toxic to a variety of cells in vitro. Exp. Biol. Med. 2010, 235, 741−750.

(21) Li, D.; Chen, S.; Bellomo, E. A.; Tarasov, A. I.; Kaut, C.; Rutter, G. A.; Li, W. H. Imaging dynamic insulin release using a fluorescent zinc indicator for monitoring induced exocytotic release (ZIMIR). Proc. Natl. Acad. Sci. U. S. A. 2011, 108, 21063−21068.

(22) Jayaraman, S. A novel method for the detection of viable human pancreatic beta cells by flow cytometry using fluorophores that selectively detect labile zinc, mitochondrial membrane potential and protein thiols. Cytometry, Part A 2008, 73A, 615−625.

(23) Gee, K. R.; Zhou, Z. L.; Qian, W. J.; Kennedy, R. Detection and imaging of zinc secretion from pancreatic beta-cells using a new fluorescent zinc indicator. J. Am. Chem. Soc. 2002, 124, 776−778.

133

(24) Horton, T. M.; Allegretti, P. A.; Lee, S.; Moeller, H. P.; Smith, M.; Annes, J. P. Zinc-Chelating Small Molecules Preferentially Accumulate and Function within Pancreatic beta Cells. *Cell Chem. Biol.* **2019**, *26*, 213−222.

(25) Zhang, X. A.; Hayes, D.; Smith, S. J.; Friedle, S.; Lippard, S. J. New strategy for quantifying biological zinc by a modified zinpyr fluorescence sensor. *J. Am. Chem. Soc.* **2008**, *130*, 15788−15789.

(26) Chyan, W.; Zhang, D. Y.; Lippard, S. J.; Radford, R. J. Reaction-based fluorescent sensor for investigating mobile Zn²⁺ in mitochondria of healthy versus cancerous prostate cells. *Proc. Natl. Acad. Sci. U. S. A.* **2014**, *111*, 143−148.

(27) Zastrow, M. L.; Radford, R. J.; Chyan, W.; Anderson, C. T.; Zhang, D. Y.; Loas, A.; Tzounopoulos, T.; Lippard, S. J. Reaction-Based Probes for Imaging Mobile Zinc in Live Cells and Tissues. *ACS Sens.* **2016**, *1*, 32−39.

(28) Que, E. L.; Domaille, D. W.; Chang, C. J. Metals in neurobiology: probing their chemistry and biology with molecular imaging. *Chem. Rev.* **2008**, *108*, 1517−1549.

(29) Kulkarni, R. N.; Mizrachi, E. B.; Ocana, A. G.; Stewart, A. F. Human beta-cell Proliferation and Intracellular Signaling: Driving in the Dark Without a Road Map. *Diabetes* **2012**, *61*, 2205−2213.

(30) Bernal-Mizrachi, E.; Kulkarni, R. N.; Scott, D. K.; Mauvais-Jarvis, F.; Stewart, A. F.; Garcia-Ocana, A. Human beta-Cell Proliferation and Intracellular Signaling Part 2: Still Driving in the Dark Without a Road Map. *Diabetes* **2014**, *63*, 819−831.

(31) Lavis, L. D.; Chao, T. Y.; Raines, R. T. Fluorogenic label for biomolecular imaging. *ACS Chem. Biol.* **2006**, *1*, 252−260.

(32) Chen, H.; He, X.; Su, M.; Zhai, W.; Zhang, H.; Li, C. A General Strategy Toward Highly Fluorogenic Bioprobes Emitting across the Visible Spectrum. *J. Am. Chem. Soc.* **2017**, *139*, 10157−10163.

(33) Blencowe, C. A.; Russell, A. T.; Greco, F.; Hayes, W.; Thornthwaite, D. W. Self-immolative linkers in polymeric delivery systems. *Polym. Chem.* **2011**, *2*, 773−790.

(34) Alouane, A.; Labruere, R.; Le Saux, T.; Schmidt, F.; Jullien, L. Self-Immolative Spacers: Kinetic Aspects, Structure-Property Relationships, and Applications. *Angew. Chem., Int. Ed.* **2015**, *54*, 7492−7509.

(35) Roth, M. E.; Green, O.; Gnaim, S.; Shabat, D. Dendritic, Oligomeric, and Polymeric Self-Immolative Molecular Amplification. *Chem. Rev.* **2016**, *116*, 1309−1352.

(36) Shen, W.; Taylor, B.; Jin, Q.; Nguyen-Tran, V.; Meeusen, S.; Zhang, Y. Q.; Kamireddy, A.; Swafford, A.; Powers, A. F.; Walker, J.; Lamb, J.; Bursalaya, B.; DiDonato, M.; Harb, G.; Qiu, M.; Filippi, C. M.; Deaton, L.; Turk, C. N.; Suarez-Pinzon, W. L.; Liu, Y.; Hao, X.; Mo, T.; Yan, S.; Li, J.; Herman, A. E.; Hering, B. J.; Wu, T.; Martin Seidel, H.; McNamara, P.; Glynne, R.; Laffitte, B. Inhibition of DYRK1A and GSK3B induces human beta-cell proliferation. *Nat. Commun.* **2015**, *6*, 8372.

(37) Kelkar, S. S.; Reineke, T. M. Theranostics: combining imaging and therapy. *Bioconjugate Chem.* **2011**, *22*, 1879−903.

134

Native zinc catalyzes selective and traceless release of small molecules in β-cells

Miseon Lee[1,2,7], Basudeb Maji[1,2,3,7], Debasish Manna[1,2,3,7], Sevim Kahraman[2,6], Ruth M. Elgamal[1,2,3], Jonnell Small[1,4], Praveen Kokkonda[1,2], Amedeo Vetere[1], Jacob M. Goldberg,[5] Stephen J. Lippard,[5] Rohit N. Kulkarni[2,6], Bridget K. Wagner[1], and Amit Choudhary[1,2,3,4,*]

[1]Chemical Biology and Therapeutics Science, Broad Institute of MIT and Harvard, Cambridge, MA 02142, USA
[2]Department of Medicine, Harvard Medical School, Boston, MA 02115, USA
[3]Divisions of Renal Medicine and Engineering, Brigham and Women's Hospital, Boston, MA 02115, USA
[4]Chemical Biology Program, Harvard University, Cambridge, MA, USA
[5]Department of Chemistry, Massachusetts Institute of Technology, 77 Massachusetts Avenue, Cambridge, Massachusetts 02139, United States
[6]Joslin Diabetes Center, Islet Cell and Regenerative Biology, Boston, MA, USA; Harvard Stem Cell Institute, Boston, MA, USA
[7]These authors contributed equally to this work

*Correspondence: achoudhary@bwh.harvard.edu (A.C.)

*To whom correspondence should be addressed:

Amit Choudhary
Chemical Biology and Therapeutics Science
Broad Institute of MIT and Harvard
415 Main Street, Rm 3012
Cambridge, MA 02142
Phone: (617) 714-7445
Fax: (617) 715-8969
Email: achoudhary@bwh.harvard.edu

135

Dose and Time-dependent of beta-cell specific hydrolysis with DA-ZP1
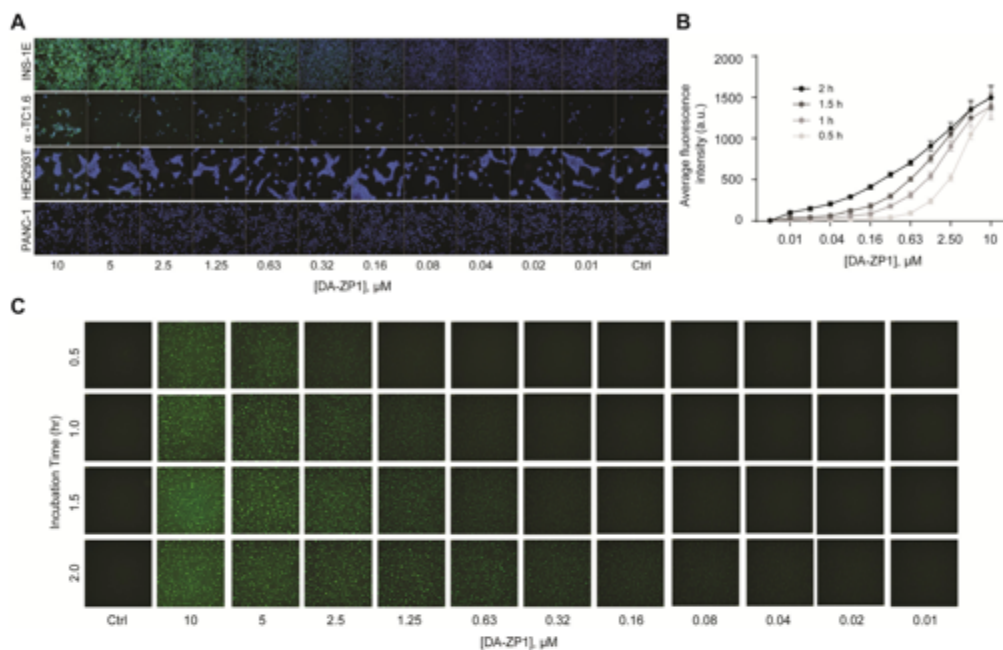
Figure S1. **(A)** β-cell-specific hydrolysis of DA-ZP1 unmasks fluorescence in a dose-dependent manner after 1 h of compound incubation at different concentrations. Each panel represents a merged FITC and DAPI channel. **(B)** Fluorescence release kinetics in INS-1E cells at increasing concentrations of DA-ZP1. **(C)** Time-dependent unmasking of DA-ZP1 in INS-1E cells imaged with the FITC channel.

S17

136

Appendix 2: Harnessing reaction-based probes to preferentially target pancreatic β-cells and β-like cells

Attribution:

Sevim Kahraman, Debasish Manna, Ercument Dirice, Basudeb Maji, **Jonnell Small**, Bridget K Wagner, Amit Choudhary, Rohit N Kulkarni[*]

Author Contribution:

JS designed the confocal microscopy imaging protocol for quantifying DA-ZP1 in EndoC-βH1 cells, and assisted in the writing and editing of the manuscript.

Research Article

Check for updates
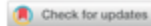
Harnessing reaction-based probes to preferentially target pancreatic β-cells and β-like cells

Sevim Kahraman[1] ⓘ, Debasish Manna[2,3,4,*], Ercument Dirice[1,*] ⓘ, Basudeb Maji[2,3,4], Jonnell Small[2,5], Bridget K Wagner[2] ⓘ, Amit Choudhary[2,3,4,5] ⓘ, Rohit N Kulkarni[1] ⓘ

Highly sensitive approaches to target insulin-expressing cells would allow more effective imaging, sorting, and analysis of pancreatic β-cells. Here, we introduce the use of a reaction-based probe, diacetylated Zinpyr1 (DA-ZP1), to image pancreatic β-cells and β-like cells derived from human pluripotent stem cells. We harness the high intracellular zinc concentration of β-cells to induce a fluorescence signal in cells after administration of DA-ZP1. Given its specificity and rapid uptake by cells, we used DA-ZP1 to purify live stem cell–derived β-like cells as confirmed by immunostaining analysis. We tested the ability of DA-ZP1 to image transplanted human islet grafts and endogenous mouse pancreatic islets in vivo after its systemic administration into mice. Thus, DA-ZP1 enables purification of insulin-secreting β-like cells for downstream applications, such as functional studies, gene-expression, and cell–cell interaction analyses and can be used to label engrafted human islets and endogenous mouse islets in vivo.

Introduction

Restoring normoglycemia independent of exogenous insulin injections can be achieved by islet cell replacement therapy. However, the limited number of donors and the need for lifelong immunosuppression pose a continuing challenge to the success of islet transplantation approach (Gamble et al, 2018). Human pluripotent stem cells (hPSCs), which have unlimited proliferation potential, provide an excellent source for cell replacement therapies. With recent successes in generating functional pancreatic β-like cells derived from hPSCs, the use of stem cells for the treatment of diabetes is promising (Kahraman et al, 2016). Several laboratories have published protocols to generate functional pancreatic β-like cells in vitro (Pagliuca et al, 2014; Rezania et al, 2014; Russ et al, 2015), and follow-up studies have optimized the protocols to improve the number and function of β-like cells (Zhu et al, 2016a;

Ghazizadeh et al, 2017; Nair et al, 2019; Velazco-Cruz et al, 2019; Hogrebe et al, 2020). However, several limitations have emerged with the directed differentiation of hPSCs for research and therapy. First, current protocols for making hPSC-derived β-like cells result in cell cultures that consist of a mixture of cell types, including non-β endocrine cells and cells with tumorigenic potential, which could develop into tumors after transplantation (Nair et al, 2019; Veres et al, 2019). The second concern is the known variability across hPSC lines, which results in generation of variable numbers of insulin-expressing cells at the final stage of the differentiation protocol (Thatava et al, 2013). To circumvent these issues, several groups have developed methods to isolate and purify insulin-secreting β-like cells for transcriptional and functional analyses. One such approach uses $INS^{GFP/w}$ human embryonic stem cells (hESCs) to facilitate isolation of insulin-expressing cells (Micallef et al, 2012). However, this approach depends on generating a reporter line and is not convenient when using other unmodified hPSC or patient-derived induced pluripotent stem cell (iPSC) lines (Zhu et al, 2016b). Other approaches include cellular fixation followed by intracellular immunofluorescence and sorting (Hrvatin et al, 2014); although this is useful for transcriptional analyses, it cannot be used for downstream functional studies requiring live cells. Other groups have reported using cell surface antibodies to alternately sort pancreatic progenitors or endoderm cells to increase the yield of β-like cells during the terminal differentiation stages (Kelly et al, 2011; Ameri et al, 2017; Cogger et al, 2017). Although this method allows elimination of undifferentiated human embryonic stem cells, further differentiation of sorted pancreatic progenitors into β-like cells results in generation of C-peptide+ (CPEP) cells at varying efficiencies. Recently, magnetic cell sorting of β-like cells using the cell surface marker, CD49a, has been reported to enrich β-like cells derived from hPSCs; however, this method requires antibody staining (Veres et al, 2019).

A small-molecule–based method for sorting has several advantages over the aforementioned genetic- and biologic-based methods. First, unlike biologics, small molecules can be easily delivered into cells through passive diffusion allowing targeting of

[1]Islet Cell and Regenerative Biology, Joslin Diabetes Center, Department of Medicine, Brigham and Women's Hospital, Harvard Stem Cell Institute, Harvard Medical School, Boston, MA, USA   [2]Chemical Biology and Therapeutics Science Program, Broad Institute of MIT and Harvard, Cambridge, MA, USA   [3]Department of Medicine, Harvard Medical School, Boston, MA, USA   [4]Divisions of Renal Medicine and Engineering, Brigham and Women's Hospital, Boston, MA, USA   [5]Chemical Biology Program, Harvard University, Cambridge, MA, USA

Correspondence: Rohit.Kulkarni@joslin.harvard.edu; achoudhary@bwh.harvard.edu
Ercument Dirice's present address is Department of Pharmacology, New York Medical College of Medicine, Valhalla, NY, USA
*Debasish Manna and Ercument Dirice contributed equally to this work

cell-specific markers located intracellularly or on cell surface without cellular fixation, reducing both effort and cost, and allowing scaling up of cell sorting processes. Second, unlike genetic methods, small molecules act rapidly requiring as little as a few minutes for their activity (Que et al, 2008). Such rapid kinetics allows precision dose- and temporal-control and enables fine-tuning of the activity and specificity of the sorting method. Third, small molecules are typically not immunogenic and thereby enable in vivo applications. Finally, small molecules have the advantage of being able to be produced *en masse* and at low cost with little batch-to-batch variability. Prior efforts have used the zinc content in β-cells to sort human and murine pancreatic β-cells, using fluorescent probes such as TSQ (6-methoxy-8-p-toluenesulfonamido-quinoline) (Klochendler et al, 2016), FluoZin-3-AM (Jayaraman, 2008), or Newport Green (Parnaud et al, 2008). TSQ has also been used for purification of β-like cells derived from hPSCs based on intracellular zinc content (Davis et al, 2019). Here, we employed a reaction-based probe, diacetylated Zinpyr1 (DA-ZP1), to label and isolate insulin-expressing cells both in vivo and in vitro. DA-ZP1 is non-fluorescent in the absence of zinc ions [Zn(II)], but binding of Zn(II) selectively and rapidly mediates hydrolytic cleavage of the acetyl groups, providing a detectable fluorescence response (Chyan et al, 2014). Lippard and co-workers (Zastrow et al, 2016) demonstrated the Zn(II) specificity of this reaction over those of other biologically relevant metal ions, including Fe(II), Cu(II), Mn(II), Co(II), and Ni(II). Insulin-secreting cells are selectively enriched for Zn(II), whereas α cells and pancreatic exocrine cells exhibit relatively less abundance of the ion (Toroptsev et al, 1974; Jindal et al, 1992). Indeed, insulin-containing cells are highly enriched for Zn(II) to a magnitude of 10–20 mM in insulin granules (Li, 2014), making them an excellent target cell type for zinc-dependent fluorescence labeling (Jindal et al, 1992).

Furthermore, tracking β-cell mass in vivo serves an important role for assessing outcomes of therapeutic interventions for diabetes. In this context, high β-cell specificity relative to neighboring endocrine and exocrine cells is an essential parameter for successful in vivo imaging of β-cell mass (Sweet et al, 2004).

Considering Zn(II) is considerably enriched in pancreatic β-cells compared with neighboring cells and no toxicity is observed in in vivo studies (Rice et al, 2016), zinc-based reaction probes are promising candidates for β-cell imaging. In efforts to label pancreatic β-cells in vivo, we also tested a chelator-based strategy to monitor engrafted human islets and endogenous mouse islets. Our work shows that systemic administration of DA-ZP1 leads to its enrichment in pancreatic β-cells and has the potential to be developed for measuring β-cell mass, sorting, and targeting.

In this study we report the in vitro use of zinc- and small-molecule–based reaction probes to label and image live insulin-secreting β-like cells in real time. Our data indicate that DA-ZP1 preferentially labels insulin-positive cells and can be used to enrich live insulin-positive cells for multiple downstream applications, including gene expression analysis, functional studies, cell–cell interaction analyses, in vivo imaging, and β-cell directed activation of bioactive small molecules.

Results

DA-ZP1 is preferentially unmasked in pancreatic β-cells in a time- and dose-dependent manner without affecting function

To begin, we tested DA-ZP1 in human pancreatic β-cells for fluorescence imaging over time. EndoC-βH1 cells were treated with 5 μM DA-ZP1 and fluorescence intensity was measured over 1 h (Fig 1A). An increase in the intracellular fluorescence signal was observed in cells 2 min after administration of DA-ZP1 and the signal increased significantly over 1 h (Fig 1B). Starved cells displayed stronger fluorescence signal compared with non-starved cells possibly because starvation induces an enhanced ability to detect Zn(II) in pancreatic β-cells (Toroptsev et al, 1974). To ensure that the unmasking of DA-ZP1 fluorescence in cells was not catalyzed by an
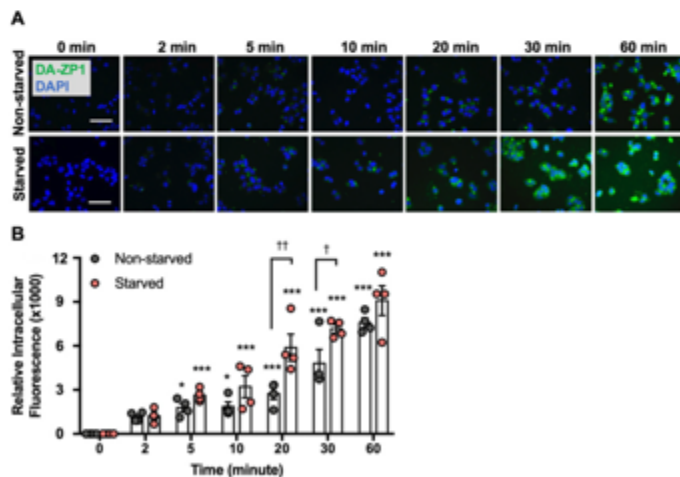
Figure 1. Time course accumulation of DA-ZP1 in human pancreatic β-cells.
(A) Starved (3-h starvation in DMEM containing 2 mM glucose) or non-starved EndoC-βH1 cells were treated with 5 μM DA-ZP1 for 0, 2, 5, 10, 20, 30, or 60 min and then fixed in 4% paraformaldehyde. Representative images show presence of DA-ZP1 (green) in EndoC-βH1 cells at the different times. Nuclei stained with DAPI (blue). Scale bar is 500 μm. **(B)** Quantification of intracellular fluorescence 0, 2, 5, 10, 20, 30, or 60 min after DA-ZP1 treatment. Relative intracellular fluorescence was measured using Image J. Staining was conducted in a 96-well format (n = 4 replicates/condition), and at least four images per condition were captured per well. Data are represented as mean ± SEM. *$P < 0.05$, ***$P < 0.001$ versus 0 min, †$P < 0.05$, ††$P < 0.01$ starved versus non-starved. Two-way ANOVA followed by the Holm–Sidak method.

139

esterase and the fluorescence is specific to Zn(II) binding, we synthesized a DA-ZP1 analog (DM-1) lacking the Zn(II)-binding ligand (and contains the esters) (Fig 2A and B) and tested its effects on EndoC-βH1 cells. As expected, EndoC-βH1 cells treated with DM-1 exhibited little to no fluorescence compared with DA-ZP1–treated cells, even up to 48 h after treatment (Fig 2C). DA-ZP1, on the other hand, generated strong fluorescence, which was significantly increased in the first 6 h and then significantly declined at 48 h. Prolonged treatment with DA-ZP1 showed that the fluorescence signal could be detected even after 7 d (Fig 2D). Whereas the half-life of DA-ZP1 for highly active porcine esterase is in the range of

hours the same for Zn(II) is ~8.1 s, indicating a kinetic specificity to the DA-ZP1 scaffold for Zn(II) (Chyan et al, 2014). Furthermore, DA-ZP1 is a PET-based zinc sensor that requires Zn(II)-triggered hydrolysis of a tethered acetate ester to turn-on fluorescence and is insensitive to intracellular esterases (Zastrow et al, 2016).

"Mobile" Zn(II) is found in concentrations between 0.4 and 1.5 nM in the cytosol and at substantially higher concentrations (1~100 μM) in insulin-containing secretory vesicles in pancreatic β-cells (Vinkenborg et al, 2009; Rutter et al, 2016). Consistently, we observed presence of the fluorescence signal in subcellular compartments in the EndoC-βH1 cells colocalizing with insulin (Fig 3A). Since DA-ZP1
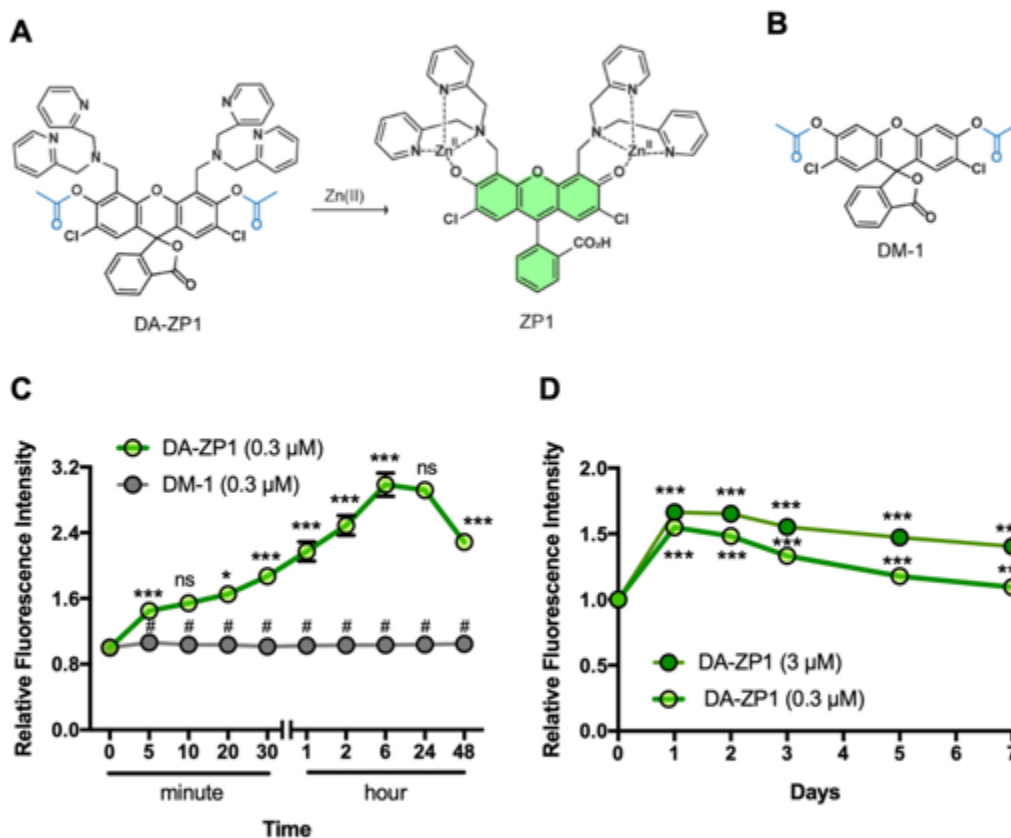
Figure 2. DA-ZP1 and DM-1 staining of human pancreatic β-cells.
(A) Chemical structure of DA-ZP1. Zn(II)-mediated deacetylation of DA-ZP1 releases active fluorophore ZP-1. **(B)** Chemical structure of control compound DM-1 which is a DA-ZP1 analog lacking the Zn(II)-binding ligand. **(C)** EndoC-βH1 cells were treated with DA-ZP1 (0.3 μM) or DM-1 (0.3 μM) for 0, 5, 10, 20, 30 min, or 1, 2, 6, 24, or 48 h. Staining was conducted in a 96-well format (n = 4 replicates/condition). Fluorescent images were acquired using an automated system (9 images/well) and intracellular fluorescence was measured by MetaXpress software. Relative fluorescence intensity showed presence of DA-ZP1 (green line) and DM-1 (gray line) at different time points in EndoC-βH1 cells. #$P < 0.0001$ DA-ZP1 versus DM-1, ***$P < 0.0001$ DA-ZP1 5 versus 0 min, 30 versus 20 min, 1 h versus 30 min, 2 versus 1 h, 6 versus 2 h, 48 versus 24 h, *$P < 0.05$ DA-ZP1 20 versus 10 min, ns indicates not significant 10 versus 5 min, 24 versus 6 h. Two-way ANOVA followed by Tukey's method. **(D)** Relative fluorescence intensity was measured for 7 d after treatment of EndoC-βH1 cells with DA-ZP1 (0.3 μM; light green, 3 μM; dark green, n = 8 replicates/condition). Data are represented as mean ± SEM. Two-way ANOVA followed by Dunnett's method. ***$P < 0.0001$ versus 0 min.

140
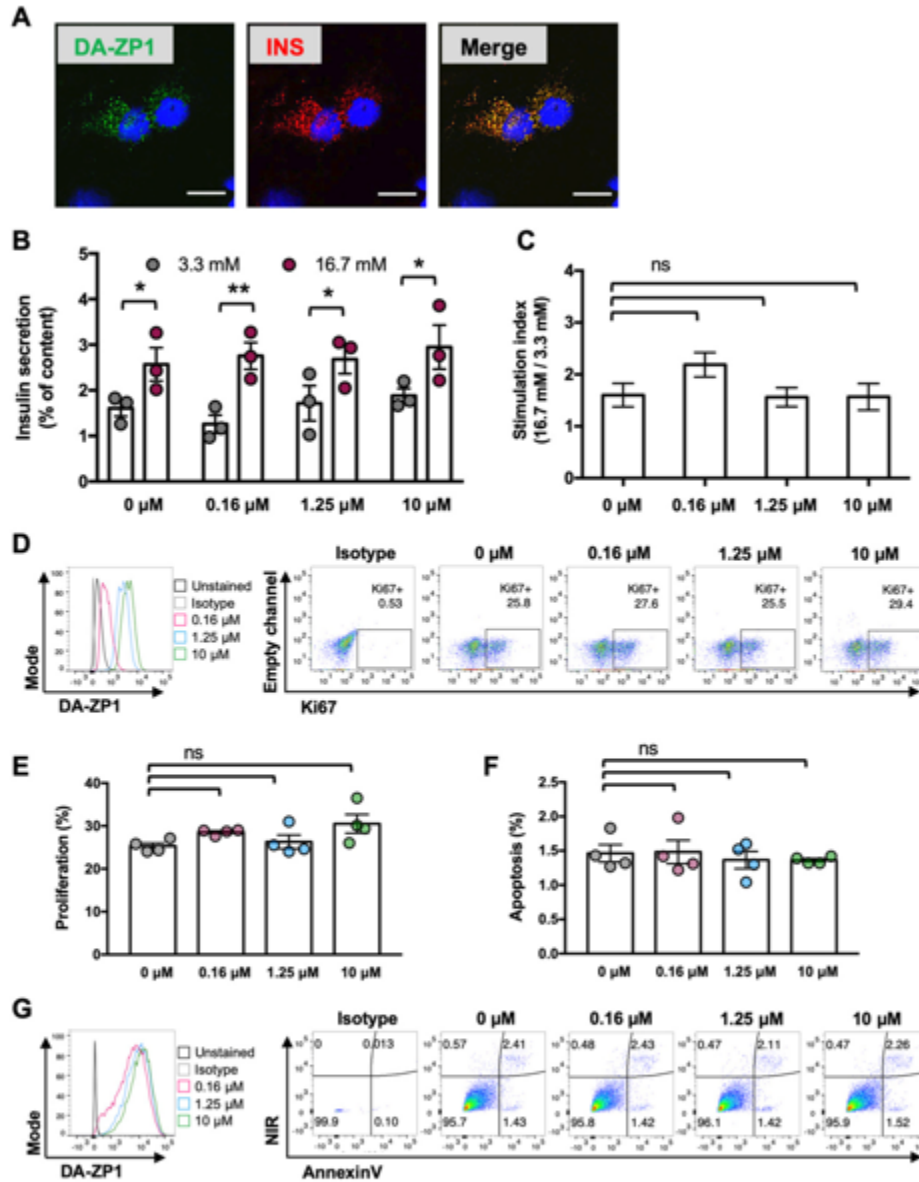
Figure 3. DA-ZP1 treatment does not impair β-cell function.
(A) Confocal imaging of EndoC-βH1 cells stained with DA-ZP1 (60 min, 5 µM DA-ZP1) and subsequently fixed and co-stained for insulin showing DA-ZP1 staining in subcellular compartments of the cells. Nuclei stained with DAPI (blue). Scale bar is 20 µm. **(B)** Glucose stimulated insulin secretion assay performed after treatment of EndoC-βH1 cells with 0, 0.16, 1.25, or 10 µM DA-ZP1 (n = 3 independent replicates/condition). Insulin secretion plotted as % of total insulin content. Data are represented as mean ± SEM. *$P < 0.05$, **$P < 0.01$. P-values were calculated by unpaired multiple t test to determine differences between 16.7 and 3.3 mM. **(C)** The stimulation index was calculated as the fold increase in insulin release measured in 16.7 over 3.3 mM glucose (n = 3 independent replicates/condition). P-values were calculated by one-way ANOVA with Dunnett for multiple comparison versus 0 µM. **(D, E, F, G)** Effects DA-ZP1 treatment on proliferation (D, E) and apoptosis (F, G) in EndoC-βH1 cells (n = 4 replicates/condition). P-values were calculated by one-way ANOVA followed by Dunnett's method. Data are represented as mean ± SEM. ns indicates not significant.
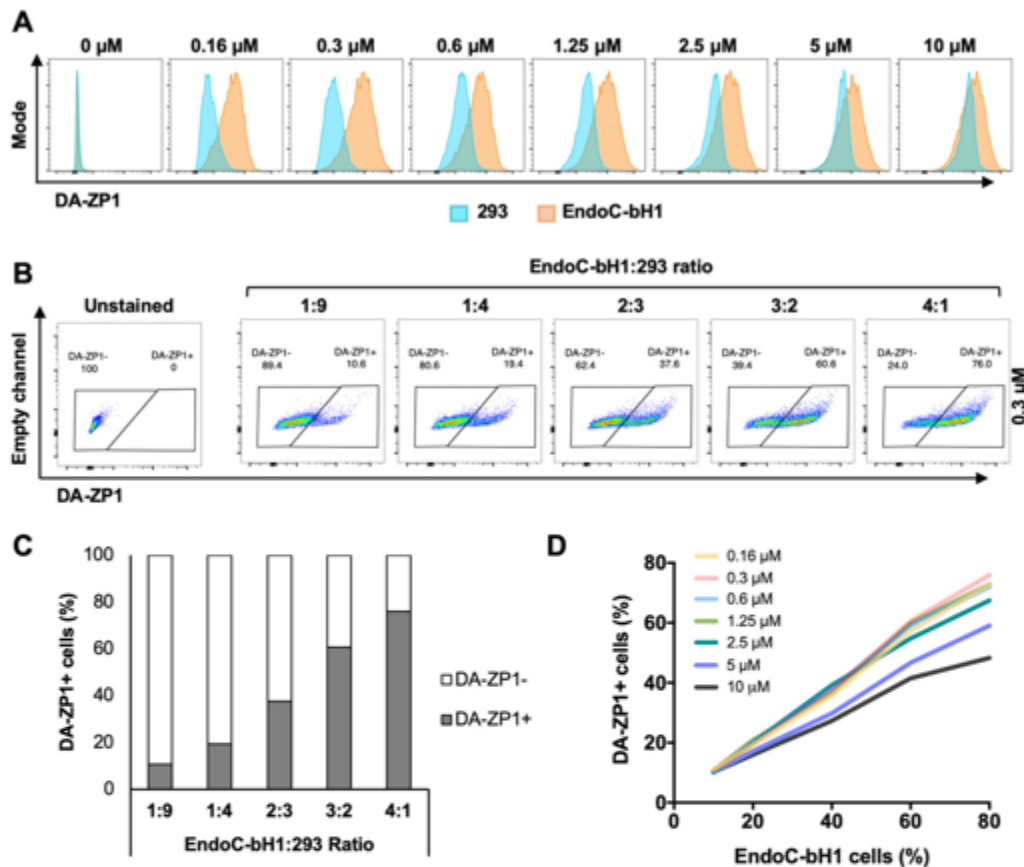
Figure 4. Low concentrations of DA-ZP1 differentiate β-cells from non-β cells.
(A) EndoC-βH1 and 293 cells were treated with different concentrations of DA-ZP1 for 30 min and then analyzed by flow cytometry (n = 3 replicates for each dose/group). Blue histogram shows 293 cells and orange histogram shows EndoC-βH1 cells. See also Fig S1A. **(B)** EndoC-βH1 cells were mixed with 293 cells in different proportions (EndoC-βH1:293 ratio; 1:9, 1:4, 2:3, 3:2, and 4:1), stained with 0.3 μM DA-ZP1 for 30 min, and analyzed by flow cytometry (n = 5 samples). See also Fig S1B for other concentrations of DA-ZP1. See also Fig S2A and B. **(C)** Quantification of percentage of DA-ZP1+ cells shows correlation with EndoC-βH1 proportion in the cell mixture (n = 5 samples). See also Fig S1C for other concentrations of DA-ZP1. See also Fig S2C. **(D)** Correlation of percentage of DA-ZP1+ cells and percentage of EndoC-βH1 cells in the mixed samples stained with different concentrations of DA-ZP1 (n = 5 samples) (Pearson's correlation r = 0.99 for each concentration). See also Fig S2D.

less β-cell targeting efficiency of TSQ. We also demonstrated enrichment of mouse β-cells after DA-ZP1 treatment (~88% insulin positive cells) that was comparable with the classical granularity/auto-fluorescence-based enrichment process (~90% insulin positive cells) (Fig S7A–C) (Pipeleers et al, 1985).

Next, we assessed whether we could use DA-ZP1 to image transplanted human islets in vivo. Human islets were transplanted under the kidney capsule of NSG mice, and kidneys containing the grafts were excised 3 d posttransplantation and treated with DA-ZP1 for 30 min. DA-ZP1–treated grafts were detectable because of their strong fluorescent signal, whereas virtually no fluorescence was detected in the kidney tissue or in the untreated grafts (Fig 7B). To

test whether DA-ZP1 can also be used in vivo, mice bearing human islet transplants were housed for a month to allow vascularization of the islet grafts, followed by i.v. injection with 10 mg/kg.b.wt. DA-ZP1 or DMSO. 1 h after the injection, a strong fluorescent signal was detected in the human islet grafts from mice treated with DA-ZP1, whereas no signal was evident in the islet grafts of DMSO-treated animals (Fig 7C). As expected, we also detected fluorescence in the islets of endogenous pancreas of DA-ZP1–injected mice, whereas no signal was observed in the surrounding organs including metabolic tissues such as the liver, adipose tissue, or skeletal muscle in either DA-ZP1– or DMSO-treated animals (Fig 7D). Iso-lation of pancreatic islets and pancreatic exocrine cells showed

142
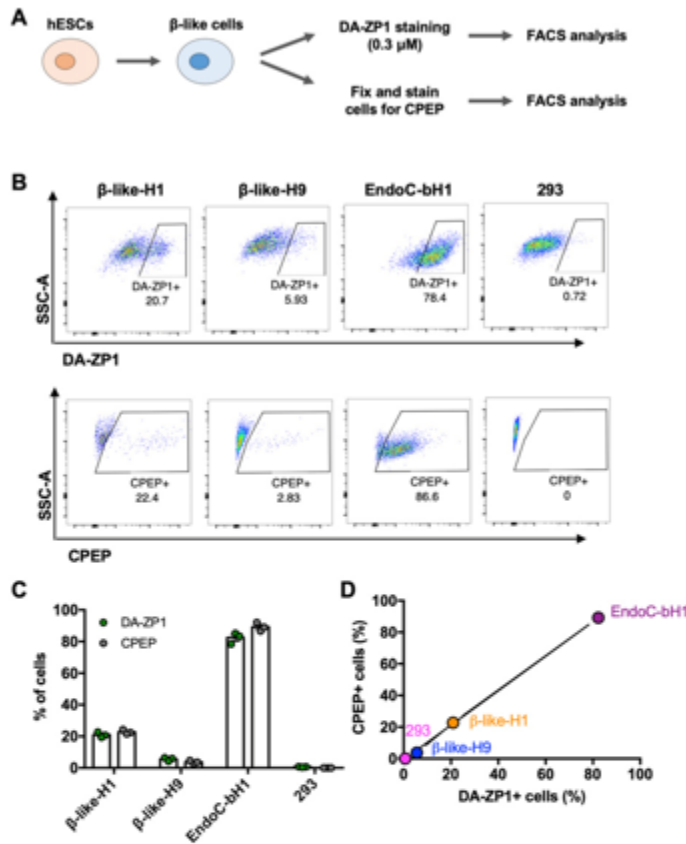
Figure 5. Percentage of DA-ZP1+ cells correlates with percentage CPEP+ cells.
(A) Human embryonic stem cells were differentiated to β-like cells and first stained for DA-ZP1 (0.3 μM) followed by CPEP staining. Composition of human embryonic stem cell differentiation media is available in Table S1. **(B)** FACS analysis of β-like cells derived from two different human stem cell lines (β-like-H1 and β-like-H9), EndoC-βH1, and 293 cells stained for DA-ZP1 (0.3 μM) or CPEP (n = 3 replicates). See also Fig S4. **(C)** Quantification of FACS data for percentage of DA-ZP1+ cells and CPEP+ cells (n = 3 replicates). Data are mean ± SEM. **(D)** Correlation of percentage of DA-ZP1+ cells and percentage of CPEP+ cells (Pearson's correlation r = 0.99) (n = 3 replicates). See also Fig S4.

that the source of the fluorescence signal in the pancreas was the pancreatic islets, and not exocrine cells (Fig S8A and B). These results indicate that intravenously administered DA-ZP1 specifically reaches the targeted tissue.

Discussion

The use of fluorescent zinc probes for sorting insulin-positive cells is promising because it satisfies several important criteria: (1) it offers high selectivity for insulin-positive β-cells compared with insulin-negative non-β cells; (2) it is nontoxic to the cells; and (3) it elicits a significant and rapid fluorescent response upon zinc binding, which can be captured by flow cytometry (ex: 495 nm, em: 500–650 nm), minimizing autofluorescence and avoiding UV-induced tissue damage, as might be caused by zinc probes described in earlier reports such as TSQ (Huang & Lippard, 2012).

A recent study showed the importance of endocrine cell clustering for functional maturation of β-like cells in vitro (Nair et al, 2019). They demonstrated that enrichment of GFP+ β-like cells derived from $INS^{GFP/w}$ reporter hESC line (~90%) and their aggregation into cell clusters improved dynamic insulin secretion and calcium signaling in response to secretagogues. In this context the zinc-based DA-ZP1 fluorescence we propose is a very sensitive and reproducible method for purification of β-like cells derived from hESC or iPSC lines and could be applied to generate highly pure β-like cell clusters for improved functional maturation.

Until now, antibody-based methods have been used in an attempt to enrich β-cells from islets. For example, in efforts to study individual human islet cell types, a panel of cell–surface markers was developed (Dorrell et al, 2008, 2016) wherein live human pancreatic β-cells were isolated by depleting other cell types. More recently, NTPDase3 was reported to be a cell–surface biomarker and used to purify human β-cells in combination with negative selection markers (Saunders et al, 2019). To our knowledge,

143
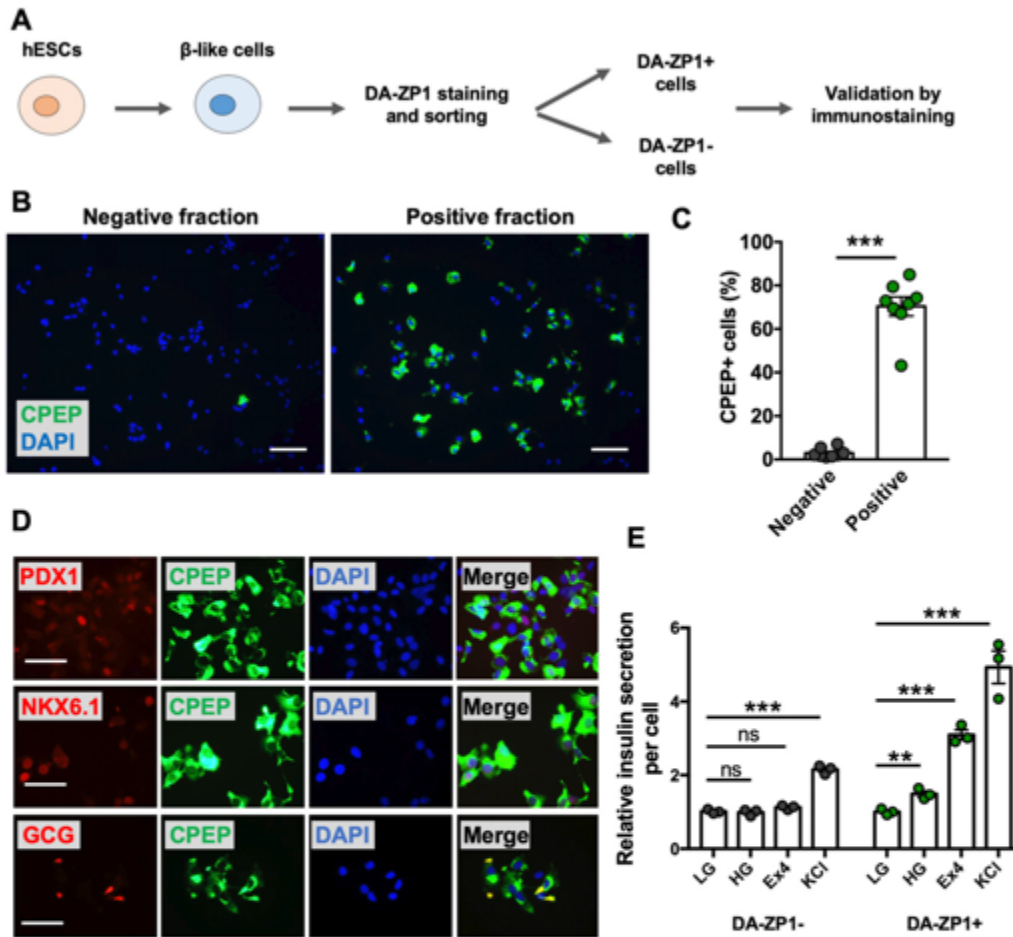
Figure 6. Enrichment of CPEP+ cells in DA-ZP1 positive fractions.
(A) Overview of DA-ZP1 analysis and experimental approach. **(B)** β-like cells derived from two human embryonic stem cell lines were stained and DA-ZP1+ and DA-ZP1– cells were collected after FACS. Representative images show CPEP staining (green) in DA-ZP1+ and DA-ZP1– fractions. Nuclei stained with DAPI (blue). Scale bar is 100 μm. **(C)** Quantification of percentage of CPEP+ cells in DA-ZP1+ and DA-ZP1– fractions. Staining was conducted in a 96-well format (n = 8, two biological replicates with four technical replicates). At least six images per condition were captured and >1,000 cells were analyzed per well. Data are represented as mean ± SEM. ***P < 0.001, P-value is calculated by two-tailed t test. **(D)** Immunostaining of DA-ZP1+ cells that were collected after FACS for markers of pancreatic β-cells (n = 3 technical replicates). PDX1 (red), NKX6.1 (red), GCG (red), CPEP (green), and DAPI (blue). Scale bar is 50 μm. **(E)** Static insulin secretion test was performed on DA-ZP1 sorted positive and negative cells at β-like cell stage (n = 3 replicates/condition, repeated twice using two different human embryonic stem cell lines). Human insulin secretion was calculated by dividing the secreted insulin by the total number of cells. The amount of insulin secretion was normalized to the amount of insulin secreted in LG condition. LG, low glucose (1 mM); HG, high glucose (20 mM); Exendin-4 (Ex4), 10 nM Ex4 in the presence of 20 mM glucose; KCl, 30 mM KCl. Data are represented as mean ± SEM. ns indicates not significant. **P < 0.01, ***P < 0.001 versus LG. P-values were calculated by multiple t test followed by the Holm–Sidak method.

NTPDase3 has not been tested using its cell surface marker properties to show whether it enables isolation of β-like cells. In another study, CD49a, which is not specific to human β-cells, was reported as a surface marker of stem cell-derived β-like cells (Veres et al, 2019). Anti-CD49a labeling followed by magnetic sorting was used to purify β-like cells up to 80%. Compared with these antibody selection approaches, DA-ZP1 is very rapid, inexpensive, and can be applied to sort insulin-positive β-like cells without the need for cell surface marker expression. Isolation of a viable β-like population with robust enrichment should enable transcriptional studies and functional assays such as static glucose stimulation and other metabolic analyses.

144

A   Human islets *in vitro*

B   Human islet graft on kidney

C   Human islet graft on kidney

D   Other tissues
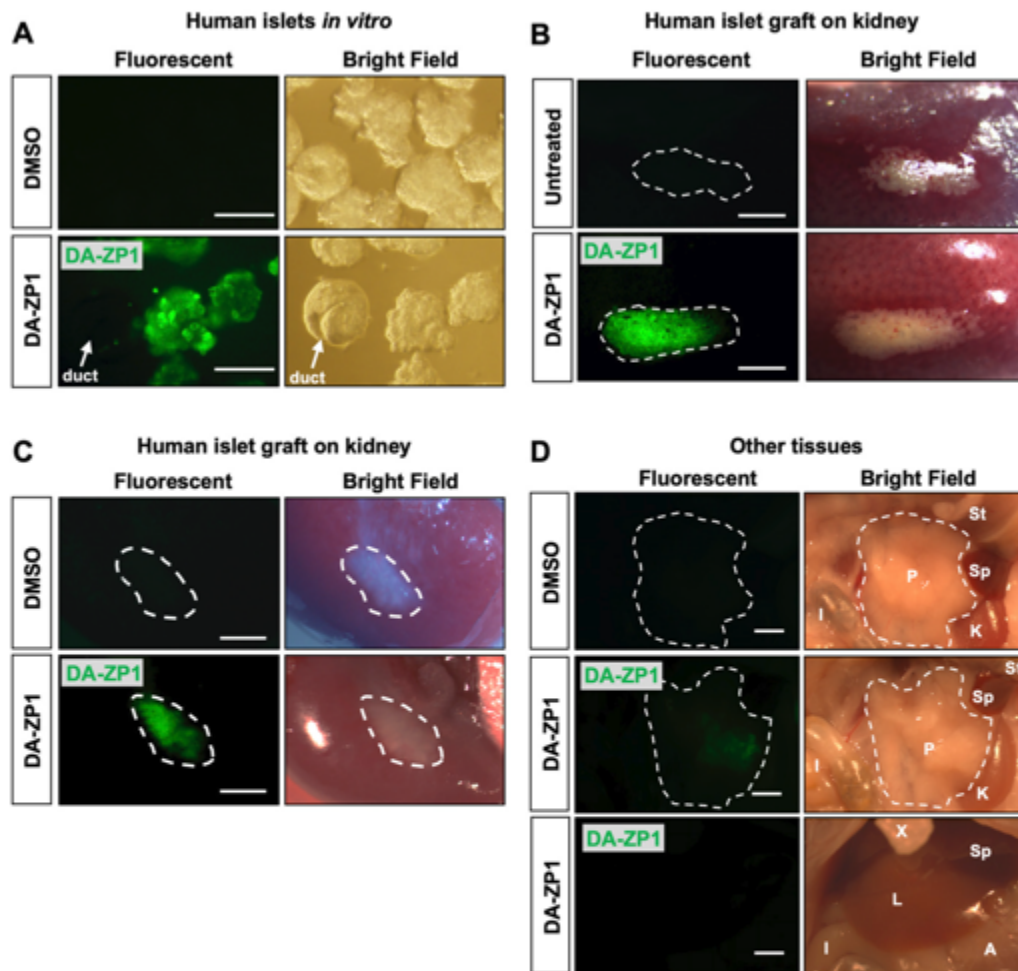
Figure 7.   Imaging of human pancreatic islet graft after administration of DA-ZP1.
(A) Representative images of human pancreatic islets treated with DMSO or 0.8 μM DA-ZP1 for 30 min in vitro. Staining was performed in a 12-well plate (n = 3 replicates) with 25 islets per well. White arrow points to DA-ZP1 negative human pancreatic duct cluster. Scale bar is 200 μm. See also Fig S5. **(B)** Kidneys with grafts were excised 3 d posttransplantation and placed in media with or without DA-ZP1 for 30 min (n = 3 mice/group). No fluorescent signal was detected from untreated graft (top panel); DA-ZP1 treated grafts displayed strong fluorescent signal (bottom panel). The grafts are outlined by white broken lines for better comprehension. Scale bar is 0.15 cm. **(C)** 10 mg/kg BW DA-ZP1 or DMSO was administrated i.v. to mice 1-mo post transplantation (n = 3 mice/group). 1 h after the injection, a strong fluorescent signal was detected in the human islet grafts of DA-ZP1 injected mice, whereas no signal was detected in the grafts of DMSO injected mice. The grafts are outlined by white broken lines for better comprehension. Scale bar 0.15 cm. **(D)** Fluorescent signal was detected only in the pancreas of DA-ZP1 injected mice but not in the DMSO group and no fluorescence signal was detected in any surrounding tissues in both DMSO and DA-ZP1 group (n = 3 mice/group). The pancreas is outlined by white broken lines for better comprehension. St, stomach; P, pancreas; Sp, spleen; K, kidney; I, intestine; X, xiphoid; L, liver; A, adipose. Scale bar 0.15 cm. See also Fig S8.

Our data confirm the selective presence of the zinc-reaction probe DA-ZP1 in pancreatic islets in vivo and demonstrate the potential utility of the system as a tool for β-cell imaging. Development of near infrared (NIR)–emitting zinc-selective sensors could permit visualization of tissues that are located anatomically deep from the surface effectively, and could enable noninvasive imaging of dynamic changes in β-cell mass (Hilderbrand & Weissleder, 2010; Smith et al, 2010). Therefore, future studies are warranted to evaluate if NIR zinc-selective sensors can be used to noninvasively monitor changes in the mass of transplanted human islets or endogenous

145

β-cells. Zinc-reaction probes could also be developed for applications such as β-cell-targeted delivery (Horton et al, 2019; Lee et al, 2020). For example, drugs with an appended zinc-reaction probe could be delivered selectively to pancreatic β-cells to enhance function, and promote survival, or proliferation of target cells. Zn(II)-mediated hydrolytic cleavage is able to release the drug from zinc-reaction probes and switch the inactive drug to an active compound. The ability of the Zn(II)-mediated switch to deliver active compounds warrants in vivo experiments to evaluate the safety and efficacy of drug-attached zinc-reaction probes as a β-cell-specific delivery method.

Finally, the zinc-based approach can be applied to improve the yield of pure β-like cells in differentiation approaches currently being used. Although several protocols can generate functional β-like cells by stepwise differentiation of hESC lines or patient-derived iPSC lines, they also include non-β cells likely because of variable differentiation efficiency (Thatava et al, 2013; Nishizawa et al, 2016). The use of zinc-binding fluorescence probes allows enrichment of β-like cells containing insulin granules and holds an advantage over the cell surface antibody approach that does not necessarily enrich for functional insulin-positive cells.

In sum, the use of zinc-binding fluorescence probes such as DA-ZP1 provides a unique opportunity for enrichment and purification of insulin-positive β-like cells, for a better understanding of human β-cell development, investigation of disease mechanisms (in vitro disease modeling), and for drug discovery.

Materials and Methods

Cell culture

All cells (cell lines and primary cells) were cultured at 37°C, 5% CO_2, and 95% humidity and manipulated in a sterile laminar flow hood. Human embryonic kidney 293 cells were cultured in DMEM High Glucose media supplemented with 10% FBS and maintained at low passage number <10. The EndoC-βH1 cells were cultured and passaged as previously described (Ravassard et al, 2011). Briefly, the culture flask was coated with DMEM HG (glucose 4.5 g/l) containing penicillin–streptomycin (1%), fibronectin (2 μg/ml), and ECM (1% vol/vol) and incubated for at least 1 h in 5% CO_2 at 37°C before the cells were seeded. EndoC-βH1 cells were grown on ECM/fibronectin coated culture flasks containing DMEM LG (glucose 1 g/l), BSA fraction V (2% wt/vol), β-mercaptoethanol (50 μM), nicotinamide (10 mM), transferrin (5.5 μg/ml), sodium selenite (6.7 ng/ml), and penicillin–streptomycin (1%).

hPSC culture and in vitro differentiation

The hESC lines, H1 and H9, were grown on vitronectin (VTN-N; Thermo Fisher Scientific) coated dishes using chemically defined Essential 8 medium (E8; Thermo Fisher Scientific) and regularly confirmed to be mycoplasma-free by MycoAlert Mycoplasma Test Kit (Lonza). The medium was changed every day, and cells were passaged every 5–6 d using 0.5 mM EDTA. The iPSC lines iAG16102, iN805-6, and iN65-51 were derived from human fibroblasts and

have been reported previously (Teo et al, 2013). Cells were grown on VTN-N–coated dishes using E8 medium and regularly confirmed to be mycoplasma-free. The medium was changed every day, and cells were passaged every 5–6 d using 0.5 mM EDTA. hESCs or iPSCs were differentiated towards β-like stage (Stage 6) using previously published protocols with some modifications (Pagliuca et al, 2014; Rezania et al, 2014). Briefly, hESCs or iPSCs were dissociated into single cells using TrypLE (Thermo Fisher Scientific) and plated on VTN-N coated plates in E8 medium supplemented with 10 μM Rho-associated protein kinase (ROCK) inhibitor Y-27632 (Chemdea) at >90% confluency 1 d before initiation of differentiation. Cultures were rinsed with DPBS without Mg^{2+} and Ca^{2+} (Gibco) and differentiation medium was added. Differentiation medium used for each stage is given in Table S1.

Human islet processing

Human islets were obtained from the Integrated Islet Distribution Program. Human islets were processed for DA-ZP1 treatment or transplantation. Joslin Diabetes Center Institutional Review Board declared studies on de-identified autopsy tissue does not qualify as human subject research. Upon receipt, islets were centrifuged at $200g$ for 1 min and resuspended in Miami media (Mediatech). Islets were then transferred to 10 cm culture dishes and cultured overnight to 24 h. Healthy islets were handpicked and washed with DPBS. For transplantation experiments 500 IEQ were transplanted under the kidney capsule of NSG (NOD-scid-IL2Rg^{null}; Jackson Laboratory) mice as previously described (Kahraman et al, 2011). For DA-ZP1 staining, islets were incubated in culture medium containing DA-ZP1 for 30 min at 37°C. At the end of incubation time, cells were washed and cell pellet was resuspended in DA-ZP1 free Miami media. Donor demographic information is summarized in Table S2.

Immunostaining

Dissociated islet cells were immediately seeded after sorting in matrigel (Corning) coated flat bottom 96 well plates and fixed next day. Cells growing in culture dishes were fixed in 4% PFA (Wako) for 15 min at room temperature and washed with PBS three times. For confocal imaging, EndoC-βH1 cells were fixed in cold methanol to preserve fluorescence (Jamur & Oliver, 2010). Cells were then permeabilized with PBS containing 0.25% Triton-X for 30 min at room temperature and blocked with PBS containing 0.25% Triton-X and 5% donkey serum (Sigma-Aldrich) for 1 h at room temperature. Primary antibody was diluted in antibody dilution buffer (Dako) and added to the wells for overnight incubation at 4°C. Cells were washed three times with PBS and the secondary antibody, diluted in PBS, was added to the wells for 1 h at room temperature. Cells were washed three times with PBS and DAPI (Sigma-Aldrich) was added to the wells. Images were captured using an Olympus IX51 Inverted Microscope and cellSens Standard Software Zeiss LSM 710 NLO confocal laser scanning microscope. Pancreatic islets and ductal clusters were fixed in 10% formalin and then stained using the whole-mount immunostaining method as described by Rezanejad et al (2019). Antibody information is given in Table S3.

146

In vitro imaging assays

Staining was conducted in 96-well format. DA-ZP1 or DM-1 was dissolved in DMSO and added to the DMEM cell medium without phenol red (Thermo Fisher Scientific) at final concentration. The culture medium was then replaced with compound-containing medium for 30 min at 37°C. At the end of incubation time, cells were washed with DPBS and fresh cell medium containing DAPI was added to the wells. The cells were imaged immediately or fixed in 4% PFA for 15 min at room temperature and washed with PBS for imaging later. Images were acquired using an automated system (n = 9 images/well) and analyzed by using MetaXpress software. For the Figs 1 and S8A, fluorescent images were taken by Olympus IX51 Inverted Microscope and relative intracellular fluorescence was measured by Image J. Briefly, ~40 cells were randomly selected and integrated density was measured for each cell (4 samples/group). Background fluorescence was subtracted to calculate corrected total cell fluorescence. For the Fig S8A, 15 islets or exocrine clusters were randomly selected for each group and the mean fluorescent intensity was measured (n = 3 mice/group).

DA-ZP1 treatment and FACS

Cells were harvested using trypsin and neutralized in DMEM containing 10% FBS. Cell pellet was resuspended in DA-ZP1 containing cell media and incubated in 37°C for 30 min. At the end of incubation time, cells were washed with DPBS and cell pellet resuspended in fresh DA-ZP1–free media. Cells were analyzed and sorted by Aria (Joslin Flow Cytometry Core). Increase in sorting time does not alter staining patterns because fluorescence response is maintained by cells after treatment with DA-ZP1. For TSQ staining, cell pellet was resuspended in TSQ (Enzo) containing FACS Buffer (2% FBS in PBS) and cells were exposed to TSQ during sorting. For cell tracking experiments (Fig S2), EndoC-βH1 and 293 cells were labeled with either the Violet or Far Red fluorescent dye (Thermo Fisher Scientific), respectively. Briefly, five million cells were harvested, pelleted, resuspended in 5 ml staining solution (1 μM fluorescent dye in DPBS), and incubated in 37°C for 20 min. Fluorescently labeled cells were washed with 25 ml DMEM 10% FBS and incubated in 37°C for 5 min. Cells were spun down, stained with Zombie Red viability dye (BioLegend) followed by DA-ZP1 staining, fixed and analyzed by flow cytometry (BD LSRFortessa High Throughput Sampler; BD Biosciences, Joslin Flow Cytometry Core). Analysis of flow cytometry data was completed using FlowJo 10.4.2 (FlowJo LLC). Gating strategy is shown in Fig S2.

FACS

For Ki67 staining, EndoC-βH1 cells were treated with DA-ZP1 (0, 0.16, 1.25, 10 μM) for 1 h and cultured in DA-ZP1–free media for 24 h. Cells were trypsinized, washed with DPBS, and stained with Zombie NIR Viability dye (BioLegend) and then fixed in 4% PFA for 15 min at room temperature. Cells were then spun and washed with cold FACS buffer (5% FBS in PBS). Permeabilization and blocking were carried out on ice for 1 h in PBS containing 5% donkey serum and 0.2% TritonX. Antibody staining was performed 1 h at 4°C. Antibody information is given in Table S3. For CPEP staining, cells were

harvested and fixed in 4% PFA for 15 min at room temperature. Cells were then spun and washed with cold FACS buffer (5% FBS in PBS). Permeabilization and blocking was carried out on ice for 1 h in PBS containing 5% donkey serum and 0.2% TritonX. Antibody staining was performed overnight at 4°C followed by incubation with secondary antibody for 1 h on ice. Cells were washed with FACS buffer, resuspended, and filtered through a 30-μm filter before analysis by LSRII (BD Biosciences, Joslin Flow Cytometry Core). Gating was determined according to the secondary-only or isotype controls.

Apoptosis detection

Cells were trypsinized, washed with DPBS, and stained with Zombie NIR Viability dye (BioLegend) for 15 min at RT. Cells were washed first with medium containing 10% FBS, followed by a wash with 1× binding buffer, and resuspended in 1× binding buffer containing APC Annexin V (1:20; BD Biosciences). Cells were incubated for 15 min at RT and analyzed by FACS LSRII (Joslin Flow Cytometry Core). Apoptotic cell rate was determined as percentage of Annexin V+ and Zombie NIR– cells.

Ex vivo imaging

NSG adult male mice were obtained from Jackson Laboratories at 8–12 wk of age for human islet transplantation studies. Mice were maintained at Joslin Animal Facility on a 12:12 h light:dark cycle with ad lib access to water and standard rodent chow. All procedures were approved by the Joslin Diabetes Center Institutional Animal Care and Use Committee and performed in accordance with National Institutes of Health (NIH) guidelines. Human islet transplanted kidneys were excised 3 d posttransplantation and placed in Miami media containing 0 or 3 μM DA-ZP1 and incubated in 37°C water bath for 30 min. Human islet grafts were imaged using SteREo Discovery V8 dissection microscope equipped with 0.63× objective, X-Cite series 120Q light source, and Axiocam 512 color camera. Images were analyzed by using Zen 2.3 lite software.

10 mg/kg BW DA-ZP1 was prepared in 125 μl saline solution and injected via tail vein into mice bearing human islet grafts 1-mo posttransplantation. 1 h after the injection, mice were anesthetized by ketamine 100 mg/kg/xylazine 10 mg/kg injection (i.p.). The kidney with the graft was exposed through an incision and imaged using SteREo Discovery V8 dissection microscope equipped with Axiocam 512 color camera. Abdominal V-incision was made to image liver, pancreas, and surrounding tissues.

Pancreatic islet and exocrine tissue isolation

Pancreatic islets and exocrine cells were obtained from 8-wk-old NSG mice 1 h after DA-ZP1 or DMSO injection. Mice were anesthetized by i.p. ketamine/xylazine injection and 2.6 ml CIzyme RI solution (30k CDA U, resuspended in RPMI 1640; VitaCyte) was injected through the pancreatic duct using 27 g-needle. Inflated pancreas was transferred to a 50 ml tube for digestion in 37°C water bath for 17 min. The tubes were hand-shaken vigorously for 5–10 s and washed twice with ice-cold RPMI containing 10% FBS. Tissue was filtered through a 424 μm sieve to remove undigested tissue and fat. The islets and exocrine cells were separated using a

147

Histopaque 1077 (Sigma-Aldrich) density gradient. The islets were collected from the top interface and the exocrine cells were collected from the pellet and transferred to new 50 ml tube. After three washes with RPMI 1640 medium containing 10% FBS, purified islets and exocrine cells were handpicked under the dissection microscope and transferred to a 12 well plates. Cells were stained with Propidium Iodide (1 μg/ml; Sigma-Aldrich) to determine cell viability. Fluorescent and bright field images of live cells were taken immediately by Olympus IX51 Inverted Microscope.

Insulin secretion assay

EndoC-βH1 cells were starved overnight in 2.8 mM glucose followed by 1 h incubation in Krebs Ringer Buffer (KRB) containing NaCl (115 mM), $NaHCO_3$ (24 mM), KCl (5 mM), $MgCl_2$ (1 mM), $CaCl_2$ (1 mM), Hepes (10 mM), BSA (0.2% wt/vol), and 0.5 mM glucose. Static insulin secretion assays were then initiated by adding KRB containing 3.3 or 16.7 mM glucose for 1 h. Aliquots of supernatants were removed for later analysis and ice-cold acid ethanol was added to extract insulin content from cells. Insulin secretion and content were measured by the human insulin ELISA (Mercodia) according to the manufacturer's instructions.

β-like cells were starved 1 h in KRB containing 0.5 mM glucose. Insulin secretion was stimulated by adding KRB containing 1 mM glucose (LG), 20 mM glucose (HG), and 10 nM Exendin-4 (Sigma-Aldrich) in the presence of 20 mM glucose or 30 mM KCl for 1 h. Supernatant samples were collected, cell debris were removed by centrifugation, and insulin levels were measured. Human insulin secretion was calculated by dividing the secreted insulin by the total number of cells.

Statistical analysis

Statistical analysis was performed by t test or ANOVA. All values are ± SEM, and statistical significance was set at $P < 0.05$.

Data Availability

The data that support the findings of this study are available from the corresponding author upon reasonable request.

Supplementary Information

Supplementary Information is available at https://doi.org/10.26508/lsa.202000840.

Acknowledgements

Author Contributions

S Kahraman: conceptualization, data curation, formal analysis, investigation, methodology, and writing—original draft, review, and editing.
D Manna: methodology and writing—review and editing.
E Dirice: methodology and writing—review and editing.
B Maji: data curation and writing—review and editing.
J Small: data curation and writing—review and editing.
BK Wagner: supervision, funding acquisition, project administration, and writing—review and editing.
A Choudhary: supervision, funding acquisition, project administration, and writing—review and editing.
RN Kulkarni: conceptualization, resources, supervision, funding acquisition, investigation, project administration, and writing—original draft, review, and editing.

Conflict of Interest Statement

The authors declare that they have no conflict of interest.

References

Ameri J, Borup R, Prawiro C, Ramond C, Schachter KA, Scharfmann R, Semb H (2017) Efficient generation of glucose-responsive beta cells from isolated GP2+ human pancreatic progenitors. Cell Rep 19: 36–49. doi:10.1016/j.celrep.2017.03.032

Chyan W, Zhang DY, Lippard SJ, Radford RJ (2014) Reaction-based fluorescent sensor for investigating mobile Zn2+ in mitochondria of healthy versus cancerous prostate cells. Proc Natl Acad Sci U S A 111: 143–148. doi:10.1073/pnas.1310583110

Cogger KF, Sinha A, Sarangi F, McGaugh EC, Saunders D, Dorrell C, Mejia-Guerrero S, Aghazadeh Y, Rourke JL, Screaton RA, et al (2017) Glycoprotein 2 is a specific cell surface marker of human pancreatic progenitors. Nat Commun 8: 331. doi:10.1038/s41467-017-00561-0

Davis JC, Helman A, Rivera-Feliciano J, Langston CM, Engquist EN, Melton DA (2019) Live cell monitoring and enrichment of stem cell-derived β cells using intracellular zinc content as a population marker. Curr Protoc Stem Cell Biol 51: 1–6. doi:10.1002/cpsc.99

Dorrell C, Abraham SL, Lanxon-Cookson KM, Canaday PS, Streeter PR, Grompe M (2008) Isolation of major pancreatic cell types and long-term culture-initiating cells using novel human surface markers. Stem Cell Res 1: 183–194. doi:10.1016/j.scr.2008.04.001

Dorrell C, Schug J, Canaday PS, Russ HA, Tarlow BD, Grompe MT, Horton T, Hebrok M, Streeter PR, Kaestner KH, et al (2016) Human islets contain four distinct subtypes of β cells. Nat Commun 7: 1–9. doi:10.1038/ncomms11756

Emdin SO, Dodson GG, Cutfield JM, Cutfield SM (1980) Role of zinc in insulin biosynthesis. Some possible zinc-insulin interactions in the pancreatic B-cell. Diabetologia 19: 174–182. doi:10.1007/BF00275265

Gamble A, Pepper AR, Bruni A, Shapiro AMJ (2018) The journey of islet cell transplantation and future development. Islets 10: 80–94. doi:10.1080/19382014.2018.1428511

Ghazizadeh Z, Kao D-I, Amin S, Cook B, Rao S, Zhou T, Zhang T, Xiang Z, Kenyon R, Kaymakcalan O, et al (2017) ROCKII inhibition promotes the maturation of human pancreatic beta-like cells. Nat Commun 8: 298. doi:10.1038/s41467-017-00129-y

Hilderbrand SA, Weissleder R (2010) Near-infrared fluorescence: Application to in vivo molecular imaging. *Curr Opin Chem Biol* 14: 71–79. doi:10.1016/j.cbpa.2009.09.029

Hinkle DE, Wiersma W, Jurs SG (2003) Correlation: A measure of relationship, 5th edn *Applied Statistics for the Behavioral Sciences*. USA: Houghton Mifflin.

Hogrebe NJ, Augsornworawat P, Maxwell KG, Velazco-Cruz L, Millman JR (2020) Targeting the cytoskeleton to direct pancreatic differentiation of human pluripotent stem cells. *Nat Biotechnol* 38: 460–470. doi:10.1038/s41587-020-0430-6

Horton TM, Allegretti PA, Lee S, Moeller HP, Smith M, Annes JP (2019) Zinc-chelating small molecules preferentially accumulate and function within pancreatic β cells. *Cell Chem Biol* 26: 213–222.e6. doi:10.1016/j.chembiol.2018.10.019

Hrvatin S, Deng F, O'Donnell CW, Gifford DK, Melton DA (2014) MARIS: Method for analyzing RNA following intracellular sorting. *PLoS One* 9: e89459. doi:10.1371/journal.pone.0089459

Huang Z, Lippard SJ (2012) Illuminating mobile zinc with fluorescence from cuvettes to live cells and tissues. *Methods Enzymol* 505: 445–468. doi:10.1016/b978-0-12-388448-0.00031-0

Jamur MC, Oliver C (2010) Permeabilization of cell membranes. *Methods Mol Biol* 588: 63–66. doi:10.1007/978-1-59745-324-0_9

Jayaraman S (2008) A novel method for the detection of viable human pancreatic beta cells by flow cytometry using fluorophores that selectively detect labile zinc, mitochondrial membrane potential and protein thiols. *Cytometry A* 73: 615–625. doi:10.1002/cyto.a.20560

Jindal RM, Taylor RP, Gray DW, Esmeraldo R, Morris PJ (1992) A new method for quantification of islets by measurement of zinc content. *Diabetes* 41: 1056–1062. doi:10.2337/diabetes.41.9.1056

Kahraman S, Dirice E, Hapil FZ, Ertosun MG, Ozturk S, Griffith TS, Sanlioglu S, Sanlioglu AD (2011) Tracing of islet graft survival by way of in vivo fluorescence imaging. *Diabetes Metab Res Rev* 27: 575–583. doi:10.1002/dmrr.1216

Kahraman S, Okawa ER, Kulkarni RN (2016) Is transforming stem cells to pancreatic beta cells still the holy grail for type 2 diabetes? *Curr Diab Rep* 16: 70. doi:10.1007/s11892-016-0764-0

Kelly OG, Chan MY, Martinson LA, Kadoya K, Ostertag TM, Ross KG, Richardson M, Carpenter MK, D'Amour KA, Kroon E, et al (2011) Cell-surface markers for the isolation of pancreatic cell types derived from human embryonic stem cells. *Nat Biotechnol* 29: 750–756. doi:10.1038/nbt.1931

Klochendler A, Caspi I, Corem N, Moran M, Friedlich O, Elgavish S, Nevo Y, Helman A, Glaser B, Eden A, et al (2016) The genetic program of pancreatic β-cell replication in vivo. *Diabetes* 65: 2081–2093. doi:10.2337/db16-0003

Lee M, Maji B, Manna D, Kahraman S, Elgamal RM, Small J, Kokkonda P, Vetere A, Goldberg JM, Lippard SJ, et al (2020) Native zinc catalyzes selective and traceless release of small molecules in β-cells. *J Am Chem Soc* 142: 6477–6482. doi:10.1021/jacs.0c00099

Li YV (2014) Zinc and insulin in pancreatic beta-cells. *Endocrine* 45: 178–189. doi:10.1007/s12020-013-0032-x

Micallef SJ, Li X, Schiesser JV, Hirst CE, Yu QC, Lim SM, Nostro MC, Elliott DA, Sarangi F, Harrison LC, et al (2012) INSGFP/whuman embryonic stem cells facilitate isolation of in vitro derived insulin-producing cells. *Diabetologia* 55: 694–706. doi:10.1007/s00125-011-2379-y

Nair GG, Liu JS, Russ HA, Tran S, Saxton MS, Chen R, Juang C, Li M, Nguyen VQ, Giacometti S, et al (2019) Recapitulating endocrine cell clustering in culture promotes maturation of human stem-cell-derived β cells. *Nat Cell Biol* 21: 263–274. doi:10.1038/s41556-019-0316-3

Nishizawa M, Chonabayashi K, Nomura M, Tanaka A, Nakamura M, Inagaki A, Nishikawa M, Takei I, Oishi M, Tanabe K, et al (2016) Epigenetic variation between human induced pluripotent stem cell lines is an indicator of differentiation capacity. *Cell Stem Cell* 19: 341–354. doi:10.1016/j.stem.2016.06.019

Pagliuca FW, Millman JR, Gürtler M, Segel M, Van Dervort A, Ryu JH, Peterson QP, Greiner D, Melton DA (2014) Generation of functional human pancreatic β cells in vitro. *Cell* 159: 428–439. doi:10.1016/j.cell.2014.09.040

Parnaud G, Bosco D, Berney T, Pattou F, Kerr-Conte J, Donath MY, Bruun C, Mandrup-Poulsen T, Billestrup N, Halban PA (2008) Proliferation of sorted human and rat beta cells. *Diabetologia* 51: 91–100. doi:10.1007/s00125-007-0855-1

Pipeleers DG, in't Veld PA, Van de Winkel M, Maes E, Schuit FC, Gepts W (1985) A new in vitro model for the study of pancreatic A and B cells. *Endocrinology* 117: 806–816. doi:10.1210/endo-117-3-806

Que EL, Domaille DW, Chang CJ (2008) Metals in neurobiology: Probing their chemistry and biology with molecular imaging. *Chem Rev* 108: 1517–1549. doi:10.1021/cr078203u

Ravassard P, Hazhouz Y, Pechberty S, Bricout-neveu E, Armanet M, Czernichow P, Scharfmann R (2011) Technical advance A genetically engineered human pancreatic β cell line exhibiting glucose-inducible insulin secretion. *J Clin Invest* 121: 3589–3597. doi:10.1172/jci58447

Rezanejad H, Lock JH, Sullivan BA, Bonner-Weir S (2019) Generation of pancreatic ductal organoids and whole-mount immunostaining of intact organoids. *Curr Protoc Cell Biol* 83: 1–16. doi:10.1002/cpcb.82

Rezania A, Bruin JE, Arora P, Rubin A, Batushansky I, Asadi A, O'Dwyer S, Quiskamp N, Mojibian M, Albrecht T, et al (2014) Reversal of diabetes with insulin-producing cells derived in vitro from human pluripotent stem cells. *Nat Biotechnol* 32: 1121–1133. doi:10.1038/nbt.3033

Rice DR, Vacchina P, Norris-Mullins B, Morales MA, Smith BD (2016) Zinc(II)-dipicolylamine coordination complexes as targeting and chemotherapeutic agents for leishmania major. *Antimicrob Agents Chemother* 60: 2932–2940. doi:10.1128/aac.00410-16

Russ HA, Parent AV, Ringler JJ, Hennings TG, Nair GG, Shveygert M, Guo T, Puri S, Haataja L, Cirulli V, et al (2015) Controlled induction of human pancreatic progenitors produces functional beta-like cells in vitro. *EMBO J* 34: 1759–1772. doi:10.15252/embj.201591058

Rutter GA, Chabosseau P, Bellomo EA, Maret W, Mitchell RK, Hodson DJ, Solomou A, Hu M (2016) Intracellular zinc in insulin secretion and action: A determinant of diabetes risk? *Proc Nutr Soc* 75: 61–72. doi:10.1017/s0029665115003237

Saunders DC, Brissova M, Phillips N, Shrestha S, Walker JT, Aramandla R, Poffenberger G, Flaherty DK, Weller KP, Pelletier J, et al (2019) Ectonucleoside triphosphate diphosphohydrolase-3 antibody targets adult human pancreatic β cells for in vitro and in vivo analysis. *Cell Metab* 29: 745–754.e4. doi:10.1016/j.cmet.2018.10.007

Smith BA, Akers WJ, Leevy WM, Lampkins AJ, Xiao S, Wolter W, Suckow MA, Achilefu S, Smith BD (2010) Optical imaging of mammary and prostate tumors in living animals using a synthetic near infrared zinc(II)-dipicolylamine probe for anionic cell surfaces. *J Am Chem Soc* 132: 67–69. doi:10.1021/ja908467y

Sweet IR, Cook DL, Lernmark Å, Greenbaum CJ, Wallen AR, Marcum ES, Stekhova SA, Krohn KA (2004) Systematic screening of potential β-cell imaging agents. *Biochem Biophys Res Commun* 314: 976–983. doi:10.1016/j.bbrc.2003.12.182

Teo AKK, Windmueller R, Johansson BB, Dirice E, Njolstad PR, Tjora E, Raeder H, Kulkarni RN (2013) Derivation of human induced pluripotent stem cells from patients with maturity onset diabetes of the young. *J Biol Chem* 288: 5353–5356. doi:10.1074/jbc.c112.428979

Thatava T, Kudva YC, Edukulla R, Squillace K, De Lamo JG, Khan YK, Sakuma T, Ohmine S, Terzic A, Ikeda Y (2013) Intrapatient variations in type 1 diabetes-specific iPS cell differentiation into insulin-producing cells. *Mol Ther* 21: 228–239. doi:10.1038/mt.2012.245

149

Toroptsev IV, Eshchenko VA, Troshkin VG (1974) Zinc content in islet cells of the mammalian pancreas in relation to the functional state of the insular system. *Bull Exp Biol Med* 77: 119–121. doi:10.1007/bf00809608

Velazco-Cruz L, Song J, Maxwell KG, Goedegebuure MM, Augsornworawat P, Hogrebe NJ, Millman JR (2019) Acquisition of dynamic function in human stem cell-derived β cells. *Stem Cell Rep* 12: 351–365. doi:10.1016/j.stemcr.2018.12.012

Veres A, Faust AL, Bushnell HL, Engquist EN, Kenty JH-R, Harb G, Poh Y-C, Sintov E, Gürtler M, Pagliuca FW, et al (2019) Charting cellular identity during human in vitro β-cell differentiation. *Nature* 569: 368–373. doi:10.1038/s41586-019-1168-5

Vinkenborg JL, Nicolson TJ, Bellomo EA, Koay MS, Rutter GA, Merkx M (2009) Genetically encoded FRET sensors to monitor intracellular Zn2+ homeostasis. *Nat Methods* 6: 737–740. doi:10.1038/nmeth.1368

Zastrow ML, Radford RJ, Chyan W, Anderson CT, Zhang DY, Loas A, Tzounopoulos T, Lippard SJ (2016) Reaction-based probes for imaging mobile zinc in live cells and tissues. *ACS Sens* 1: 32–39. doi:10.1021/acssensors.5b00022

Zhu S, Russ HA, Wang X, Zhang M, Ma T, Xu T, Tang S, Hebrok M, Ding S (2016a) Human pancreatic beta-like cells converted from fibroblasts. *Nat Commun* 7: 10080. doi:10.1038/ncomms10080

Zhu Z, Li QV, Lee K, Rosen BP, González F, Soh CL, Huangfu D (2016b) Genome editing of lineage determinants in human pluripotent stem cells reveals mechanisms of pancreatic development and diabetes. *Cell Stem Cell* 18: 755–768. doi:10.1016/j.stem.2016.03.015

150

Appendix 3: Supplementary Material for Chapter 4

A3.1. Full Kinase Profiling Results Table

DiscoveRx Gene Symbol	Entrez Gene Symbol	Percent Control (KD025)	Percent Control (SR3677)	Percent Control (H1152)
AAK1	AAK1	100	95	55
ABL1-nonphosphorylated	ABL1	92	95	58
ABL1-phosphorylated	ABL1	98	100	100
ABL1(E255K)-phosphorylated	ABL1	98	86	77
ABL1(F317I)-nonphosphorylated	ABL1	100	100	86
ABL1(F317I)-phosphorylated	ABL1	99	89	51
ABL1(F317L)-nonphosphorylated	ABL1	96	89	41
ABL1(F317L)-phosphorylated	ABL1	100	80	55
ABL1(H396P)-nonphosphorylated	ABL1	87	99	61
ABL1(H396P)-phosphorylated	ABL1	100	100	70
ABL1(M351T)-phosphorylated	ABL1	100	100	67
ABL1(Q252H)-nonphosphorylated	ABL1	100	96	82
ABL1(Q252H)-phosphorylated	ABL1	100	100	37
ABL1(T315I)-nonphosphorylated	ABL1	100	100	62
ABL1(T315I)-phosphorylated	ABL1	100	91	74
ABL1(Y253F)-phosphorylated	ABL1	100	77	55
ABL2	ABL2	100	100	97
ACVR1	ACVR1	100	100	91
ACVR1B	ACVR1B	94	99	53
ACVR2A	ACVR2A	100	85	82
ACVR2B	ACVR2B	100	88	90
ACVRL1	ACVRL1	99	80	100
ADCK3	CABC1	100	100	100
ADCK4	ADCK4	100	100	100
AKT1	AKT1	100	93	100
AKT2	AKT2	100	100	100
AKT3	AKT3	100	35	78
ALK	ALK	75	76	37
ALK(C1156Y)	ALK	100	100	48
ALK(L1196M)	ALK	100	100	100
AMPK-alpha1	PRKAA1	100	87	45
AMPK-alpha2	PRKAA2	100	75	86

A3.1. Full Kinase Profiling Results Table

ANKK1	ANKK1	100	100	100
ARK5	NUAK1	100	100	75
ASK1	MAP3K5	100	100	100
ASK2	MAP3K6	100	97	88
AURKA	AURKA	94	82	23
AURKB	AURKB	97	97	6.9
AURKC	AURKC	79	96	4.2
AXL	AXL	100	100	99
BIKE	BMP2K	52	99	19
BLK	BLK	51	70	51
BMPR1A	BMPR1A	62	80	54
BMPR1B	BMPR1B	100	100	36
BMPR2	BMPR2	100	100	100
BMX	BMX	100	100	100
BRAF	BRAF	100	100	100
BRAF(V600E)	BRAF	100	100	100
BRK	PTK6	100	100	100
BRSK1	BRSK1	100	100	70
BRSK2	BRSK2	100	100	39
BTK	BTK	85	85	89
BUB1	BUB1	96	77	61
CAMK1	CAMK1	100	98	100
CAMK1B	PNCK	44	94	89
CAMK1D	CAMK1D	100	100	85
CAMK1G	CAMK1G	100	96	100
CAMK2A	CAMK2A	100	86	43
CAMK2B	CAMK2B	100	100	100
CAMK2D	CAMK2D	100	96	61
CAMK2G	CAMK2G	100	92	90
CAMK4	CAMK4	100	83	10
CAMKK1	CAMKK1	100	91	82
CAMKK2	CAMKK2	100	94	75
CASK	CASK	100	97	96
CDC2L1	CDK11B	100	100	100
CDC2L2	CDC2L2	100	100	100
CDC2L5	CDK13	82	87	27
CDK11	CDK19	100	100	66

A3.1. Full Kinase Profiling Results Table

CDK2	CDK2	100	100	99
CDK3	CDK3	100	100	100
CDK4	CDK4	100	100	100
CDK4-cyclinD1	CDK4	81	70	65
CDK4-cyclinD3	CDK4	100	94	81
CDK5	CDK5	90	80	91
CDK7	CDK7	81	53	26
CDK8	CDK8	100	100	69
CDK9	CDK9	100	100	100
CDKL1	CDKL1	83	89	75
CDKL2	CDKL2	100	100	76
CDKL3	CDKL3	99	100	100
CDKL5	CDKL5	98	100	100
CHEK1	CHEK1	100	99	100
CHEK2	CHEK2	100	100	89
CIT	CIT	98	97	90
CLK1	CLK1	100	30	26
CLK2	CLK2	94	54	35
CLK3	CLK3	100	100	98
CLK4	CLK4	74	4.8	37
CSF1R	CSF1R	100	100	100
CSF1R-autoinhibited	CSF1R	80	81	86
CSK	CSK	100	100	100
CSNK1A1	CSNK1A1	79	76	80
CSNK1A1L	CSNK1A1L	94	92	82
CSNK1D	CSNK1D	90	99	94
CSNK1E	CSNK1E	100	100	100
CSNK1G1	CSNK1G1	100	100	100
CSNK1G2	CSNK1G2	91	75	97
CSNK1G3	CSNK1G3	100	100	100
CSNK2A1	CSNK2A1	8.5	67	62
CSNK2A2	CSNK2A2	18	91	100
CTK	MATK	99	100	99
DAPK1	DAPK1	99	100	57
DAPK2	DAPK2	100	100	93
DAPK3	DAPK3	100	100	96
DCAMKL1	DCLK1	100	98	20

A3.1. Full Kinase Profiling Results Table

DCAMKL2	DCLK2	100	100	41
DCAMKL3	DCLK3	100	77	16
DDR1	DDR1	42	100	100
DDR2	DDR2	86	97	90
DLK	MAP3K12	100	100	92
DMPK	DMPK	100	83	91
DMPK2	CDC42BPG	63	97	100
DRAK1	STK17A	98	98	100
DRAK2	STK17B	98	100	100
DYRK1A	DYRK1A	100	100	100
DYRK1B	DYRK1B	72	78	72
DYRK2	DYRK2	100	87	100
EGFR	EGFR	99	96	92
EGFR(E746-A750del)	EGFR	81	90	79
EGFR(G719C)	EGFR	90	89	84
EGFR(G719S)	EGFR	100	99	95
EGFR(L747-E749del, A750P)	EGFR	95	92	79
EGFR(L747-S752del, P753S)	EGFR	97	92	74
EGFR(L747-T751del,Sins)	EGFR	90	83	85
EGFR(L858R,T790M)	EGFR	93	95	87
EGFR(L858R)	EGFR	93	99	63
EGFR(L861Q)	EGFR	93	96	96
EGFR(S752-I759del)	EGFR	83	86	80
EGFR(T790M)	EGFR	89	84	70
EIF2AK1	EIF2AK1	97	96	81
EPHA1	EPHA1	100	100	20
EPHA2	EPHA2	100	100	95
EPHA3	EPHA3	95	100	75
EPHA4	EPHA4	100	100	84
EPHA5	EPHA5	98	84	90
EPHA6	EPHA6	100	93	83
EPHA7	EPHA7	100	100	100
EPHA8	EPHA8	97	100	100
EPHB1	EPHB1	100	100	81
EPHB2	EPHB2	100	96	100
EPHB3	EPHB3	100	100	83
EPHB4	EPHB4	100	97	88

A3.1. Full Kinase Profiling Results Table

EPHB6	EPHB6	100	97	96
ERBB2	ERBB2	97	96	56
ERBB3	ERBB3	96	100	93
ERBB4	ERBB4	92	100	69
ERK1	MAPK3	100	93	94
ERK2	MAPK1	97	86	100
ERK3	MAPK6	100	100	100
ERK4	MAPK4	100	100	99
ERK5	MAPK7	100	100	100
ERK8	MAPK15	100	100	100
ERN1	ERN1	100	100	95
FAK	PTK2	91	100	65
FER	FER	100	100	100
FES	FES	96	100	86
FGFR1	FGFR1	100	100	46
FGFR2	FGFR2	100	100	95
FGFR3	FGFR3	100	100	98
FGFR3(G697C)	FGFR3	100	100	96
FGFR4	FGFR4	100	100	98
FGR	FGR	100	100	78
FLT1	FLT1	98	97	95
FLT3	FLT3	98	80	100
FLT3-autoinhibited	FLT3	89	86	57
FLT3(D835H)	FLT3	81	71	29
FLT3(D835V)	FLT3	73	100	77
FLT3(D835Y)	FLT3	100	96	82
FLT3(ITD,D835V)	FLT3	89	92	45
FLT3(ITD,F691L)	FLT3	99	100	25
FLT3(ITD)	FLT3	93	100	79
FLT3(K663Q)	FLT3	83	88	62
FLT3(N841I)	FLT3	70	100	91
FLT3(R834Q)	FLT3	100	100	80
FLT4	FLT4	90	94	80
FRK	FRK	100	100	94
FYN	FYN	90	96	72
GAK	GAK	69	94	86
GCN2(Kin.Dom.2,S808G)	EIF2AK4	100	100	100

A3.1. Full Kinase Profiling Results Table

GRK1	GRK1	96	98	16
GRK2	ADRBK1	100	95	39
GRK3	ADRBK2	90	96	65
GRK4	GRK4	49	100	14
GRK7	GRK7	83	70	7
GSK3A	GSK3A	96	92	100
GSK3B	GSK3B	100	91	85
HASPIN	GSG2	99	19	67
HCK	HCK	100	100	90
HIPK1	HIPK1	81	79	84
HIPK2	HIPK2	100	85	90
HIPK3	HIPK3	100	93	93
HIPK4	HIPK4	92	100	94
HPK1	MAP4K1	91	89	57
HUNK	HUNK	97	100	100
ICK	ICK	94	85	81
IGF1R	IGF1R	90	83	92
IKK-alpha	CHUK	98	92	95
IKK-beta	IKBKB	100	89	99
IKK-epsilon	IKBKE	69	85	82
INSR	INSR	79	70	75
INSRR	INSRR	100	100	100
IRAK1	IRAK1	100	100	57
IRAK3	IRAK3	100	100	70
IRAK4	IRAK4	100	92	93
ITK	ITK	100	100	100
JAK1(JH1domain-catalytic)	JAK1	100	100	100
JAK1(JH2domain-pseudokinase)	JAK1	56	72	75
JAK2(JH1domain-catalytic)	JAK2	100	100	11
JAK3(JH1domain-catalytic)	JAK3	100	100	1.9
JNK1	MAPK8	99	95	82
JNK2	MAPK9	100	94	94
JNK3	MAPK10	100	100	96
KIT	KIT	100	92	100
KIT-autoinhibited	KIT	97	100	78
KIT(A829P)	KIT	100	100	73
KIT(D816H)	KIT	92	100	82

A3.1. Full Kinase Profiling Results Table

KIT(D816V)	KIT	100	99	100
KIT(L576P)	KIT	100	100	100
KIT(V559D,T670I)	KIT	100	100	100
KIT(V559D,V654A)	KIT	97	100	90
KIT(V559D)	KIT	98	100	100
LATS1	LATS1	93	100	81
LATS2	LATS2	95	61	82
LCK	LCK	100	100	73
LIMK1	LIMK1	100	100	100
LIMK2	LIMK2	100	100	100
LKB1	STK11	100	100	100
LOK	STK10	94	100	65
LRRK2	LRRK2	99	100	11
LRRK2(G2019S)	LRRK2	100	100	8.7
LTK	LTK	100	99	100
LYN	LYN	100	95	98
LZK	MAP3K13	100	100	93
MAK	MAK	100	99	68
MAP3K1	MAP3K1	100	96	77
MAP3K15	MAP3K15	93	80	70
MAP3K2	MAP3K2	100	100	100
MAP3K3	MAP3K3	81	69	75
MAP3K4	MAP3K4	90	90	69
MAP4K2	MAP4K2	100	100	28
MAP4K3	MAP4K3	100	100	76
MAP4K4	MAP4K4	95	85	62
MAP4K5	MAP4K5	99	85	79
MAPKAPK2	MAPKAPK2	100	100	100
MAPKAPK5	MAPKAPK5	100	100	94
MARK1	MARK1	100	100	97
MARK2	MARK2	95	97	24
MARK3	MARK3	100	86	27
MARK4	MARK4	100	100	92
MAST1	MAST1	66	73	55
MEK1	MAP2K1	100	100	92
MEK2	MAP2K2	100	100	97
MEK3	MAP2K3	92	86	52

A3.1. Full Kinase Profiling Results Table

MEK4	MAP2K4	97	96	90
MEK5	MAP2K5	91	85	58
MEK6	MAP2K6	100	98	97
MELK	MELK	85	84	31
MERTK	MERTK	100	90	83
MET	MET	72	78	78
MET(M1250T)	MET	89	100	91
MET(Y1235D)	MET	100	100	100
MINK	MINK1	98	87	54
MKK7	MAP2K7	100	99	99
MKNK1	MKNK1	83	95	85
MKNK2	MKNK2	100	100	9.7
MLCK	MYLK3	100	100	100
MLK1	MAP3K9	92	98	79
MLK2	MAP3K10	100	98	87
MLK3	MAP3K11	100	86	100
MRCKA	CDC42BPA	100	100	100
MRCKB	CDC42BPB	21	88	100
MST1	STK4	100	91	87
MST1R	MST1R	100	94	68
MST2	STK3	92	72	36
MST3	STK24	100	100	85
MST4	MST4	100	100	62
MTOR	MTOR	100	100	100
MUSK	MUSK	100	100	100
MYLK	MYLK	84	88	81
MYLK2	MYLK2	97	100	73
MYLK4	MYLK4	99	100	68
MYO3A	MYO3A	81	87	73
MYO3B	MYO3B	84	100	100
NDR1	STK38	100	97	91
NDR2	STK38L	100	100	100
NEK1	NEK1	100	100	100
NEK10	NEK10	61	68	78
NEK11	NEK11	95	100	100
NEK2	NEK2	100	97	95
NEK3	NEK3	73	62	65

A3.1. Full Kinase Profiling Results Table

NEK4	NEK4	98	100	100
NEK5	NEK5	100	100	100
NEK6	NEK6	88	87	98
NEK7	NEK7	100	100	100
NEK9	NEK9	70	57	53
NIK	MAP3K14	100	100	100
NIM1	MGC42105	97	91	100
NLK	NLK	100	100	100
OSR1	OXSR1	97	99	75
p38-alpha	MAPK14	100	100	100
p38-beta	MAPK11	99	100	83
p38-delta	MAPK13	100	98	81
p38-gamma	MAPK12	100	85	80
PAK1	PAK1	100	100	100
PAK2	PAK2	91	89	78
PAK3	PAK3	100	86	43
PAK4	PAK4	100	99	100
PAK6	PAK6	100	100	100
PAK7	PAK7	100	99	89
PCTK1	CDK16	99	100	97
PCTK2	CDK17	85	100	100
PCTK3	CDK18	100	100	100
PDGFRA	PDGFRA	93	99	82
PDGFRB	PDGFRB	100	100	98
PDPK1	PDPK1	93	76	98
PFCDPK1(P.falciparum)	CDPK1	85	73	68
PFPK5(P.falciparum)	MAL13P1.279	100	97	94
PFTAIRE2	CDK15	95	93	89
PFTK1	CDK14	100	100	100
PHKG1	PHKG1	4.4	100	25
PHKG2	PHKG2	100	100	26
PIK3C2B	PIK3C2B	98	96	100
PIK3C2G	PIK3C2G	59	53	57
PIK3CA	PIK3CA	97	96	96
PIK3CA(C420R)	PIK3CA	98	100	100
PIK3CA(E542K)	PIK3CA	95	89	90

A3.1. Full Kinase Profiling Results Table

PIK3CA(E545A)	PIK3CA	100	97	100
PIK3CA(E545K)	PIK3CA	87	80	83
PIK3CA(H1047L)	PIK3CA	94	85	87
PIK3CA(H1047Y)	PIK3CA	83	58	71
PIK3CA(I800L)	PIK3CA	100	100	100
PIK3CA(M1043I)	PIK3CA	86	81	85
PIK3CA(Q546K)	PIK3CA	83	80	73
PIK3CB	PIK3CB	100	100	100
PIK3CD	PIK3CD	84	77	78
PIK3CG	PIK3CG	100	100	100
PIK4CB	PI4KB	97	94	89
PIKFYVE	PIKFYVE	92	100	100
PIM1	PIM1	100	100	100
PIM2	PIM2	100	100	100
PIM3	PIM3	85	85	78
PIP5K1A	PIP5K1A	31	90	9.7
PIP5K1C	PIP5K1C	100	73	92
PIP5K2B	PIP4K2B	100	98	94
PIP5K2C	PIP4K2C	99	100	100
PKAC-alpha	PRKACA	100	63	41
PKAC-beta	PRKACB	100	62	39
PKMYT1	PKMYT1	100	97	100
PKN1	PKN1	100	88	16
PKN2	PKN2	100	55	31
PKNB(M.tuberculosis)	pknB	88	86	77
PLK1	PLK1	99	90	96
PLK2	PLK2	95	75	91
PLK3	PLK3	100	95	95
PLK4	PLK4	83	75	12
PRKCD	PRKCD	100	100	17
PRKCE	PRKCE	100	100	0
PRKCH	PRKCH	84	70	0
PRKCI	PRKCI	98	93	61
PRKCQ	PRKCQ	79	100	26
PRKD1	PRKD1	97	85	100
PRKD2	PRKD2	100	96	100
PRKD3	PRKD3	100	60	52

A3.1. Full Kinase Profiling Results Table

PRKG1	PRKG1	100	76	34
PRKG2	PRKG2	100	86	7.1
PRKR	EIF2AK2	100	88	97
PRKX	PRKX	100	100	21
PRP4	PRPF4B	98	99	100
PYK2	PTK2B	90	92	75
QSK	KIAA0999	100	100	83
RAF1	RAF1	100	100	100
RET	RET	99	99	62
RET(M918T)	RET	100	95	64
RET(V804L)	RET	100	90	78
RET(V804M)	RET	100	93	91
RIOK1	RIOK1	77	91	48
RIOK2	RIOK2	91	87	95
RIOK3	RIOK3	88	100	55
RIPK1	RIPK1	100	100	100
RIPK2	RIPK2	100	100	100
RIPK4	RIPK4	64	56	47
RIPK5	DSTYK	100	100	100
ROCK1	ROCK1	79	0	0
ROCK2	ROCK2	2	0	0
ROS1	ROS1	100	100	69
RPS6KA4(Kin.Dom.1-N-terminal)	RPS6KA4	100	96	86
RPS6KA4(Kin.Dom.2-C-terminal)	RPS6KA4	100	96	93
RPS6KA5(Kin.Dom.1-N-terminal)	RPS6KA5	100	98	97
RPS6KA5(Kin.Dom.2-C-terminal)	RPS6KA5	100	100	100
RSK1(Kin.Dom.1-N-terminal)	RPS6KA1	79	100	100
RSK1(Kin.Dom.2-C-terminal)	RPS6KA1	100	100	11
RSK2(Kin.Dom.1-N-terminal)	RPS6KA3	97	100	63
RSK2(Kin.Dom.2-C-terminal)	RPS6KA3	88	95	45
RSK3(Kin.Dom.1-N-terminal)	RPS6KA2	100	100	95
RSK3(Kin.Dom.2-C-terminal)	RPS6KA2	100	100	27
RSK4(Kin.Dom.1-N-terminal)	RPS6KA6	95	94	49
RSK4(Kin.Dom.2-C-terminal)	RPS6KA6	100	100	24
S6K1	RPS6KB1	100	94	78
SBK1	SBK1	62	98	87
SGK	SGK1	97	73	74

A3.1. Full Kinase Profiling Results Table

SgK110	SgK110	92	100	100
SGK2	SGK2	90	97	71
SGK3	SGK3	98	87	65
SIK	SIK1	95	97	77
SIK2	SIK2	96	92	45
SLK	SLK	100	100	70
SNARK	NUAK2	99	65	8.2
SNRK	SNRK	96	89	77
SRC	SRC	100	100	98
SRMS	SRMS	100	100	100
SRPK1	SRPK1	92	82	36
SRPK2	SRPK2	90	90	27
SRPK3	SRPK3	85	100	22
STK16	STK16	100	100	100
STK33	STK33	100	88	67
STK35	STK35	100	100	98
STK36	STK36	98	97	100
STK39	STK39	79	90	65
SYK	SYK	100	100	100
TAK1	MAP3K7	98	85	74
TAOK1	TAOK1	100	100	11
TAOK2	TAOK2	89	90	75
TAOK3	TAOK3	100	100	42
TBK1	TBK1	94	94	88
TEC	TEC	100	100	100
TESK1	TESK1	100	100	100
TGFBR1	TGFBR1	100	100	100
TGFBR2	TGFBR2	99	76	64
TIE1	TIE1	100	100	100
TIE2	TEK	96	100	66
TLK1	TLK1	100	100	100
TLK2	TLK2	100	98	100
TNIK	TNIK	89	100	72
TNK1	TNK1	100	100	65
TNK2	TNK2	100	100	94
TNNI3K	TNNI3K	94	100	98
TRKA	NTRK1	100	100	52

A3.1. Full Kinase Profiling Results Table

TRKB	NTRK2	100	100	64
TRKC	NTRK3	100	85	70
TRPM6	TRPM6	80	86	79
TSSK1B	TSSK1B	95	100	100
TSSK3	TSSK3	81	95	66
TTK	TTK	100	96	100
TXK	TXK	100	100	93
TYK2(JH1domain-catalytic)	TYK2	100	100	16
TYK2(JH2domain-pseudokinase)	TYK2	98	100	93
TYRO3	TYRO3	100	100	100
ULK1	ULK1	100	98	2.1
ULK2	ULK2	100	100	18
ULK3	ULK3	100	100	98
VEGFR2	KDR	88	97	67
VPS34	PIK3C3	70	84	73
VRK2	VRK2	100	100	66
WEE1	WEE1	98	90	99
WEE2	WEE2	81	87	79
WNK1	WNK1	100	100	100
WNK2	WNK2	100	100	100
WNK3	WNK3	97	89	95
WNK4	WNK4	99	100	94
YANK1	STK32A	97	98	38
YANK2	STK32B	100	99	100
YANK3	STK32C	100	100	100
YES	YES1	100	100	100
YSK1	STK25	100	98	92
YSK4	MAP3K19	100	70	100
ZAK	ZAK	100	100	99
ZAP70	ZAP70	100	100	100